

**UNIVERSITÀ DEGLI STUDI DI PADOVA**

**DIPARTIMENTO DI INGEGNERIA INDUSTRIALE**

**CORSO DI LAUREA MAGISTRALE IN INGEGNERIA ENERGETICA**

**Tesi di laurea magistrale in  
Ingegneria Energetica**

**Energy storage and Power-to-X:  
A simulation for an Offshore Wind farm**

*Relatore: **Prof. Arturo Lorenzoni***

*Laureando: **Samuele Amadi***

*Matricola: **2020218***

**ANNO ACCADEMICO 2022/2023**









# *Index*

<b>Abstract</b> .....	1
<b>Sommario</b> .....	2
<b>Introduction</b> .....	3
<b>1 Offshore Wind farms</b> .....	11
1.1 Introduction to Offshore wind Farms.....	11
1.2 State of Art of floating Offshore Wind .....	13
1.2.1 Wind Turbines .....	13
1.2.2 Floater.....	14
1.2.3 Moorings .....	16
1.2.4 Anchors .....	18
1.2.5 Electrical substation.....	22
1.2.6 Submarine cables .....	23
1.2.7 Existing Floating Offshore Wind Farms .....	27
1.3 Case study: Sardinia, Sicily and Calabria .....	28
1.4 Wind Farm Productivity .....	31
1.4.1 Comparison of the three cases .....	31
1.4.2 Calabria Wind data .....	35
1.4.3 Energy Yield estimation & Turbine Power curve .....	39
1.4.4 Wind Profile scaling .....	44
1.4.5 Array power losses estimation .....	53
1.4.6 Transformation losses estimation.....	55
1.4.7 Export cable power losses estimation .....	56
1.4.8 Wind Power profile generation .....	59
<b>2 Grid Development and Electric Market</b> .....	61
2.1 Transmission congestions .....	61
2.2 Grid Development Plans.....	65
2.3 Electric Market .....	67
2.3.1 Dispatching Services Market and Balancing Market .....	68
2.3.2 MSD ex-ante prices & volumes .....	69
2.3.3 MB prices & volumes .....	73
2.3.4 Total prices & volumes.....	75
2.3.5 Wind farm incentives.....	76

<b>3</b>	<b>Energy Storage Systems and Power-to-X review .....</b>	<b>77</b>
3.1	Compressed Air Energy Storage.....	78
3.1.1	DCAES.....	79
3.1.2	Huntorf DCAES system.....	80
3.1.3	McIntosh DCAES system.....	81
3.1.4	Technical characteristics and efficiency .....	82
3.1.5	DCAES Summary.....	83
3.1.6	ACAES.....	84
3.1.7	Commercial examples.....	85
3.1.8	ACAES Summary.....	86
3.1.9	Isothermal CAES.....	87
3.2	Liquid Air Energy Storage.....	89
3.2.1	Existing plants .....	93
3.2.2	Technical characteristics and efficiency .....	93
3.2.3	LAES Summary.....	94
3.2.4	Commercial examples.....	94
3.3	Gravity-based Energy Storage .....	95
3.3.1	Gravity-based storage concepts .....	95
3.3.2	Technical characteristics.....	96
3.3.3	Commercial examples.....	97
3.3.4	Gravity Energy Storage Summary .....	100
3.4	Liquid Carbon Dioxide Energy Storage.....	101
3.4.1	Technical characteristics.....	103
3.4.2	Commercial Examples .....	104
3.4.3	Liquid CO <sub>2</sub> Summary .....	104
3.5	Battery Energy Storage Systems.....	107
3.5.1	Technical characteristics.....	108
3.5.2	Recycling and reusing lithium-ion batteries.....	111
3.5.3	Commercial examples.....	112
3.5.4	BESS Summary .....	113
3.6	Power-to-H <sub>2</sub> .....	115
3.6.1	Hydrogen Characteristics.....	115
3.6.2	Final Uses & Market opportunities .....	116
3.6.3	Electrolyser.....	118

3.6.4	Hydrogen Storage .....	124
3.6.5	Fuel Cell .....	126
3.6.6	Commercial examples.....	128
3.6.7	Power-to-H2 Summary .....	128
3.7	Choice of the Storage System.....	129
4	<b>Connection to the Local Grid</b> .....	131
4.1	Local Energy Demand .....	131
5	<b>Coupling the Storage with the Wind farm</b> .....	133
5.1	Battery Energy Storage System Simulation.....	133
5.1.1	Operation of the Battery System .....	137
5.1.2	Energy Storage Simulation .....	140
5.1.3	Simulation 1 – Control Strategy.....	142
5.1.4	Simulation 1 – Results .....	147
5.1.5	Simulation 2 – Control Strategy.....	162
5.1.6	Simulation 2 – Results .....	164
6	<b>Business Plan</b> .....	173
6.1	Business Plan for the Electric Energy Storage.....	173
6.1.1	Business plan results.....	178
6.1.2	Comparison of the CASES .....	184
6.1.3	D.Lgs. 210/21 .....	186
7	<b>Conclusions</b> .....	193
	<b>Appendix A: Simulation 1 results</b> .....	197
	<b>Appendix B: Simulation 2 results</b> .....	203
	<b>Bibliography</b> .....	213



# Abstract

In a world with increasing renewable energy sources penetration, energy storage technologies are becoming key technologies to achieve decarbonization targets. In the past, pumped hydropower has always been the most efficient and widespread solution for energy storage, accounting for 91% of the total global storage capacity installed in 2019. Nonetheless, energy storage technologies have strongly developed over the years, and nowadays there are many alternatives to pumped hydro to be considered.

This thesis work was developed in collaboration with Elettrostudio s.r.l., an Italian company that works in the renewable energy field. The company was working on the authorization process of three offshore wind farms in Italy, and its interest was to understand the technical and economic feasibility of coupling an energy storage or a Power-to-X solution to one of the future wind farms. Therefore, in the first part, a study on the state of art and on the critical points of offshore wind farms was performed. This allowed to make realistic predictions of the characteristics of the wind farm according to the available technology and the expected developments. In order to perform the analysis, the wind farm that should be sited in Calabria was selected, and the local data about the wind availability were studied. To simulate a profile of yearly power generation, a wind profile from an onshore site was scaled to match the expected energy generation of the offshore case. Then, based on the preliminary projects of the wind farm and on the technology assumptions, the losses of power during operation were estimated so as to calculate a realistic power profile to the land. Another objective of this thesis was to study the characteristics of energy storage technologies alternative to pumped hydro, so as to evaluate the best options for investments on utility scale storage. In the second part, a review of energy storage and Power-to-X technologies was performed, and the results were used to select the technologies to be considered for the simulations.

Then, a model of operation of a battery energy storage has been developed. Data about the market prices for the dispatching services were taken from historical data of GME (Gestore dei Mercati Energetici), while data about power fluxes for a portion of the grid were given by Terna. These data, together with the previously generated power profile from the wind farm, were used to simulate the operations of a BESS (Battery energy storage system) in two different scenarios through the software MATLAB. The simulations provided useful data for the sizing of the system and the estimation of the economic feasibility of these projects. In fact, the output results of the simulations were then used for the development of a business plan, so as to investigate with more detail the economic feasibility of such project. In the end, it was found that investments on energy storage technologies might be very risky due to large uncertainties on the effective operation and to large investment costs. For this reason, it was also presented a new mechanism (currently under development in Italy) to supply the storage capacity needed by the country by providing a fixed annual remuneration after the participation to competitive bids.

# Sommario

In un mondo con crescente penetrazione di fonti energetiche rinnovabili, le tecnologie di stoccaggio dell'energia stanno diventando tecnologie chiave per raggiungere gli obiettivi di decarbonizzazione. L'idroelettrico a pompaggio è sempre stata la soluzione più efficiente e diffusa per lo stoccaggio di energia, arrivando a rappresentare il 91% della capacità di stoccaggio totale installata nel mondo nel 2019. Nonostante ciò, le tecnologie di stoccaggio dell'energia si sono fortemente sviluppate nel corso degli anni e ad oggi esistono diverse alternative all'idroelettrico a pompaggio che possono essere considerate.

Questo lavoro di tesi è stato sviluppato in collaborazione con Elettrostudio s.r.l., una società italiana che opera nel campo delle energie rinnovabili. L'azienda stava lavorando all'iter autorizzativo di tre parchi eolici offshore in Italia, ed era suo interesse valutare la fattibilità tecnica ed economica dell'abbinamento di una soluzione di accumulo di energia o di una soluzione Power-to-X con uno dei parchi eolici in sviluppo. Pertanto, nella prima parte della tesi, è stato svolto uno studio sullo stato dell'arte e sui punti critici degli impianti eolici offshore. Ciò ha consentito di effettuare previsioni realistiche riguardo le caratteristiche del parco eolico offshore sulla base delle tecnologie disponibili e degli sviluppi tecnologici previsti. Per effettuare l'analisi è stato selezionato il parco eolico in sviluppo per il sito in Calabria e sono stati studiati i dati relativi alla disponibilità del vento locale. Per simulare un profilo annuale di generazione di energia, è stato scalato un profilo reale del vento relativo ad un sito onshore in modo tale da ottenere la stessa generazione di energia attesa per il caso offshore. Successivamente, sulla base dei progetti preliminari dell'impianto eolico e delle ipotesi tecnologiche, sono state stimate le perdite di potenza durante il funzionamento in modo da poter calcolare un profilo realistico di potenza in arrivo a terra. Un altro obiettivo di questa tesi è stato quello di studiare le caratteristiche delle tecnologie di accumulo di energia alternative all'idroelettrico di pompaggio, in modo da valutare quali fossero le migliori opzioni per effettuare investimenti su stoccaggi energetici di grandi dimensioni. Perciò, nella seconda parte è stata presentata una panoramica dei sistemi di accumulo di energia e dei sistemi Power-to-X, i cui risultati sono stati utilizzati per selezionare le tecnologie da considerare per le simulazioni.

In seguito, è stato poi sviluppato un modello di funzionamento di un sistema di accumulo elettrochimico. I dati sui prezzi di mercato per i servizi di dispacciamento sono stati ricavati dai dati storici del Gestore dei Mercati Energetici, mentre i dati sui flussi di potenza per una porzione di rete sono stati forniti da Terna. Questo gruppo di dati, insieme al profilo di potenza precedentemente calcolato per il parco eolico, sono stati utilizzati per simulare le operazioni annuali di una soluzione di accumulo a batteria in due diversi scenari attraverso il software MATLAB. Le simulazioni hanno fornito dati utili per il dimensionamento e la stima della fattibilità economica di questi progetti. Infatti, questi risultati sono stati poi utilizzati per lo sviluppo di un business plan, in modo da approfondire più nel dettaglio la fattibilità economica del progetto. Infine, è emerso che gli investimenti nelle tecnologie di stoccaggio potrebbero essere molto rischiosi a causa delle grandi incertezze sull'effettivo funzionamento dei sistemi e a causa degli elevati costi di investimento. Per questo motivo è stato poi presentato anche un nuovo meccanismo (attualmente in fase di sviluppo in Italia) per fornire la capacità di stoccaggio necessaria al Paese tramite aste che prevedono una remunerazione fissa annua.

## Introduction

Over the years, the energy sector has been crucial to provide the means for human development, economic growth and high-quality life. In recent years the energy sector has become one of the most interesting as it is undergoing a lot of changes due to the increasing concern about the environment. In particular, the topic of Climate Change has gained a large relevance. Climate changes refers to the Greenhouse effect generated by human activities, which emit greenhouse gases in the atmosphere. The presence of these gases modifies the thermal balance of the earth, causing a gradual overheating of the planet. One of the main responsible gases is CO<sub>2</sub>, whose emission is highly related to energy uses. The variation of the average temperature of the surface of the planet over the years can be seen in the following [Fig.1](#) by NASA.



Fig.1 Global average temperature variations over the years [0.4]

As it can be seen in the figure, in the recent years we reached a global average temperature increase of around +1°C with respect to preindustrial levels. It is expected that between 2030 and 2052 the temperature increase will reach +1.5 °C according to IPCC [0.5]. Among the effects that will probably be caused by this temperature variation there are increases of hot extremes in inhabited regions, heavy precipitations in several regions, higher probability of drought and precipitation deficits in some regions. Furthermore, one of the consequences will be the rising of the sea, that in the case of limiting the temperature increase to 1.5 °C is expected to range between +0.26 and +0.77 m by 2100. Additionally, there will be impacts on biodiversity, terrestrial and marine ecosystems. Food and water availability, human health and economic growth might be affected too. The main objective is therefore to limit as much as possible this temperature increase to avoid larger negative effects on the environment and on humanity itself. Different pathways have been proposed along the years to achieve the objective of limiting the temperature increase to 1.5 °C by reducing the GHG emissions, and in particular the CO<sub>2</sub> emissions.

Nevertheless, CO<sub>2</sub> concentration in the atmosphere is still growing year after year, as it can be seen in the following [Fig.2](#) by NASA.



Fig.2 CO<sub>2</sub> concentration in the atmosphere by [\[0.4\]](#)

As it can be seen in the following plot ([Fig.3](#)), according to data from IPCC in 2014, the electricity and heat production sector accounted for 25% of the global emissions. Additionally, another 10% was related to the energy sector as it accounted for emissions in the extraction, refining and transportation of fuels. Considering that in the future more and more of the other energy uses will be electrified, the generation of electric energy with the lowest possible amount of GHG emissions gains even a higher importance.

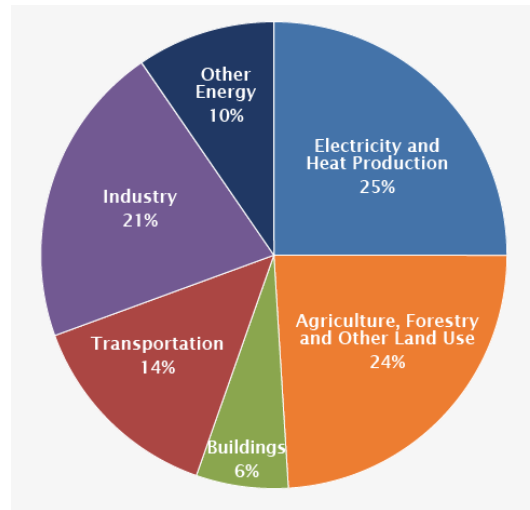


Fig.3 Global GHG emissions by economic sector by [\[0.6\]](#)

In order to face climate change and try to limit its effects, many initiatives have been taken on global and local level over the years. In 1992 the secretariat of UNFCCC (United Nations Framework Convention on Climate Change) was established by the United Nations [\[0.3\]](#). Its purpose is to support a global response to face the challenges related to the climate change. Over the years, 198 parties have signed and



applied to the convention. The milestones that defined the path towards climate neutrality up to now are cited in the following. The first and the most famous achievement was the Kyoto Protocol.

On 11 December 1997 the Kyoto protocol was adopted during the III Conference of Parties (COP3) [0.7]. This protocol has been signed by 192 parties and it represents one of the first commitments to reduce greenhouse gas emissions establishing national individual targets. In particular, it set higher emission reduction targets for highly industrialized countries, recognizing their larger responsibility on causing climate change. Overall, the countries achieved an average emission reduction of 5% compared to the emission levels of year 1990 over the period between 2008 and 2012. After this, on 8 December 2012, during COP18, the Doha Amendment to the Kyoto Protocol was adopted for a second commitment period, starting in 2013 and lasting until 2020. With this second commitment, the parties committed to reduce emissions by 18% compared to the levels of year 1990.

Another important milestone on the path to mitigate the effects of climate change took place on 12 December 2015, when 196 parties adopted the Paris Agreement at the XXI Conference of Parties (COP21) [0.8]. This treaty has the goal of limiting as much as possible the global warming and the effects of climate change. In particular, the parties agreed to limit the increase in global average temperature to well below 2°C above pre-industrial levels, and preferably to below 1.5°C. In order to achieve this, the parties agreed to reach the peak of greenhouse gas emissions as soon as possible and then a rapid reduction of emissions towards climate neutrality. The Paris Agreement is based on a 5-year cycle over which the countries communicate nationally determined contributions (NDCs) and apply the actions to reduce GHG emissions and to build resilience to adapt to increasing global temperatures.

On 11 December 2019 the European Commission announced the European Green Deal to transform the EU into the first climate neutral continent by 2050 [0.2]. This represents the first step of the EU towards the objective of zero net GHG emissions by 2050. On January 2020, Italy approved the PNIEC, National Plan for Energy and Climate [0.10]. The plan presented the measures through which Italy aimed at reducing the GHG emissions of 40 % by 2030 compared to 1990, in accordance with the EU Green Deal. Then, on 19 November 2020, according to the 2050 objective, the EU presented its strategy regarding the development of offshore wind [0.9]. With this strategy, it was proposed to increase the offshore wind capacity from 12 GW of 2020 to 60 GW by 2030 and to 300 GW by 2050. Additionally, it was proposed the use of tidal energy and floating photovoltaic energy. This strategy proves that in the future there will be huge investments in the offshore wind field and that wind energy has key role in Europe to achieve the objective of the climate neutrality. From this point of view, the development of EU regulation should help increasing security on this field.

In 2020 the outbreak of the pandemic strongly affected the European and global economy. Therefore, important measures were taken to support the restart of the European economy while trying to achieve the energetic and climatic objectives. In this period, the NextGenerationEU was realized as a temporary instrument for recovery with an invested value of 806.9 billion € (750 b€ in 2018 prices) [0.1]. Together with the long-term budget for 2021-2027, the total package was worth 2.018 trillion € (1.8 t€ in 2018 prices). The largest part of the NextGenEU was destined to the Recovery and Resilience Facility (RRF), with a total of 672.5 b€ in 2018 prices, of which 312.5 b€ as grants and 360 b€ as loans to be delivered

between 2021 and 2026 [0.1]. Conversely, the React-EU package was used for the short-term recovery with relatively smaller investments.

Among the instruments available from the NextGenerationEU, the Recovery and Resilience Facility grants 191.5 billion € to Italy for the period 2021 – 2026 (of which 68.9 b€ are grants and 122.6 b€ are loans). In order to be able to access these funds, Italy presented its National Plan for Recovery and Resilience (PNRR) “Italia Domani” [0.11], which shows the plan to achieve the six main missions through the available funds. According to the RRF, the plan includes a minimum of 37% of the expenditure dedicated to the climate investments and a minimum of 20% of the expenditure to digitalization investments. The energy sector is mainly interested by the mission regarding the green revolution and energy transition, to which 59.46 b€ are assigned. Four different components are distinguished inside this mission. Our main focus is on the second component, which is dedicated to renewable energy, hydrogen and sustainable mobility. According to the plan, this component should receive 23.78 b€ from the funds. These investments should boost the transition towards a carbon-neutral Italy, as part of the larger objectives of the EU Green Deal and also of Fitfor55 in the new version. Just to highlight some of the most interesting investments, it should be mentioned the promotion of offshore innovative plants, but also the development of biomethane production and agrivoltaics. Once again, this shows that offshore wind has a great opportunity to develop in the next years in Italy thanks to these funds. Of great interest is also the investment on the development of the production, distribution, and use of Hydrogen. In fact, hydrogen could be useful both in hard-to-abate sectors and as energy storage to balance the overgeneration of renewable energy sources. According to the plan, investments should promote the local production and use of green hydrogen, building the so called “hydrogen valleys”. Some of the mentioned possibilities are the supply of hydrogen to local industries, the transport through trucks and the blend with natural gas through the national gas grid. Supporting decarbonization in hard-to-abate sectors, green hydrogen could serve the production of chemicals like ammonia and methanol, but also provide thermal energy in the production of steel, concrete, glass and paper. Finally, the PNRR investments should support the use of hydrogen in road transports and railways, but also the research and development on hydrogen. According to the last public consultation for the “promotion of innovative plants (including offshore)” [0.12], Italy might provide funds to projects which include floating offshore wind or photovoltaics and energy storages, and integrated plants with floating wind /photovoltaics /tidal energy. In particular, for plants with size larger than 20 MW, up to 10% of the expenses could be covered by the public support. Therefore, it might be interesting to evaluate the possibility of integrating offshore wind with the abovementioned solutions to achieve better economic results and to reduce the initial investment needed thanks to the public support.

On 14 July 2021, the European Union adopted a package of more ambitious proposals, with the aim of reducing GHG emissions of 55% (instead of the 40% previously mentioned) by 2030 [0.13]. This means accelerating once again the energy transition to renewable energy sources in most of the European countries, increasing the renewable penetration objective of 2030 from 32% to 40%.

In the beginning of 2022, a new crisis affected the EU and Italy particularly. The outbreak of the conflict between Russia and Ukraine, caused the reaction of the EU, which introduced economic sanctions to Russia as a response. These conditions of degraded political relations with Russia, also affected the EU

on the economic and energy supply side. In fact, the EU is a large importer of natural gas and petrol from Russia. As stated by IEA [0.14], “In 2021, the European Union imported 155 billion cubic meters of natural gas from Russia, accounting for around 45% of EU gas imports and close to 40% of its total gas consumption”. Focusing on Italy, according to the Ministry for the Ecological Transition [0.15], in 2020, 43.3 % of Italian natural gas imports were from Russia, for a total amount of 28.7 billion cubic meters. This large energy dependance, still ongoing, affects the electric energy production, the industry, and the residential sector. While on one side the emergency situation could be partially solved by increasing natural gas imports from other countries, the new challenge is to try to generate and use energy without being energy-dependent from other countries, so improving the use of local resources like renewable energies. Therefore, in addition to the increasing renewable energy targets for environmental reasons, the energy dependance problem raised further attention on the energy transition. Once again, in this complex political situation, offshore wind and hydrogen production could help Europe on its path towards energy independency.

On 18 May 2022, as a response to Russian fossil fuel dependance, the European Union introduced the REPowerEU plan [0.16]. This last plan aims at reducing energy consumption, increasing the clean energy production, and achieving diversification of energy imports. Among the short-term measures mentioned in the plan, there is the rapid realization of solar and wind energy projects together with the development of renewable hydrogen to reduce by 50 billion cubic meters the natural gas imports. Regarding the long-term measures, instead, there is an additional increase in the target of renewable energy penetration from the previously set 40% to a new 45% by 2030. This means an increase in the expected renewable installed capacity from 1067 GW (as planned on the “FitFor55” package) to 1236 GW by 2030. For Italy, the new target of additional renewable capacity has yet to be defined, but it should reach around 80 GW by 2030. Regarding the production and use of hydrogen, a new target is set for its generation supply chain: the objective of 17.5 GW installed of electroliers should be reached by 2025 to achieve an internal production of 10 billion tons of renewable hydrogen. The use of green hydrogen and the electrification process should help reducing the fossil fuels use on European industry. In order to accelerate the startup of the hydrogen market, on 15 July 2022, the EU approved the first Important Project of Common European Interest in the hydrogen sector “IPCEI Hy2Tech” [0.17]. This project supports research, development and first applications for most of the hydrogen value chain processes. Hydrogen generation, fuel cells, storage, transportation, distribution, and even some final uses are interested by this project, which involves 35 companies and a total of 41 different projects.

Given the national and European policies, it is interesting to evaluate what are the trends for renewable energy, energy storages and hydrogen in Italy. These trends and the projections for the future are presented in the DDS 2022 (“Documento di Descrizione degli Scenari”) by Terna and Snam [0.18]. The document reports different scenarios based on current policies for the future years up to 2050. These scenarios are useful to understand the possible developments that will likely happen in the energy sector. In particular, for year 2030 two scenarios are proposed: one following the current policies and according to the objective of Fitfor55, and one in contrast with the current policies which is the Late Transition scenario, where European objectives are reached with 5 to 10 years delay. For year 2040, instead, three scenarios are proposed: the Late Transition, similarly to the one for 2030, and then the Distributed Energy Italy and Global Ambition Italy. These last two scenarios start from Fitfor55 and determine the

intermediate objectives to reach the ones of 2050. In the Global Ambition scenario, it is expected a large use of the carbon capture technology and a decrease of the demand together with renewables. In the alternative Distributed Energy scenario, instead, it is forecasted a larger renewable penetration with energy storages and electrolyzers to prevent overgeneration. The benchmark of the document is the expected decrease of the population in Italy together with a decreasing rate of growth of the GDP (PIL). A gradual decrease of the final energy consumption is expected both for 2030 and 2040.

Regarding the electric energy demand, it is expected a large increase over the next years due to the electrification of final uses. Starting from the 320 TWh of year 2019, for 2030 the scenarios expect a demand (including grid losses) ranging between 331 and 366 TWh, while for 2040 it is expected a demand ranging between 389 and 418 TWh. According to the Fitfor55 scenario for 2030, it is expected that renewable energy may cover 65% of the electric energy demand with a generation of 239 TWh. Conversely, it is forecasted a decrease of the electric energy generation from natural gas from 138 to 75 TWh (- 46%). In order to achieve these levels of renewable generation, the Fitfor55 scenario requires the addition of 102 GW of renewable capacity between solar and wind power plants. Starting from year 2019, it would be necessary the addition of 12 GW of distributed photovoltaics, 42 GW of utility scale photovoltaics, 7 GW of onshore wind and 9 GW of offshore wind. According to the late transition scenario, the additional capacity would be lower, but still 71 GW of renewable energy might be deployed. The 2040 scenarios are affected by larger uncertainties, but still are representative of possible paths towards the climate neutrality objective. Regarding the renewable installed capacity in these scenarios, it should be ranging between 140 and 156 GW to achieve the European objectives, while it is estimated to be equal to 104 GW in the Late Transition case. To achieve the European objective, offshore wind capacity may reach 15.5 to 18.5 GW.

To allow the transition to this high penetration of renewable energy, it is forecasted also the increase of electric energy storage capacity installed by around 95 GWh to achieve the 2030 Fitfor55 objective. It is estimated that 16 GWh could come from energy communities and small distributed plants, 8 GWh have already been assigned by the capacity market auctions, while the remaining 71 GWh will be utility scale storages assigned from new auctions. Regarding the distribution of these energy storage systems, it is expected an increase of small capacity storages mostly in the North of Italy together with distributed photovoltaics, while most of the storage capacity is expected in the South where many utility-scale renewable plants should be developed (like utility solar and offshore wind). The large renewable fluctuations will have to be balanced and because of the large amount of solar the need for energy shifting capacity will grow. It is forecasted also an increase of the equivalent operation hours of the existing and new energy storages. It is said that indicatively an energy storage plant in the South of Italy with Energy/power ratio of 8 hours might work for 3600 equivalent hours during the year: 2000 hours in charge mode and 1600 hours in discharge mode.

Another useful instrument for grid balancing and absorption of the renewable overgeneration is the electrolyser. The electrolyzers might be used for green hydrogen production while providing useful services to the electrical grid. Then, the produced Hydrogen could be used as an electrical energy storage or as a fuel for transports or as a chemical product and others. According to the report by Terna, these systems could be dimensioned so as to operate for an efficient number of hours between 1700 to 2000,

when the electricity market prices are low. This typically means during spring and summer months, when the solar photovoltaics production might generate too large amounts of energy, that could not be otherwise absorbed or exported through the electrical grid. Regarding the perspectives for electrolyzers in the different scenarios, they should be able to absorb 9 TWh to comply with the Fitfor55 by 2030 and between 16 and 18 TWh by 2040. Regarding the demand for hydrogen, by 2030, 23 TWh of this energy vector might be required for energy generation and storage, for production of biofuels, chemicals, and fertilizers, but also for industrial final uses in hard-to-abate sectors and in the transport sector. By 2040, instead, the demand may vary between 77 and 127 TWh depending on the level of electrification of final uses. These large amounts of hydrogen could difficultly be fully produced in Italy. Therefore, it is assumed that part of the demand will be covered by hydrogen imports from other countries. This, considering also that some renewable plants could be dedicated only to hydrogen production through electrolysis. From this perspective, the Hydrogen Backbone concept would be optimal for import and export of hydrogen between European countries in combination with the import and export of liquid hydrogen through ships. The scheme of the backbone is presented in Fig.4.

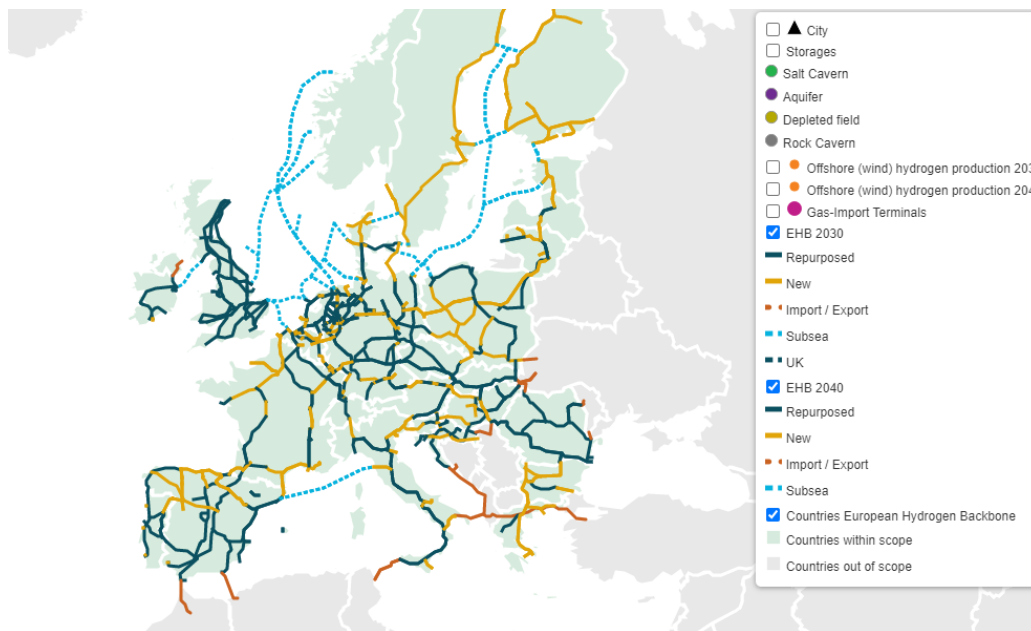


Fig.4 Map of the Hydrogen Backbone Initiative [0.19]

The presented scenarios show that a large effort will be needed to achieve the fixed objectives, to move towards energy self-sufficiency and to reduce the environmental impact of power generation. Offshore wind, hydrogen and energy storages will be fundamental in this path, and thus it is worth investigating these technologies. In this context, this master thesis was developed with Elettrostudio s.r.l., a company active in the renewable energy field, currently working on the authorization process of three floating offshore wind farms in the South of Italy. The company wanted to investigate the possibility of coupling an energy storage system to one of the offshore wind farms, so as to permit its operation without curtailments due to congestions and to reduce the disturbs introduced into the electrical grid. Therefore,

the main aims of this work were to look for the best storage opportunity available and to assess the feasibility of such system for the selected case.

Here it is reported a brief description of the structure of the analysis that has been carried out. In the first part of the thesis, it was described the floating offshore wind state of art, in order to provide some background on the technology and some views on its current development. Then, one of the three wind farms under development was taken as a reference to focus the study on a single case. Based on the available preliminary productivity assessment, a wind power profile was generated, to be later used in the simulations of the coupling with the storage system. In the second part, the Italian electric market was presented, as the storage simulations would have included the participation to the markets. In this section, the historical market data and their elaboration for the simulations were presented too. In the third part of the work, a review of some energy storage technologies was presented, as the company was interested in possibilities different from the pumped hydro energy storage, which was already known. From this review, a single technology was chosen for the wind-storage simulation, based on the pros and cons of the analyzed storage types. In the following part, a storage model was created in MATLAB, and different scenarios were simulated based on the company's needs. From the simulations results, a storage size was chosen in accordance with the company to later perform a business plan to evaluate the economic feasibility of an investment.

# 1 Offshore Wind farms

## 1.1 Introduction to Offshore wind Farms

Thanks to the technology advancements and to the growth of the scale of wind turbines, there is growing movement towards the realization of offshore wind farms. This is particularly of interest in Italy, because of the wind availability and because of the approval process problems.

In fact, in Italy the approval process of onshore wind farms is frequently jeopardized by their visual and environmental impact on the installation site. Moreover, they are often not well accepted by the local population because of the noise and because of the damage to the landscape that may affect the tourism. Offshore wind farms, instead, are designed to be placed several kilometers from the coast, thus minimizing the impact on the landscape. This is fundamental in Italy, as the country has important landscape, naturalistic, and historical sites to be preserved. So, placing a wind farm at sea may present many advantages as it may avoid most of the visual and environmental problems, while being more socially accepted.

Regarding wind availability, Italy has not a large abundance of wind resource on land. Usually, the regions with the highest amount of wind resource on land are located on the mountains and on the southern regions as it can be seen in [Fig.5](#). This limited resource has to face also the problem of the limited number of sites suitable for wind farms. In fact, the plants should not be placed on sites of national interest like natural reserves or historical sites. On the other side, offshore wind farms present the advantage of a larger availability of sites at sea and a consequent lower risk of saturation. According to Wind Europe, a total potential of 42.9 GW of potential wind power could be placed offshore in Italy. This means that Italy has the largest potential in the Mediterranean Sea, as the total potential in the area estimated by Wind Europe is 70 GW [[1.4](#)].

Generally, in addition to the possibility of avoiding authorization problems, offshore wind farms are able to exploit the larger wind availability of the sea compared to the one of the lands, allowing to produce more renewable energy. Moreover, offshore sites usually present lower wind turbulences, positively affecting the durability of the mechanical parts of the turbines.

On the other side other complexities of installing wind generators at sea have to be overcome. Firstly, it is fundamental the resistance of the components to the corrosive environment because of presence of the marine water. Additionally, the resistance to fatigue has to be carefully addressed, as waves and strong wind velocities may significantly reduce the components' lifetime. In the case of deep water depth, floating solutions are possible, but this may introduce significant challenges regarding the floating base, the moorings and the submarine cables. All these problems, added to the complexity of the installation and maintenance operations, strongly affect the costs of realizing and operating these power generation plants.

The great interest in offshore wind is demonstrated by the huge amount of connection requests that Terna, the Italian TSO, has received during 2022. By November 2022, a total of 95 GW of requests were received by the company. While this represents a great opportunity for Italy to achieve energy security

and European environmental targets, it also shows a huge challenge for the Italian electrical grid. In fact, around 80% of the requests refer to offshore wind farms located in the South and on the islands: a situation that may generate strong imbalances and congestions. Therefore, grid reinforcements and energy storages will be fundamental in the next years to be able to support this new renewable capacity.



Fig.5 Wind Availability map in Italy according to NEWA [1.1]



## 1.2 State of Art of floating Offshore Wind

Offshore wind farms are gaining a higher importance in the energy sector as they allow the access to higher wind resources available on sea sites that were not accessible before. Among the potential sites for wind farms, shallow water sites present a water depth lower than 60 m, while deep water sites present larger water depths up to around 2000 m. In the case of deep-water sites, they can be exploited only with the floating technology. The use of floating platforms is complex and more costly than shallow water plants, but nonetheless it allows to exploit more windy sites. According to Eurek et al. (2017), as mentioned by [1.2], 80% of the global offshore wind resource is located in waters deeper than 60 m.

### 1.2.1 Wind Turbines

Regarding the turbines used for offshore wind applications, a good reference is given by the “Definition of the IEA 15-Megawatt Offshore Reference Wind Turbine” by NREL [1.6]. The size of wind turbines for offshore applications was 6.8 MW on average in 2018, but now the market is moving above the 10 MW threshold. For this reason, the new reference size was chosen as 15 MW. This is in accordance with the development of floating offshore, which should make a larger wind resource available. The reference wind turbine is a Class IB direct-drive machine, with three blades, a rotor diameter of 240 m and a hub height of 150 m. This is comparable to some of the new commercial offshore three-blade wind turbines: GE Heliade X (12-14 MW) presents a rotor diameter of 220 m, Vestas V236-15.0MW has a rotor diameter of 236 m, while MingYang MySE 16.0-242 has 242 m diameter length.

Nevertheless, different solutions are still proposed on the market. An example is the HyMed project, by Aquaterra energy and Seawind Ocean technologies [1.7]. This project might become the largest floating offshore wind farm in the world, with a size of 3.2 GW. Its particularities are that 1 GW should be destined exclusively to green hydrogen production, and that the wind turbines should be of the two-blade type. According to Seawind [1.8], the company is developing two-blade large size wind turbines for marine applications. The first one is a 6 MW wind turbine with a diameter of 126 m, while the second one should have a size of 18 MW with 260 m of diameter. This shows interest also in other solutions different from the well-established three-blade wind turbine. These two-blades turbines should work at higher rotation speed, with active yaw control and no blade pitching. The lack of one additional blade should reduce the investment cost and the weight of the structure.

The wind turbines for offshore applications should be able to withstand corrosion as they are exposed to the action of the saline environment at sea. In addition, they should be equipped with transformers to transmit power at high voltage, and with switchgears (typically Gas Insulated Switchgears). Regarding the switchgears, it would be preferable the use of SF<sub>6</sub>-free systems, but still GIS with SF<sub>6</sub> insulation are a common solution for such high voltage applications.

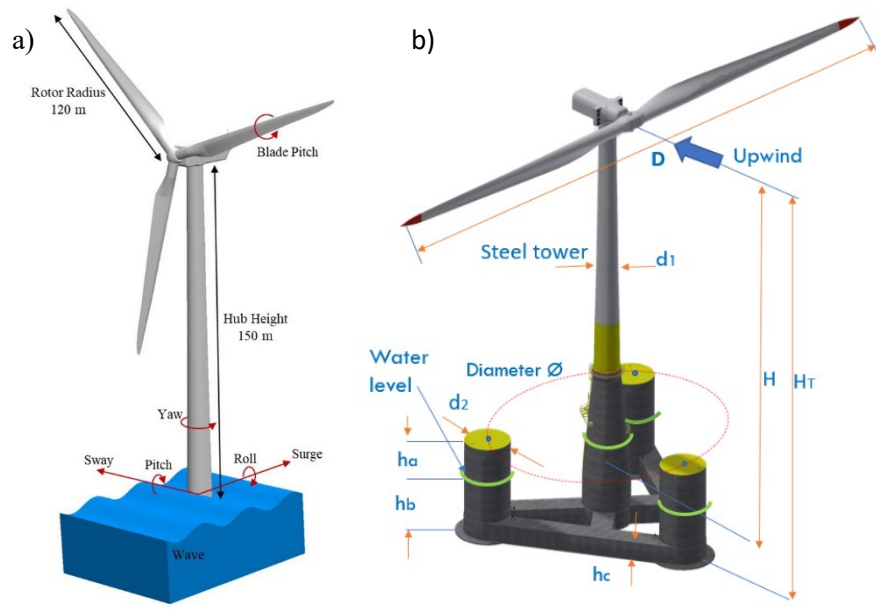


Fig.6 a) Rotation and movement axes, and dimensions of the IEA 15 MW reference wind turbine in an offshore environment. [1.9]

Fig. b) Schematic representation of the Seawind two-blade floating concept [1.8]

### 1.2.2 Floater

Most of the technologies regarding the floating platforms and the mooring lines for the turbines and electrical substations come from the world of oil&gas, where these technologies were used for the extraction of hydrocarbons at sea. The knowledge from this sector has been adapted and further developed for offshore wind, with new concepts. The main floating platform types for wind turbines are represented in Fig.7.

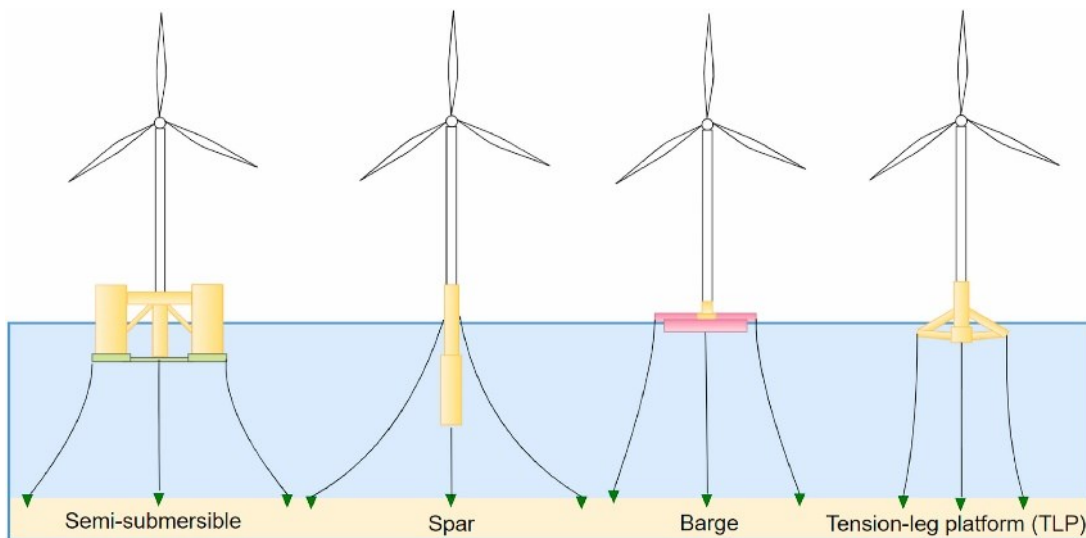


Fig.7 Floating offshore wind platforms [1.2]

Among the possible floating platforms, different stabilization concepts can be identified [1.11]. The spar type is stabilized through a ballast, while the barge system is buoyancy stabilized and the TLP is tension stabilized through the mooring lines.

- Spar

The spar type floating base consists of a steel or concrete cylinder. This base is filled with a ballast of water and gravels so as to keep the center of gravity below the center of buoyancy [1.10]. Usually, the length of the platform is equal or larger than the height of the turbine tower. This introduces a constraint for the water depth that needs to be sufficiently high. One of its disadvantages is that the spar platforms have to be assembled offshore.

- Semi-submersible

The Semi-submersible type of floating platform consists of large columns connected by tubular elements. The wind turbine might be placed on one of the columns or on the geometric center of the platform. This kind of platform is also called column-stabilized platform, as the columns provide the stability. One of its advantages is that the platform is suitable also for shallow water sites. A well-established concept is Windfloat, the one by Principle Power, which has three columns. According to this company, the platform can be modularly built and then assembled. The turbine can be installed with onshore operations at the harbor and the ensemble can be transported to the offshore site as in Fig.8.

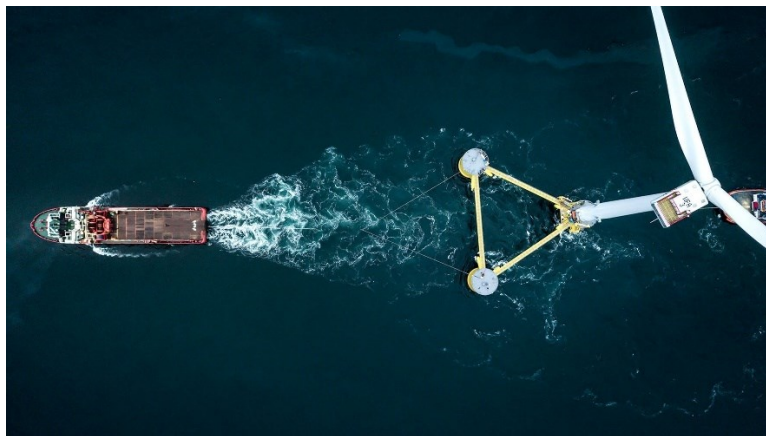


Fig.8 Windfloat transportation on site – Principle Power [1.13]

- Barge

Barge type floaters are large box-shaped structures that may be realized with concrete or steel. These structures achieve stability through buoyancy and a large plane area [1.12]. An example of commercial solution is the platform developed by Ideol, which is a barge with a damping pool. This technology has been used in the Floatgen project, and it can be used also for floating electrical substations. According to Ideol, this floating technology can be used also for very shallow water sites, with water depths of 30 m.

- TLP Tension Leg Platform

The Tension Leg Platform (TLP) can have different designs, but its main characteristic is that its stability relies on the mooring lines. Some particular designs can rely both on buoyancy and tension stabilization [1.11]. Examples of TLP platforms are the Pelastar concept by Glosten, the Blue H by Blue H engineering and the Float4wind by Sbm offshore. According to Sbm [1.14], the transport to the site from the harbor can be done by the addition of Temporary buoyancy modules, that are then removed once the ensemble is on place. Moreover, the floater should be modularly built and then assembled, similarly to the previously mentioned Windfloat semi-submersible floater.

### 1.2.3 Moorings

The moorings are fundamental in floating offshore wind, as they should keep the turbines in place and guarantee limited movements so as to keep stable operation of the wind generator. Additionally, they should not exceed the movement limitations imposed by the electric cable bending. Some of the moorings exploited in offshore wind applications are catenary lines, tension leg systems and taut leg systems [1.10].

- Catenary mooring

Catenary lines are moorings commonly used for shallow waters. Their particularity is that the floating platform is kept in place thanks to the weight of the mooring lines. These lines are way longer than the water depth of the site, and they partially lie horizontally on the seabed, as it is shown in Fig.9. Any change in the suspended length, determines an increase of the weight acting on the platform and of the consequent restoring force. For high water depth, their cost becomes relevant and therefore they are less economically convenient. For water depths lower than 100 m, the all-chain catenary concept can be applied as it is usually done in the oil&gas.

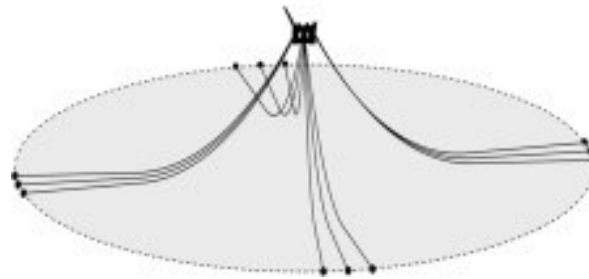


Fig.9 Catenary mooring [1.10]

- Tension leg moorings

The tension leg moorings are tubular steel legs made of multiple steel members, called tendons. These moorings are kept under tension thanks to the buoyancy of the offshore platform and to the anchorages on the seabed. This kind of mooring allows for small horizontal movements of the platform, while damping vertical movements. An example of tension leg mooring for oil&gas application can be seen in the following Fig.10.

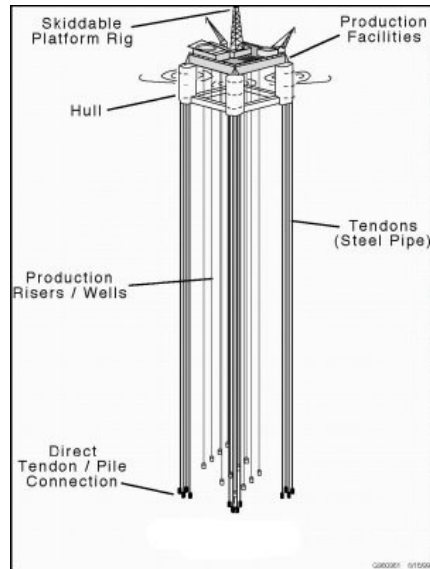


Fig.10 Tension Leg mooring

- Taut leg mooring

Taut leg moorings are anchored to the seabed under normal pretension, and differently from catenary moorings there is no change in the suspended portion of the line. The lines allow some movement of the floating platform because of the elastic stretch of the lines. Usually, the moorings have an angle between the horizontal and the platform of 30 to 45 degrees. Compared to catenary lines, taut leg moorings present much shorter lines, but they need to have sufficient elasticity to absorb the floater wave motions without overloading. Additionally, the anchorages have to withstand both horizontal and vertical uplift forces. An illustration of a taut leg mooring is presented in [Fig.11](#). These kinds of moorings could be used for water depths larger than 200 m thanks to the smaller footprint and because of the better station-keeping performance with respect to the catenary.

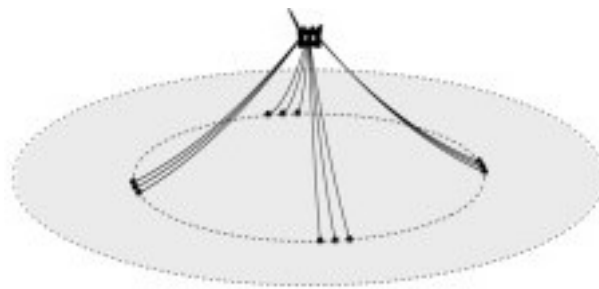


Fig.11 Taut Leg mooring [1.10]

Regarding the materials that could be used for the moorings, the main options are steel chains, but also synthetic fibers. In particular, synthetic fibers have been used in the oil&gas sector for deep and ultra-deep waters with taut and semi-taut configurations. Their main advantages are the lower weight, the better fatigue resistance and the low stiffness, that should allow cost savings.

## 1.2.4 Anchors

The anchoring system needed for the moorings is mainly a function of the type of the seabed of the site and consequently it has to be chosen after a detailed survey. Additionally, it is function of the mooring configuration and of the holding capacity required. Usually, catenary mooring configurations use drag-embedded anchors, while taut-leg mooring configurations typically use driven piles, suction piles, vertically loaded or gravity installed anchors to be able to face the vertical loads applied by the mooring lines. Since offshore wind farms are composed of many floating platforms, a possible option is to use piles as anchorages and to share them between different wind turbines. The main anchorage types are presented in the following Fig.12.

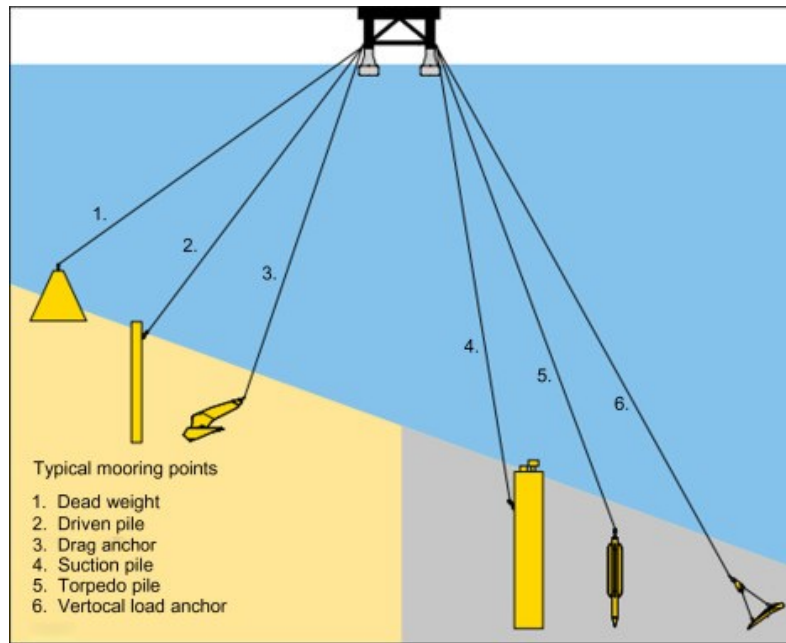


Fig.12 Examples of possible anchorages for floating applications [1.10]

- Suction piles

Suction piles are cylindrical anchors of a large diameter, typically from 4 to 6 m. Their installation relies partially on their weight and partially on the suction process. By pumping through a valve on the top, a pressure differential is induced between the internal and the external part of the pile, which allows a higher penetration on the ground. This pumping process is operated through a remotely operated vehicle (ROV). The suction piles are particularly effective with clay soils, as they are relatively impermeable and leakage flows through the soil are negligible. Their length may vary depending on the soil conditions, and they usually present low thickness of the walls. They are used both on TLPs, catenary and taut moorings.

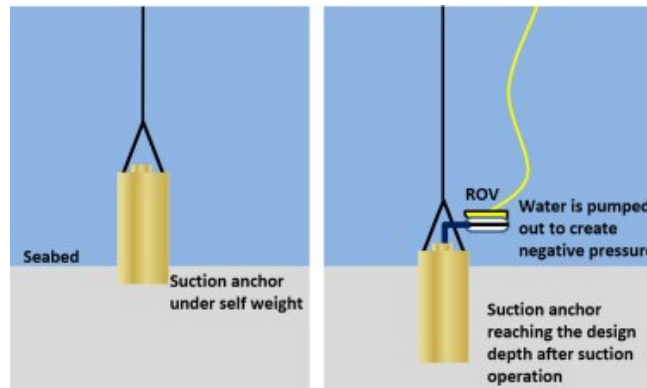


Fig.13 Schematization of Suction Pile installation process [1.10]

- Driven piles

Driven piles are open pipes with a diameter varying between 1 and 3 m. They can be driven 100 m in the seabed mobilizing the soil and gaining high uplift resistances. For this reason, they are common where vertical loads are important, like TLPs and taut leg moorings. Nevertheless, they can be used also in catenary moorings. These anchors are less common for high water depths because of the complexity of installation. In fact, they require the use of hydraulic hammers which operate underwater. New technologies made it possible to use these anchorages even at 2400 m depth.

- Drag-embedment anchor (DEA)

The drag-embedment anchor is a bearing plate that sinks into the seabed if dragged by a chain. Of particular importance is the control of the angle of inclination of the anchor, which allows the sinking process. This angle depends on the type of soil. These anchors are less expensive than the previous ones, however they present some limitations: it cannot be precisely placed in a specific position, and its load resistance is dependent on the sinking depth which cannot be precisely predicted either. This anchor provides mainly resistance to horizontal loads, but minimal resistance to vertical loads in case of low depth penetration. This happens with sand and stiff clay soil, while in the case of soft clay the sinking depth can be higher, thus providing higher resistance to vertical loads.

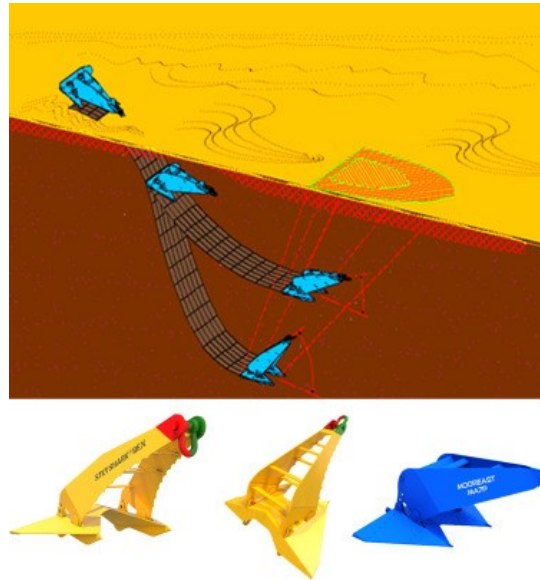


Fig.14 Drag Embedment Anchors installation procedure and commercial examples by Vryhof [1.10]

- Vertically loaded anchors (VLA)

Vertically loaded anchors (VLA) are installed similarly to DEA, but in addition to that they present a releasable shank that can be opened after installation. This additional part allows for a larger resistance to vertical loads. These anchors are suitable for soft and layered clay soils. Their resistance to the loads is function of their final orientation and of the penetration depth in the soil, for this reason it is critical the prediction of the installation outcome.

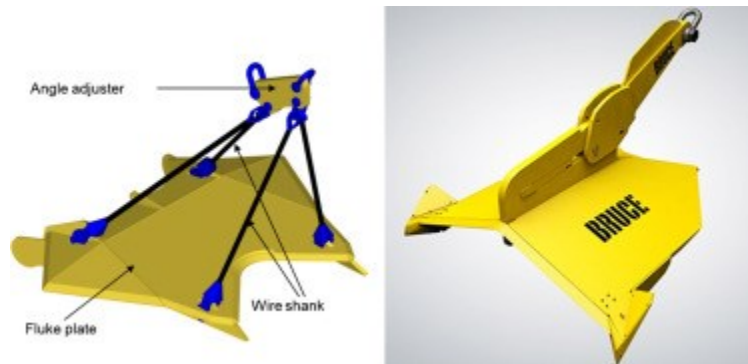


Fig.15 Vertically Loaded Anchors commercial examples by Vryhof and Bruce [1.10]

- Suction embedded plate anchors (SEPLA)

Suction embedded plate anchors (SEPLA) are a combination of suction piles and plate anchors. In particular, the suction pile is used to provide further sinking of the plate anchor and it is then removed by reverse operation of the pump. The vertical plate anchor is then turned perpendicularly to the mooring direction. This positioning allows to support also vertical loads, and so the anchor is suitable also for taut leg moorings. Its use is limited to the soft clay type of soil.



- Deadweights

Dead weight anchors are simply composed of concrete or scrap steel materials, and they are deployed without penetration on the seabed. They are less frequently used, but useful in the case of rocky seabed. These anchors have low holding capacity, as the vertical load resistance depend on the submerged weight while horizontal loads depend on the friction with the seabed.

- Torpedo piles

Torpedo anchors are gravity-installed devices that sink into the seabed thanks to their shape and their large weight. They are usually released around 100 m above the seabed, and they may reach a final velocity of 30 to 50 m/s. These anchors are usually installed with soft or medium clay soils. Their deep sinking provides large holding capacity both to vertical and horizontal loads, resulting in suitability both for catenary and taut moorings. Torpedo's main advantage is the simple and economical installation process.

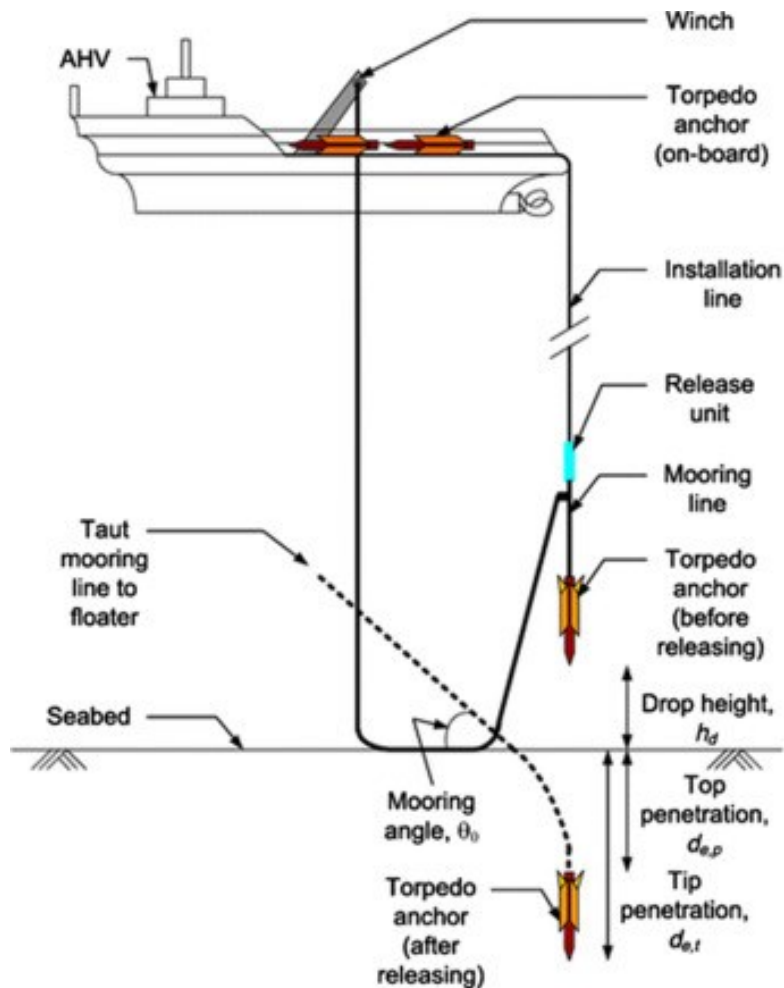


Fig.16. Torpedo anchors and their installation procedure [1.10]

### 1.2.5 Electrical substation

Another important element for floating offshore wind farms is the electrical substation. In the case of close to the coast wind farms, the electrical substation could be placed onshore. In this case the power generated by the turbines could be sent to the land through 33 or 66 kV cables, without too high-power losses because of the low cable length. This solution could be economically sustainable thanks to the lower investment. However, for large wind farms placed far from the coast, a bottom-fixed or a floating electrical substation could be needed to elevate the voltage level offshore for the power transmission to the land. This should significantly reduce the power losses through the submarine cable to land. Of course, this solution requires a further complication in the design of the plant and a larger investment cost, but it might be more economically performing in the long term. The optimal choice has to be assessed depending on the specifications of each particular plant. In any case, once the submarine cables get to land, it is necessary to perform a junction with the onshore cables and to connect them to an onshore substation, which links the plant with the national grid. Regarding the offshore electrical substation, once again the choice between the floating and the bottom-fixed solution lies on the water depth and its technical and economic feasibility. With the development of new wind farms in deep and ultradeep waters it is expected that there will be a consistent growth in the field of floating substations. However, this still represents one of the critical points for the development of floating offshore wind, as no utility scale systems have yet been realized. Some solutions have been studied and proposed by some companies, but still only renderings of floating substations are available. An example of a floating electrical substation solution is the one developed by Hitachi Energy, sustained by a four-pillars floater, which is represented in [Fig.17](#) [1.15]. As it is highlighted, these structures are subject to the continuous action of waves, to vibrations, to a saline environment and they have to withstand extreme weather events. Consequently, it is important that all the appliances of the substation are protected from this environment and are tested to support the effect of the movements and vibrations typical of the offshore environment. In particular fatigue, resonance frequencies and shock loads have to be studied. Due to permanent water currents, the possibility of a continuous inclined operation has to be considered too. This requires a longer period of study and testing before the commercialization of the products. Another critical point in this part of the projects is the lack of common legislation and standardization, which could improve and accelerate the development of floating projects.

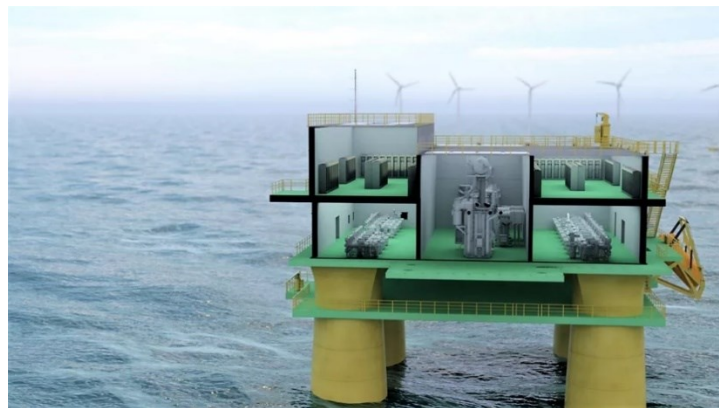


Fig.17 Floating electrical substation by Hitachi Energy [1.15]

According to Repower’s general technical report for the offshore plants [1.21], these substations should include not only the electrical appliances (like transformers) and their auxiliaries, but also emergency generators, safety systems, fire protection systems, communication systems, temporary accommodations for operators. In a similar way to floating wind turbines, these substations should be assembled on the floater and then transported on site through tug ships. According to Hitachi Energy, AC floating substations should be available by 2025 once all the components will be proven and tested. Conversely, for DC floating substations, they are expected to be available between 2028 and 2030 as the development of this solution has been planned but it has not started yet.

## 1.2.6 Submarine cables

Among the possible submarine cables, a first distinction might be between the static and dynamic cables. The main distinction between the dynamic and the static ones, is that dynamic cables have a double layered armor to provide protection and stability [1.2]. Differently from conventional submarine cables, the dynamic ones have additional floating components to enable their movement with the floating platform of the turbine/substation. Additionally, it is necessary to add bend stiffener connectors, which limit the curvature of the cable in correspondence to the connection with the floating platform. In case the cable touched the seabed, it is also necessary to add a further protection on the touchdown point, as this part is subject to abrasion with the seabed. Two different shapes may be used for these kinds of cables: the “W-shaped” cables and the “S-shaped” cables which are also called “lazy wave” [1.16]. These cables get their particular shape thanks to the presence of the buoyancy modules. The W-shaped cable may be used as a connection between the floating wind turbines or between the offshore substation and the wind turbines. The Lazy wave cable configuration may instead be used as an inter-array or export cable. Two examples are represented in the following Fig.18.

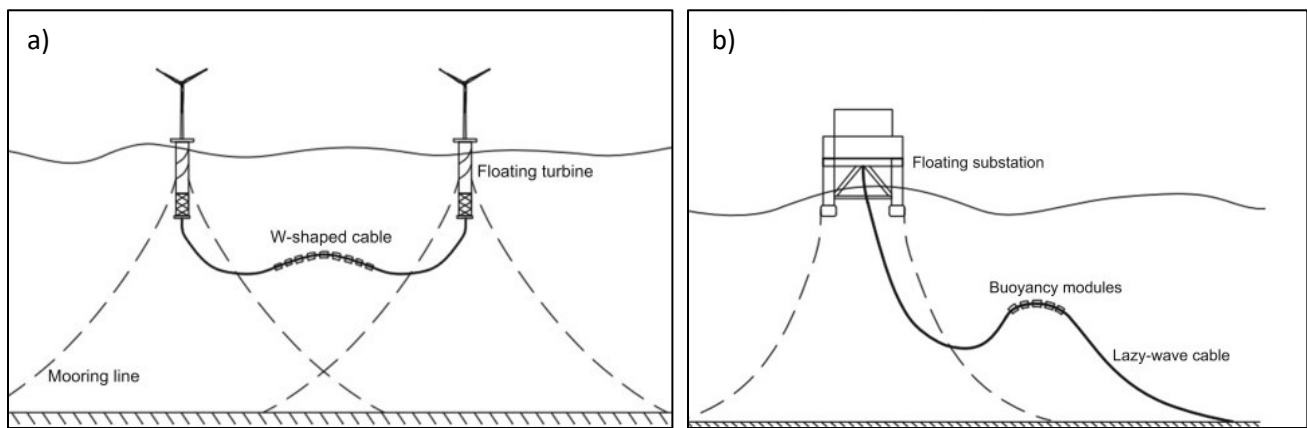


Fig.18. a) Example of “W” inter-array cable between two floating turbines

b) Example of Lazy wave shape of a dynamic cable [1.16]

Differently from dynamic cables, the static cables are deployed on the seabed, where they can be buried or protected through an external protection. This kind of protection is additional to their metallic armor, and it is made to avoid damages due to marine operations like fishing, to anchors deploying and to strong

hydrodynamic actions. The external protection of the cable could be done with natural rocks or concrete mattresses placed above, or alternatively through the use of cast iron shells assembled on the cable itself. Usually, static cables are used for the power transmission from the wind farm to the land.

In the realization of an offshore wind farm, we should distinguish the inter-array cables between the turbines and the offshore substation, and the transmission cables to the land. Usually, the inter-array cables operate at voltage levels like 33 and 66 kV. The first one is suitable for wind turbines up to 7 MW, while the second one is suitable for turbines of size equal or larger than 8 MW, so the 66 kV will be more and more used with the growing size of offshore wind. Additionally, in the future it is expected that 132 kV inter-array cables will be available for turbines with 15 – 18 MW size. Regarding transmission cables from the farm to the land, they can work at very high voltage level like 275 or 380 kV to reduce as much as possible the cable losses. However, the export cable represents another critical point for the realization of offshore wind farms, as the technology is still not fully commercially available for all operative conditions. As an example, for ultra-deep-water conditions (water depth of around 2000 m), it is expected that in 2024 AC export cables working with 220/275 kV will be available. However, 380 kV cables seem not yet to have been planned for a future commercial release. Even if a further voltage increase might be expected for the future, up to now there is no certainty on when this technology will be available. Therefore, lower voltage solutions might impact the operation of future plants with not negligible losses in currently developed plants.

Inter-array cables are usually of the dynamic type, as they are designed to withstand the constant movements due to the offshore operation. Latest advancements for these cables led to the development of the 66 kV solution, which can be used for medium to large size wind turbines with lower losses. Nonetheless, one of the critical components for offshore wind farms is the export cable to the land. This cable is usually a static cable placed or buried in the seabed. The critical points are that it should allow large power transportation with the lowest possible losses over long distances. The longer the distance from the land, the higher the resistance and losses through the cable. In addition, in the case of AC transmission at high voltage levels, the reactive losses might be relevant in long cables. This represents a technical but also an economical challenge due to the large investment needed, and to the large economic value of the transmission losses that might occur over the system lifetime. Evaluating all the available possibilities, historically HVAC has been the most common solution. Anyway, HVDC is gaining more and more interest due to its potential for long distance connections [1.17].

- HVAC

Alternate current is used in most portions of the electrical grid for high voltage transport of the electrical energy, so it represents the first solution for bulk power transmission to the land. In AC conditions the voltage can be easily adjusted through transformers, and in fact one of the main advantages of AC connections is the higher efficiency of the transforming substations. Typical reference value for transformation substation loss is 0.1 % of the input power received [1.17]. Additionally, transformers cost less if compared to the converters needed for the DC power transportation. However, talking about the power transmission, HVAC systems tend to generate large amounts of reactive power, so compensation reactors are also needed. All in all, for long distance connections, the power losses in

HVAC cables might higher compared to the ones of HVDC cables. Additionally, compared to DC solutions, AC cables need larger section solutions because of the skin effect and self-inductance resistance to achieve the same capacity according to [1.2].

- HVDC

The second possibility for the export of the generated energy is the use of the Direct Current technology. According to [1.2], HVDC cables generally perform economically better than HVAC in subsea applications for distances larger than 60 km. In [1.17], a review of different studies is reported, many of them with different results but with the common agreement that HVDC offers some advantages for long distance connections. Just to report some of them: the power flow is controlled, eventual AC faults are not transferred to the rest of the network, there are no skin effects and self-inductances, and the DC cable power losses are lower. Therefore, it might be an interesting solution for large offshore wind farms. Of course, site specific optimization should be carried out based on the plant characteristics.

HDVC connections use mainly two types of converters: line commutated converters (LCC) and voltage source converters (VSC). These converters are required at both ends of the line, to provide AC/DC conversion and vice versa. The VSC technology has the advantage of being able to provide black start to the grid and the advantage of being more compact. Additionally, it doesn't require a transformer converter, as AC transformers can be used, differently from LCCs. However, this technology generates higher losses compared to the LCC. Nevertheless, it seems the most promising one for renewable energy transmission like offshore wind farms because of the black start capability. The LCC technology instead, is mostly used to transport bulk energy for very long distances [1.18]. Recent developments of VSC technology have made its losses lower and closer to LCC. For VSC, the losses are in the order of 1.3 % of the rated power, while LCC losses are typically lower than 1%. Another point that makes these technologies interesting is the weight reduction that has occurred over the years for the converters, that may make their offshore use easier.

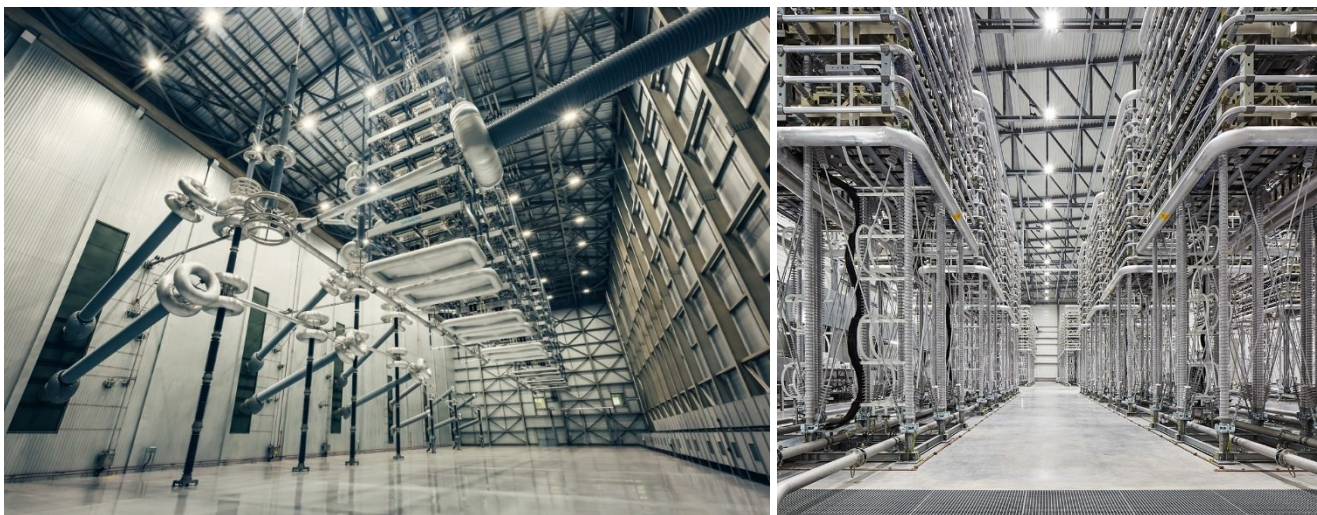


Fig.19 LCC converters (left) and VSC converters (right) by Siemens.

For HVDC submarine cables, a typical solution is a monopolar connection, a single DC pole line which separates the rectifier and the inverter. DC submarine cables connected to VSCs can work at very high voltages reaching 500 kV and consequently reducing power losses. An example is the Skagerrak 4 link between Denmark and Norway, which is partially an overhead line and partially a submarine cable. Regarding their capacity, it is constantly growing to provide market solutions for very large wind farms. An example can be the TSO Tennet, which is working on the development of a 2 GW HVDC static submarine cable. For lines connected to LCCs, the voltage levels can be even higher. An example is the Zhundong – Sichuan overhead line in China, which reaches 1100 kV and transmits power over 2600 km. A comparison of the performances of HVAC and HVDC power transmission is reported in [1.19]. The paper shows that the DC losses are kept low at around 4 % for distances up to 150 km, similarly to what is declared in [1.2]. Conversely, AC losses in the cable may reach 19 % for a length of 150 km, which would be clearly unacceptable. While the use of DC connections for long distances could be very interesting for offshore wind farms, once again the technology seems to be not yet ready for nowadays applications mainly because of the converters. In fact, these systems have yet to be tested for floating applications, as they comprise a large set of micro-components that could be affected by the vibrations and movements of floating substations. Additionally, these systems are typically large and very tall for large power applications and therefore they must be carefully designed together with the floating substations to balance the weight and the size of the system. Another point that has to be developed is the use of dynamic HVDC cables, that seem to not be yet ready for high depth submarine applications.

All in all, the technology to be used for offshore floating wind farms is almost ready, with some critical developments needed on dynamic cables, floating substations, DC converters and GIS. Moreover, with the growing investments on this technology, a local supply chain will have to be created to satisfy the future demand together with the development of suitable infrastructures for the manufacturing and installation of large structures in the coastal areas. Finally, another key point to accelerate the development of floating applications is also the regulation of the sector, that will give references and security for investors.



### 1.2.7 Existing Floating Offshore Wind Farms

Some examples of existing floating plants are reported in the following. Most of these plants are medium scale projects intended to prove the developed technology for commercial level. Still, they represent some of the largest projects existing in the world.

- Hywind Scotland

Hywind Scotland is the world's first commercial floating offshore wind farm as it entered in operation in 2017 off the coast of Peterhead. It consists of 5 turbines of 6 MW, which results in a total rated power of 30 MW. The site where it is located has a water depth ranging between 95 and 129 m which means relatively shallow water. The site is 25 km from the Scotland coast and the cable to the land has a length of 30 km. [1.3] Regarding the technologies that have been used for this plant, the floating base is of the spar type. Each of these bases, are kept in place by the moorings: three steel chains connected to suction bucket anchors. This plant reached a capacity factor of 57 % in 2020, a very high value if compared to the average one for onshore plants, that for the UK is 25.2 % [1.4], demonstrating the higher productivity of offshore wind. Regarding the economic performance of this plant, it achieved an LCOE of 211.43 €/MWh. If compared to the current bottom-fixed offshore wind farms in the UK the floating option seems unfavorable, as their LCOE reached 64.60 €/MWh [1.2].

- Kincardine

The Kincardine offshore wind farm is located in Scotland like Hywind, and it consists of five 9.5 MW wind turbines plus a single 2 MW turbine, for a total power of almost 50 MW [1.3]. This project has started its operation in 2021 (after the pilot operation of the 2 MW turbine alone), and it is located 15 km from the coast, in a site where the water depth ranges between 60 and 80 m. Regarding the technologies implemented in this plant, its floating platform is of the semi-submersible type, and each of these platforms is linked to four steel chain mooring lines with drag-embedment anchor.

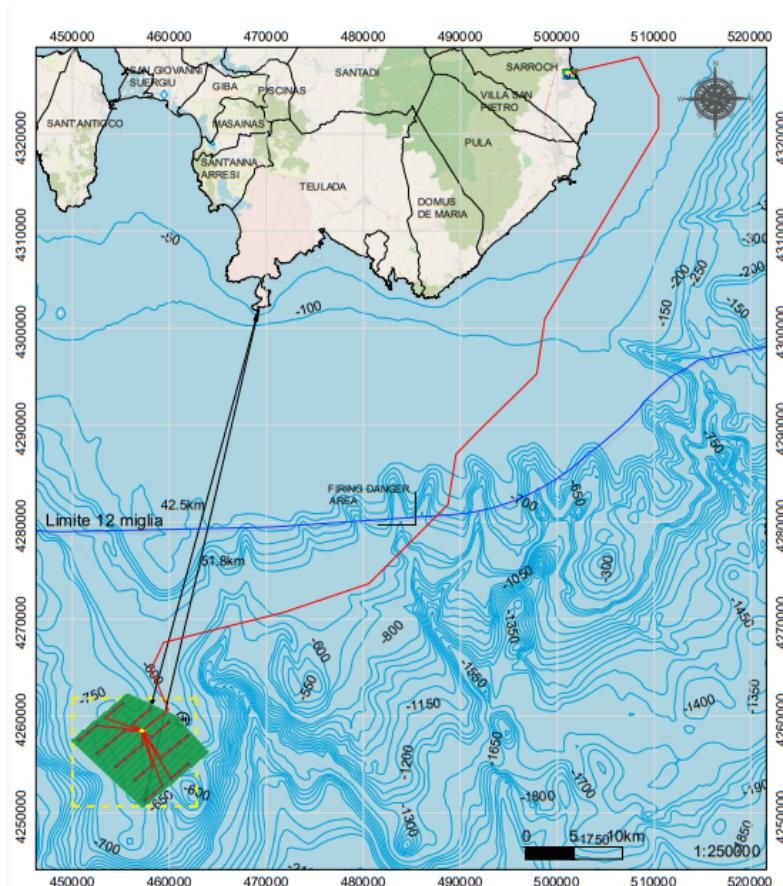
- Hywind Tampen

Another important project is Hywind Tampen, which entered operation in 2022. This is an 88 MW project, composed by 11 turbines with 8 MW size each. The plant is located in Norway, 140 km from the land, where the seabed is between 260 and 300 m deep. According to Equinor [1.5], these turbines are placed on concrete floaters.

### 1.3 Case study: Sardinia, Sicily and Calabria

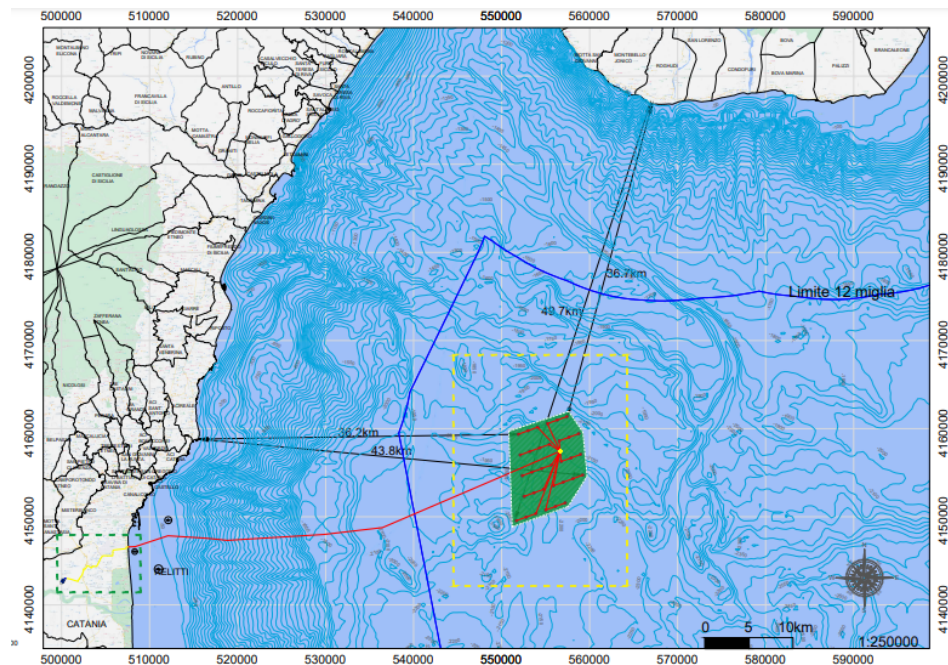
Three offshore wind farms are under development by Repower renewable s.p.a. in the southern regions of Italy, and they should be connected to the regions of Sardinia, Sicily and Calabria. The three offshore wind projects have the same size of 495 MW, as they should be composed of 33 wind turbines of 15 MW each. In all these cases the depth of the seabed is relevant for the chosen sites, so the wind farms will be of the floating type. Each wind farm will have its own floating electrical substation, responsible for the transformation to very high voltage level to transport the generated power onshore. The connections between the wind turbines and the floating substation will be composed by submarine cables working at high voltage 66 kV. Starting from the floating substation, the submarine cables will connect the floating wind farm to the land. It is supposed that in the next years 380 kV HVAC submarine cables will be available, while actually in most of the current offshore plants 275 kV HVAC submarine cables are present. The submarine cables will be connected to other onshore cables heading to the electrical substation, which then connects the plant to the national grid. The wind farms will be subdivided in 10 sub-arrays each, which will be composed by a maximum number of 4 turbines in series, as it can be seen from the following figures. The specifications of the three projects will be briefly presented in the following.

The Sardinian wind farm should be placed south of Sardinia, at a minimum distance of 42.5 km from the coast (Fig.20).

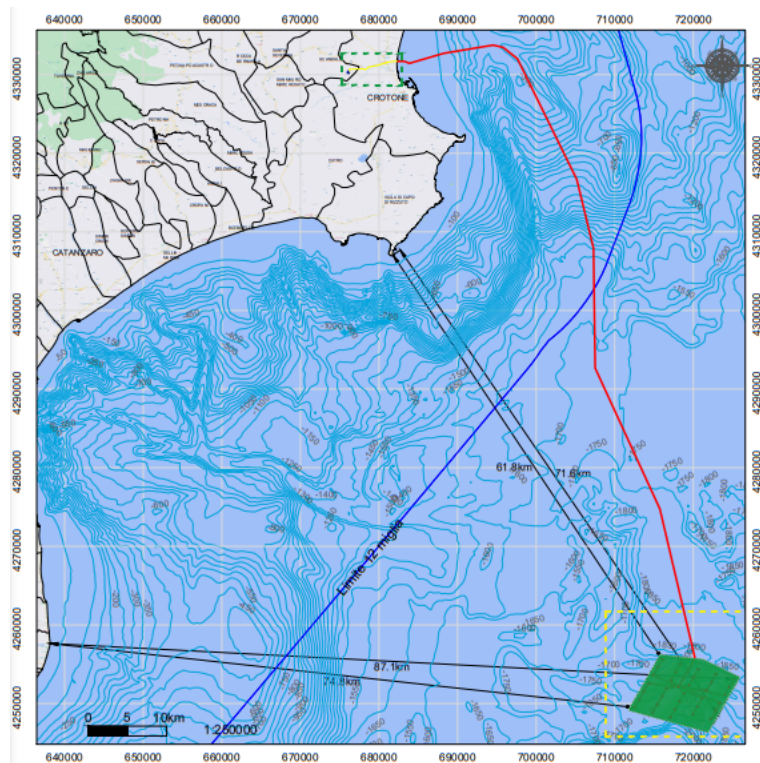




The wind farm in Sicily should be placed at sea in front of the city of Catania. The chosen site has a minimum distance of 36.2 km from the coast of Sicily and 36.7 km from the coast of Calabria (Fig.21).



The third wind farm has a minimum distance of 61.8 km from Capo Rizzuto in Calabria, and it is 74.8 km distant from Monasterace Marina (Fig.22).



Here in Tab.1 is a comparison of the main specifications for the three wind farms.

Location	Sardinia	Sicily	Calabria
Minimum distance from the coast	42.5 km	36.2 km	61.8 km
Bathymetry plant area	-620 m / -780 m	-2020 m / -2200 m	-1680 m / -1860 m
Area interested by the plant	89 km <sup>2</sup>	86.7 km <sup>2</sup>	86.2 km <sup>2</sup>
Offshore cable length	105 km	51.1 km	104.9 km
Onshore cable length	1 km	10.1 km	6.6 km
Total cable length	106 km	61.2 km	111.5 km

Tab.1 Main project data of the three wind farms

It is possible to see that all of the plants should be placed very far from the coast, thus minimizing the visual impact on the landscape from the coast. However, the distance from the coast affects the length of the cables needed to connect the farms to land and consequently increases the power losses and the investment costs. The path of the cable towards land, however, is dependent on many other parameters including the morphology of the seabed and interactions with marine infrastructures, environmental and biological protected zones, military zones. In fact, the cable length for the three plants is significantly different from the distance from the coast as a result of the preliminary study. The detailed surveys may detect particular needs for the path and further affect the total length. In the cases of Sardinia and Calabria, the cable length is particularly relevant and very challenging.

Another important parameter to notice is the depth of the seabed. In the case of Sardinia, the depth is relevant but still much lower compared to the other plants. This represents an economic advantage, as the location surveys and the installation process should be easier to carry out. Additionally, the investment for the moorings should be significantly lower. This is a critical point for the other two cases.

## 1.4 Wind Farm Productivity

### 1.4.1 Comparison of the three cases

During the preliminary studies about the three above mentioned plants, the analysis about the productivity of the site has been carried out by Tecnoconsult Engineering Construction S.r.l., as it is reported in [1.21]. Part of the results of this study are reported in this chapter. This analysis allowed to estimate the expected production of the wind farms and consequently to evaluate the possible revenues. In particular, the aim of this study was to estimate the values of the capacity factor (and equivalent hours of operation) and the P50. The P50 value represents the expected yearly productivity of the plant that has a probability of 50 % of being overcome.

The methodology that has been followed is the same for all the plants. It has been used the simulation software Windsim, which is based on CFD analysis. Some of the main inputs of this software, needed to estimate the available wind resource, are the orography and roughness of the site. Therefore, the map of the orography was taken from the remote sensor Advanced Spaceborne Thermal Emission and Reflection Radiometer (ASTER), while the info about the surface roughness was taken from the project “Corine Land Cover 2006”. Since no physical sensors were available on site, the characterization of the wind availability was carried out through the “New European Wind Atlas” (NEWA) database, which exploits satellite meteorological data. Three points located near each site and at a height of 150 m were considered to extract the data for the simulations. These data were referred to a period of time of 10 years: from 2009 to 2018.

Regarding the choice of the wind turbine to be used, a three-blade turbine with a rated power of 15 MW was considered. In particular, the data about the turbine were taken from the commercial turbine by Vestas: the offshore model V236-15.0MW. Its main characteristics are here reported in Tab.2:

V236-15.0MW	
Turbine rated power	15 MW
Rotor diameter	236 m
Swept Area	43742 m <sup>2</sup>
Cut-in wind velocity	3 m/s
Cut-out wind velocity	30 m/s
Design lifetime	25 years

Tab.2 Offshore turbine data

Considering that the height of the hub can be adjusted depending on the site characteristics, it was considered a hub height of 150 m, which results in a total height of 268 m accounting both for the tower and the blades. Since the characteristic curves of the new turbine were not available, the productivity analysis was carried out referring to the characteristics of a similar size turbine. The curves that were used are here reported in Fig.23.

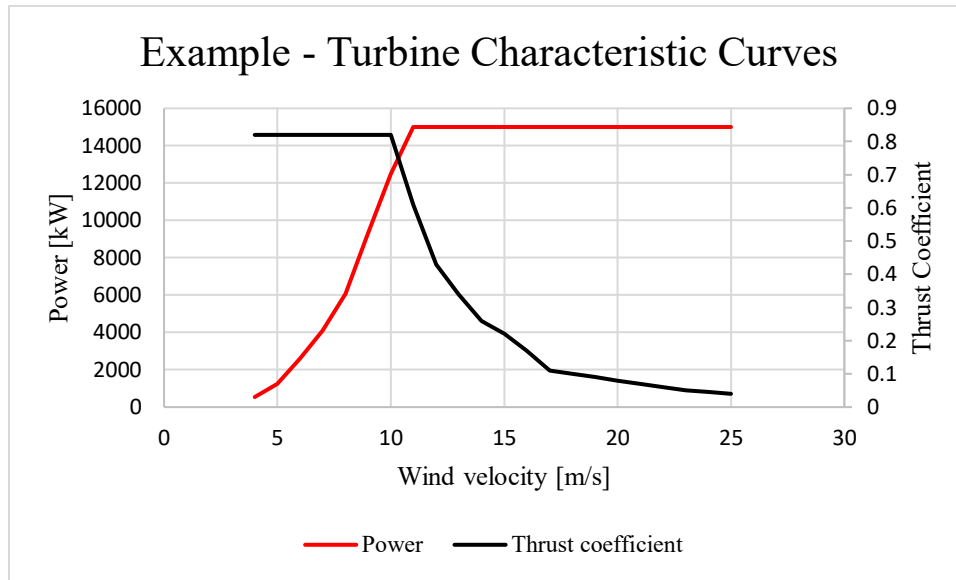


Fig.23 Turbine characteristic curves by [1.21]

Looking at the curves, it is possible to see that with the increasing wind velocity we have the increase of the power generated up to the rated power. Once the rated power has been reached, a further increase in the wind velocity does not affect the generated power, thanks to the power control strategy that reduces the power coefficient. This allows to keep the generated power constant and to avoid too high rotation velocities.

The main climatic data regarding the three plants are here reported in Tab.3.

	<b>Sardinia</b>	<b>Sicily</b>	<b>Calabria</b>
Newa points - Average velocities	7.65 – 7.70 m/s	6.81 – 7.26 m/s	7.24 – 7.41 m/s
Yearly average wind velocity	7.67 m/s	7.02 m/s	7.32
Main Wind directions	North-West	North / North-West	North / North-West / South-West
Height	150 m	150 m	150 m
Average Temperature	20 °C	18.5 °C	20 °C
Considered Air Density	1.217 kg/m <sup>3</sup>	1.217 kg/m <sup>3</sup>	1.217 kg/m <sup>3</sup>

Tab.3 Meteorological data of the three locations

The wind velocities reported in the above table are a resume of the characteristics of the 9 points from NEWA considered for the wind availability. Each point presents its own wind velocity and orientation distribution probability. In Fig.24, the plots for one of the points considered for Sardinia is reported as an example.

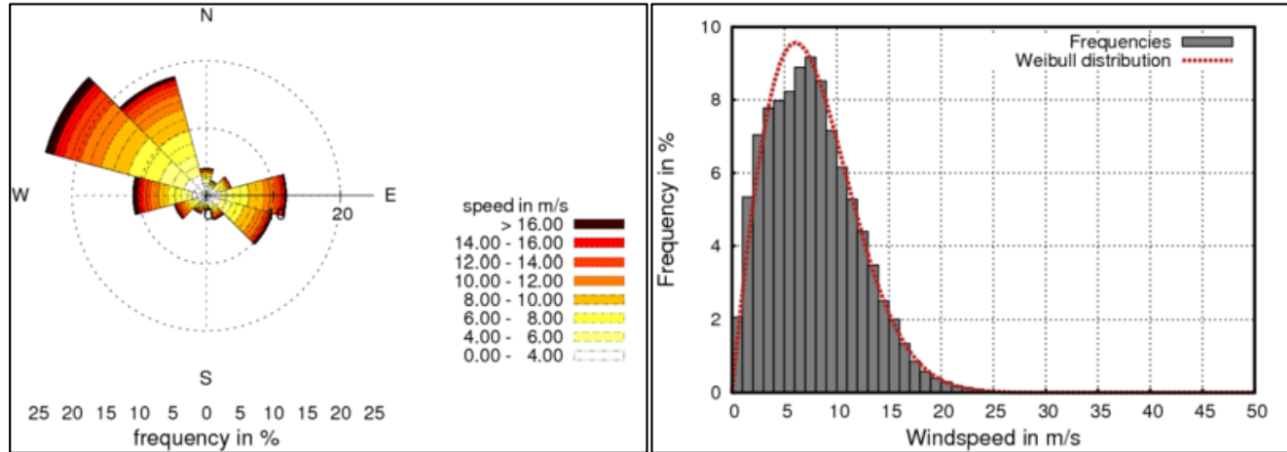


Fig.24 Wind data availability for one of the points considered in the Sardinia project.

In order to produce a valid estimation of the production of the plants, the wake losses were calculated through the software. These losses refer to the rotationality imprinted to the wake, which reduces the power extracted from the air flow. Moreover, this effect has to be considered to better understand the interaction between different sub-arrays of turbines. In fact, the rows of turbines positioned after the first one, may receive a lower wind velocity. In addition, the wind farm blockage effect was considered.

For this reason, the spatial configuration of the turbines is important to limit this kind of losses. A larger distance between the turbines allows to minimize the influence that one turbine has on the following ones. As it is usually done in literature, for these plants the distance between the turbines of different sub-arrays was set to 10 times the rotor diameter size, while the distance between the turbines of the same array was set to 5 times the rotor diameter.

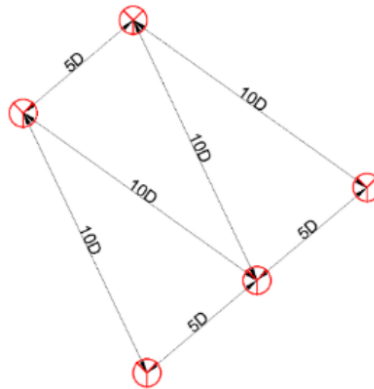


Fig.25 Schematic plot of the distance between the turbines of the array

The wake losses were calculated through two different wake models: the Jensen model and the Larsen Model. While the first one is the most frequently used, the second one is more precise for offshore plants. These models are not investigated, as their result is used as one of the inputs of the following analysis. In [Fig.26](#) the wake losses calculated with the Larsen model for the Sardinian power plant are shown.

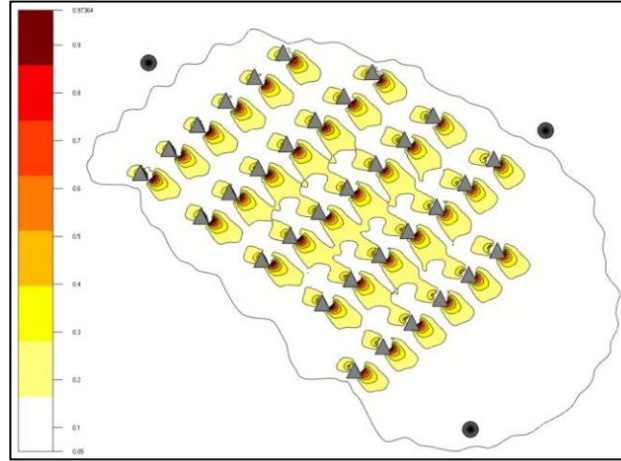


Fig.26 Plot of the wake velocity loss for the Sardinia plant project.

Both models showed that the wake losses are not negligible. In particular, the Jensen model showed losses that might reach 10.7% for singular turbines, while the Larsen model showed losses up to 7.8%. Considering that Larsen model should be more accurate for these cases, the result was acceptable as in any case the losses were lower than 8%. It should be highlighted that this effect is way lower for the first row of the array, which receives an undisturbed air flow. On the other hand, the central rows are the ones that suffer the highest wake losses.

Given all the previous data, it was possible to perform the productivity estimation and calculate the energy generated by each turbine over a year, with both kind of wake models and even without considering wake losses. The results of the overall simulations of productivity are here shown in Tab.4.

	<b>Sardinia</b>	<b>Sicily</b>	<b>Calabria</b>
Gross Energy Generation	1866 GWh/year	1649 GWh/year	1682 GWh/year
Energy Generation with Jensen losses	1737 GWh/year	1528 GWh/year	1546 GWh/year
Incidence of Jensen losses	6.9 %	7.3 %	8.1 %
Capacity Factor - Jensen	40.1 %	35.2 %	35.7 %
Energy Generation with Larsen losses	1769 GWh/year	1559 GWh/year	1582 GWh/year
Incidence of Larsen losses	5.2 %	5.4 %	5.9 %
Capacity Factor - Larsen	40.8 %	36 %	36.5 %
P50 [Larsen]	1648 GWh/year	1452 GWh/year	1474 GWh/year
P50 [Jensen]	1618 GWh/year	1423 GWh/year	1440 GWh/year

Tab.4 Productivity of the three wind farms

Comparing the results with the different models it is possible to notice that the Jensen model presents around 2 % higher losses compared to the other model. The results of the Jensen method will be used as a reference for the future analysis, as it provides a conservative productivity value.

Starting from the results of the two models, the capacity factors were calculated as in the following eq.

$$\text{Capacity Factor} = \frac{\text{Equivalent hours at rated power}}{8760}$$

In the end, the value of the P50 was estimated by considering the electrical losses and the losses due to unavailability and exceptional weather events. The overall losses added to get the P50 value were 6.85% of the previously calculated net productivity.

Comparing the three plants, it is possible to see that the highest expected energy production comes from the plant in Sardinia, thanks to the higher average wind availability. The difference with the other plants is relevant, as it accounts for 200 GWh/year more than the others. The productivity of the other two plants is more similar, but the farm in Calabria suffers the highest value of losses between them all. Nonetheless, the wind farm in Calabria shows a higher expected energy generation than Sicily thanks to its good wind availability. However, the result for all the three plants might be considered satisfactory, as the values of the capacity factors are pretty high for wind farms in Italy. According to Wind Europe [1.4], the average offshore capacity factor in Italy is 35.9 % (achieved by the only operating plant in Taranto), while in northern Europe the values are way higher thanks to the abundance of wind resource in the North Sea, like in Denmark where the offshore capacity factor reaches 53.6 %.

Overall, the wind farm in Sicily might be considered as the worst, because of the lower generation and because of the challenge caused by its very high-water depth. Similarly, the wind farm located in Calabria presents medium level generation but challenging objectives for the water depth and the cable length. On the other hand, the plant located in Sardinia might be the most promising one, as it is expected to generate the largest amount of energy while being located in a site with more shallow water. Nonetheless, for this plant the challenge remains the long submarine cable to the land.

## 1.4.2 Calabria Wind data

In order to base the following analysis on energy storages on a “real” plant, the wind farm located in Calabria was chosen as a reference because of data availability and because of the critical grid congestions present in the region, as it will be explained in the next chapter.

Therefore, the windiness data of the location were further analyzed to determine a power duration curve for the turbines by using the software MATLAB. Starting from [1.21], the data about the windiness of three points at sea near the installation site were available. In particular, the average wind speed, the shape and the scale factors of the Weibull distribution and the frequency of the wind from each direction were available. The Weibull factors were then used to determine the probability density for wind velocity in each direction with the following equation:

$$D(v) = \frac{k}{s} \cdot \left(\frac{v}{s}\right)^{k-1} \cdot \left[-\left(\frac{v}{s}\right)^k\right]$$

Here,  $D(v)$  represents the probability density of registering a wind velocity  $v$  on the site,  $k$  represents the shape factor and  $s$  represents the scale factor. The shape factor is frequently dependent on the site, as it



depends on the irregularity of the wind. In this case, as the site is located at sea, the shape factor of the zone is close to 2, a typical value for coastal areas. The scale factor, instead, is mainly influenced by the average wind speed and is therefore an indicator of the windiness of the site. Among the probability distributions calculated, the ones from the directions with highest frequency have been reported in the following Fig.27 for all the three points. It can be seen as for each wind direction we have a different probability distribution, with more or less frequent high speed of the wind. It is possible to observe that for all the points the most frequent directions of the wind are from North, West-Northwest, South-South-West and West-South-West. The same directions can be observed from the plot in Fig.28 taken from [1.21] representing point 1 of Calabria.

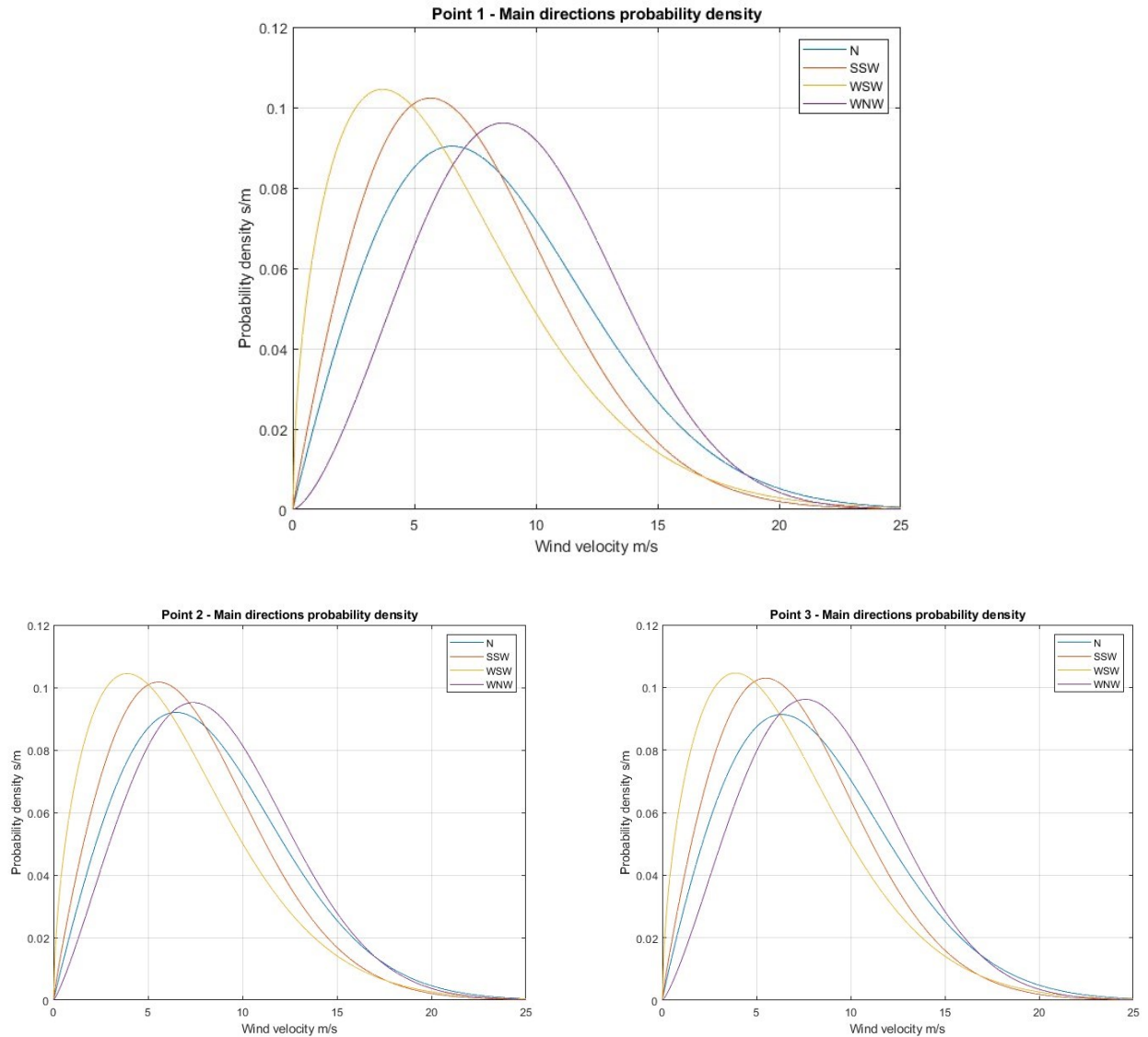


Fig.27 Weibull distributions for the most frequent wind directions in the Calabria site



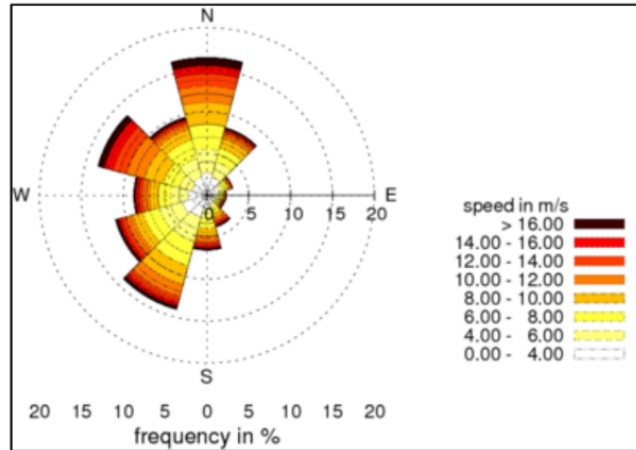
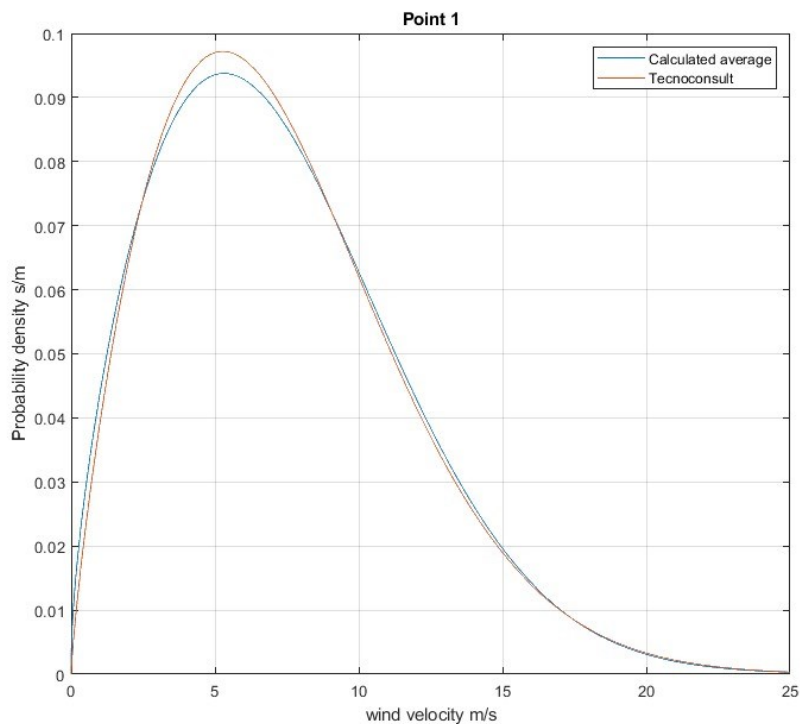


Fig.28 Distribution of wind direction frequency and intensity in the Calabria site

Given the Weibull distributions for each wind direction with its own frequency, a mean Weibull distribution for each point was calculated. The frequency of the direction of the wind was used as a weight for the probability distributions. The resulting mean distributions of the three points are shown in the following plots in Fig.29. On the same figures, it is also plotted the mean probability density calculated from the shape and scale factors reported by Tecnoconsult, the company responsible for the preliminary project of this plant.



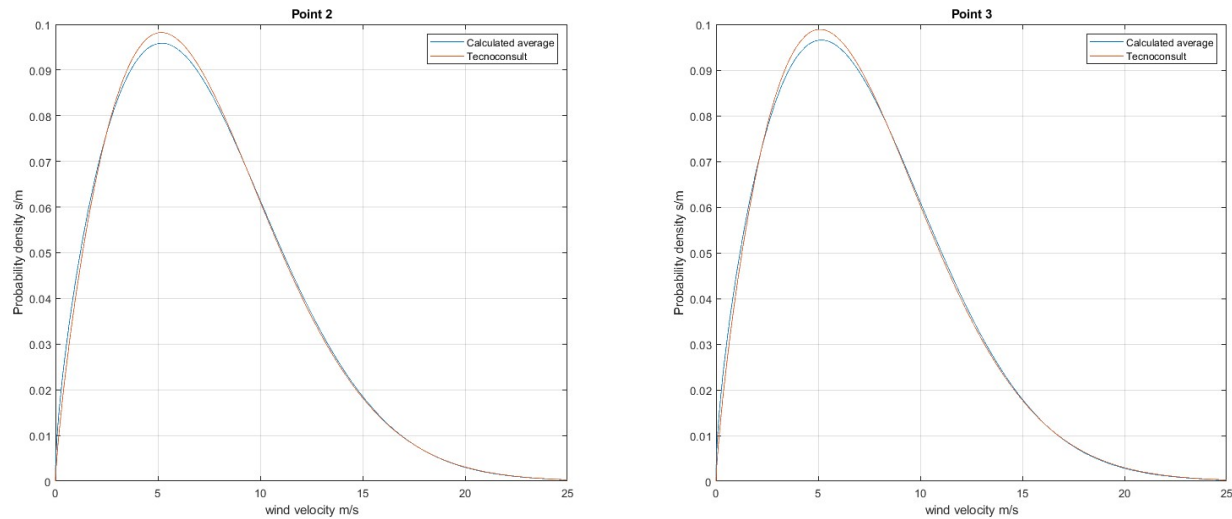


Fig.29 Average Weibull distributions representing the three examined points at sea.

It can be observed that the mean curves of all the three considered points are similar, confirming the regularity of the windiness of the zone. Slight differences are present between the calculated curves and the mean curves given in the project report [1.21]. In particular, the curves from the report show a higher wind probability of achieving a lower speed wind, close to the peak around the velocity of 5 m/s. Regarding higher wind speeds, a lower probability is predicted for velocities in the range from 8.5 to 16 m/s, while higher probability is expected for higher wind speeds. These difference, however, are not so relevant as it will be explained in the following. The probability distributions of the three points were then combined averaging them in a single Weibull distribution representing the windiness of the whole site. This site probability distribution is reported in the following Fig.30 including the curve calculated from all the directions distributions and the curve calculated from the mean curves presented by the company. Once again, slight differences similar to the previous ones can be observed.

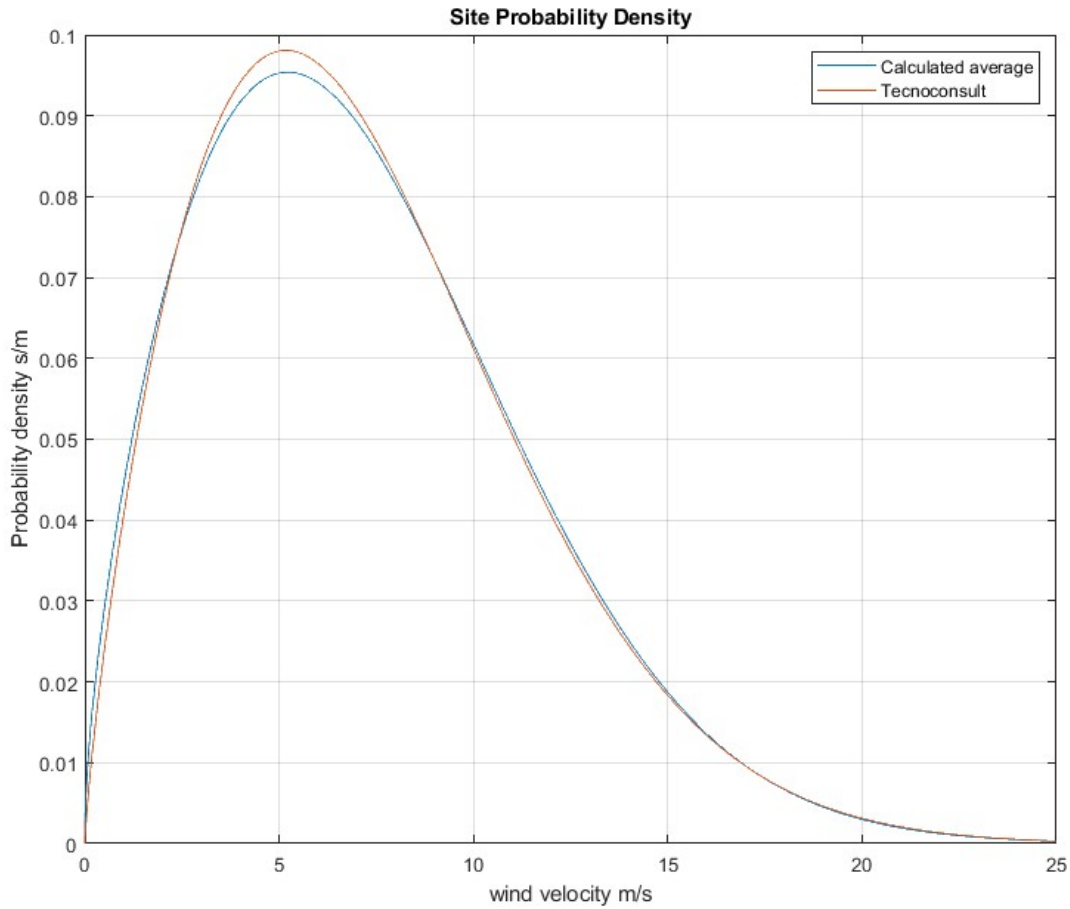


Fig.30 Average Weibull distributions representative for the site

### 1.4.3 Energy Yield estimation & Turbine Power curve

Given the probability of occurrence of the wind velocities, it was needed the calculation of the amount of time over a year during which each windiness condition occurs. Therefore, a curve for the specific hours of occurrence per wind velocity was calculated by using the following equation:

$$D(v) \cdot dv = \frac{dt}{\Delta t_{tot}}$$

Here,  $D(v)$  represents the curve of probability density previously calculated for the site,  $dv$  represents the path between the considered velocities and  $\Delta t_{tot}$  represents the total period of time considered. Therefore, the hours of occurrence for each velocity were calculated as:

$$dt = D(v) \cdot dv \cdot \Delta t_{tot}$$

The calculation was made for a year, therefore considering  $\Delta t_{tot} = 8760$  and with two possible spacings between velocities. In both cases the wind velocities considered were between 0 m/s and 30 m/s, as in this range it is included the turbine operation range. The spacings between velocities considered were of

0.1 in the first case and 0.01 m/s size in the second case. The resulting curves are reported in the following Fig.31.

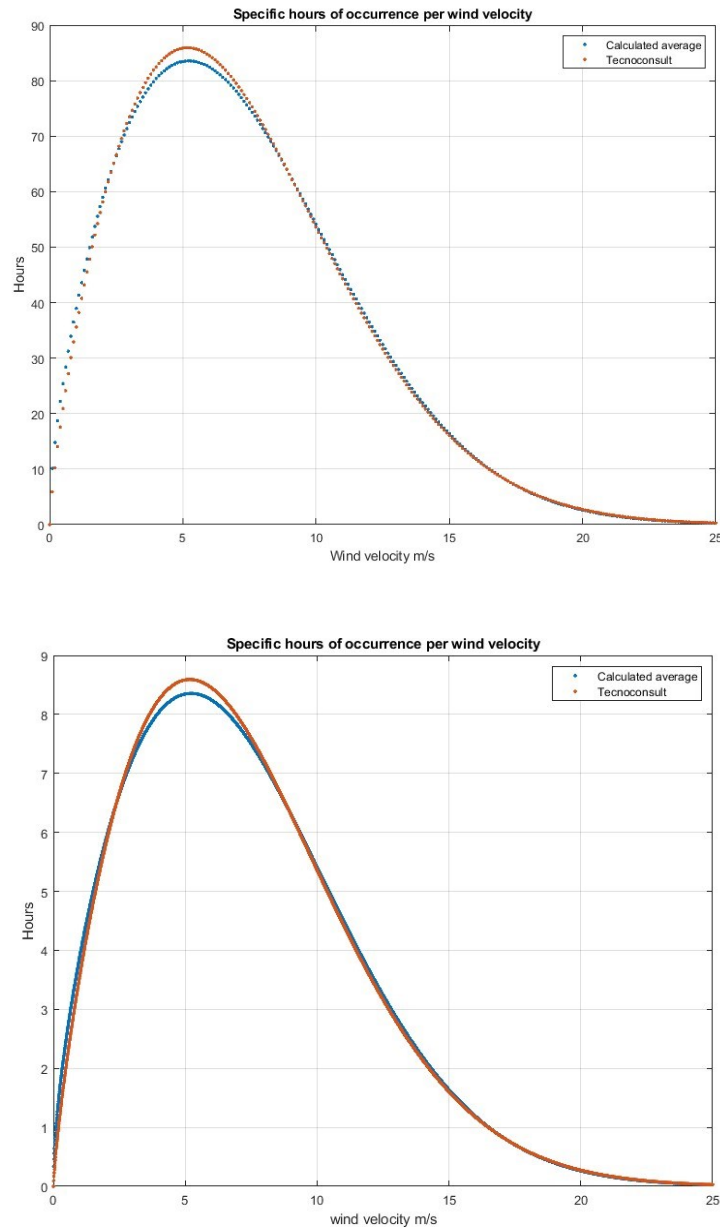


Fig.31 Plots of the specific hours of wind occurrence – (plot 1  $dv = 0.1$ ) – (plot 2  $dv = 0.01$ )

From the first plot it is possible to distinguish the singular spots, while in the second plot they cannot be distinguished because of the lower spacing. The values on the y axis represent the number of hours in which the velocities reported on the x axis are expected to be registered. The difference in the spacing affects the values on the y axis by a factor 10, but the curves represent the same concept.

In order to add the power duration curve, it was necessary to elaborate the turbine power curve previously reported in Fig.23 and used by Tecnococonsult in the preliminary project. In particular, the previous plot of the curve was done with discontinuous data with spacing 1 m/s between wind velocities. Therefore,

in order to allow the power calculation with more precision, the section between cut-in and rated power was interpolated through a spline function. In the following Fig.32, the blue dots represent the data taken from the report [1.21], while the red line represents the function interpolating the power curve between 3 and 11 m/s velocities. Then, after 11 m/s and up to 30 m/s the curve was constant and the power was equal to the turbine rated power, so the curve didn't need to be interpolated up to the cut-off point.

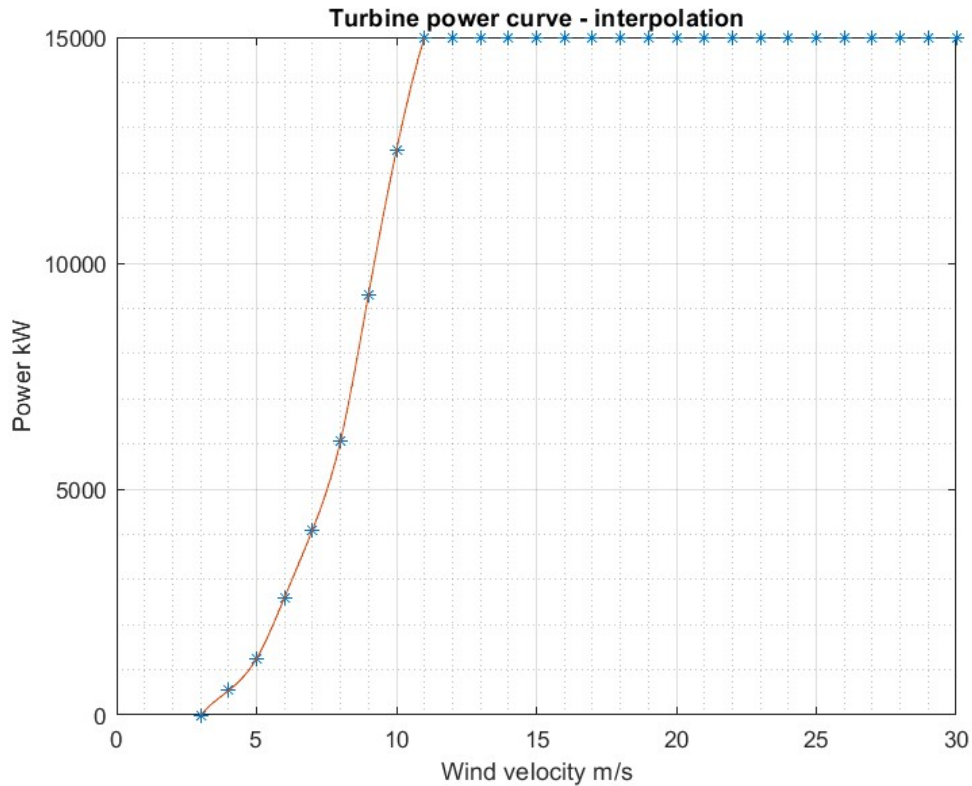


Fig.32 Interpolation of the turbine power curve data

The resulting final curve in Fig.33 was then represented point by point considering a velocity spacing of 0.01 m/s.

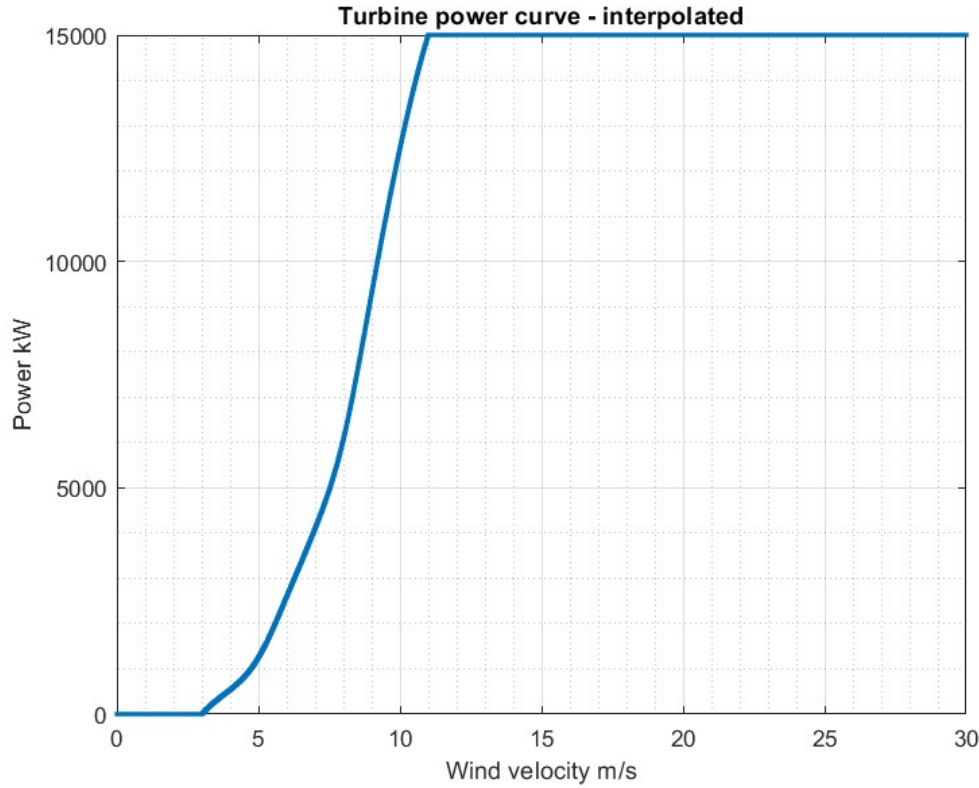


Fig.33 Final 15 MW turbine power curve

After this, the turbine power curve was used to calculate the expected energy generation over a year. This calculation was done by using the power curve and the probability density function of the wind through the following equation:

$$E = \Delta t_{tot} \int_{v_{in}}^{v_{off}} P(v) \cdot D(v) \cdot dv$$

Once again, as a whole year was considered  $\Delta t_{tot} = 8760 \text{ hours}$ . To make this calculation, first the product between the power curve and the velocity density probability was calculated and plotted. The result of  $P(v) \cdot D(v)$  can be seen in the plot Fig.34. From the plot it can be seen that the turbine should start generating power for velocities larger than 3 m/s and that the product increases up to around 10.5 m/s. Then, because of the decreasing probability and of the upper limit of the power curve (after 11 m/s), the product decreases rapidly.

The expected energy generation was calculated considering  $dv = 0.01 \text{ m/s}$  for both the curves: one considering the  $D(v)$  calculated and one with the  $D(v)$  elaborated from the company report. The results obtained are the following:

$$E_{calc} = 51.5541 \text{ GWh/year}$$

$$E_{Tecniconsult} = 51.2648 \text{ GWh/year}$$

As it can be seen, the overall difference between the two is of around 289 MWh, which is an error in the order of 0.5%. These energy yield results were referred to a single turbine subject to undisturbed wind at

150 m height from the sea level (hub height). The results could be considered to be confirmed as the report [1.21] estimated a gross yield between 51.2 and 51.3 GWh/year for the turbines in the first row.

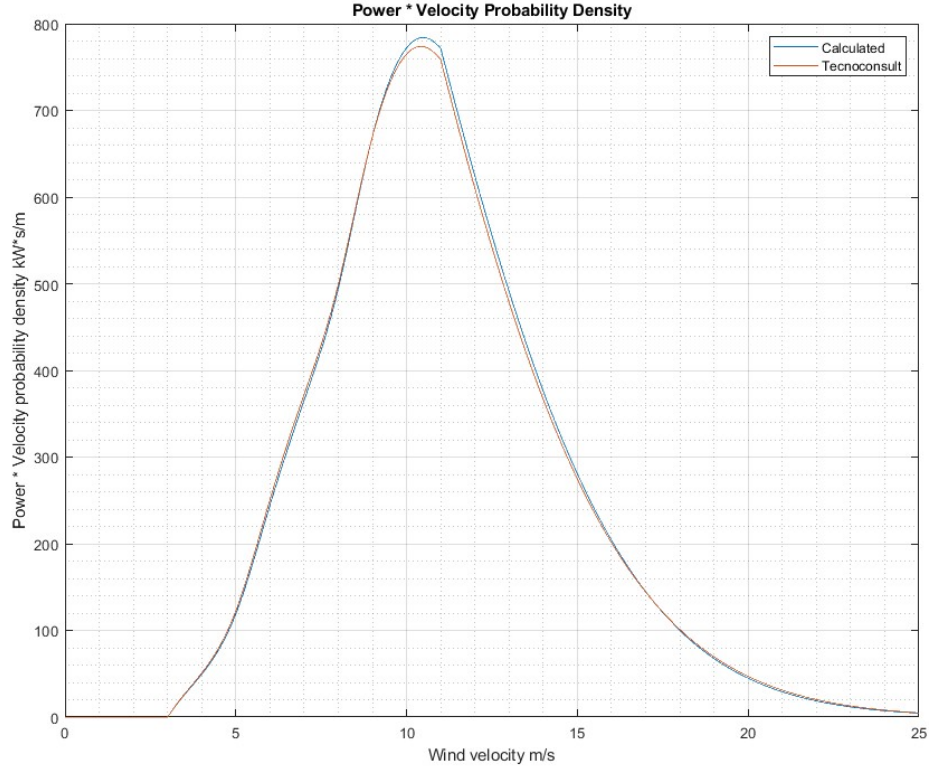


Fig.34  $D(v) \cdot P(v)$  curves

Given the turbine power curve, which links the output power with the wind speed, and the specific hours of occurrence per wind velocity, which links the hours “of operation” and the wind velocity, it was built the power duration curve. In order to do this, the hours of operation for each power level of the turbine were calculated as integral of the “specific hours of wind occurrence” curve between the corresponding velocity and the cut-off velocity.

$$T_{operation\ P} = \int_{v_p}^{v_{off}} dt = \int_{v_p}^{v_{off}} D(v) \cdot dv \cdot \Delta t_{tot}$$

The resulting ideal power duration curve is reported in [Fig.35](#). Here, “ideal” means that the turbine wake losses were not yet considered.

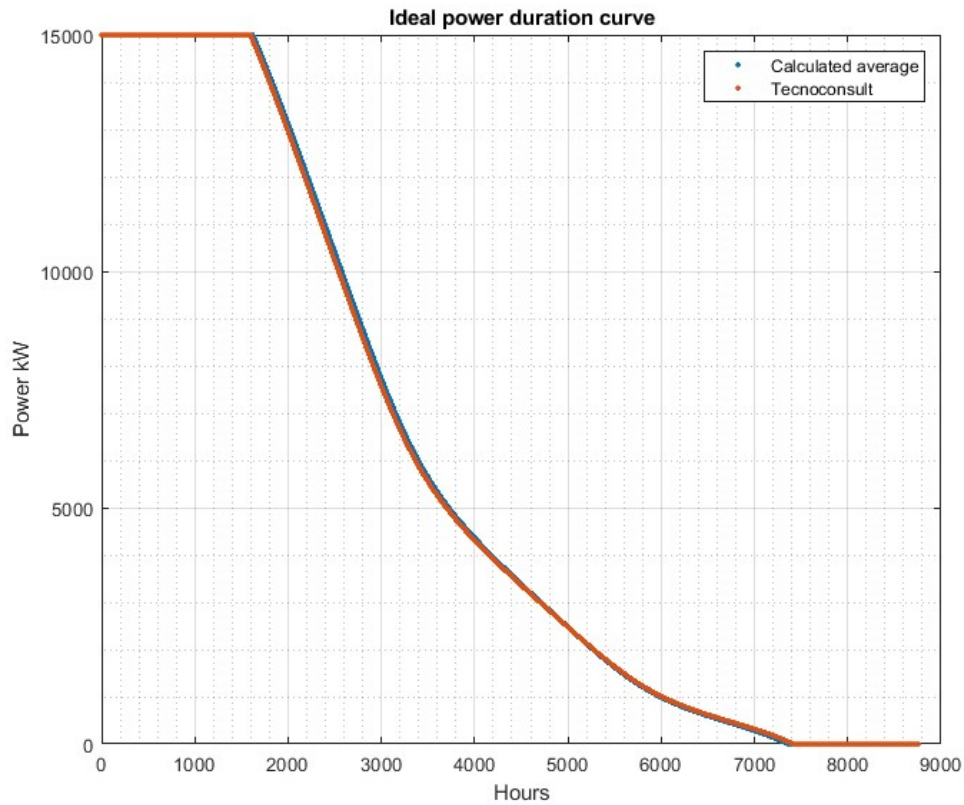


Fig.35 Ideal power duration curves

According to the calculated ideal curve, the plant should be in operation for around 7354 hours/year, while according to the data from Tecnococonsult the operation time should be of 7414 hours/year. This difference is due to the larger probability of getting low wind speeds in the data by the company. Regarding the rated power, the plant should be able to achieve it for 1620 hours according to the calculated curve, while for 1596 hours according to the company's data. However, this ideal curve did not include the wake losses and the other losses that led to the P50 calculation.

#### 1.4.4 Wind Profile scaling

In order to analyze the problem with a deterministic approach rather than a probabilistic one, a yearly wind availability profile was needed. In particular, this degree of detail was needed for the following study on the energy storage use, which needed to determine when the wind power was available or not. Given the unavailability of measurements on site, a yearly wind profile for an onshore plant from Repower was provided. The data refer to measurements made at a height of 10 meters from the ground and they report values with 1-hour timestep. The plot of the yearly profile is here represented in [Fig.36](#) together with a representation of the probability density based on the number of occurrences of each wind velocity in [Fig.37](#). Of course, the windiness of this site does not well represent the conditions that can be found on offshore sites, but it provides a realistic trend of the wind that can be registered during a year. Therefore, these data were considered to be later scaled and to simulate the offshore wind conditions.



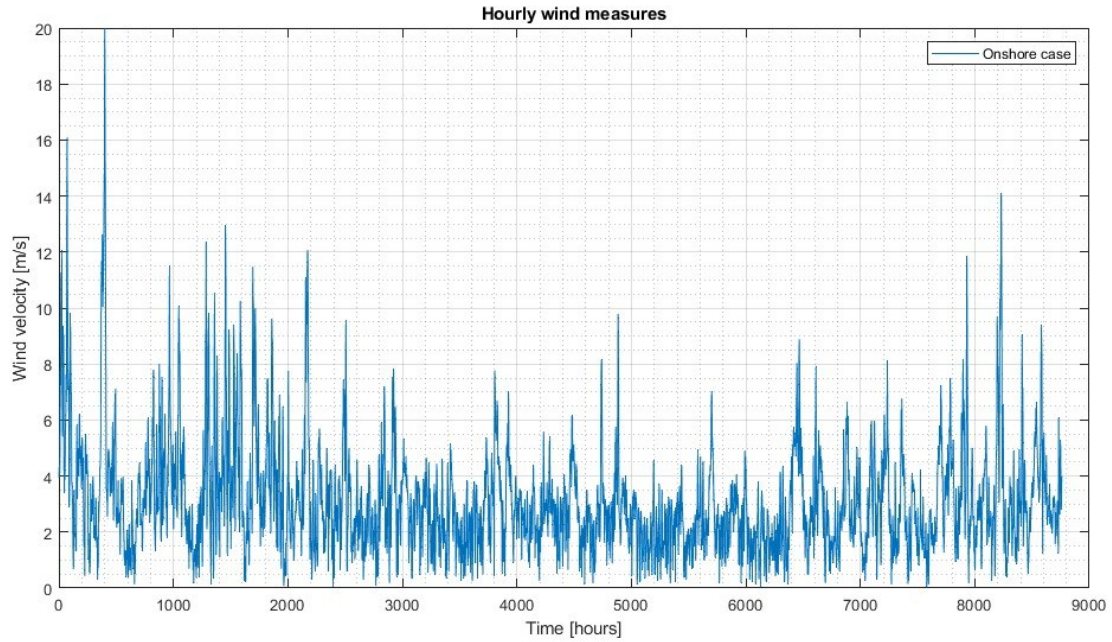


Fig.36 Onshore Wind profile

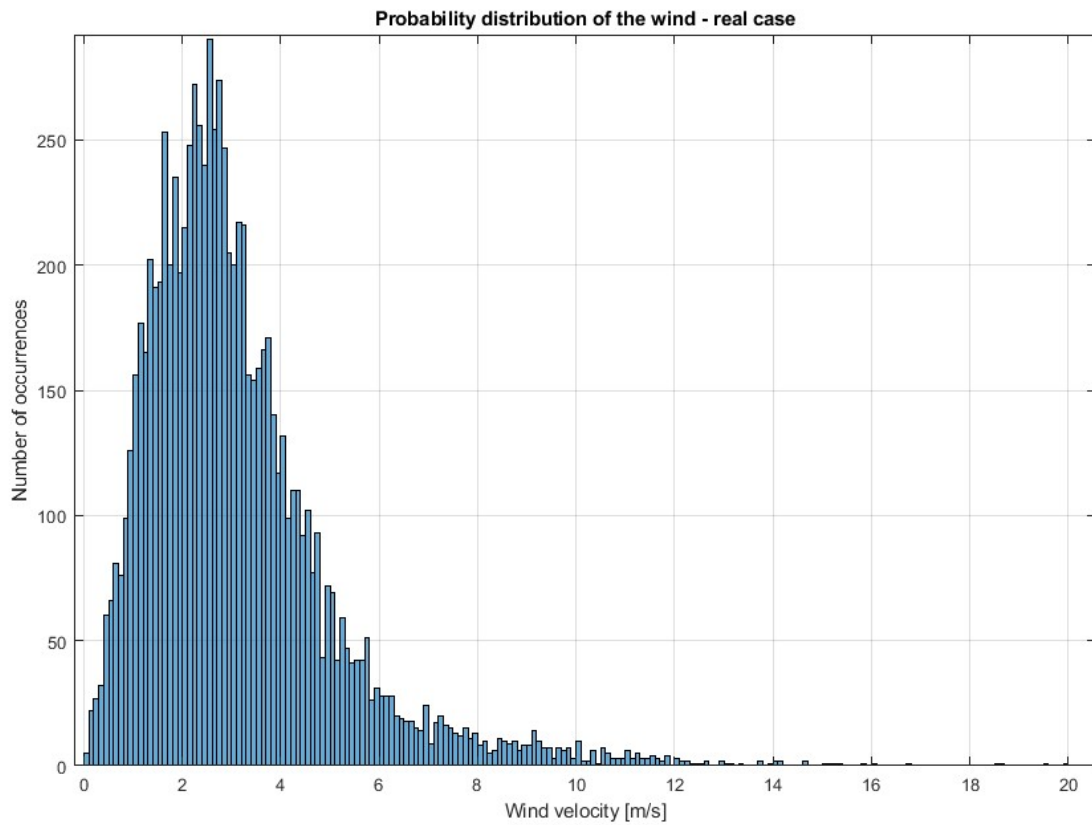


Fig.37 Histogram of Onshore Wind distribution

At first, given the onshore data, the scaled wind profile was obtained through the average of the wind speed. In particular, an objective average wind speed of 7.32 m/s was taken from the point 2 data of wind probability from the report [1.21]. Then, a scale factor was calculated as the ratio between the objective average wind speed (related to the offshore site) and the onshore average wind speed.

$$Scale\ factor = \frac{\overline{v_{offshore}}}{\overline{v_{onshore}}} = 2.35$$

Each value of the onshore wind profile was then multiplied by the scale factor to obtain a new wind profile that could approximate realistic conditions for the offshore site. The new profile had an average wind speed corresponding to the objective and its plot is represented in the following Fig.38 to be compared with the previous profile.

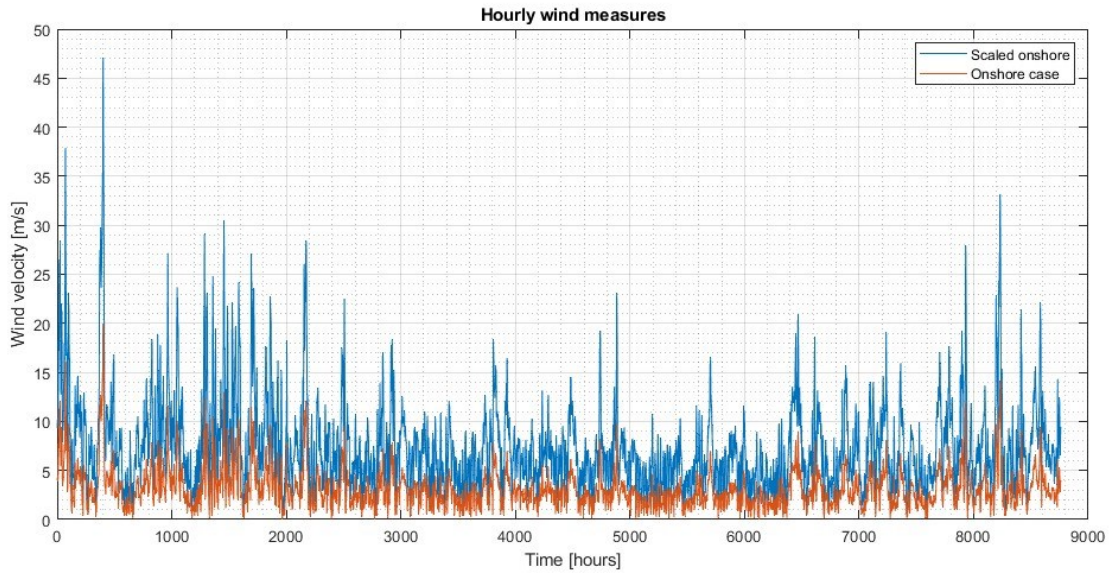


Fig.38 MEAN-Scaled and Onshore wind profiles.

Additionally, the comparison of the probability density between the two profiles is shown as a histogram in Fig.39, where the occurrences of each wind velocity are counted. It is possible to see how scaling the wind data, the frequency of low wind speeds decreased while medium and high velocity wind speeds increased their frequency. On the base of the raw data, it was possible to calculate the shape and scale parameter of the Weibull distributions through the MATLAB function “wblfit” and then plot the probability distribution functions to compare them as in Fig.40. The comparison of the Weibull distributions shows the change from the original data of the “onshore case” to the “scaled onshore” case, that is pretty close to the “offshore” distribution reported from the report regarding the wind farm productivity [1.21]. However, this scaled profile provided a gross energy generation of 1500 GWh over a year, a value significantly different from the 1682 GWh expected. Here, the gross energy yield was calculated considering the power generation of 33 turbines with the previously interpolated turbine power curve and with the wind profile.

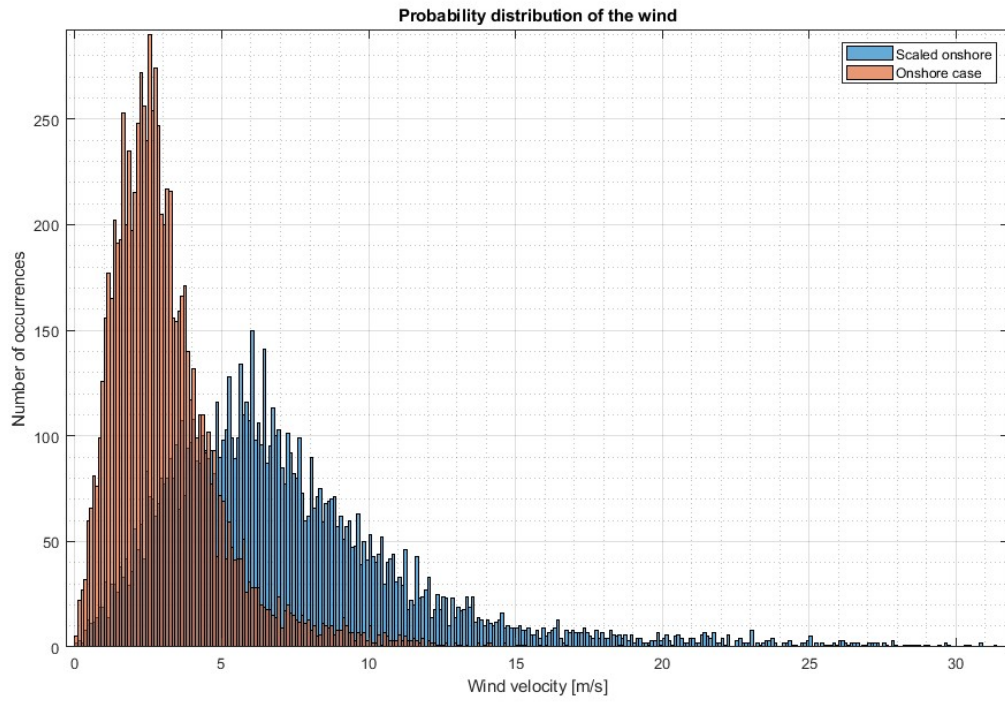


Fig.39 Histogram of Onshore and MEAN-Scaled wind probability distribution.

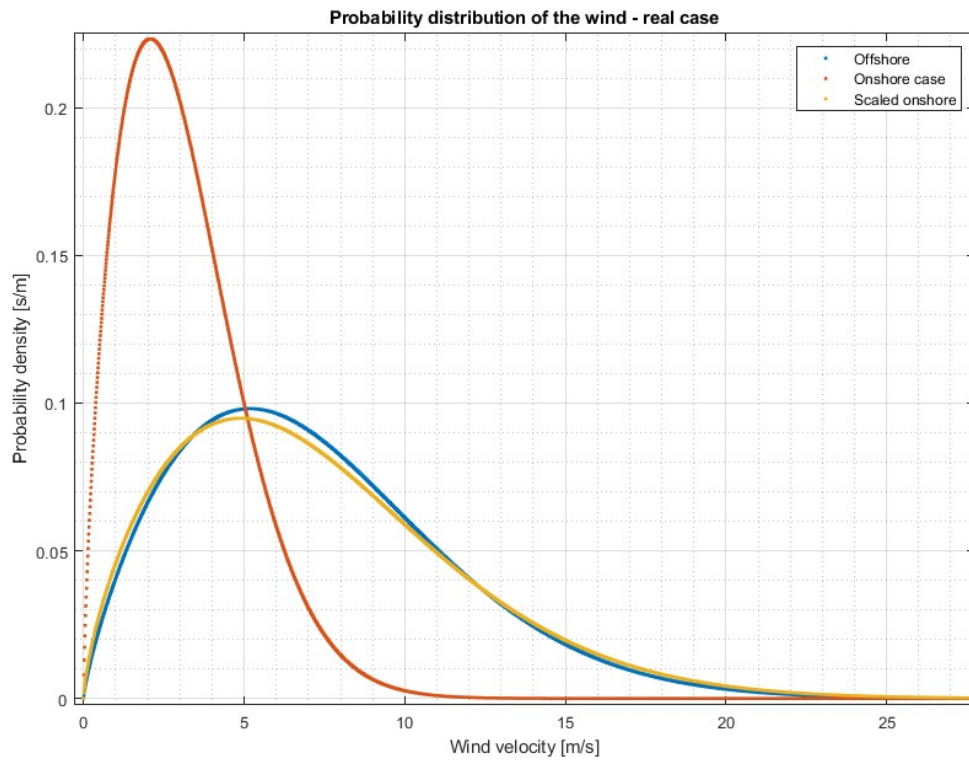


Fig.40 Comparison of the Weibull probability distributions with MEAN-scaled profile

From the plot in Fig.41, it is possible to see how the gross energy yield was expected to be 1682 GWh/year, in accordance with the report. This plot was made by using random wind profiles generated by the Weibull curve given in the report [1.21] representing the offshore wind availability.

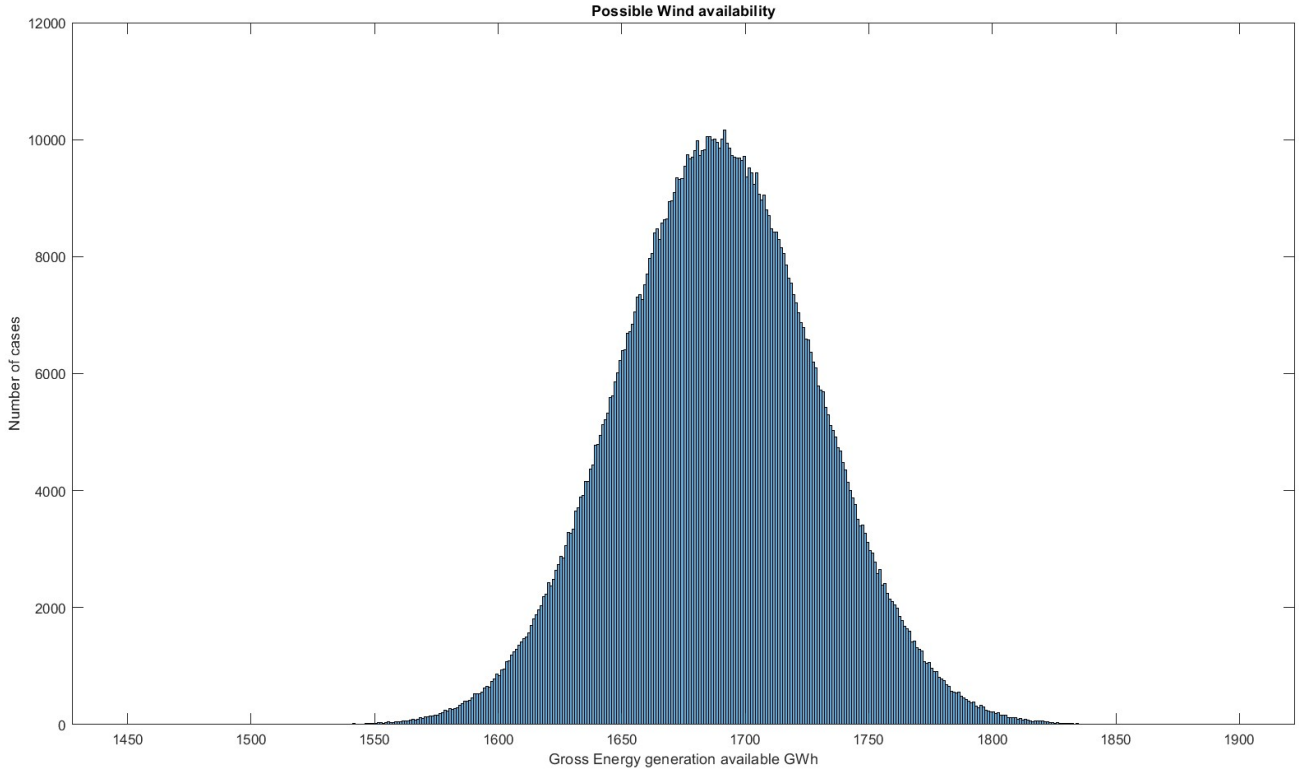


Fig.41 Probability distribution of yearly gross energy yield based on offshore Weibull curve

Therefore, to better fit the gross energy yield, a new scaled profile was generated by scaling through the median wind speed. The objective median speed was set to 6.6573 m/s, a value that was calculated through the following equation:

$$\widehat{v_{offshore}} = s_{offshore} \cdot \log(2)^{\frac{1}{k_{offshore}}} = 6.6573 \text{ m/s}$$

Here,  $k_{offshore}$  and  $s_{offshore}$  represent the shape and scale factors of the offshore Weibull distribution.

$$Scale \ factor = \frac{\widehat{v_{offshore}}}{\widehat{v_{onshore}}} = 2.4566$$

The scale factor was higher compared to the previous case with the mean wind speed. Once again, each wind speed value from the original wind speed profile was multiplied by the scale factor to obtain a new scaled wind profile. In Fig.42 it is reported the Weibull probability density distribution of the wind profile scaled on the median speed, as calculated by the MATLAB function “wblfit”. Nonetheless, even in this case, the gross energy yield resulted to be not suitable, as it was of 1608.7 GWh. In fact, this would have caused an underestimation as for the mean-scaled profile.

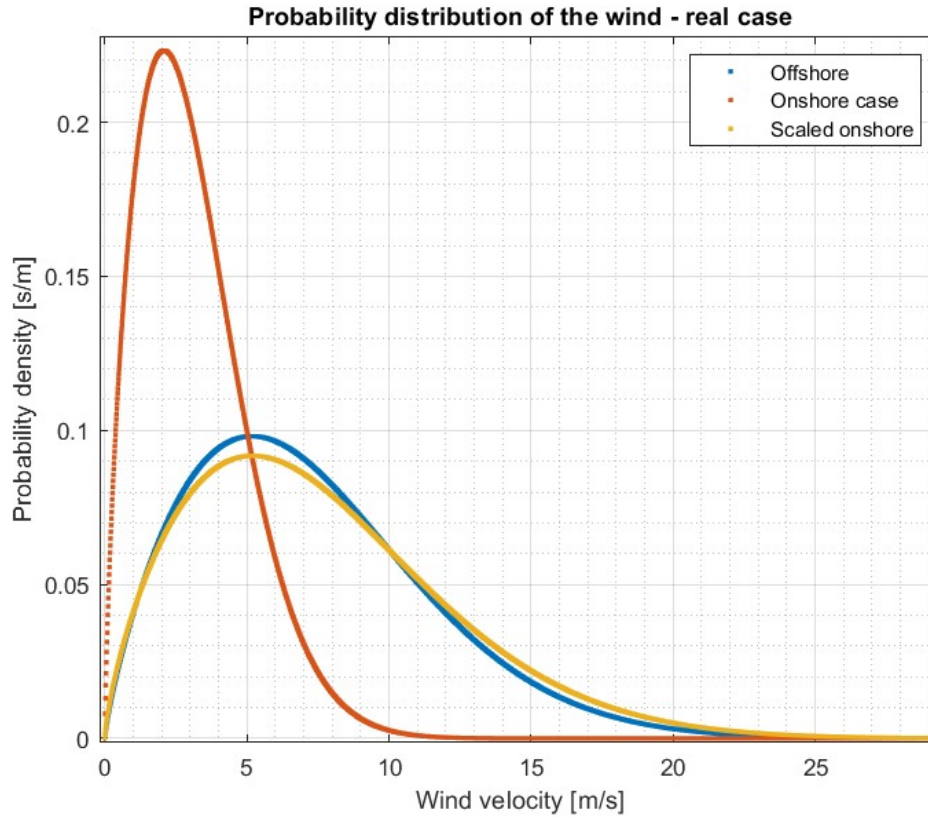


Fig.42 Comparison of the Weibull probability distributions with MEDIAN-scaled profile

The Weibull distribution of the new scaled profile was still similar in shape to the reference offshore curve, but it presented higher probabilities for high wind speeds and lower probabilities in the peak zone. Therefore, in order to match the expected gross yearly yield, the onshore wind profile was scaled with a customized scale factor of 2.5299. In addition, considering that with this scale factor some wind speed values would have reached over 50 m/s (which represent extreme weather conditions), the scale factor was selectively reduced to 1.8 for onshore wind speeds larger than 14 m/s. This allowed to achieve exactly a gross energy yield of 1682 GWh while keeping reasonable wind speed values. The custom scaled profile is shown in the following [Fig.43](#) and compared to the original wind profile for the whole year. As it can be seen, the selective reduction of the scale factor allowed to achieve maximum wind speeds of around 37 m/s. Then, the new histogram of occurrences is plotted to show the change in distribution of the wind speed values in [Fig.44](#). In the end, the Weibull distribution of the new Gross Yield-scaled wind profile was once again calculated through the MATLAB function “wblfit”. The new Weibull probability density curve was then compared to the offshore reference one with the [Fig.45](#) plot. This last plot shows once again a probability density increasing for high velocities and decreasing for medium/low velocities. Even if Weibull distributions are not identical, the new profile was considered to be suitable as it provided the desired gross energy yield for a year.



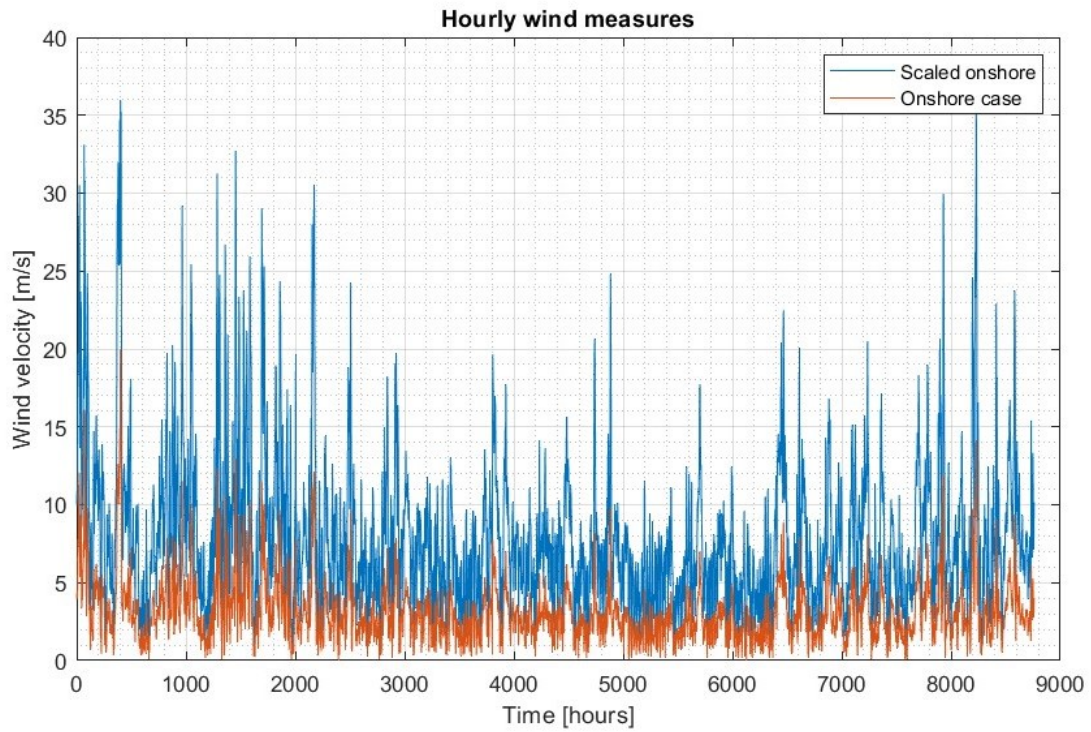


Fig.43 Gross Yield - Scaled and Onshore wind profiles

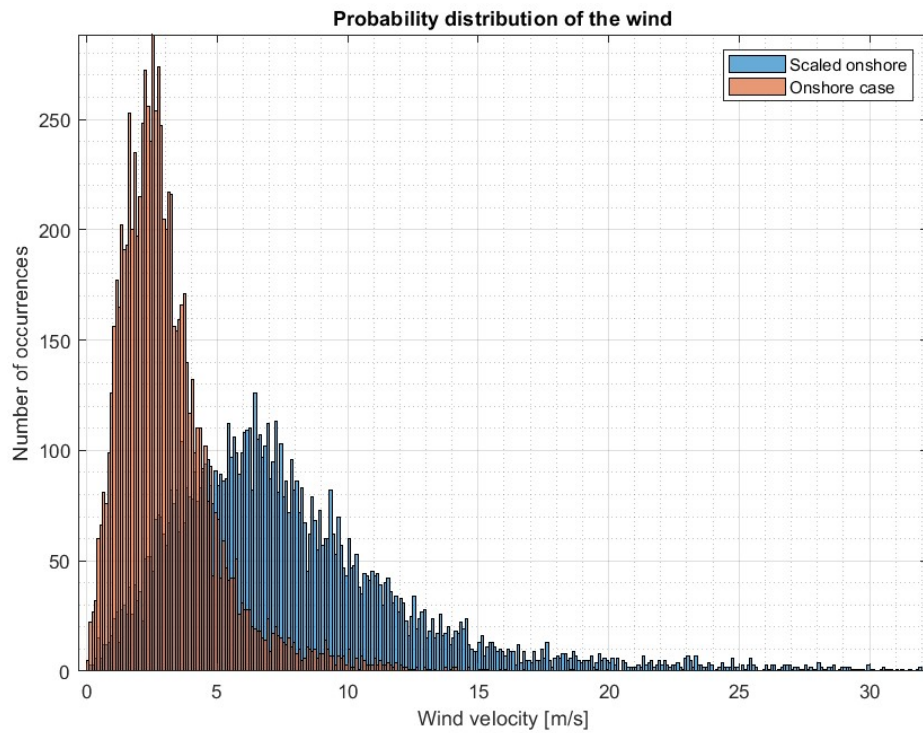


Fig.44 Histogram of Onshore and Gross Yield-Scaled wind probability distribution

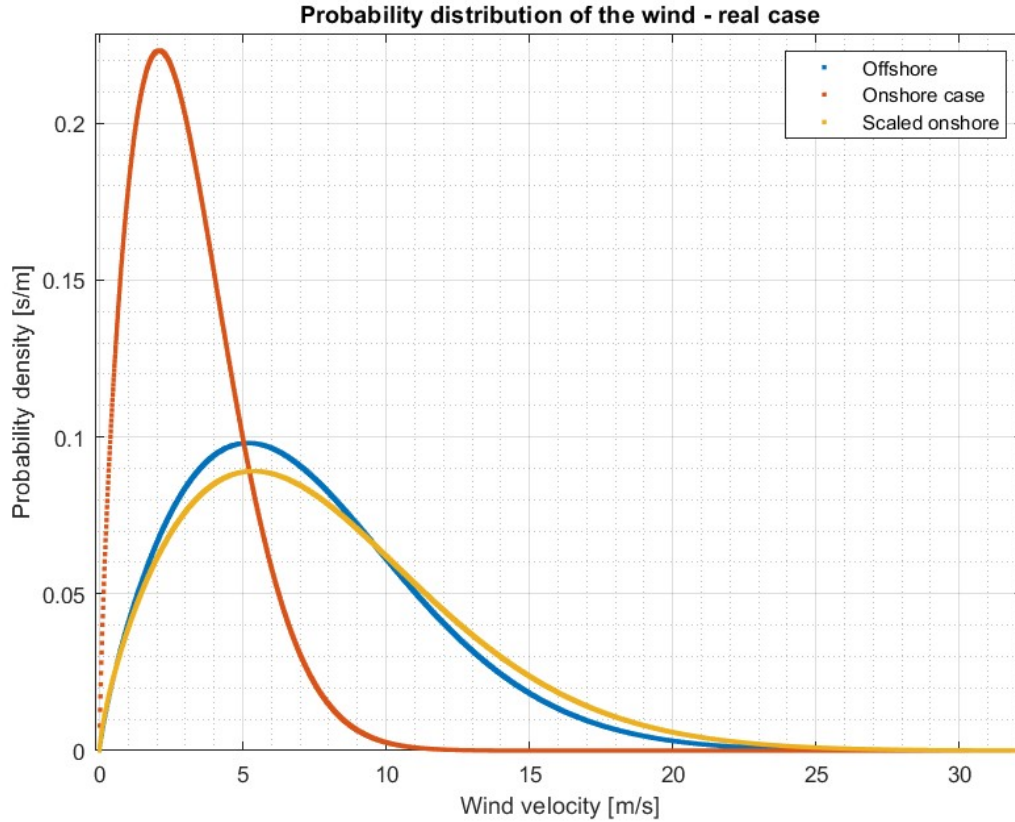


Fig.45 Comparison of the Weibull probability distributions with Gross Yield-scaled profile

Given the selected Gross Yield-scaled wind profile, in order to use it to estimate a profile of power generation of the offshore wind farm, the wake losses were introduced at the wind profile level. According to the report [1.21], it was also necessary to consider the electrical losses of the generator, the blade degradation losses and the unavailability losses. These losses could be difficultly added to an hourly model of a yearly profile. According to the report, the Jensen wake losses reduced by 8.1% the energy yield, while the other losses reduced it by another 6.85%. Here, the Jensen wake losses were considered instead of the Larsen ones as they were more suitable for project bankability estimation. In order to include this kind of losses in the wind power generation profile, it was decided to assume a wind velocity reduction that would correspond to the energy reduction caused by these losses. In particular, the wind profile was once again scaled, with a 9.38 % speed reduction. This speed reduction allowed to achieve the expected P50 value of 1440 GWh/year, as reported in the report. Of course, this represented a simplification, but it allowed to generate a realistic wind power profile coherent with the expected yearly generation. In Fig.46 it is reported a particular of the scaled wind profile compared to the one including the wake and P50 losses, so that it is possible to see the wind speed reduction applied. In the following, this wind profile will be addressed as P50 wind profile, as it provides the P50 values as energy yield.

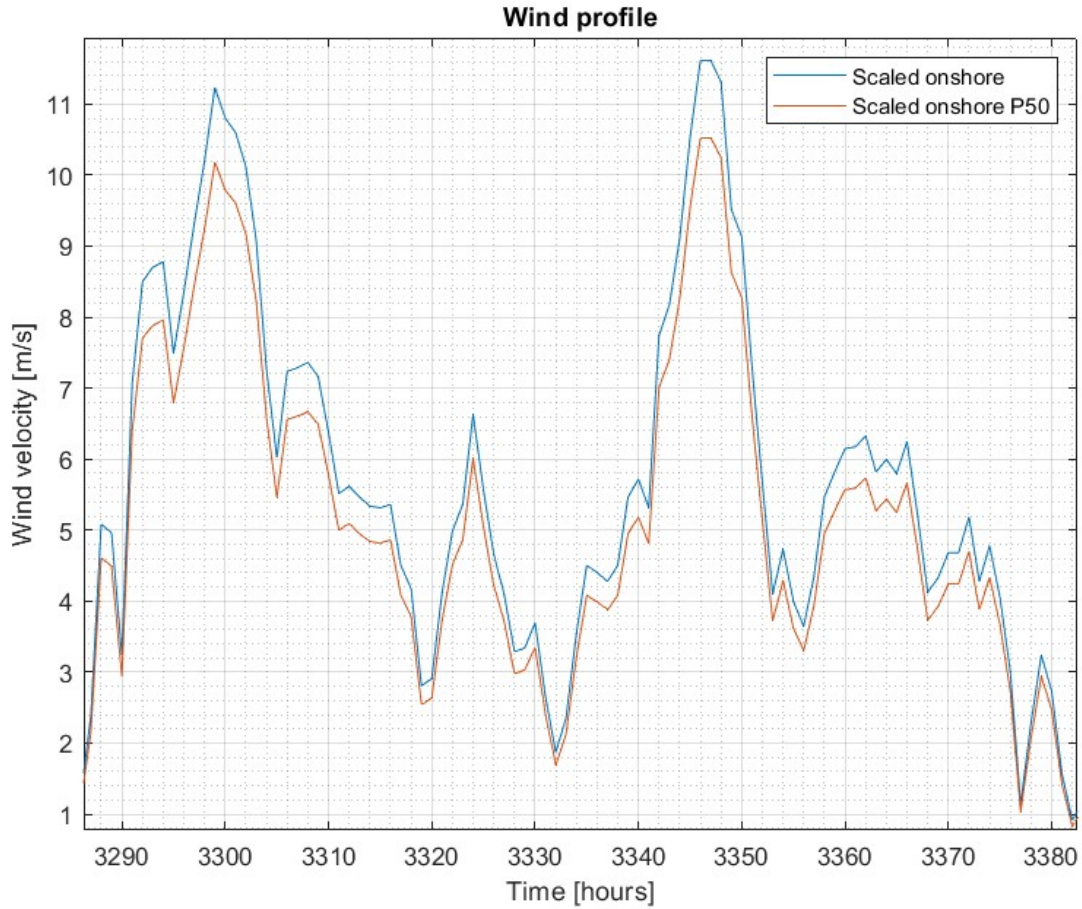


Fig.46 Scaled and P50 wind profiles compared.

After the generation of the P50 wind profile, the data were discretized. This was made because the grid power data by Terna were given every 15 minutes while the wind profile from the onshore plant was given with a timestep of an hour, and the wind power generation (calculated from this profile) would have been later compared to grid data. In particular, the intermediate points between the ones previously defined were calculated by subdividing the velocity difference between two hourly values in four equal portions, so as to consider a continuous constant variation of the wind speed. Of course, this represents an approximation, but nonetheless it is in accordance with the general trend of the wind profile, and it should provide small local errors that shouldn't affect the overall yearly performance of the wind farm simulation. In the following [Fig.47](#), it is shown a portion of the discretized P50 wind profile.



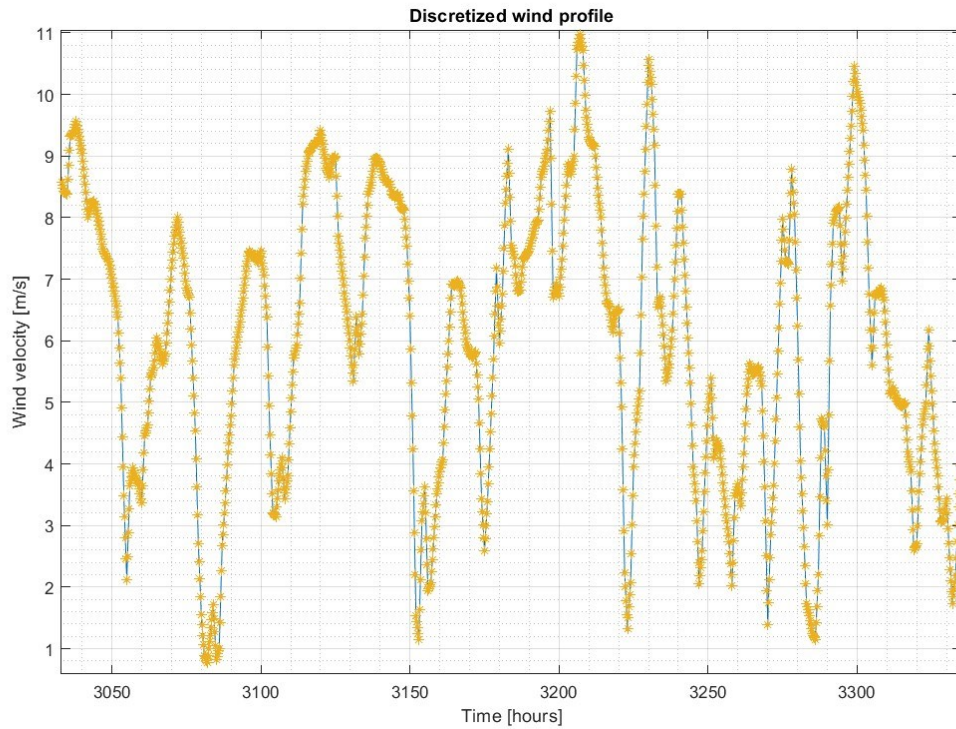


Fig.47 Portion of the discretized wind profile

### 1.4.5 Array power losses estimation

Given the wind availability and the previously calculated turbine power curve, it was necessary to evaluate the power losses to estimate a power profile to the land. First of all, the power losses due to the Joule losses in the array cables were considered. The scheme of the considered plant with the array connections is reported in [Fig.48](#).

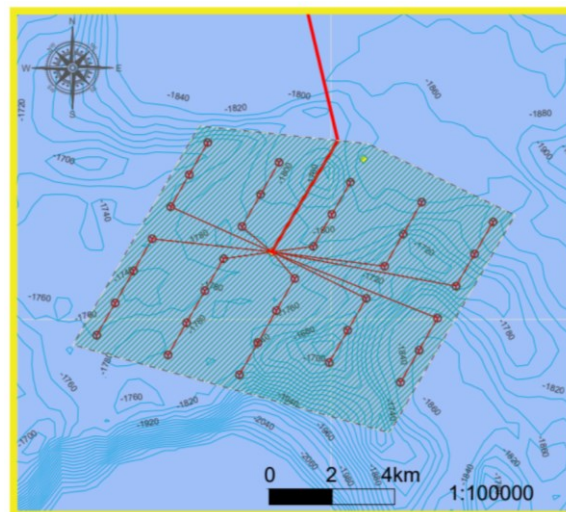


Fig.48 Offshore wind farm configuration

Considering the data available from [1.21], it was assumed to use increasing sections of the cable along the series of the turbines of each subfield. The sections were set by the company who developed the preliminary project of the plant, which decided to keep the tension drop below 2%. The table reporting the sections and the lengths considered is reported in Tab.5.

	WT1 -WT2	WT2 -WT3	WT3 -WT4 or Substation	WT4 - Substation
Cable section	95 mm <sup>2</sup>	185 mm <sup>2</sup>	240 mm <sup>2</sup>	500 mm <sup>2</sup>
Cable length Subfield 1	1200 m	1200 m	3550 m	-
Cable length Subfield 2	1200 m	1200 m	1250 m	-
Cable length Subfield 3	1200 m	1200 m	1350 m	-
Cable length Subfield 4	1200 m	1200 m	3650 m	-
Cable length Subfield 5	1200 m	1200 m	6000 m	-
Cable length Subfield 6	1200 m	1200 m	5700 m	-
Cable length Subfield 7	1200 m	1200 m	3400 m	-
Cable length Subfield 8	1200 m	1200 m	1200 m	1150 m
Cable length Subfield 9	1200 m	1200 m	1200 m	1150 m
Cable length Subfield 10	1200 m	1200 m	1200 m	3850 m

Tab.5 Inter-array cable sections and lengths

In order to evaluate these losses, a matrix containing the length of each cable was built. Based on the company values, a resistivity of 0.0276  $\Omega \cdot \text{mm}^2/\text{m}$  was used to calculate the kilometric resistance of the array cables:

$$r_{km} = \frac{0.0276 \frac{\Omega \cdot \text{mm}^2}{\text{m}} \cdot 1000}{S_{cable} \text{ mm}^2}$$

By using the matrix of lengths of the cables, a matrix of resistances was calculated, considering for each cable its specific section:

$$R_{cable} = r_{km} \cdot L_{cable}$$

After this, for each power generation condition determined by the wind, the current flowing through each cable was estimated supposing a  $\cos\varphi$  value of 0.9 and a tension of 66 kV.

$$I_{cable}(w) = \frac{P_{gen}(w) [W]}{\sqrt{3} \cdot V_{array} [V] \cdot \cos\varphi} [A]$$

Finally, the power loss of the array for each wind condition was calculated as the sum of the power losses in each cable subject to the corresponding current. Here,  $w$  represents the wind speed for which the power loss was calculated.

$$P_{loss array}(w) = \sum_1^{m \text{ cables}} 3 \cdot R_{cable} \cdot I_{cable}(w)^2 [W]$$

The resulting curve of power losses as function of the wind speed is reported in the following Fig.49. It can be observed that when nominal power is reached, the power loss in array cables would reach around 2.9 MW, while below nominal conditions the losses are lower thanks to the lower current.

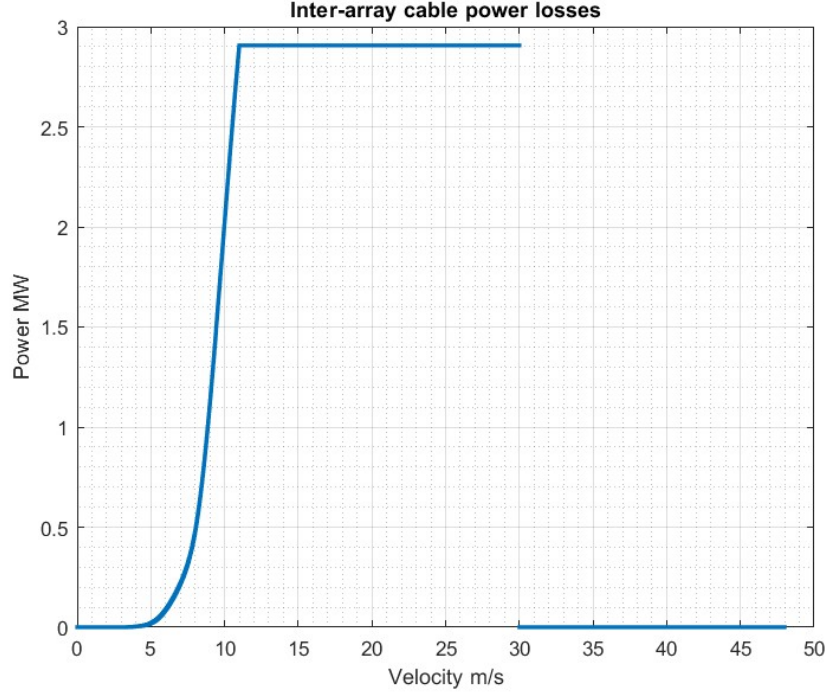


Fig.49 Array cable power losses as function of the wind speed

The resulting power curve to the substation was obtained by subtracting the inter-array power losses to the power generation of the wind farm for each wind velocity condition.

$$P_{in\ substation}(w) = P_{wind\ farm}(w) - P_{loss\ array}(w) [MW]$$

#### 1.4.6 Transformation losses estimation

After the array power losses, another important component to be considered was the electrical substation, where the tension is raised before the export trough the submarine cable. Here, the tension should be raised from 66 kV to the export cable voltage level. For this step it was considered an efficiency of  $\eta_{transformation} = 98\%$ , as usually these machines work with very few losses. Transformers for power transmission can reach efficiency levels higher than 99%, however it was assumed a lower efficiency level to consider also the power absorbed by the auxiliaries and to consider part of the cable losses caused by reactive power. The transformation losses in the turbine tower transformers were not considered separately, as they were included in the P50 calculation. The power to the submarine export cable was calculated by applying a constant value efficiency to every power level coming from the inter-array cables.

$$P_{out\ substation}(w) = \eta_{transformation} \cdot P_{in\ substation}(w) [MW]$$

### 1.4.7 Export cable power losses estimation

Regarding the export cable to the land, this element represents one of the critical points of the wind farm project. According to the preliminary project, it was expected to export energy through 380 kV AC submarine power cables. In particular, three unipolar cables should have been used (one for each phase), with a cable section of  $1000 \text{ mm}^2$  for each of them. However, the depths of installation made it impossible to use nowadays' 380 kV power cables. As explained previously in Chapter 1, 220 & 275 kV submarine cables should be available on the market by 2024 for this kind of applications. This time horizon was considered to be coherent with the approval and construction time of a new offshore wind farm, and therefore it was supposed to adopt the 275 kV cable type for the simulation. DC solutions were not considered because of the low technology readiness for floating offshore applications.

The company then proposed the use of two tripolar submarine cables. Each cable should be able to sustain the whole output of the wind farm for redundancy, so as to avoid losing energy generation opportunities in case of faults on the transmission line. This is very important in offshore wind applications as the maintenance might be complex and require weeks of work. Long periods of stop would cause significant economic losses for the wind farm. Among the proposed solutions, there are tripolar cables with sections varying between  $1600 \text{ mm}^2$ ,  $2000 \text{ mm}^2$  and  $2500 \text{ mm}^2$ . All these sections should allow operation at full power in case of fault on one of the cables, considering Joule losses only. Economic optimization would be needed to correctly choose the cable size to be used, as larger cables imply higher costs but generally cause lower power transmission losses.

Another relevant issue in AC power transmission through submarine cables is given by the generation of reactive power [1.17]. In fact, transmission cables generate mainly capacitive reactive power, differently from overhead transmission lines. This is due to the proximity between the conductors and the external sheath, which causes high capacitance values. According to [1.20], capacitance values can be 20 to 60 times higher in cables compared to overhead lines. Conversely, inductance values are lower in cables, around 0.3 to 0.6 times the inductance of overhead lines.

High reactive power generation in long cables can cause reductions in the power transmission capacity. Therefore, reactive power compensation is needed to limit the effects of the high capacitance. Shunt reactors should be inserted to absorb capacitive reactive power. Once again, an optimization would be required to decide where to apply the reactors and how much compensation it would be needed. In general, it is supposed that compensation will be made at the beginning and at the end of the transmission cables, so on the floating substation and on the land. This optimization in the choice of the submarine cable was considered to be beyond the scope of the study, and therefore it was not analyzed. It was supposed to operate with two 275 kV cables with  $1600 \text{ mm}^2$  section, and with a  $\cos\varphi$  value of 0.98. The choice of the smallest section was made to partially overestimate the Joule power losses, as the other loss components were not considered. In practice, it is expected that the  $1600 \text{ mm}^2$  section will not be enough, and at least a  $2000 \text{ mm}^2$  section will be chosen.

As it was done for the array cable power losses, a copper resistivity of  $0.0276 \Omega \cdot \text{mm}^2/\text{m}$  was used. The total length of the cables, according to the preliminary project, was estimated to be 111.503 km. The kilometric resistance was calculated as in the previous case with the following equation:

$$r_{km} = \frac{0.0276 \frac{\Omega \cdot \text{mm}^2}{\text{m}} \cdot 1000 \text{ m}}{1600 \text{ mm}^2} = 1.72 \cdot 10^{-5} \frac{\Omega}{\text{km}}$$

Then, the total cable resistance was calculated.

$$R_{\text{export cable}} = r_{km} \cdot L_{\text{cable}}$$

The current flowing through the cables was calculated for each power level as:

$$I_{\text{export cable}}(w) = \frac{P_{\text{out substation}}(w) [W]}{n_{\text{cables}} \cdot \sqrt{3} \cdot V_{\text{export cable}} [V] \cdot \cos \varphi} [A] = \frac{P_{\text{out substation}}(w)}{2 \cdot \sqrt{3} \cdot 275000 \text{ V} \cdot 0.98}$$

It was supposed a normal operation condition, with both export cables operative. Then, for each power generation condition, the export current was used for the estimation of power losses.

$$P_{\text{loss export cable}}(w) = n_{\text{cables}} \cdot 3 \cdot R_{\text{export cable}} \cdot I_{\text{export cable}}(w)^2 [MW]$$

In the end, the power to the land was calculated by subtracting the export cable power losses to the power exiting from the substation for each wind velocity condition.

$$P_{\text{land}}(w) = P_{\text{out substation}}(w) - P_{\text{loss export cable}}(w) [MW]$$

In the following [Fig.50](#), it is plotted the final power curve of the wind farm that reports an estimation of the power that should reach the land for each wind velocity condition. In nominal operation conditions, around 479 MW should reach the land. This power curve represents the reference that was considered to transform the P50 wind profile into a wind power profile.

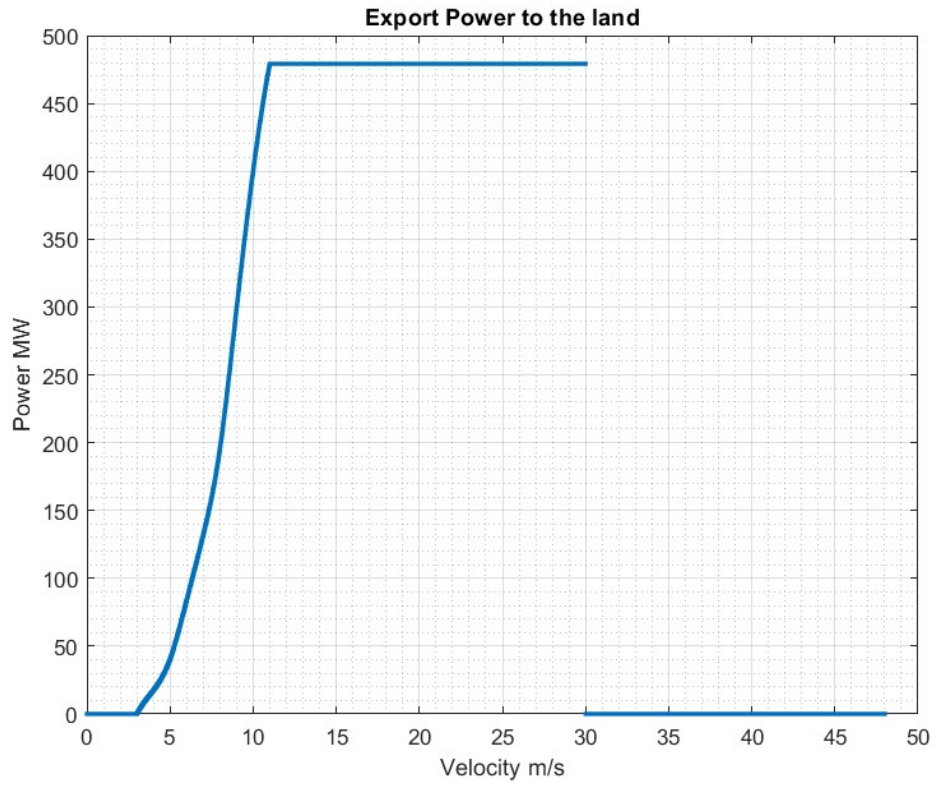


Fig.50 Estimation of the export power that should reach the land as function of the wind velocity.



### 1.4.8 Wind Power profile generation

By exploiting the calculated export power curve and the scaled P50 wind profile, a wind power profile was generated. In particular, each power value from the export power curve was substituted to the corresponding wind velocity that occurred in the previously calculated wind profile. The result was a yearly wind power profile defined with a timestep of 15 minutes. The plot of a portion of the result is shown in the following [Fig.51](#). This result represents one of the inputs of the simulations of the storage-wind farm coupling.

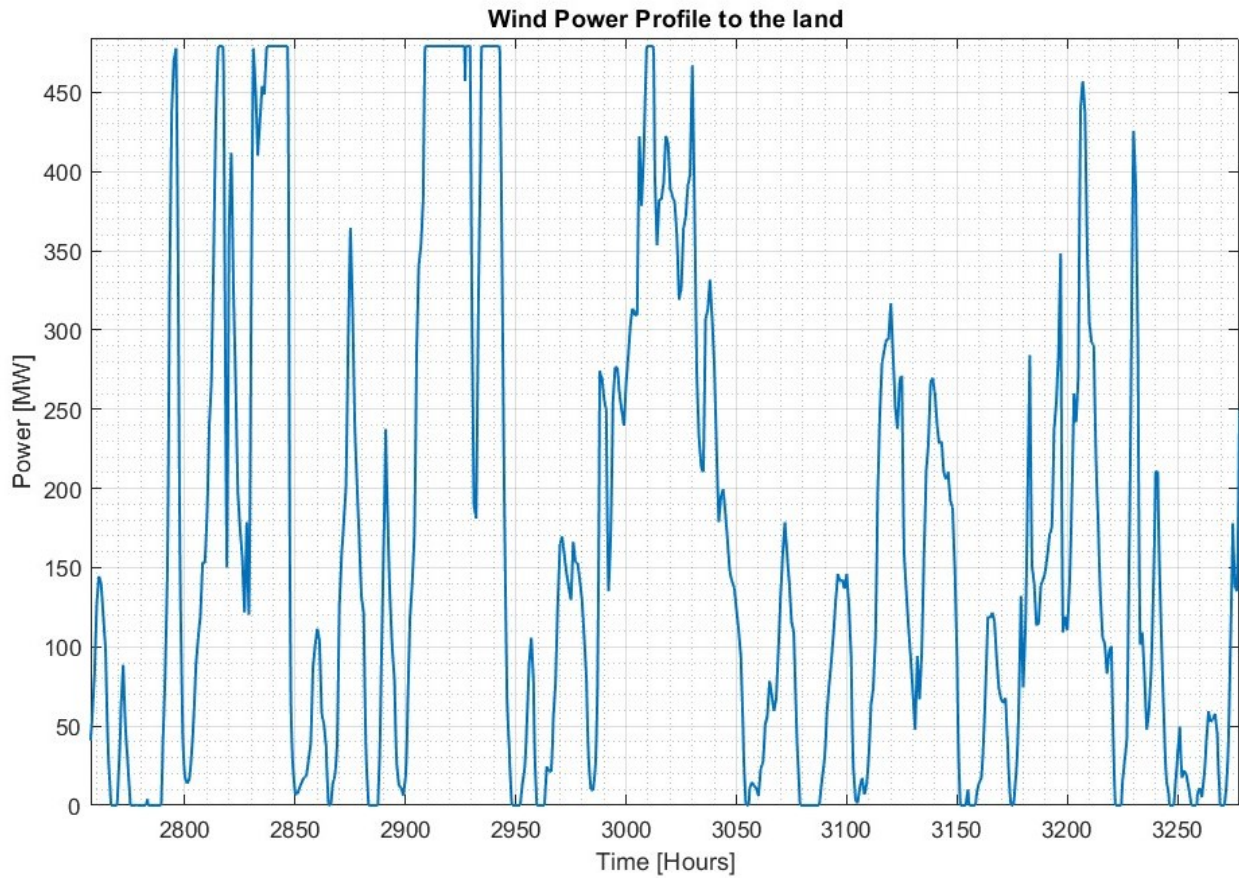


Fig.51 Portion of the generated yearly wind power profile





## 2 Grid Development and Electric Market

### 2.1 Transmission congestions

Due to the renewable intermittency and its local variability, the electricity transmission grid may undergo overload conditions, as the local production may exceed the local demand. In these cases, connections with different zones are fundamental to bring the energy where it is actually needed. However, these interconnection lines have a limited capacity, and when it is almost saturated by the excess production, we may have congestion phenomena. These conditions can be spotted both by looking at the data about zonal electricity demand and exchange [2.3] and at the local market prices [2.1]. Considering the location of the offshore wind farms, the zones of Sardinia, Sicily and Calabria are used as an example.

Terna, the Italian TSO (Transmission System Operator), provides public data about the electrical power load requested every 15 minutes from each region. Moreover, Terna provides also the power fluxes exchanged every hour between the internal zones (inside the Italian country) and external zones (foreign countries). Given the imports and the exports of energy through the links with other zones and countries, it is possible to get an estimation of the local (zonal) electric energy power generation.

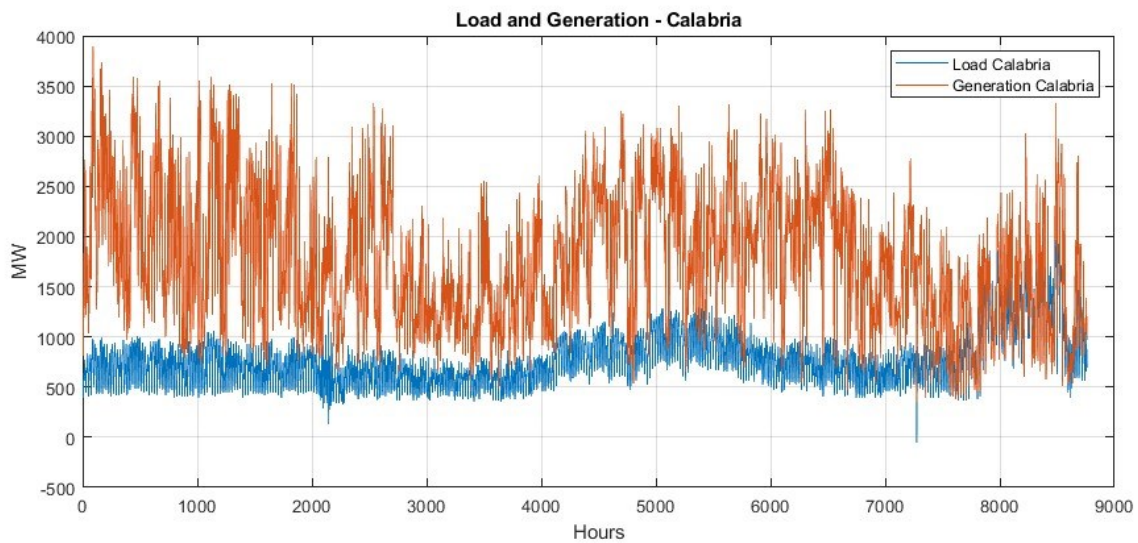
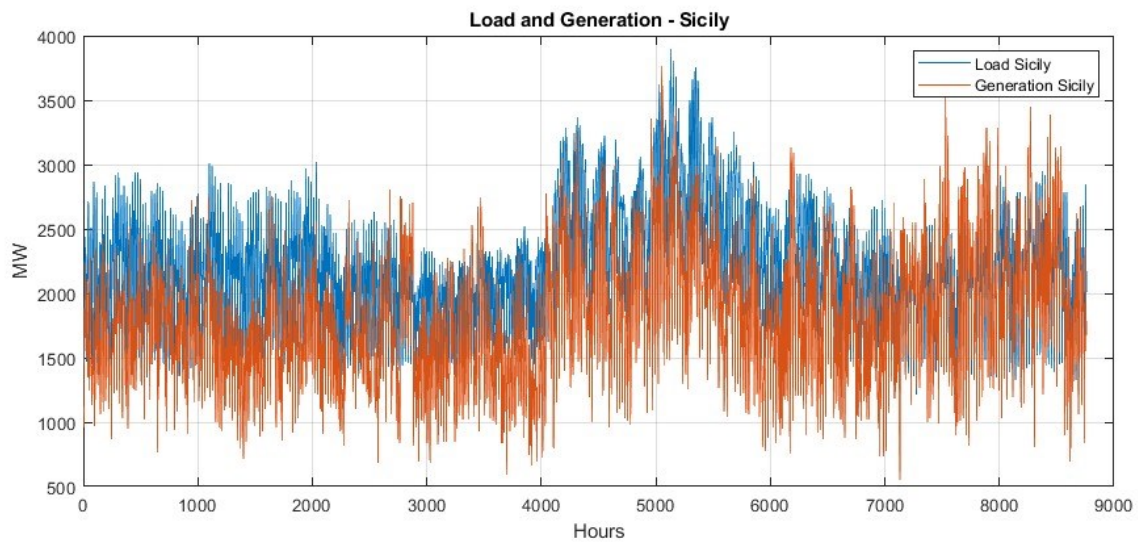
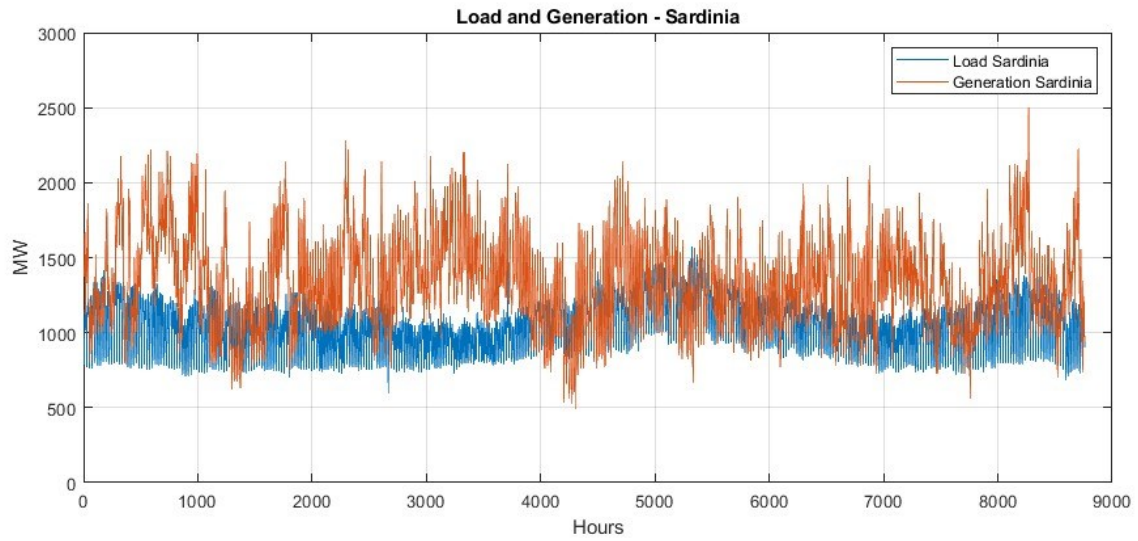
$$Generation \approx Load - Imports + Exports$$

In order to assess existing congestions, it was chosen year 2021, as it provides the most recent data. Moreover, to carry out this estimation it was considered an hourly average of the electrical zonal load (instead of quarter of hour values).

For Sardinia, the main links to be considered were the ones through submarine cable with the Centre-North zone of Italy, with the Centre-South zone of Italy and with Corse (France). For Sicily, the main links through submarine cables were the ones with the Calabria zone and with the island of Malta. Regarding Calabria, its links were with the Sicily zone and the South zone of Italy. The results of the estimated hourly production and demand for each zone are plotted in [Fig.52](#).

In [Fig.52](#) we can observe that the generation in Calabria and Sardinia was way higher than the actual local demand of energy. This might cause congestions more frequently if the interconnections with other zones didn't have enough capacity to transport the excess energy. In these cases, utility scale energy storages might be useful to avoid these grid overloads by absorbing and storing the excess energy.

Differently from the other two zones, in Sicily we frequently had a lower power generation than the one actually requested by the grid. The power needed frequently came from the link with Calabria, which exported its excess power generation. The zone was therefore less subject to this kind of congestions, as it rarely presented overgeneration that could not be absorbed by the region itself. Nonetheless, no information was available on congestions inside the zone due to local power fluxes.



A further study had to be carried out to spot the congestions phenomena. In fact, it is possible to look at the market prices hour by hour for each zone and compare them. When a congestion occurs, the market prices of the zone may significantly reduce, differently from a “non-congested” adjacent zone where they are more stable (dependently on the marginal costs of the last generation technology in-use). This price decrement gives a signal of excess of energy, and it may be useful for energy storage systems to exploit arbitrage mechanisms.

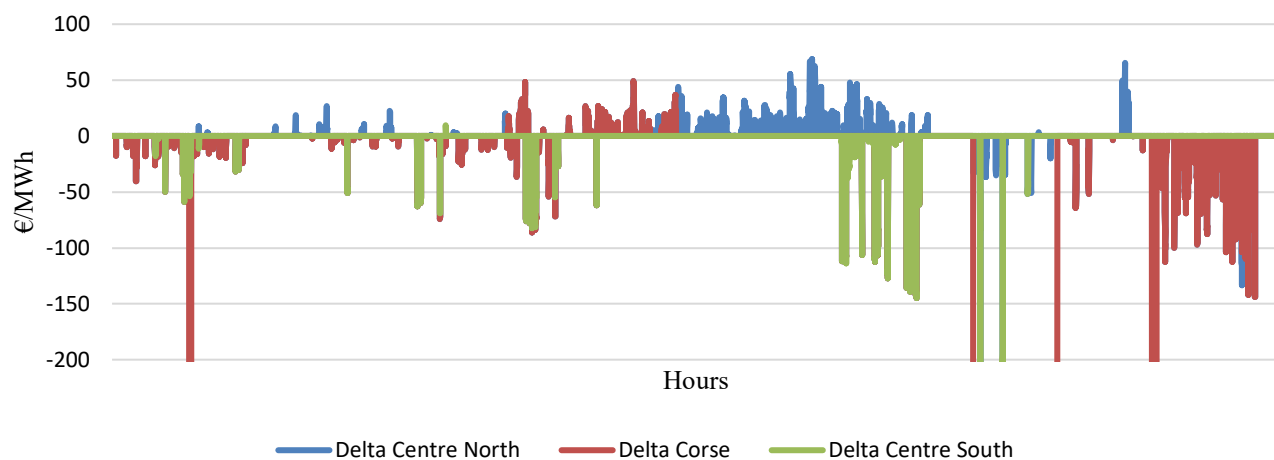
In addition, this means that by calculating the difference of price between the connected zones, it is possible to spot the hours of the year when significant congestions happened. In particular, it can be assessed the presence of a congestion when the difference of price is negative (excluding too small local variations of prices).

If the market price differences with the other zones are plotted for each region of interest, we get the results of [Fig.53](#).

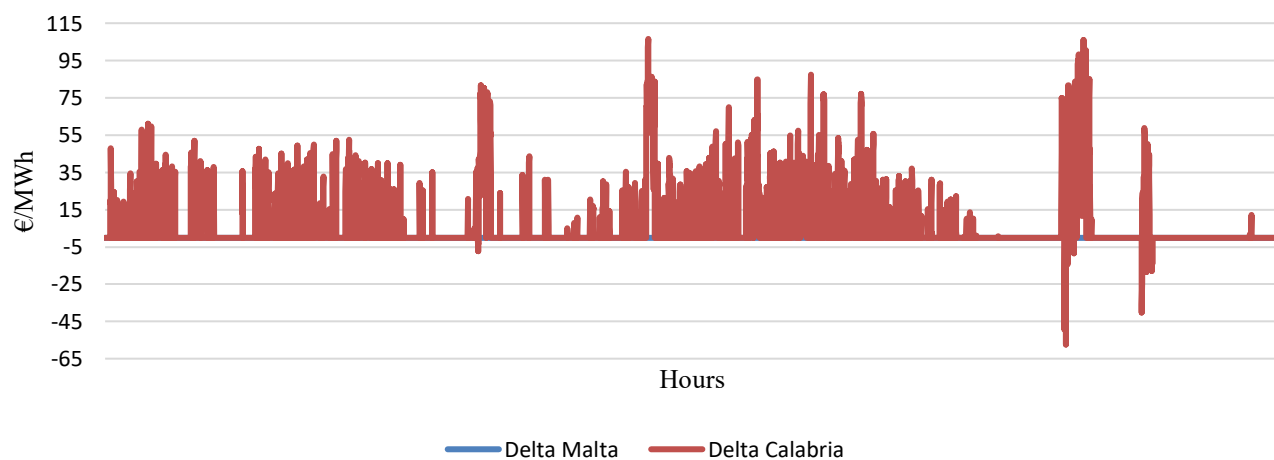
The second diagram clearly shows that for most of the year 2021, the price difference with the adjacent zones was positive. This result confirms that actually Sicily rarely presents congestions in the links with other regions, as Sicily mostly imports energy. However, it is expected that congestions may happen there in the future as more and more renewable power generation capacity is added to the island. In fact, the southern regions are more favorable from the economic point of view in Italy because of the larger availability of wind and solar sources. Therefore, it is necessary to prevent these phenomena investing on transmission and storages to be able to exploit as much as possible the available renewable power.

The first and the third diagrams, instead show a more variable trend of the price differences. Sicily only accounted for 24 hours of congestions in 2021. Regarding Calabria, a total of 1801 hours of congestions could be seen for the same year. These congestions were not evenly distributed, in fact, only 24 hours of those simultaneously interested both the connections with the other zones. Regarding Sardinia, the connection with Corse was not considered due to some anomalies on the prices, that locally spiked up to 1250 €/MWh. Therefore, comparing Sardinia with the Centre North and Centre South of Italy, 1391 hours of congestions could be spotted, of which 805 were more severe as they interested both the connections with the other zones. These numbers highlight the difficulties that the transmission grid has to sustain, and they justify the interest on the use of energy storage systems to provide useful services to the grid. On the other hand, this shows that great investments are needed to improve the grid reliability and its readiness for future renewable generation, as it will be later shown in the Grid Development plans chapter.

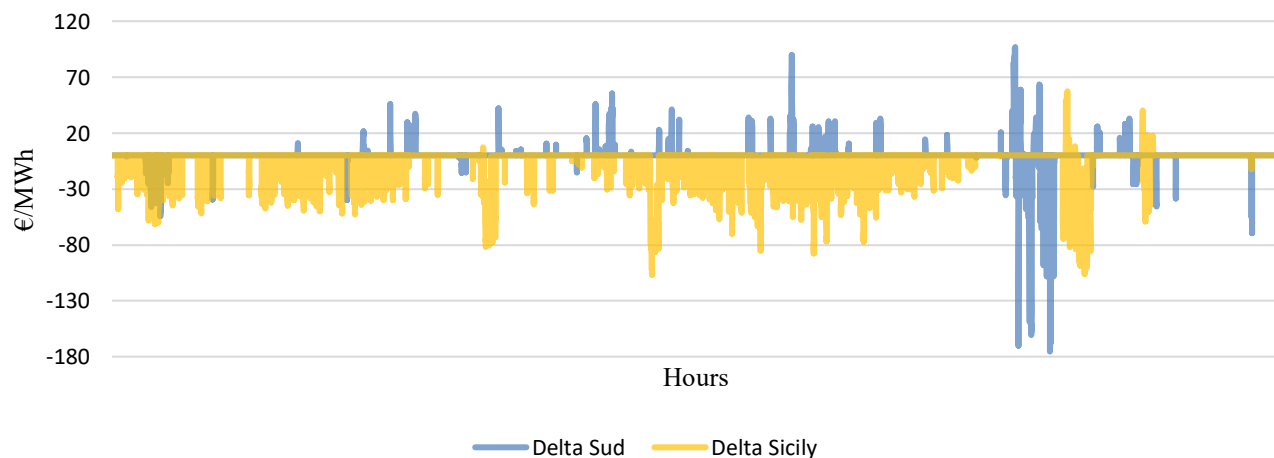
### Market price difference - Sardinia



### Market price difference - Sicily



### Market price difference - Calabria



## 2.2 Grid Development Plans

The achievement of renewable energy targets in future years will need grid improvements, as explained in Terna's Development Plan 2021 [2.2]. In particular, the rearrangement of some portions of the grid and new connections will be needed to increase the transmission capacity, reduce congestions, and increase reliability and resiliency. Focusing on the regions of southern Italy, some important interconnections will be deployed, like the Tyrrhenian link, a submarine line that will connect Sardinia with Sicily and Campania, and the SACOI 3 the line connecting Sardinia with Tuscany. Additionally, a new HVDC line between Puglia and Greece will be built, together with the connection between Sicily and Tunisia.

Between the critical points of the Italian grid, according to the report by Terna, there are the 400 kV connections from Calabria towards the North. This confirms that the congestions in this region are frequent because of the overgeneration of the zone, and because of the consequent high export power flow. For this reason, a new line has been planned between Laino and Altomonte to provide a new way for the power to move towards the central and northern regions. Additionally, it is said that inside the region, the presence of limited capacity lines may cause overloads on high voltage lines because of the high-power wind capacity installed. Among the lines interested by this phenomenon there are the 150 kV ones near Crotona and near Feroleto, proving that the addition of new wind capacity in the area might further unbalance the grid. In addition to the improvements of the transmission lines in the north of the region, a new line has also been planned in the South: the 380 kV connection Bolano-Paradiso between Calabria and Sicily. The representation of this new line is reported in Fig.54.

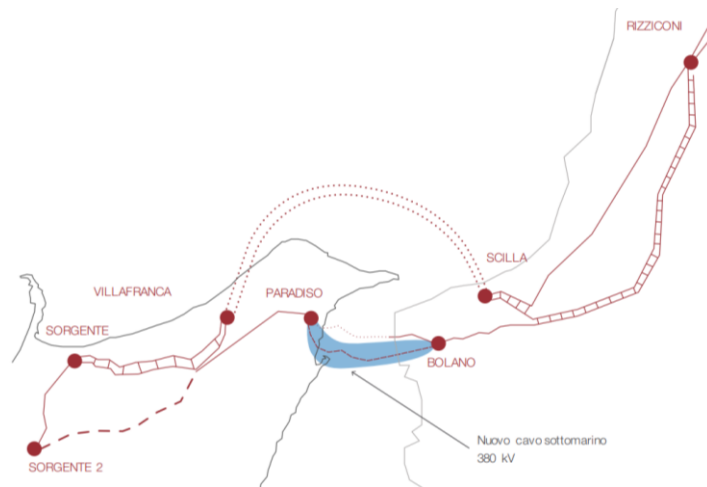


Fig.54 Scheme of the new connection Calabria-Sicily [2.2]

While this could allow less congestions in the Sicilian import from Calabria, the new link was mainly planned considering that Sicily will undergo a large increase on its renewable capacity installed. This opera will allow an increase of the transmission capacity to 1750 MW, and it is expected that it might be increased again to 2000 MW. According to the Development plan, the transmission capacity between Calabria and the South zone will remain stable to a max export value of 2350 MW. However, the new guidelines of the RepowerEU plan led to a larger expected increase of renewable power capacity (mainly

concentrated in the south regions) and consequently to a larger need of investments on the national electrical grid. Therefore, a new planning of grid developments will be presented in 2023. In DDS 2022 [0.18] an estimation of new power transmission capacity between the zones are reported in Fig.55.

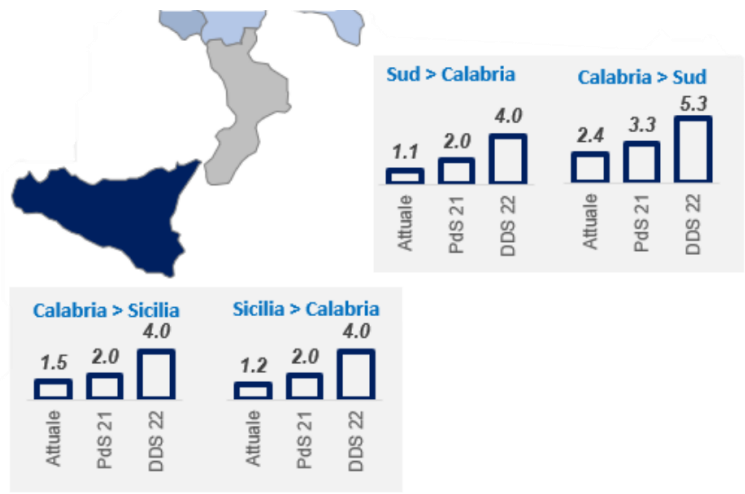


Fig.55 Estimation of transmission capacity between the zones in the South

These new data show that the transmission capacity towards Sicily will have to be increased to 4 GW, while towards the South zone it will have to be increased up to more than 5 GW.

## 2.3 Electric Market

The Italian Electric Market is divided in 4 different markets [2.1]. The first one is the MGP (Mercato del Giorno Prima), which is based on auctions. This market is used to provide the energy needed by the Italian grid by stating the amounts of energy that will be bought and sold and their corresponding prices in advance. In particular, the market sessions are held up to one day before the delivery of the energy. Every energy operator has to offer his maximum and minimum values for quantity and price of energy to be sold or bought. At the end of the market session, the offers are accepted according to the economical merit order and to the limits of transmission capacity between the zones. At this point, for every hour of the considered day, each operator has an assigned profile of energy to be delivered according to the market outcome. The prices that are corresponded to the accepted offers are equal to the marginal prices of the zone to which they belong. The ensemble of the zonal prices contributes to the PUN, the unique national price of Italy, which is equal to the average of prices of the zones weighted on the amounts of energy sold.

The second important market is the MI (Mercato Infragiornaliero). In this market, it is possible to adjust the programs resulting from the MGP with additional offers to buy or sell electricity. In order to perform this, three auction sessions are carried out and a continuous negotiation session is also adopted.

A third market is the MPEG (Mercato dei prodotti giornalieri), where the negotiations for daily products with energy delivery obligation are carried out. Here, negotiations are carried out continuously. The products that can be negotiated in this market refer to both baseload and peak load services.

Finally, the fourth market is the MSD (Mercato per il Servizio di Dispacciamento). This market is used to provide Terna, the Italian Transmission System Operator, for the resources needed to control and manage the national grid. In particular, it is used to solve congestions, to generate energy reserve and to balance the grid. In this case, Terna is the subject which accepts and manage the offers of the MSD. Two different phases are distinguished in the MSD: the programming phase (MSD ex-ante), and the Balancing Market (MB). The MSD ex-ante is based on six subphases in which the offers are presented and accepted or refused, while the Balancing Market is a continuous market. The MSD represents one of the key instruments to allow a good management of the grid by Terna. During the programming phase, the TSO programs the resolution of congestions, and acquires resources for the secondary and tertiary reserve. This allows to reduce the gap between the forecast of energy demand and renewable generation and the energy market results, and also to provide reserves in addition to real time grid management. Then, through the Balancing Market, in addition to the congestion solving and reserve retrieval, the TSO keeps the equilibrium between the generation and the loads of the electrical grid. The types of reserve that are managed through the MSD are briefly described in the following. The power primary reserve is the most flexible resource for the electrical grid, and it must be provided by all the suitable plants. This reserve is used to correct the instantaneous imbalances between total production and total demand of the entire interconnected European electricity system as a response to frequency variations. The power secondary reserve is meant to balance the difference between the demand and production of the national grid, re-establishing the power exchange levels at the borders of the country. These first two mechanisms can be activated automatically by Terna with response times in the order of seconds and contribute to the European frequency regulation. The ready tertiary reserve is meant to re-establish the secondary power

reserve and it consists of the increase or decrease in production which can be performed within 15 minutes of the request from Terna. For units to operate as part of this reserve it is required a fast ramp-up and down velocity, with a gradient of at least 50 MW/min. In the end, the tertiary replacement reserve is meant to cover the ready tertiary reserve in case of variations of the demand, renewable sources unprogrammed injections and damages to the production units. In this case the reserve consists of the increase or decrease in production which can be performed within 120 minutes of the request from Terna without duration limitations. In tertiary reserve management, dispatchment orders are sent, differently from the primary and secondary reserve, where autonomous regulation devices are used both in frequency and voltage regulation.

### **2.3.1 Dispatching Services Market and Balancing Market**

For energy storage applications, the operation on the MSD market results to be very interesting for arbitrage, as it may allow to buy energy at low prices and to sell at very high prices. This is possible as this market works with the pay-as-bid method, differently from the other markets like MGP and MI. In the MSD, two different offer and price types are defined in Italy: “a salire” and “a scendere”. In the case of offers “a salire”, they are referred to offers to increase the energy generation or to decrease the energy consumption to meet the energy demand. Conversely, in the case of “a scendere” offers, they are referred to a decrease of the energy generation or an increase of the energy consumption to meet certain grid requirements. Taking as a reference congestion events, these phenomena need to be solved by reducing the power generation or increasing consumption where needed. From this point of view, energy storage technologies may act as an additional load if needed, helping to solve congestions and storing energy for a second use. In a future with a large excess of renewable energy, they could help integrating intermittent sources with the national grid. Then, the energy stored could be sold in traditional markets like MGP or MI, or it could be offered in the MSD to provide energy in peak cases. Additionally, energy storages could be used to provide services like voltage and frequency regulation. One of the particularities of the dispatching services, it is that units that may be called to solve congestions or provide grid services might be very far from the critical point of the grid. Therefore, in order to see a full picture of the market behavior, it was suggested to consider more than one zone of the market.

For the following simulation of an energy storage system, it was supposed to be able to operate on the market of dispatching services MSD and on the Balancing Market MB, as they would probably be the most profitable ones. It should also be remembered that the MSD works with bids, that can be accepted or rejected, therefore any expected economical result depends on the selection process by Terna, which accepts the best solution to correctly manage the grid.

The market data were extracted by historical data of GME [2.1]. Considering that the offshore plant subject of the analysis should be located in Calabria, both Calabria and the whole Centre-South of Italy were used to provide market data for the different simulations. The choice of including the zones of the Centre-South was done because the storage could eventually participate in the balancing, congestion solving and frequency regulation as a response to disturbs located in the other regions. Therefore, the volumes and prices of the other zones could provide valuable information about the possible size and characteristics of the market where the storage would operate. The zones included in the market data



were South, Centre-South, Calabria, Rossano, Sicily. The Calabria zone is relatively recent as it was first adopted in 2021, therefore in the previous years it was partially included in the South and in the Rossano zone.

### 2.3.2 MSD ex-ante prices & volumes

The prices “down” (used as “a scendere”) were used in the energy storage simulation as a reference to define the prices applied to the buying & charging energy process. In practice, these prices also refer not to a physical buying and taking energy from the grid, but also to a decrease of the electricity to be provided to the grid that was previously stated in the other markets. In this way, producers might be able to avoid part of the generation by paying part of what it was initially given to them in the other markets. As an example, it is shown in [Fig.56](#) the plot of the hourly prices “a scendere” of MSD ex-ante for the zones of Centre-South of Italy between year 2018 and 2021. Each hourly price was plotted against its corresponding total power required by the zones. It is possible to observe how prices may vary significantly, probably because of the bidding process and because of differences in terms of necessities for the grid. Nonetheless, plotting the average of the values for each power level required (in orange), it is possible to see a trend that highlights how for a larger energy excess the prices to buy it back tend to be lower.

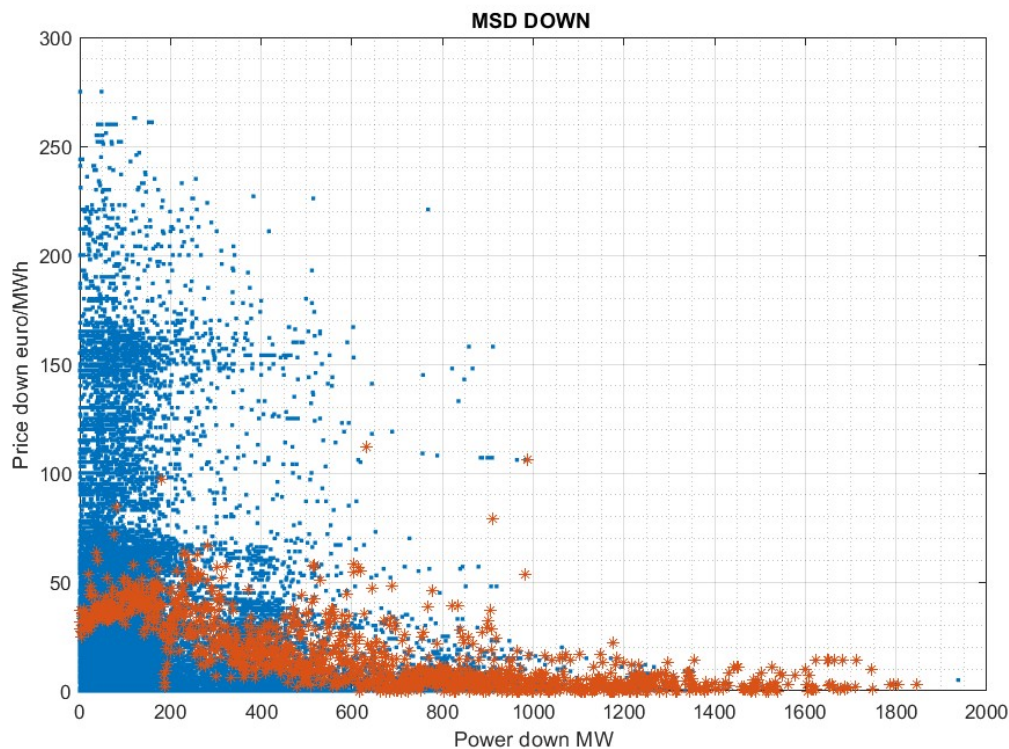


Fig.56 MSD ex-ante Prices “down” / “a scendere” between 2018 and 2021

Differently, prices “up” (used as “a salire”) refer mainly to increase of energy generation. In the case study of an energy storage, their values were used to evaluate the opportunities to discharge & sell the

energy of the storage. In a similar way to what it was done previously, also the prices “up” of MSD ex-ante were plotted for the southern regions in the period of time between 2018 and 2021. Once again, it can be observed a huge variability of prices, probably due also to influences of other variable market prices (like natural gas, which affects thermoelectrical power generation). Nonetheless, it can be again noticed a trend that correlates the power required by the grid with the average price level for each power required. The result is represented in Fig.57.

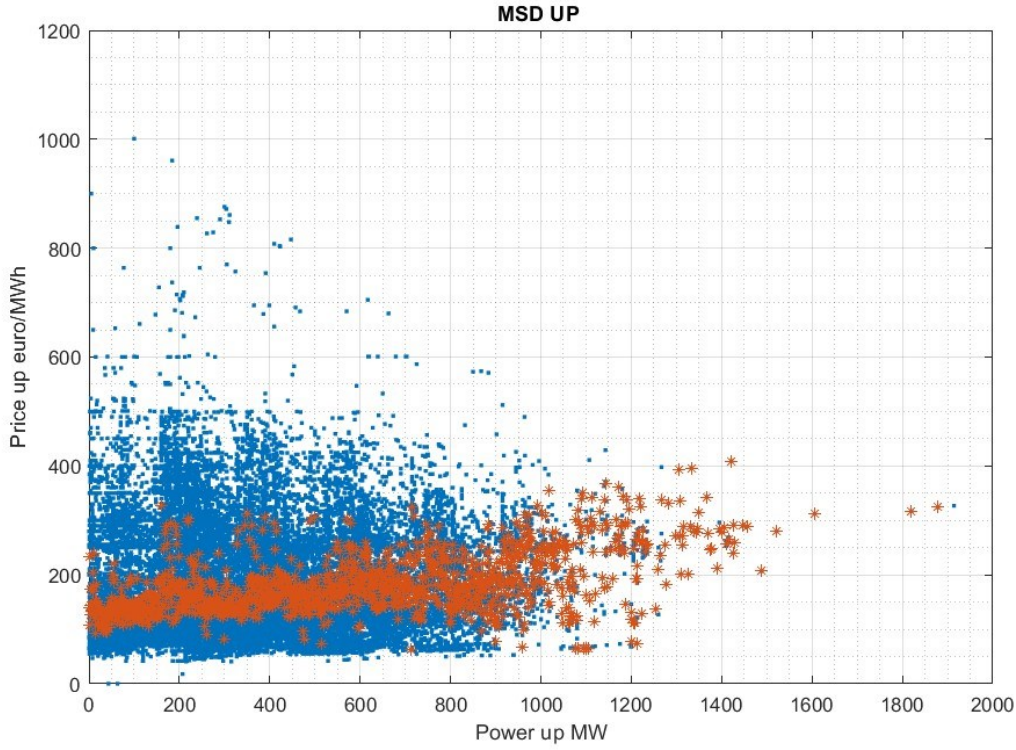


Fig.57 MSD ex-ante Prices “up” / “a salire” between 2018 and 2021

In order to perform the simulations, the zonal price profiles were condensed into unique yearly profiles. For each year between 2018 and 2022, it was calculated the weighted average of the prices “up” and “down” for each hour of the year and for each market session (MSD ex-ante). The weights used consisted of the volumes of energy sold or bought for the hour considered, as reported in the following equations.

$$price_{up}(h) = \sum_{zones} price_{up(zone)}(h) \cdot \frac{Energy\ up_{zone}(h)}{Energy\ up_{total}(h)}$$

$$price_{down}(h) = \sum_{zones} price_{down(zone)}(h) \cdot \frac{Energy\ down_{zone}(h)}{Energy\ down_{total}(h)}$$

This calculation process allowed to get yearly price profiles suitable for the simulation. In particular, this was done 2 times, one referred to Calabria only (SUD + ROSN for years 2018-2020 & CALA for years 2021-2022) and one referred to the whole Centre-South (SUD + ROSN/CALA + SICI + CSUD). This

was done to provide information about the prices of a local market like the one of Calabria, and also to gain information about the prices of a larger market, that might be used to evaluate the operation of the storage to provide services to the whole south of Italy. However, given that the market is based on bids, during some hours of the day the prices could be undefined because of the absence of accepted offers. As an example, the weighted price profiles for year 2019 in the Centre-South zones are reported in Fig.58. Looking at the profiles, it is possible to see how the prices “up” can reach significantly high values, while prices “down” are typically low. The large variability in the plot of prices “down” is due to the non-accepted offers, which are represented with a price = 0 value. The advantage of buying energy from the MSD is shown in Fig.60, where the same prices “down” are compared to the PUN hourly value for the same year 2019. The same applies to selling energy on the MSD ex-ante, where the average price was 141 €/MWh, compared to an average PUN of 52 €/MWh. The average buying price in MSD ex-ante, instead, was 25 €/MWh. However, this advantage is mostly theoretical as the possibility of winning the bids is not straightforward, and still dependent on many parameters monitored by Terna.

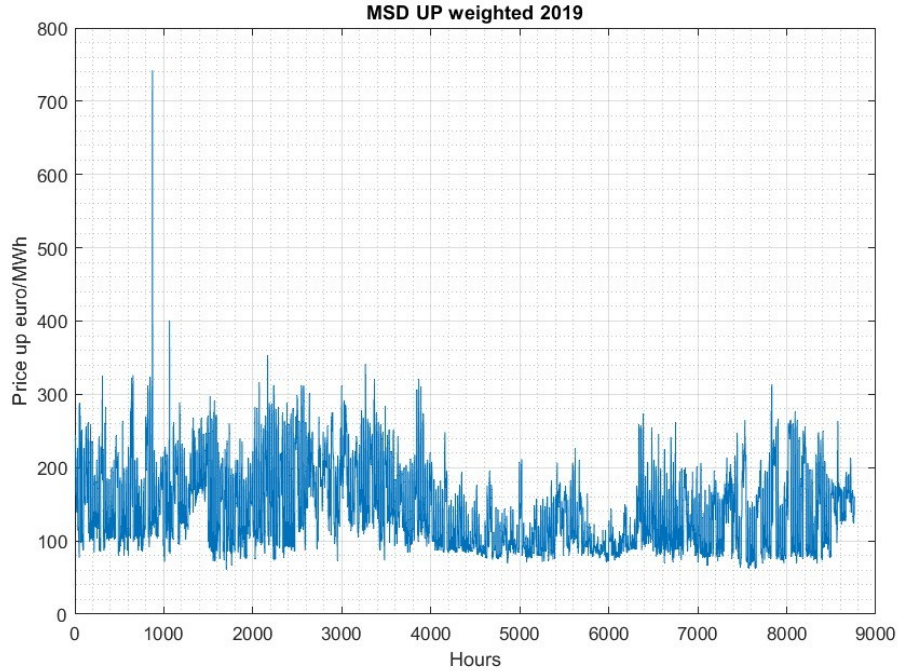


Fig.58 MSD ex-ante Prices “up” / “a salire” during year 2019 in the Centre-South

In addition to the prices, also the volumes “up” and “down” were extracted from GME historical data for the years 2018-2022. In this case, both the yearly profiles for volumes “up” and “down” were elaborated:

$$Volume_{up\ CALA}(h) = Vol_{ROSN}(h) + Vol_{SUD}(h) \quad or \quad Volume_{up\ CALA}(h) = Vol_{CALA}(h)$$

$$Volume_{up\ CENTRE\ SOUTH}(h) = Vol_{ROSN/CALA}(h) + Vol_{SUD}(h) + Vol_{CSUD}(h) + Vol_{SICI}(h)$$



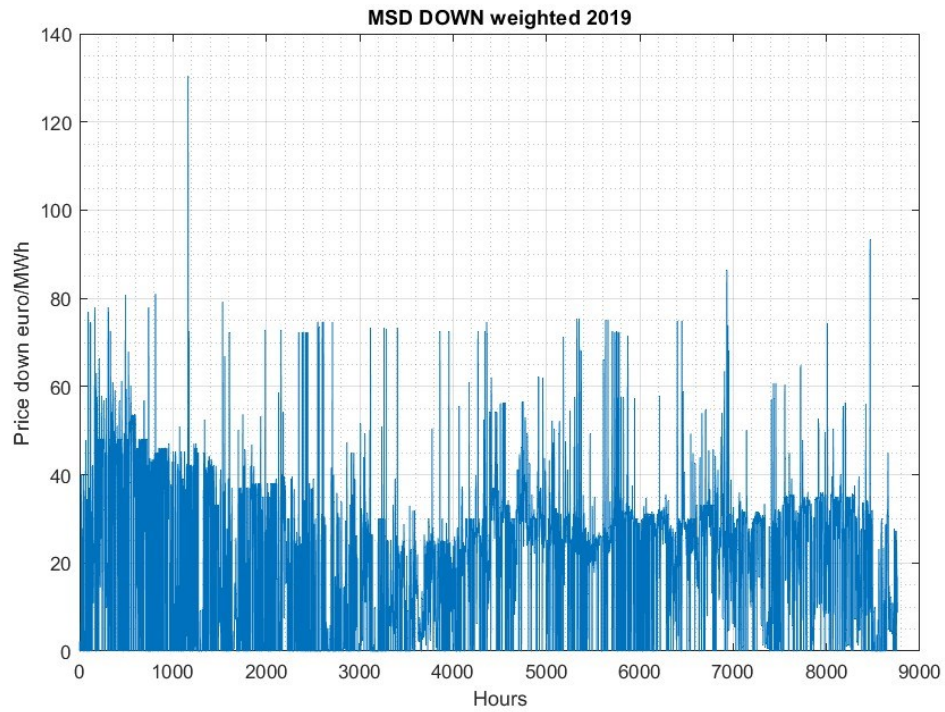


Fig.59 MSD ex-ante Prices “down” / “a scendere” during year 2019 in the Centre-South

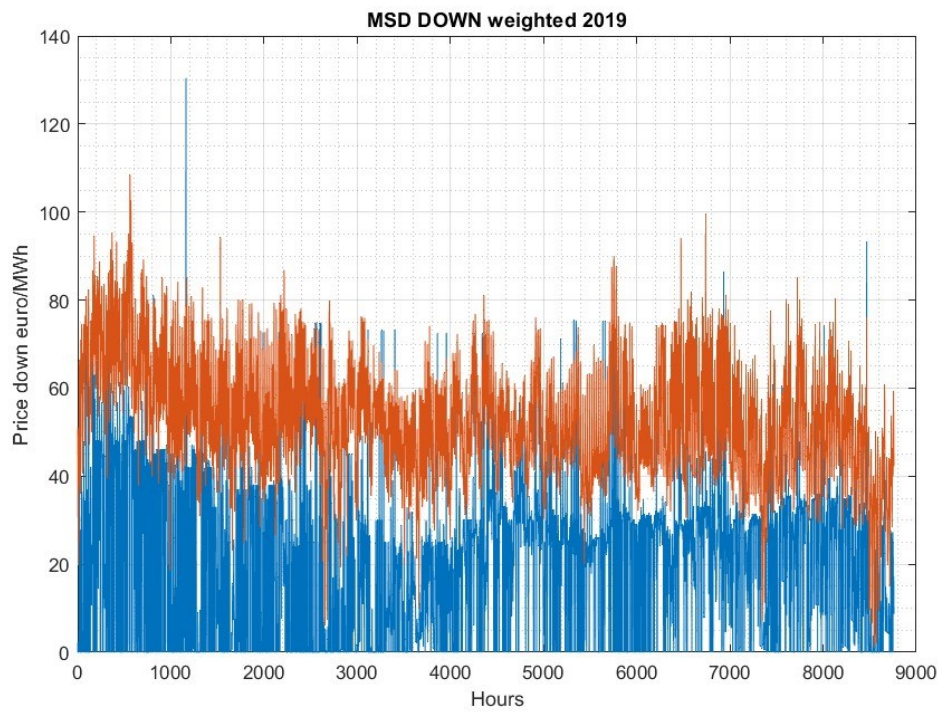


Fig.60 MSD ex-ante Prices “down”/“a scendere” during year 2019 in the Centre-South compared to PUN

In the following graph, the average values of PUN and prices “up” and “down” from the MSD ex-ante results in the Centre-South zones are reported for each considered year. These indicative values show how the prices of MSD could be exploited for energy storage technologies. In addition, it highlights how prices are not stable and frequently variable. In year 2020 it can be seen the effect of the pandemic, which caused a general decrease of energy prices, while in 2021 it can be seen a large increase of prices due to the restart of the economies and in 2022 a further spike in prices due to the effect of the war in Europe.

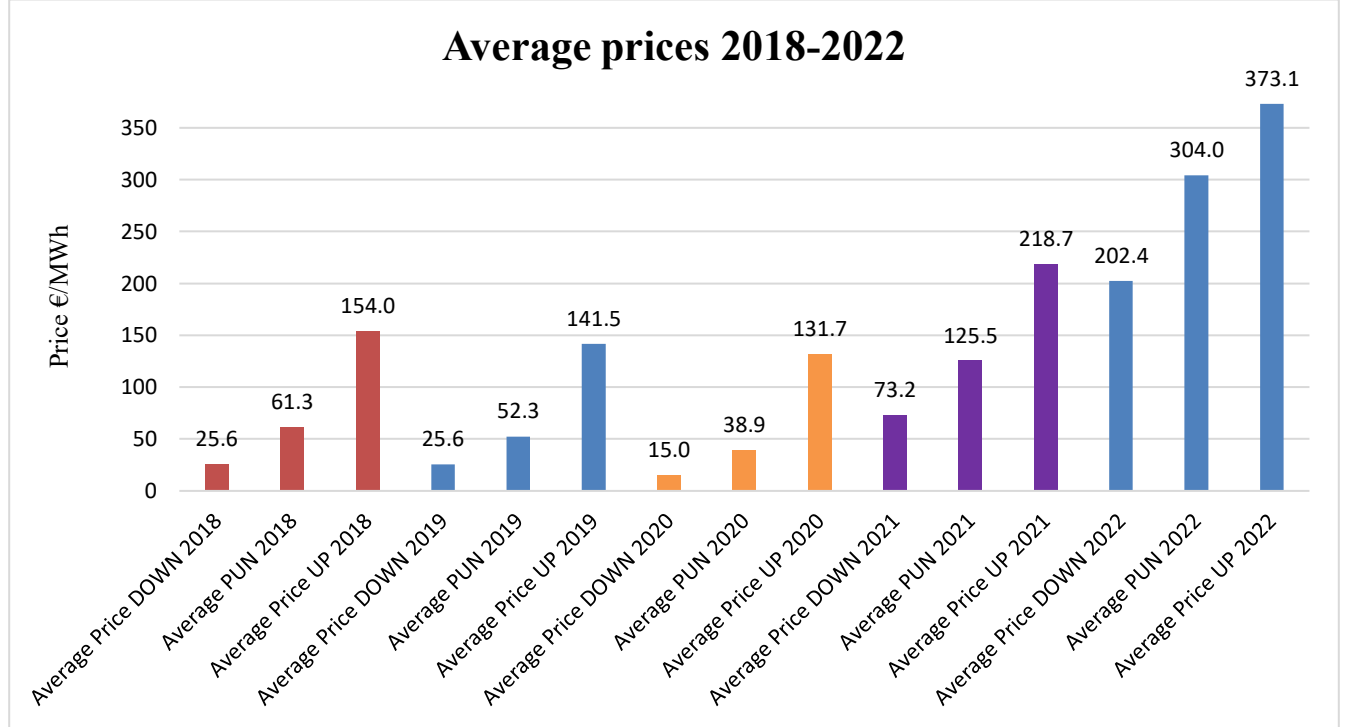


Fig.61 Average prices for years 2018 to 2022 [MSD ex-ante & PUN]

### 2.3.3 MB prices & volumes

In addition to the MSD ex-ante, also the historical results of the Balancing Market session were considered. The process applied to calculate a yearly profile of the prices “up” and “down” was the same of the MSD ex-ante results. The prices were weighted with the volumes managed on the market in the different zones, both considering Calabria only and the whole Centre-South zones.

$$price_{up}(h) = \sum_{zones} price_{up(zone)}(h) \cdot \frac{Energy_{up_{zone}}(h)}{Energy_{up_{total}}(h)}$$

$$price_{down}(h) = \sum_{zones} price_{down(zone)}(h) \cdot \frac{Energy_{down_{zone}}(h)}{Energy_{down_{total}}(h)}$$

Equally, also the volumes “up” and “down” from the results of the Balancing Market were extracted and used to generate yearly profiles both for Calabria only and the Centre-South of Italy.

$$Volume_{up\ CALA}(h) = Vol_{ROSN}(h) + Vol_{SUD}(h) \quad or \quad Volume_{up\ CALA}(h) = Vol_{CALA}(h)$$

$$Volume_{up\ CENTRE\ SOUTH}(h) = Vol_{ROSN/CALA}(h) + Vol_{SUD}(h) + Vol_{CSUD}(h) + Vol_{SICI}(h)$$

As it was done for the results of MSD ex-ante, the weighted price profiles “up” and “down” for the Centre-South regions in 2019 are shown as an example in the next figures [Fig.62](#).

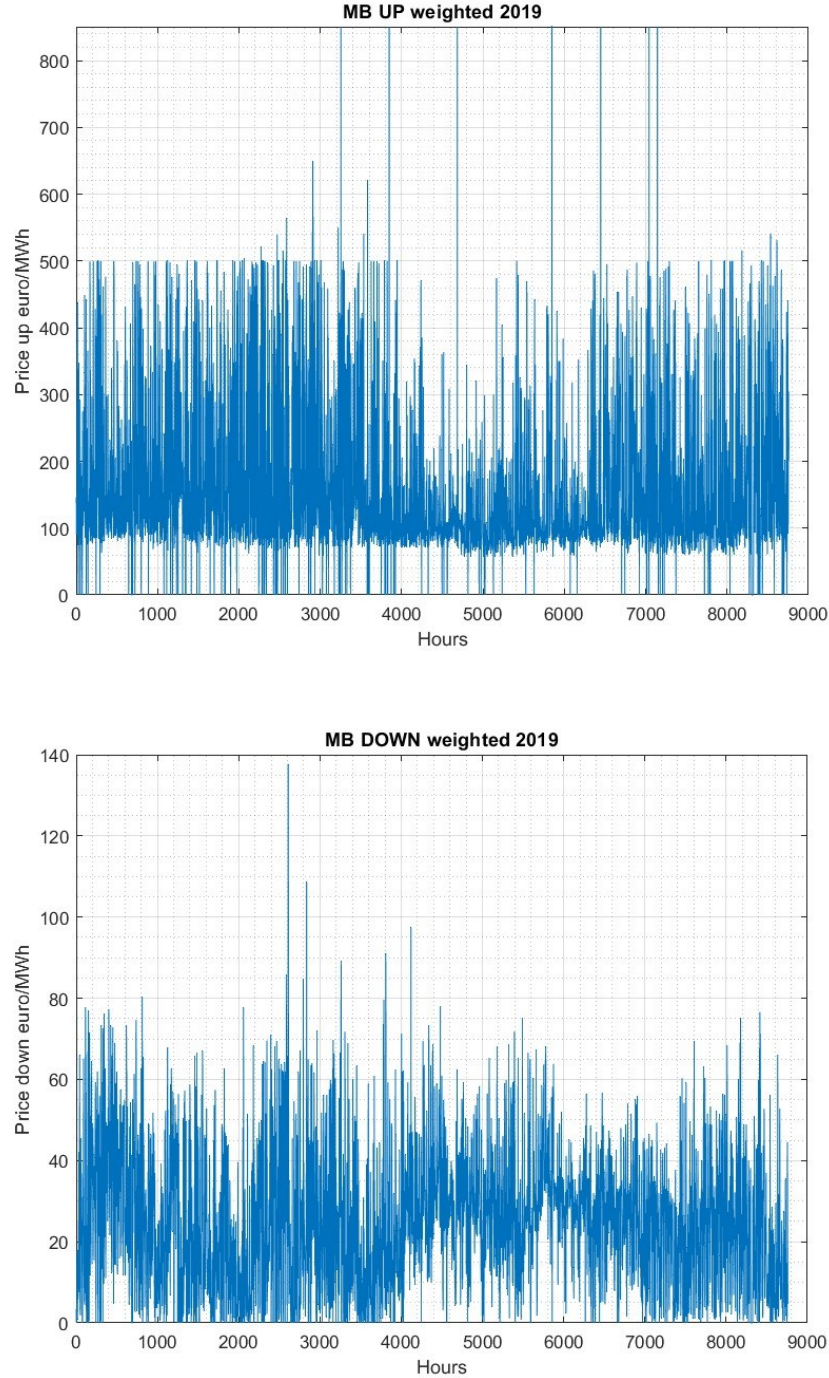


Fig.62 MB Prices “up” and “down” during year 2019 in the Centre-South

### 2.3.4 Total prices & volumes

Considering that both results of the markets refer to services that can be provided by a storage, it was supposed to be able to participate to both sessions and to be able to be awarded with dispatching orders on both markets. Even if the two market sessions are carried out in different periods of time, and therefore the scheduling of the storage would happen in different times, for the sake of simplicity both markets were considered as equal to identify the required demand of services and the relative possible revenues. For this reason, the data about the two markets were unified, both for the case of Calabria and for the case of the Centre-South. The hourly volumes of the two markets were summed, while for the prices once again they were weighted on the volumes of the respective markets.

$$Volume_{up}(h) = Vol_{up\ MSD}(h) + Vol_{up\ MB}(h)$$

$$Volume_{down}(h) = Vol_{down\ MSD}(h) + Vol_{down\ MB}(h)$$

$$Price_{up\ tot}(h) = Price_{up\ MSD}(h) \cdot \frac{Energy_{up\ MSD}(h)}{Energy_{up\ MSD\ \&\ MB}(h)} + Price_{up\ MB}(h) \cdot \frac{Energy_{up\ MB}(h)}{Energy_{up\ MSD\ \&\ MB}(h)}$$

$$Price_{down\ tot}(h) = Price_{down\ MSD}(h) \cdot \frac{Energy_{down\ MSD}(h)}{Energy_{down\ MSD\ \&\ MB}(h)} + Price_{down\ MB}(h) \cdot \frac{Energy_{down\ MB}(h)}{Energy_{down\ MSD\ \&\ MB}(h)}$$

The yearly profiles obtained were used in the storage simulations to estimate the possible operation of the system on the two markets. In the following are reported the price curves obtained by the combination of the two market session results for year 2019 in the Centre-South of Italy.

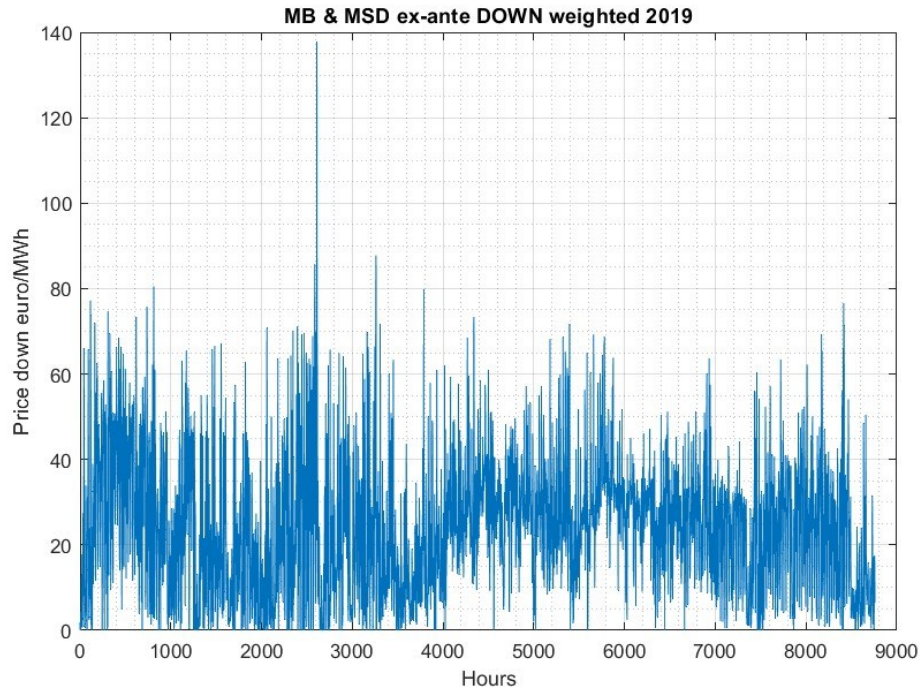


Fig.63 MB & MSD ex-ante prices “down” / “a scendere” during year 2019 in the Centre-South



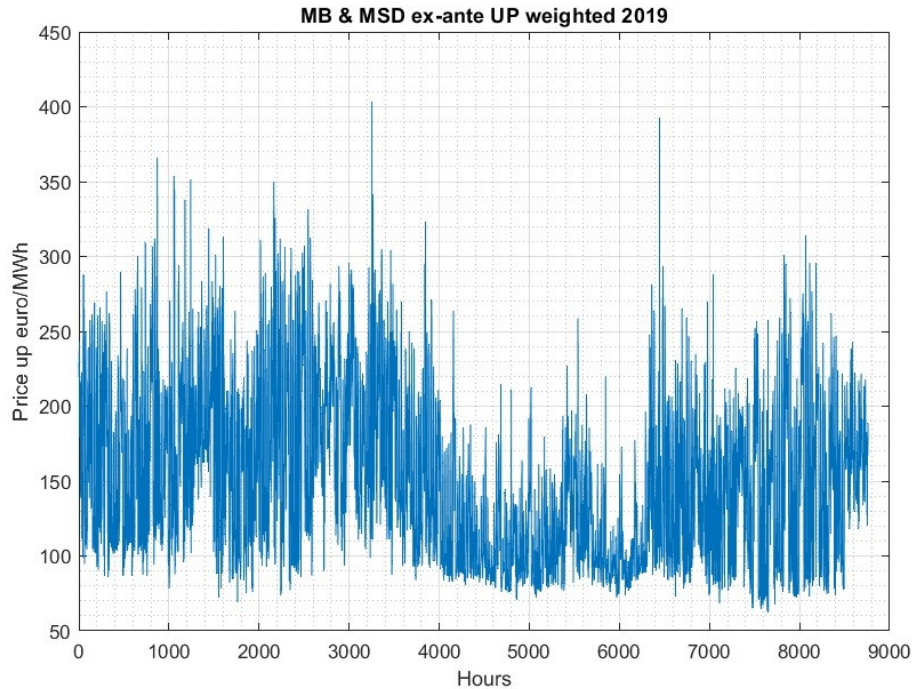


Fig.64 MB & MSD ex-ante prices “down” / “a scendere” during year 2019 in the Centre-South

The weighted average of the MSD ex-ante and MB keeps the trend of the prices clear if compared with the previous plot, but it also allows to mitigate the effect of some outliers, like selling prices higher than 2000 €/MWh that were present in the MB data.

### 2.3.5 Wind farm incentives

Regarding the offshore wind farm subject of this analysis, the plant should typically sell energy on the traditional energy markets like MGP and MI. However, over 2022, a draft of the decree FER II was published, providing the possibility of receiving a fixed price remuneration for energy produced by selected renewable power plants [2.4]. Among the renewable energy sources eligible for this form of incentive there is also floating offshore wind, with a maximum cumulative power of 3.5 GW that can be awarded. This kind of incentive should be awarded with competitive bids among the producers, starting from a maximum tariff of 185€/MWh. This form of incentive could help covering the high costs of the development of these plants and assure a reasonable return of the investment with relatively low risk. On the contrary, the participation to the traditional markets without any incentive could make the investment on offshore floating wind unfeasible or very risky, due to the variable and relatively low prices captured. Even if the definitive version of the decree has not been published yet, large variations from the draft are not expected, and this fixed tariff is considered as a reference also for the company. In fact, it is forecasted that the lack of awarding of the tariff would probably result in the cancellation of the project.



### **3 Energy Storage Systems and Power-to-X review**

Energy storage and Power-to-X technologies might be used for a variety of purposes. The most classic use of energy storage is the energy arbitrage, where the electric energy is bought from the grid in low price periods to be later sold when prices are higher. However, this kind of operation requires sufficiently high price spreads, which are more and more difficult to find according to [3.1]. In addition, they could provide ancillary services, like voltage and frequency regulation, as well as energy imbalance services, congestion solving, energy reserve and black start. Each different technology has different characteristics in terms of storage capacity, degradation and lifetime, self-discharge, energy density, round-trip efficiency and velocity of response. All of these characteristics might affect the type and quality of services provided by the storage system, and therefore they should be analyzed to better understand the possibilities offered by the different technologies.

As previously stated, the companies Elettrostudio s.r.l. wanted to investigate the possibility of adding energy storage solutions to some of their planned offshore wind farms. Given that the company already had some experience with pumped hydro energy storage, the aim of the review was to evaluate alternative storage possibilities to highlight their pros and cons. If some of the possibilities would have been considered feasible, a further investigation would have been conducted to understand if an investment would have been profitable. In this chapter the results of the review are reported, together with the description of the fundamentals of each storage technology, their main characteristics, and some commercial examples. The data acquired from this review were used also for the final simulations and in the business plan development.

### 3.1 Compressed Air Energy Storage

Compressed air energy storage systems store energy in the form of a compressed gas: air. In these systems, excess electric energy is used to run an air compressor, which increases the air pressure. The high-pressure air is then stored in a reservoir to be later used. When the grid needs more power, the reservoir can be discharged, and the high-pressure air can be used to generate electricity in a turbine. Among compressed air systems, three main different types of systems can be distinguished: Diabatic CAES (DCAES), Adiabatic CAES (ACAES) and Isothermal CAES (ICAES). All these systems will be presented in the following.

CAES systems are based on the Brayton-Joule open cycle, and so their layout is similar to conventional gas turbine power plants. Their main elements are the air compressor, the air reservoir, the heating system and the turbine. Differently from a traditional gas turbine, the compression process may not be simultaneous with the operation of the other components. In fact, during the charging phase the air is compressed and then stored in a closed space.

This space is called air reservoir, and it could be natural or artificial. Natural reservoirs might be underground caverns like natural salt caves, mines, aquifer storages, rock caverns, depleted gas fields and wells. Man-made reservoirs could be aboveground tanks or gas pipelines, but also underwater systems could be used like ballasted rigid tanks or flexible fabric containers [3.2]. Of course, the use of natural reservoirs is more cost effective than purposely built reservoirs, as it allows to have lower capex. However, the availability of natural reservoirs is not always favorable, and so it might be necessary to build or modify the existing reservoirs. In fact, it should be proved that the existing natural structures should be able to withstand the high-pressure air for long periods of time without leakages or without causing structural damages and issues. It should also be highlighted that the use of a natural reservoir represents a geographical constraint for this storage technology.

Another possible distinction that can be made is between the isochoric and the isobaric type of reservoir [3.7]. An isochoric air storage is a constant volume space, the most common for compressed air energy storage systems. Underground caverns and steel vessels are the easiest examples. These kinds of reservoirs operate with variable pressure: the air pressure is at its minimum when the storage has been discharged and at its maximum when it has been fully charged. The main constraints for these reservoirs regard the stress to which they are subject because of the pressure and temperature variations. In particular, during charge there is a temperature increase, while during discharge there is a temperature decrease inside the reservoir. An isobaric air storage works with variable volume and with constant pressure. Among the possible solutions to provide isobaric storages there are caverns with sliding barriers, liquid displacement pressurization and also underwater storage. The liquid displacement solution has been commercially developed by Hydrostor and will be presented in the following as an example for the ACAES systems.

Regarding the operation of these systems, ideally when energy is required to the grid, the high-pressure air storage is discharged, and the air drives a turbine and a generator to generate the electricity needed. However, to increase the output power of the system, it is necessary a heating phase before the inlet of

the turbine, as it happens in a Brayton-Joule Cycle. Dependently on how the heat is provided to the air flow, the three previously mentioned types of CAES systems are distinguished.

### 3.1.1 DCAES

Starting from Diabatic CAES systems, they provide heat to the air flow by burning an external fuel, which is usually natural gas. So, these systems are even more similar to gas turbines, as after the compression-storage phase there is a combustion chamber. Therefore, the turbine has to process the high-pressure exhaust gases from the combustion chamber, generating electric energy through a generator. Of course, this is one of the weaknesses of DCAES systems, as they generate CO<sub>2</sub> emissions and need fossil fuels to operate. In the following Fig.65 from [3.3], the DCAES plant scheme of Huntorf is reported. In this case, the represented air reservoir is a salt cavern, and two stages of compression and expansion are present.

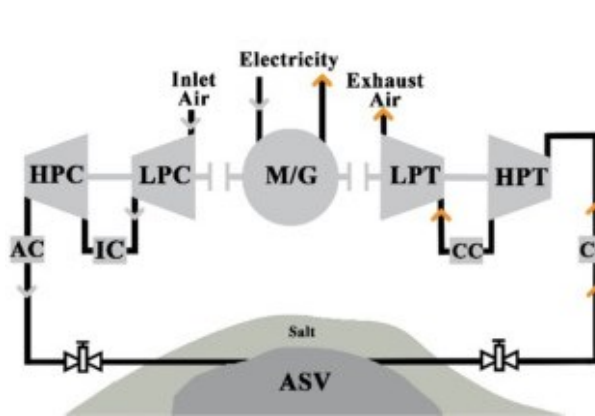


Fig.65 DCAES Huntorf plant scheme [3.3]

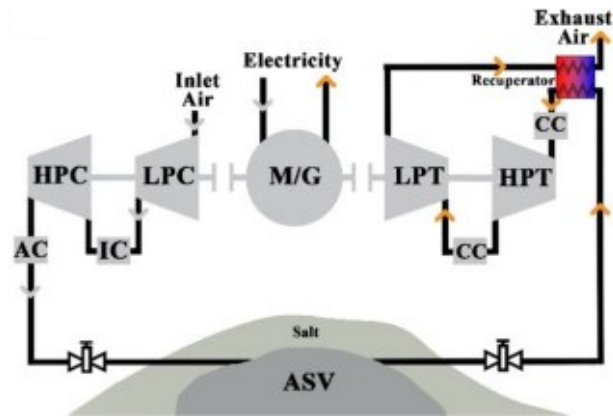


Fig.66 DCAES McIntosh plant scheme [3.3]

It should be highlighted that after the first stage of compression an inter-cooling phase is added to cool down the air, which is heated by the compression phase. Different possibilities are available for this “undesired” heat produced during compression. The first possibility is to store the hot air directly in the reservoir. This option needs an insulated reservoir not to lose the enthalpic content of the air stream, as reported by [3.4]. Therefore, it is not a valid possibility for large natural reservoirs. Moreover, the possibility of storing hot gas may affect the air density inside the storage, and the isentropic efficiency of the compression would be affected too. For this reason, the excess heat is usually removed from the air stream, as in the previous Fig.65 through inter-cooling and after-cooling. This allows to achieve greater air density and higher compression efficiency.

The heat removed during these processes can be wasted by releasing it to the environment or it can be stored for a second use during the discharge of the system (in ACAES or ICAES systems). The plant of Huntorf, which was the first commercial CAES plant, which scheme was previously presented in Fig.65, releases to the environment the heat removed during the compression phase.

The Huntorf plant was built from 1969 to 1978 in Germany, while a second CAES system, the McIntosh plant was commissioned in 1991 in Alabama, in the USA. The scheme of the McIntosh plant is shown in the following Fig.66. These two commercial systems are the main examples of this technology, as they are the only two large size plants still in operation.

### 3.1.2 Huntorf DCAES system

The Huntorf plant is the first commercial CAES ever. Its storage is constituted by two caverns artificially built to store the compressed air, one of 140000 and one of 170000 m<sup>3</sup> for a total volume of 310000 m<sup>3</sup>. These caverns are located around 700 m deep in the ground and are able to store the compressed air at pressures between 20 and 70 bar. The plant had a rated power output of 290 MW, which was increased to 321 MW after a retrofit in 2006. The storage can be fully charged in 8 hours of operation and discharged in 2 hours.

The compression phase of the CAES system relies on two compressors, one for the low and one for the high-pressure stage, for a total nominal power of 60 MW. The low-pressure compressor is of the axial type, while the high pressure one is of the centrifugal type with 6 stages of compression. After each compression stage, two after coolers are used to extract the excess heat, which is released to the environment. During the discharge phase, the air stream reaches a first combustion chamber fed by natural gas and then the high-pressure stage of the turbine. After the first expansion, the gas stream enters a second combustion chamber for a post-combustion before the low-pressure turbine. The main plant specifications are summarized in the following Tab.6.

Description	Value
Round trip efficiency	0.42
Input per kWh el. of Output [3.7]	0.8 kWh el. & 1.6 kWh natural gas
Charging/discharging flow ratio	1/4
“Energy content”	642 MWh
Charging phase	8 h - 2.5 bar/h
Discharging phase	2 h - 10 bar/h
Time to full load	6 minutes
Expansion	
Output power (min/max)	100 – 321 MW (290 before retrofit)
Mass flowrate (max/nominal)	455 – 417 kg/s
HP section inlet pressure	41.3 bar
HP section inlet temperature	490 °C
LP section inlet pressure	12.8 bar
LP section inlet temperature	945 °C
Expansion exhaust temperature	480 °C
Compression	
Nominal electric power	60 MW
Air mass flowrate	108 kg/s
Storage	
Storage volume	140,000 and 170,000 m <sup>3</sup>
Cavern depth (top/bottom)	-650 to -800 m

Tab.6 Huntorf plant specifications

As it can be seen from the table, the storage system is able to achieve an overall round trip efficiency of 42 %, where the RTE is defined as:

$$RTE = \frac{El. \text{ energy output}}{El. \text{ energy input} + Fuel \text{ energy input}}$$

### 3.1.3 McIntosh DCAES system

The McIntosh plant is the second DCAES commercial plant ever built. It exploits a salt cavern to store air at pressures between 46 and 75 bar in a total volume of 538000 m<sup>3</sup>. The plant has a rated power output of 110 MW. At full load, the storage system can be fully charged in 38 hours and fully discharged in 24 hours. Differently from the Huntorf plant, the McIntosh CAES is equipped with a recuperator that improves its efficiency.

The compression phase of the CAES is carried out by four compressors for a total power of 50 MW, equipped with three inter-coolers and one after-cooler. These coolers waste the excess heat to the environment. During the discharge process, the air from the storage is preheated before the combustion chamber thanks to the recuperator. This additional component is a heat exchanger that exploits the high temperature exhaust gas (at around 370 °C) from the turbine outlet to heat up the compressed air (up to 300 °C). According to [3.3], this modification reduces the fuel consumption by 25 % if compared to what happens in the Huntorf plant. After this preheating phase, the hot air feeds the first combustion chamber together with natural gas and the two stages (high and low pressure) of expansion. The main characteristics of the McIntosh DCAES system are reported in the following Tab.7.

Description	Value
Round trip efficiency	0.54
Input per kWh el. of Output [3.7]	0.69 kWh el. & 1.17 kWh natural gas
“Energy content”	2640 MWh
Charging/discharging time at full load	38 h / 24 h
Startup time—normal/emergency	12 / 7 minutes
Expansion	
Output power (min – max)	10 – 110 MW
Max mass flow rate	154 kg/s
Compression	
Rated input power	50 MW
Max charging air flow rate	90 kg/s
Storage	
Storage pressure range	46 – 75 bar
Storage volume	538000 m <sup>3</sup>
Cavern depth	-450 m

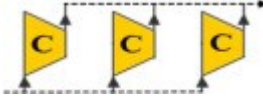
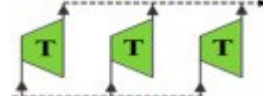
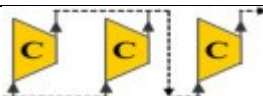
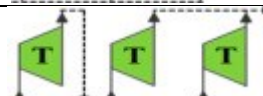


Tab.7 McIntosh plant specifications

As it is reported in the table, this kind of storage system is able to reach a round trip efficiency of 54 % thanks to the addition of the recuperator, which avoids fully wasting the energy content of the exhaust gas stream.

### 3.1.4 Technical characteristics and efficiency

In order to assess possible improvements for other plants, the role of each component in the system had to be analyzed. According to [3.3], the turbine isentropic efficiency has a relevant impact on the overall efficiency as it directly affects the power generation. In addition, also the inlet temperature of the gas before expansion has a relevant effect. For the high-pressure stages, an increase in the inlet temperature increases the RTE of the whole cycle and the power output, while for low pressure stages it would imply a larger waste energy stream in the exhaust gases. Of course, in the case of the recuperator, part of that energy would be reused. However, it should be highlighted that the addition of a recuperator increases the efficiency, but it delays the start of the generation at the start up. Regarding the compression phase, the efficiency could be increased by reaching lower temperatures thanks to the inter coolers (which improve the isentropic efficiency) and by using a larger number of compressors.

According to [3.4] an important characteristic of CAES plants is the configuration of the turbomachinery during the charge and discharge processes. In fact, the arrangement could be changed between parallel and series connection depending on the air pressure values inside the storage. As an example, at the beginning of the charge phase, the compressors might be operated in parallel to provide a larger mass flow rate. A series connection would otherwise bring the air to higher pressure but make it expand in the empty reservoir, consequently wasting energy. With the increasing pressure of the reservoir, the compressor arrangement could be gradually changed to series. Similarly, the same could be applied to the expansion process: at high pressures of the reservoir the turbines could operate in series, while for low pressure levels the turbines could operate in parallel configuration. An example of the schematic variations of the arrangement are shown in the following Tab.8. For underground caverns, however, a minimum pressure should be kept inside the reservoir in order to prevent the collapse of the cavern because of the weight of the surrounding ground. This means that if the pressure level is high enough, the turbomachinery should be able to work always in a series configuration, without making the system more complex.

Air storage pressure (bar)	Compressors arrangement	Turbines arrangement
$P \leq 4$		
$4 < P \leq 16$		
$16 < P \leq 64$		

Tab.8 Compressor and turbine arrangements

Regarding the reservoir characteristics, its size affects only the storage capacity and the charge/discharge time. However, it is very important to verify the injected air pressure and temperature limits in order to avoid damages to the cavern structure and leakages. If these limits are correctly established, the operation of the CAES system should be safe, as it is demonstrated by the Huntorf plant. In fact, after more than twenty years of operation, in 2001, the cavern was inspected proving limited changes in the storage dimensions.

### 3.1.5 DCAES Summary

Overall, for these systems the availability of natural caverns as air reservoirs is fundamental, both from the technical and economical point of view. In particular, aquifers and salt caverns are more economical than hard rock caverns, and if a natural reservoir is not present a large investment is required to provide one. The possibility of building such systems is therefore highly site dependent.

Another issue for these storage systems is the need for fossil fuels, which makes them less attractive in a carbon-free future perspective. Additionally, this makes them subject to the volatility of prices of fossil fuels, which may make them very costly. In the end, it should be remembered that CO<sub>2</sub> emissions are regulated by the Emission Trading System, adding a further cost to the operation. According to [3.2], CAES systems have low energy and power density as they need very large volumes to store and release energy. Frequently, being the reservoir underground, the large volume needed does not represent a particular problem. However, particular care should be taken to avoid any environmental impact due to the modifications of the caverns. Concerning the efficiency of DCAES systems, the values are quite low as they range between 30 and 55 % depending on the load. Positive aspects of DCAES systems are the well-proven technology, which is based on gas turbines, and the long life of the asset, which is expected to last for more than 40 years. Regarding the economic performance, the Levelized Cost of Storage is pretty low for this technology, but still subject to the market prices variations of fossil fuels. In the end, these systems can mainly be used for energy-shifting of large amounts of energy thanks to their large storage capacity for large periods of time, and so they are suitable for avoiding renewable curtailment during periods of overgeneration. The regulation services, in terms of voltage and frequency, cannot be provided by these plants as they would need a faster response. Additionally, they can provide black start to the grid. The main characteristics of DCAES systems, based on the existing plants, are reported in the following Tab.9.

Power	Discharge time	Lifetime	RTE	Energy Density	CAPEX [3.6]
100 – 320 MW	2 – 24 hours	30-50 years	29 – 54 %	2 – 5 kWh/m <sup>3</sup>	400 – 1200 €/Kw

Tab.9 DCAES summary

Where the Energy Density was calculated as:

$$En. Density = \frac{P_{out} \cdot T_{discharge}}{V_{reservoir}}$$

An example of a DCAES commercial solution is the one proposed by Siemens [3.13], which offers solutions for the compression and expansion train. Regarding the compression train, the company proposes a rated power up to 125 MW per train, while for the expansion train it proposes a maximum power output up to 160 MW. Regarding the responsiveness of these system, the company claims a 4-minute time to achieve full power compression and 10 minutes time to achieve full power generation. Additionally, it is reported the possibility to operate the firing process with 50% hydrogen and natural gas co-firing, with the objective of 100 % hydrogen fuel by year 2030.

### 3.1.6 ACAES

In order to achieve higher efficiencies and better environmental performances, other types of CAES systems have been developed, like Adiabatic CAES (ACAES). Differently from DCAES, ACAES systems are able to exploit the heat that is generated during the compression of air. This way, it is not needed an external source of heat, and the round-trip efficiency of the storage should be higher. Moreover, by removing the need of fossil fuel firing, this storage solution presents the advantage of avoiding GHG and pollutant emissions.

In order to achieve this, the inter and after coolers (during compression) and the preheaters should exchange heat with the additional hot and cold thermal energy storages. A schematic of the ACAES concept is shown in Fig.67.

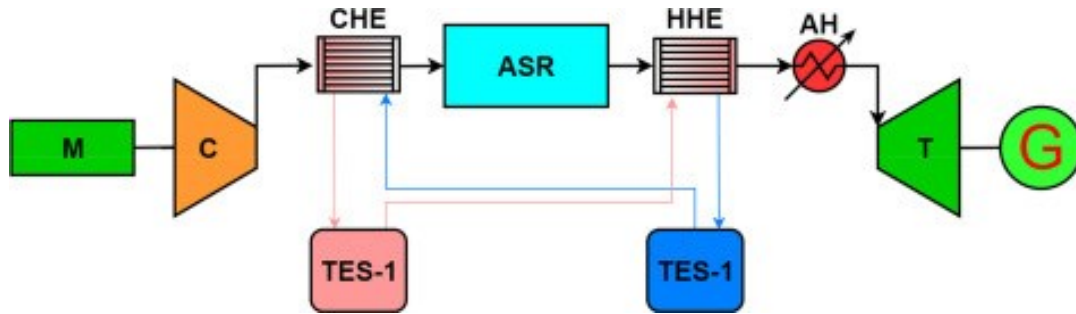


Fig.67 ACAES concept scheme from [3.4]

According to [3.5], the compressor discharge temperature could exceed 600 °C during the charge phase. This high temperature stream can be cooled through an after cooler and the heat can be stored in a hot storage. During the discharge phase, the heat from the thermal storage can be sent to another heat exchanger to preheat the compressed air before the expansion train. If the heat was not enough before the expansion, external heat could be provided through an auxiliary heater, as it is shown in the figure. However, the objective of ACAES is to avoid the need of external heat sources.

The thermal energy storages used for these systems could be liquid thermal storages or of the packed bed type, with beds of particulate rock or brick/concrete lattices [3.7]. Considering that the system works with high pressure air, this introduces some constraints for the thermal storages. In particular, for liquid thermal storages, the heat exchanger liquid-air should withstand high pressure on the air side. For packed bed thermal storage, instead, the storage itself should support high internal pressures, as the air flows through the bed both during charge and during discharge, exchanging heat with the bed materials. These requirements may increase the costs of the system. For liquid thermal storage, the fluid choice should be optimized depending on the temperature levels reached. Usually, water would be the preferred choice, but its use for higher temperature storages requires high pressure levels. Possible alternatives are also the use of molten salts or thermal oils, which are used also in solar thermal applications [3.5; 3.4].

Some challenges that compressed air systems have to face regard the use of air compressors. In fact, the pressure increase during the charge is relevant, as for CAES systems it is suggested to operate between 40 and 100 MPa. The temperature increases during compression have to be managed carefully in order to get good compressors efficiency and to recover heat useful for the thermal storage. Another issue regards the heat exchangers, which should be able to recover as much energy as possible minimizing



pressure drops and exergy destruction. Therefore, the heat should be stored at the highest possible temperature. Finally, some issues have to be addressed also for the turbines. In fact, the turbines for compressed air systems usually work with lower temperatures and higher pressures compared to the ones of traditional gas turbines. Therefore, condensation or freezing problems during expansion should be avoided or kept between sustainable limits. Moreover, the high air density may increase the frictional pressure losses [3.7].

### 3.1.7 Commercial examples

Among the different concepts presented for CAES systems, the Canadian company Hydrostor [3.8] presented a slightly different version of underground storage. In their storage system, the air is compressed and stored in artificial caverns built underground, and it is kept under pressure through hydrostatic compensation. An artificial lake aboveground stores the water used by the plant: when the air storage is charged the water moves upwards to the lake and keeps the pressure level thanks to the water column. When the system is discharged, instead, the water forces the air out of the cavern, gradually filling the underground reservoir and emptying the aboveground lake. This solution seems to balance the advantages of isochoric and isobaric storage systems.

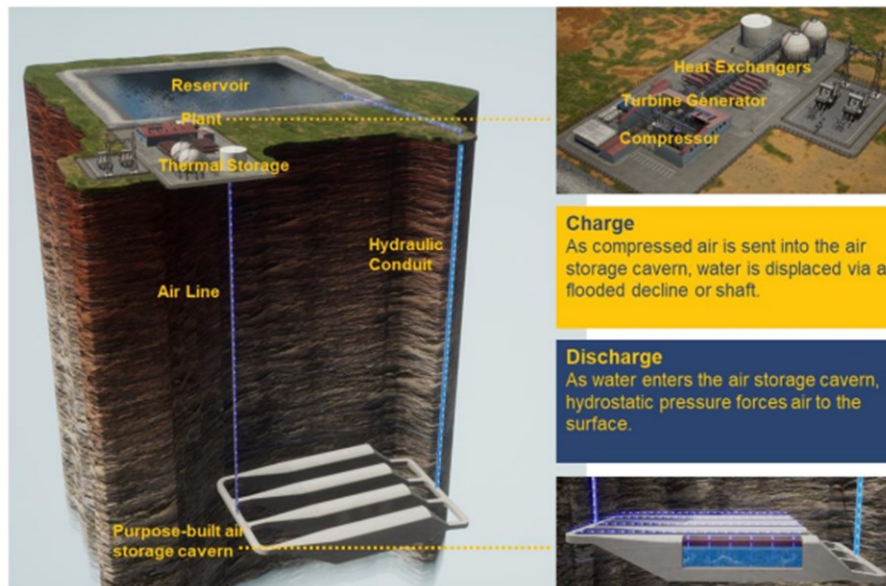


Fig.68

The company realized the first ACAES commercial plant in the world: a small-scale system in Goderich, Ontario, Canada. According to the company, the plant has an output rated power of 1.75 MW, an input rated power of 2.2 MW and a total storage capacity of around 10 MWh.

Other projects that are being developed by the company can show the potential future applications of the ACAES technology. A large-scale project example is the Willow rock energy storage center, in California, USA. This project should have a capacity of 4 GWh, with a rated power output of 500 MW and 8 hours duration. Another example in California is the Pecho Energy Storage Center project, which should have a 3.2 GWh capacity with a rated power of 400 MW and 8 hours duration. This shows how ACAES could be useful for utility scale energy storage as pumped hydro.

### 3.1.8 ACAES Summary

ACAES systems are based on the same concept of DCAES systems and have the potential to achieve better efficiencies avoiding GHG emissions. The additional complexity due to the addition of thermal storages introduces the challenges previously reported. In these plants, the thermal management is the critical point. The power and capacity potential characteristics of these plants is similar to DCAES plants and could even reach the GWh scale for suitable sites. Also, the expected lifetime of the plants is similar to the one of DCAES systems: Hydrostor [3.8] declares 50 years of lifetime. However, the investment costs result to be higher as the systems are not yet commercially widespread, as highlighted by EASE [3.5].

Power	Discharge time	Lifetime	RTE	Energy Density	CAPEX [3.5]
100 -500 MW	8 – tens of hours	30 – 50 years	40 - 75%	2 – 5 kWh/m <sup>3</sup>	1200 - 2000 €/kW

Tab.10 ACAES summary

According to [3.7], ACAES systems should be able to reach high round trip efficiencies in the range 65 – 75 %, while EASE [3.5] claims that efficiencies might be larger than 70%. Another example is given by [3.10], where a small experimental system, the TICC-500 has reached an efficiency of 33 %, with a design target of 41.03 %. The TICC-500 system scheme is reported in the following Fig.69. Differently, according to [3.11], a low temperature ACAES concept may reach efficiencies ranging between 52 and 60%. Considering that utility scale plants have not been deployed yet, uncertainties are still wide, but with technological developments it is expected that round trip efficiencies may realistically reach around 60%.

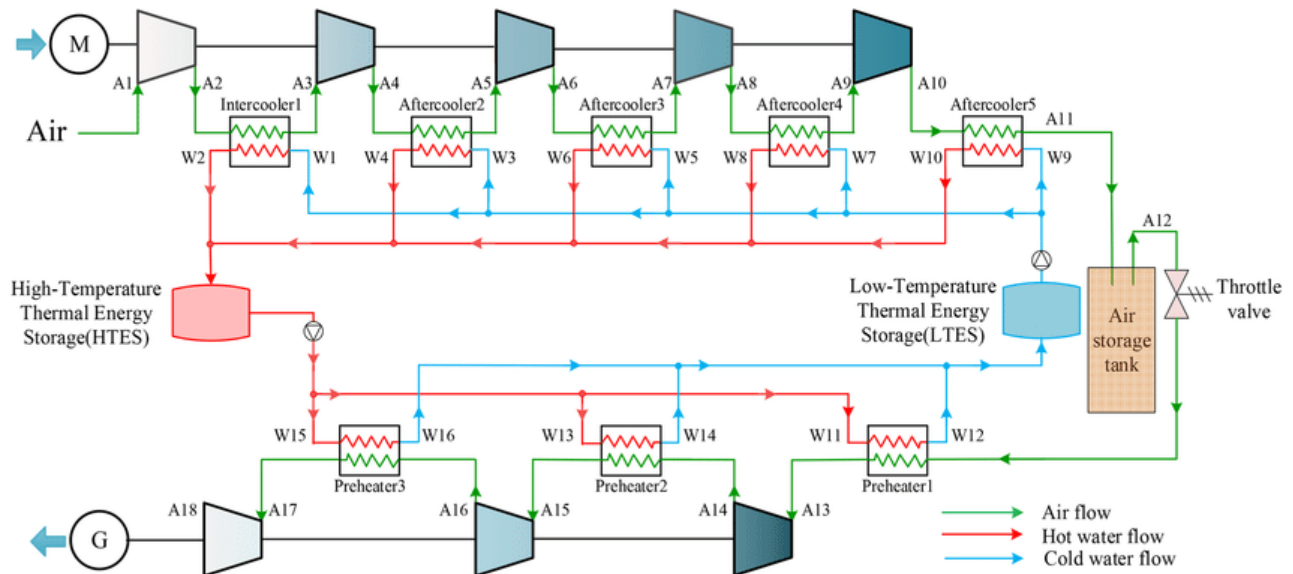


Fig.69 TICC-500 ACAES plant scheme [3.9]

### 3.1.9 Isothermal CAES

Isothermal CAES is still a research topic for energy storages. This technology is based on isothermal compression, a process through which the air is compressed without any increase of its temperature. Different solutions have been developed and are being studied to achieve quasi-isothermal compression [3.7]. The main characteristics of each of these methods are reported in the following and illustrated in Fig.70.

- Direct heat transfer enhancement

This first solution is based on achieving a larger heat transfer with the mechanical components of the compressor, which would then transfer this heat to the environment. This result could be obtained with finned compressors.

- Indirect heat transfer

This second method relies on the presence of a secondary fluid in the compression chamber, which should absorb most of the heat generated during compression. Some examples have been developed with water injection. However, the moisture content should be managed carefully to avoid corrosion or condensation that may affect the operation of the system.

- Liquid piston

The third solution is based on the use of liquid displacement to compress and expand the air. During charge, a liquid is pumped in the vessel containing air, slowly compressing the air volume. During discharge the air pressure gradually releases as the liquid drives a turbine. The slow processes involved allow a near-isothermal compression. An advantage of this method is the use of hydraulic pumps and turbines, which are usually less costly and highly efficient.

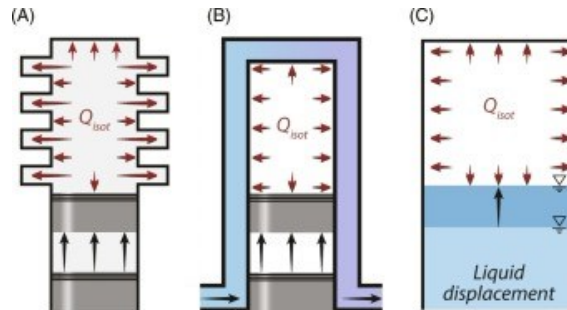


Fig.70 Isothermal compression methods

The heat extracted from the compressor and the cold generated during the expansion, could be used for some heating and cooling applications to increase the overall energy utilization. However, a higher power output is obtained storing the heat of compression and providing it during discharge before the expansion, as it happens in Adiabatic CAES. According to [3.12], aiming mainly at the power generation, ICAES systems may reach electrical round trip efficiencies of 71.8 %. Overall, Isothermal CAES is still not commercially available. Nonetheless, it has some potential as it does not need external heat sources. Moreover, higher pressure ratios can be achieved with single stage compressors thanks to the lower temperature reached that does not exceed the material's limits. According to [3.7], with isothermal compression, it should be possible to achieve high round trip efficiencies.



## 3.2 Liquid Air Energy Storage

Liquid air energy storage (LAES) store and release energy through liquefaction and regasification processes of air. Differently from compressed air energy storage, these systems can store energy with low pressure, and they reach very low temperatures, therefore it is a cryogenic type of storage. Schematically, when excess energy needs to be absorbed, the system starts the liquefaction process of air. This liquid air is then stored in cryogenic tanks to later be used, while the heat extracted during liquefaction is stored in hot thermal tanks. When additional energy is requested from the grid, the LAES system discharges the accumulated energy pumping, heating and expanding in turbine the air. During the discharge, the cold energy removed is stored for a later use during the following liquefaction process through cold thermal tanks. The concept is illustrated in the following Fig.71 by [3.18].

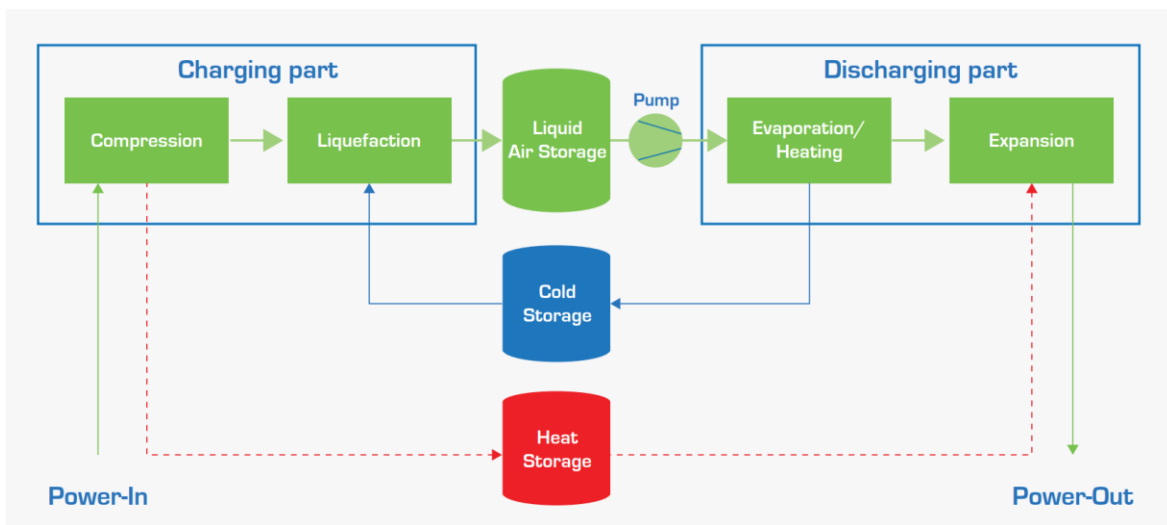


Fig.71 General LAES system scheme [3.18]

The liquefaction process typically is performed at high pressures, as it allows to achieve liquid state at higher temperatures [3.15]. As it happens in compressed air energy storage systems, the air compression phase generates some heat which is undesired. Consequently, this heat has to be removed through heat exchangers during the multi-stage compression to be able to achieve liquefaction and to improve the efficiency of the compression phase. In order to achieve higher round trip efficiencies, the removed heat is usually stored in a hot thermal storage to be used in the subsequent power generation cycle. Then, to reach the cryogenic temperatures needed for liquefaction the air flow releases heat to a series of cold thermal storages, which are usually liquid refrigerants like methanol or propane, but they could also be packed bed thermal storages. Frequently, different refrigerants are used to achieve good cooling efficiencies for each temperature range of operation. The temperature level that has to be reached to achieve condensation depends on the pressure at which the system works. In the example reported by [3.15], the temperature here may reach  $-190\text{ }^{\circ}\text{C}$ . After condensation is complete, the pressure is usually reduced through a cryogenic turbine or an expansion valve, and the temperature is further reduced during expansion. In case of expansion to the atmospheric pressure, the air reaches a temperature of  $-196\text{ }^{\circ}\text{C}$ . After the expansion, there is a mixture of liquid and gas, and consequently a separation of the two phases

has to be carried out. After this, the liquid air is stored at low pressure in a vessel until the discharge of the system is required.

The liquefaction processes can be carried out through different cryogenic inverse cycles. For air liquefaction, the Linde-Hampson cycle could be performed. In this cycle, the air is compressed up to 200 bars approximately, and then it is cooled through some heat exchangers up to cryogenic temperatures. Then, the air is expanded through a Joule-Thomson expansion valve. In order to achieve a further reduction in temperature and the formation of a liquid vapor mixture, the Joule-Thomson coefficient has to be positive. Furthermore, the temperature needs to be sufficiently low, otherwise the expansion doesn't enter the saturation curve as it can be seen in 3'-4' in Fig.72.

$$\mu = \left(\frac{dT}{dP}\right)_h > 0$$

After the expansion, the liquid and the gas are separated, and the gas is sent back to the liquefaction heat exchangers. An ideal scheme of the cycle is presented in the following Fig.72.

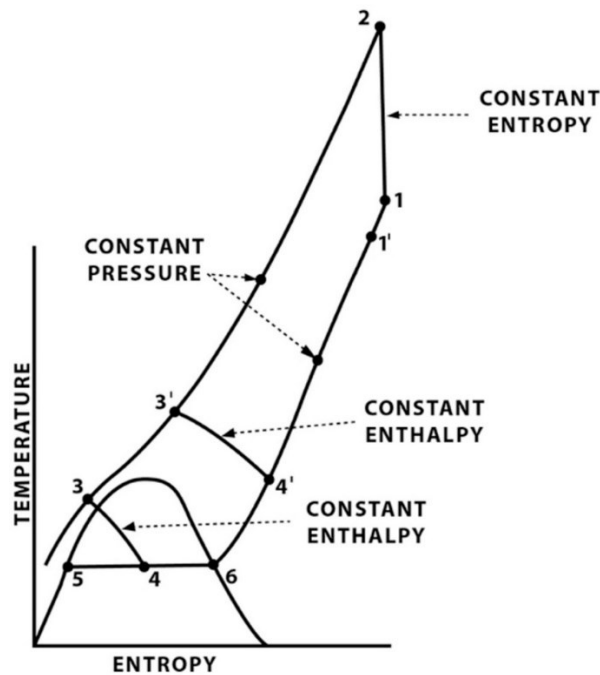


Fig.72 Linde-Hampson ideal cycle by [3.15]

Unfortunately, this cycle is considered to be unfeasible for commercial scale LAES. Its power consumption per unit of liquefied air is in the range 2.5-2.6 kWh/kg. It should be noted that actually the compression process is not isentropic as represented, but it is usually considered to be adiabatic and carried out with a series of stages with intercooling, therefore being able to consume less energy.

An alternative to the Linde cycle is given by the Claude liquefaction cycle. This one represents a modification of the original Linde cycle, where a recirculation mass flow is added. The main modification consists of part of the compressed mass flow rate being expanded through a turbine. This allows to

recover some energy while decreasing the temperature of the separated gas stream. The cold gas stream is then used to exchange heat with the incoming air flow to further cool it down. For these cycles the recirculation fraction is defined as the ratio between the recirculation and the total compressed mass flow rate:

$$r_f = \frac{m_{JT}}{m_c}$$

A further difference is given by the lower pressure level reached after compression, in the order of 50 bar. The scheme of the cycle is represented in the following Fig.73.

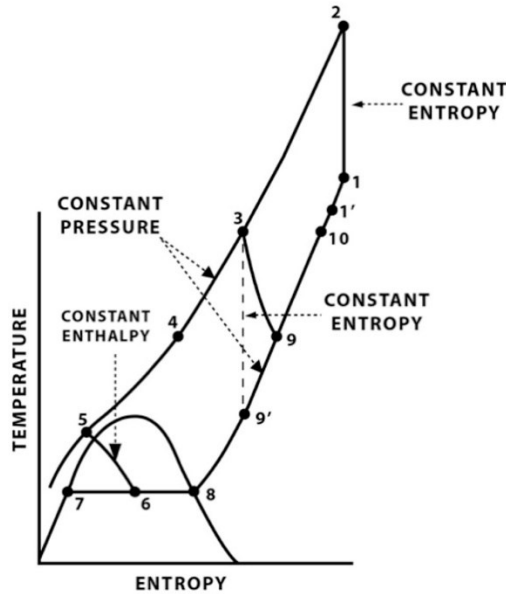


Fig.73 Claude ideal cycle by [3.15]

As for the previous scheme, the compression is represented as a single isentropic transformation, while it usually consists of a series of adiabatic compressions with inter-cooling phases. Similarly, the expansion is represented as isentropic, while in real applications it can be seen as adiabatic. These modifications to the Linde cycle allow to achieve liquefaction with lower power consumption, in the range 0.72 – 0.73 kWh/kg with a double stage compression.

Other alternative cycles are the Kapitza and the Heylandt cycles, as improvements of the Claude cycle. The Kapitza cycle's modifications consists of the removal of the low temperature heat exchanger and on the addition of a low temperature turboexpander. These modifications allow to sustain a larger flow rate while removing a component, the heat exchanger, which was responsible only for a minimal temperature reduction. For this cycle, the power consumption could be in the order of 0.71 – 0.72 kWh/kg.

The Heylandt cycle, instead, removes the high temperature heat exchanger and inserts the by-pass line for recirculation directly after the compression phase. According to different researches cited by [3.15], optimizing the specific consumption of these cycles, values around 0.5 kWh/kg could be obtained.



When the system has to be discharged, a power cycle has to be performed in order to generate electrical energy. Different possibilities are available: direct expansion of air, Rankine cycles, Brayton cycles and other combinations. In the case of Rankine cycles, as the liquid air from the tank is pumped to a high-pressure level, then it is evaporated and superheated to be finally expanded in a turbine. Firstly, the pumping process is carried out by a cryogenic pump, as it has to be able to operate at  $-196\text{ }^{\circ}\text{C}$  as in the example. Then, regarding the evaporation process, the heat is usually provided by the refrigerants in the cold storage which were previously used during the liquefaction process. This allows to achieve evaporation while recovering and storing the cold energy for the subsequent liquefaction processes. After that, the air is superheated by exchanging heat with the hot secondary fluid from the hot thermal storage. This process further improves the efficiency of the process as it provides a second use of the heat generated during air compression in the charging phase. The evaporation and superheating phases cause significant expansion of the air, in the order of 700 times. Similarly to what happened for the compression, the expansion is subdivided into many stages with superheating phases in between. The superheating allows to increase the temperature of the air and the power generation, as during each expansion in turbine the air temperature decreases. A detailed scheme of the LAES system is reported in the following Fig.74. It is possible to observe the subdivision in different stages for the compression with inter-cooling and the expansion with re-superheating. Additionally, it is possible to see the intermediate cycles for hot and cold thermal storage: the hot storage removes heat during the compression and provides it during expansion, while the cold storage removes heat during condensation and provides it during evaporation. It should also be highlighted the presence of a line that collects the air that spontaneously vaporizes inside the cryogenic storage and recirculates it to a second liquefaction process, once again recovering the cold energy with the cold storage.

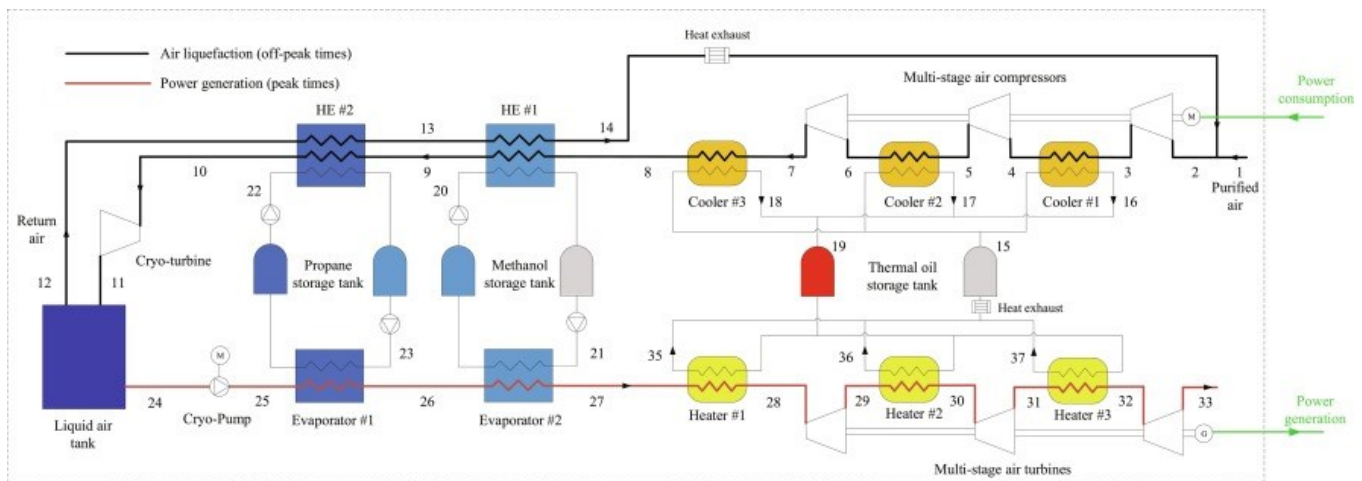


Fig.74 Detailed scheme of a standalone LAES by [3.15]

Alternative configurations for the power generation process are made by the combinations of different cycles. An example is the possible combination of Rankine cycles with Organic Rankine cycles and with Absorption or vapor compression Refrigeration Cycles. In particular, ORCs may be suitable for power generation as they allow to recover low temperature or below ambient temperature heat. These systems might be able to exploit the waste heat generated by the compression processes, while refrigeration cycles



might lower the condensation temperature of the ORC. The available combinations might allow a larger power generation and a larger RTE of the system. According to [3.15], RTE of 55.7 % could be obtained with the combination of ORC and ARC. Another possibility is given by the use of vapor compression cycles used to accumulate cold energy during off-peak periods, to later be used by the ORC.

### **3.2.1 Existing plants**

The first built LAES system has been developed by Highview power storage and the University of Leeds [3.14]. The plant was built and operated between 2009 and 2012, and it was a pilot plant with 350 kW power and 2.5 MWh storage capacity. This system can reach 80% of its nominal power with a 2-minute start-up time [3.15]. However, this first system showed a very low round trip efficiency of 8% [3.16]. Nonetheless, the system showed the possibility to operate such systems and the opportunities to improve its efficiency. In 2018, the same company, Highview, started the operation of a pre-commercial plant of relevant size in Manchester UK with 5 MW nominal power and 15 MWh storage capacity. According to [3.17], this plant has reached an RTE of 60% as a standalone system.

### **3.2.2 Technical characteristics and efficiency**

According to [3.14], the LAES systems could be able to provide frequency regulation services thanks to their quick response time of 2 minutes and half in a normal operation mode. Adopting the spin generation mode, instead, the response time of the system could be shortened to less than 10 seconds for even better frequency regulation activity. To apply this second type of operation, the air turbines should be synchronized to the grid before the dispatch is expected by the system. Another option could be to combine these systems in normal operation mode with other storages specifically for frequency regulation like batteries, supercapacitors and flywheels.

Another important feature of LAES system is the possibility to provide black start. This is possible as the system needs a minimum amount of energy to start up and start providing power to the grid. In particular, to provide black start, a battery would be needed to start up the cryogenic pump and to drive the valves of the systems. This should initiate the system discharge, energizing other plants and restoring the grid operativity.

Standalone LAES plants aim at storing liquid air and hot and cold energy to later generate electricity. Other possible configurations of LAES systems, different from the previously presented, allow to use the heat and the cold stored also for different uses. These systems need to be coupled with other final uses and are called Advanced LAES, as they are able to provide trigeneration. During the compression phase, the excess heat can be stored at around 200 °C and used for heating or for cooling applications through absorption or adsorption cycles. A good thermal management can lead LAES to provide cooling, heating and hot water services. Of course, the use for purposes different from the power generation significantly decreases the electrical efficiency of the storage system, but it leads to achieving overall higher efficiencies. According to [3.14], advanced LAES can achieve round trip efficiencies of 75%, while standalone systems for electrical power generation can achieve efficiencies in the order of 50 to 60%.

### 3.2.3 LAES Summary

Summarizing LAES main characteristics, these systems can provide frequency services, black start and hot and cold to other energy uses as previously mentioned. Moreover, LAES systems have the advantage of the possibility of storing energy at low pressure, which is better in terms of safety compared to highly pressurized solutions. However, very low temperatures have to be reached and maintained. This means that thermal management is very important to achieve high efficiency, as low temperatures can be achieved with high power consumption. Additionally, the storage insulation is fundamental not to lose cold energy because of the boil off. The liquid air storage has also the advantage of achieving a relatively high energy density, as a large amount of air can be stored in a compact volume, around 700 times smaller than CAES systems. Compared to CAES, LAES has also the advantage of not being geographically constrained, as it doesn't need a natural reservoir to store the air. Conversely, it needs a purposely built vessel to store the cryogenic liquid. Regarding the lifetime of the system, it is expected to be long as it happens for CAES systems, as according to [3.14] it may reach 40 to 60 years while according to EASE [3.18] it is expected to be between 30 and 40 years. The main characteristics of the LAES systems are summarized in Tab.11.

Power	Discharge time	Lifetime [3.14]	RTE [3.14]	Energy Density	CAPEX [3.15]
1 - 200 MW	-	>30 years	50 - 60 %	120 kWh/m <sup>3</sup>	1270 – 2090 €/kW

Tab.11 LAES summary

Here, the round-trip efficiency refers to the electrical efficiency, as the main objective was intended to be storage of electrical energy. Some studies cited by [3.15], claim that RTE up to 65% could be obtained with two packed bed cold thermal storages. Other studies cited by [3.16], claim that RTE of 64 % could be obtained with multiple fluids for cold storage optimization, while RTE up to 55 % could be reached working on the compressors and turbines isentropic efficiencies and on working pressures optimization. Integration with other systems could further improve the performances of LAES systems, like coupling with LNG regasification or Air separation Units, or even nuclear power plants. In [3.17] a comparison of different publications shows how for standalone systems the expected RTE is confirmed to be between 50 and 60 %, while for integrated systems it could be higher. Among the available possibilities for LAES, as explained by [3.14], these systems could be used also for other concepts like ammonia production or to produce liquid air and use it as an energy carrier. As an example, liquid air could be produced offshore by wind farms and then transported by ships, to be later used for power generation where required.

### 3.2.4 Commercial examples

Among the new projects for LAES systems, Highview is developing new plants in the UK, Spain and Australia [3.19]. In the UK, the company is working on two plants, the first one being a 50 MW power plant near Manchester with 300 MWh storage capacity. The second project regards a large-scale plant in the Yorkshire region, with a 200 MW power and 2.5 GWh storage capacity. In the end, in the Canary Islands, a 300 MWh capacity is under development.

### 3.3 Gravity-based Energy Storage

Gravity-based energy storage systems are mechanical energy storages which rely on the displacement of weights against gravity to accumulate potential energy. Different concepts have been developed for these systems, including above ground and underground solutions and also offshore/floating solutions. All these systems exploit a difference of height to lift and lower some weights to store and release electric energy.

$$E_{stored} = m \cdot g \cdot h$$

For these storage solutions it is of main importance to be able to exploit a large height difference between the charged and discharged configuration of the plant. The reason is that the energy that can be stored increases linearly with the height, given the weight. The main concepts of this type of storage are presented by [3.20] and schematically represented in Fig.75.

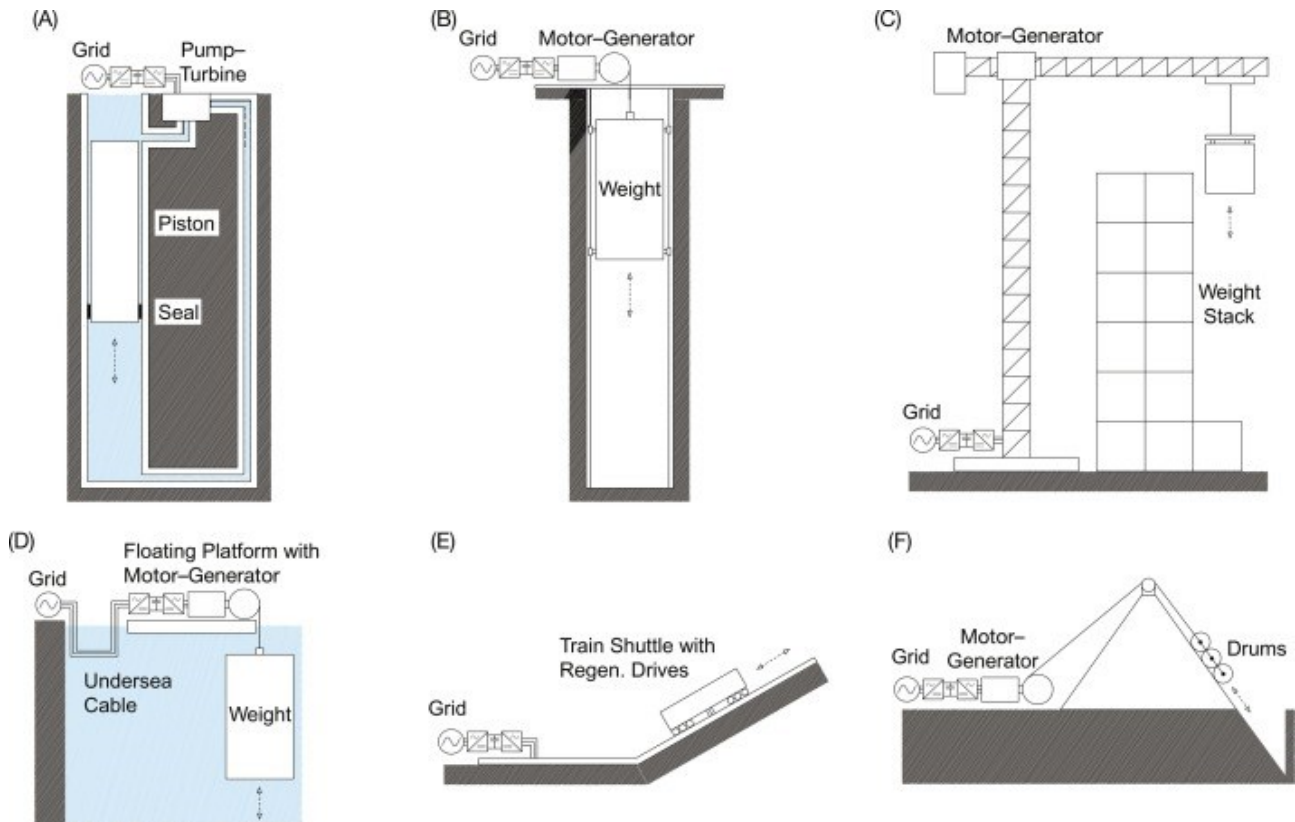


Fig.75 Schematic of different gravity-based energy storage solutions by [3.20]

#### 3.3.1 Gravity-based storage concepts

The “Gravity Power” project is an underground gravity storage system (A). According to this concept, the energy could be stored and released through the movement of a heavy piston in an underground shaft. This piston could be moved by pumping water from above to a below chamber, therefore charging the system. During discharge, instead, the weight would keep the water under pressure and drive the pump-

turbine in turbine mode, thus generating electricity. Among the underground solutions, there is also the “Gravitricity” concept (B), which is based on lifting and releasing very large weights (500 to 5000 tons) in deep underground shafts. Regarding above-ground solutions, “Energy Vault” seems one of the most promising for large scale applications (C). The storage concept consists of a central tower with six crane arms lifting and releasing weights of around 35 tons. During the charge phase, the tower lifts and stacks weights somehow building a tower made by the weight blocks. During the discharge phase, instead, the central tower lowers the blocks to the ground. Similarly, another concept is available, in which an array of blocks is lifted and stored at high floors to be later released. Regarding gravity systems operating with inclined planes, there are concepts like “Advanced Rail Energy Storage”, which relies on automate trains with regenerative traction (E). These trains should carry 45 tons weight, uphill and downhill through terrains with a maximum inclination of 8.5 %. During charge phase, the trains should be moved uphill by electric motors, while during the discharge the trains should generate electricity through regenerative braking while downhill. A similar solution is “GravitySoilBatteries”, which is based on lifting and releasing heavy drums on an inclined plane with electric motors-generators (F). In this concept, the slope is artificially created with an aboveground concrete structure and with excavated side channels to store the released drums. Finally, a proposed offshore solution is “SinkFloatSolutions”, where a weight is lifted and released into the sea from a floating platform (D). This solution in particular could be coupled in place with offshore wind. In the end, another concept is given by the buoyancy energy storage, where buoys could be placed on the seabed and connected to a motor/generator through a cable.

### 3.3.2 Technical characteristics

For above-ground systems, the weights can be moved vertically or on inclined planes. The vertical configurations should reduce friction losses, but they require more complex construction and might be unacceptable because of the landscape modification [3.20]. Conversely, underground solutions could be more easily accepted as they do not modify significantly the landscape. However, underground storages may need excavations if the shaft is not already available, therefore increasing the investment costs. To improve the economic performance of these plants abandoned mines could be used. Regarding inclined aboveground solutions, the main problem is the large area required for the operation of these systems, as the maximum inclination of the plane is very low to allow the uphill movement. However, these systems do not require large works and they might exploit the site features. For offshore concepts, the problem is to balance between the water depth availability, which represents the height difference between the charged and discharged system, and the distance from the land. Larger water depths mean larger energy storage capacity, while larger distance from the land means larger investments on transmission and larger losses. The site choice represents a fundamental part for this type of project and for its optimization.

Regarding the lifting mechanisms, most of the concepts use wire rope hoisting mechanisms. These wires can hold considerable weights (given that the world's largest crane can sustain up to 20,000 tons) and can be used in mines with more than 2000 m depth. Therefore, the potential energy capacity is relevant, but strongly dependent on the site and on the feasibility. An example based on the previous data is reported in the following equation (without considering efficiencies).

$$E_{theoretical} = m \cdot g \cdot h = 20000 \text{ ton} \cdot 9.81 \frac{m}{s^2} \cdot 2000 \text{ m} = 109 \text{ MWh}$$

Another possible lifting mechanism which has been considered is the linear electric machine. For the Gravity Power concept, the lifting mechanism consists of pressurized water, therefore this type of system relies on turbomachinery for hydropower. While using standard hydro equipment, this introduces some complications as the system works under pressure and the piston requires sealing. Given these necessities, this type of system requires shafts built on purpose or purposely modified.

Of great interest is the possibility of avoiding excavations for the other types of storage by using existing underground structures for these systems, as the excavation phase might be the largest cost component. However, the different site characteristics may affect the design of the system equipment therefore avoiding the cost reduction achievable through standardization.

Regarding the use of these systems, they might be useful for grid regulation thanks to their high responsiveness, but also for energy shifting as they are able to discharge over long periods of time and can store relevant amount of energy in case of multi-weight systems. A limit for the energy capacity of the system is given by the strength of the lifting mechanism and of the support structure. Additionally, another limit is the available space for storing the weights in the upper and lower storage areas. The tower solution by Energy Vault removes the need for an upper and lower area by piling up the weights, with the drawback of reducing the height difference and consequently the energy capacity. It should be highlighted that the horizontal movements of the weights reduce the efficiency of the storage, and the coordination of multi-weight systems is fundamental to provide a continuous power absorption or generation.

### 3.3.3 Commercial examples

Gravity based energy storage systems have not been commercially deployed yet. However, some test plants have already been deployed, and some medium/large systems are under development so in the next years these systems could spread rapidly thanks to their high efficiency levels and low costs. To mention one of them, ARES has developed its advanced rail energy storage solution “Gravityline” [3.23], claiming that it may be scalable between 5 MW up to 1 GW of installed power. In particular, each train track should provide 5 MW power for a period of time ranging between 15 minutes and around 24 hours. Additionally, they claim that their system should be able to reach the maximum charge or discharge power in around 3 seconds. The declared round trip efficiency of the system is higher than 90 % while the declared system lifetime is higher than 40 years. As reported in [3.20], instead, the efficiency of ARES should be between 78 and 80 %. The company is currently working on the development of a 50 MW project in Nevada at Gamebird Pit. This project should include a total of 210 mass cars, for a total weight of 75000 tons. The system is conceived to provide ancillary services for the California Independent System Operator (CAISO) due to the high responsivity of the storage.

Among the other companies that seem to have achieved promising results there is Energy Vault. This company has developed different types of gravity storage, among which there is the EV1 Tower. This energy storage commercial demonstration unit, sited in Castione in Switzerland, entered in operation in

July 2020. A picture of the system is shown in [Fig.77](#), while the working principle is shown in the following [Fig.76](#).



Fig.76 Energy Vault tower working principle [3.24]



Fig.77 Energy Vault CDU EV1 tower [3.24]

According to the company, this kind of system can store 20 or 35 or 80 MWh depending on the design, and it can achieve output power between 4 and 8 MW with a discharge time between 8 and 16 hours. According to [3.22], the commercial demonstration unit achieved a 75% round trip efficiency, but for the next systems the expected round trip efficiency is between 80 and 85%. Instead, [3.21] reports that the efficiency could reach values up to 90 %. It should be highlighted that for the tower concept, the visual impact might be relevant for the local acceptance of the system, as the tower is 120 m tall. The same company developed also a different modular solution: the EVx. Several EVx modules would be part of Energy Vault Resiliency Centers (EVRs), which are box-like buildings inside which 30 tons weights would be lifted and released. Each module should be able to accumulate 10 MWh with around 1300 weights, and their height could reach 120 m (but the company claims that new systems will present



40 % lower height). In terms of occupied area, as reported by [3.22], 100 MWh storage would require about 9713 m<sup>2</sup> of land. The following equation shows that the overall energy density of the system is very low, representing the main disadvantage of gravity systems.

$$\text{Energy Density} = \frac{100000 \text{ kWh}}{(9713 \text{ m}^2 * 120 \text{ m})} = 0.08 \frac{\text{kWh}}{\text{m}^3}$$

In terms of sustainability, the company claims that the weights can be made of waste and recycled materials like coal combustion residuals, fiberglass from de-commissioned wind turbine blades and waste tailings from mining processes. The declared system lifetime is of 35 years. Among the future plants, the company is developing 2 GWh EVRC and a 100 MWh storage in China [3.24] and also 1.6 GWh in the USA [3.22].

Another company that is carrying on the gravity-based storage technology development is Gravitricity. Their concept is based on the use of existing or purposely built underground shafts for weight displacement. According to [3.22], the company completed the 250 kW above-ground demonstration unit in 2021 in Edinburgh. This system was placed on a 15 m high tower, and it moved two 25-tons weight. The Gravitricity demonstrator plant is shown in the picture Fig.78. According to [3.22] this system should achieve round trip efficiencies of around 80 % and the demonstrator was able to get to full power in less than a second, proving the very high responsiveness of the system.



Fig.78 Gravitricity's demonstrator unit picture from [3.22]

The company claims that Gravitricity systems have a design lifetime of 50 years and that their power output will be ranging between 1 and 20 MW [3.25]. The company is now working on its first full scale project, which could be located in Czech Republic exploiting a decommissioned mining site. Future systems might have 4 to 8 MW size and it is claimed that multi-weight systems might have a capacity of 25 or more MWh. The masses that in the future could be used by Gravitricity might be in the order of 1000 tons size and made of high-density materials.

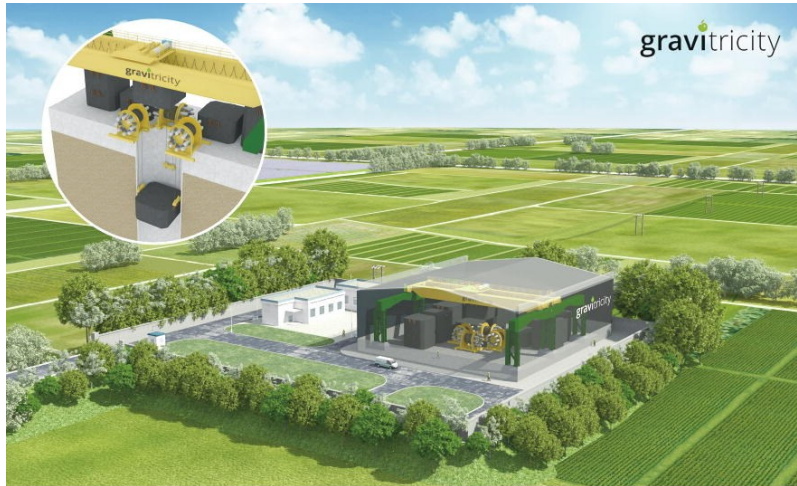


Fig.79 Gravitrlicity’s “Multi-Weight” Storage System by [3.25]

### 3.3.4 Gravity Energy Storage Summary

The data presented in the following [Tab.12](#) refer to the characteristics of the main types reported as commercial examples.

Power	Discharge time	Lifetime [3.23; 3.24; 3.25]	RTE [3.23; 3.24; 3.25]	Energy Density	CAPEX [3.21]
5 MW – 1 GW	15 min. – 24 hours	35 - 50 years	80 - 90 %	0.08 kWh/m <sup>3</sup>	1750 - 2000 \$/kW

Tab.12 Gravity energy storage summary

For gravity storage systems the power is typically low, in the order of 4 – 8 MW. However, the possibility of combining modular solutions expand the power range up to the theoretical GW scale (both for ARES and EV). For this large power range, the only limit is the availability of space required which is the weak point for these systems. Their energy density is in fact very low, as it was previously shown in the calculation for the EVRC case, and large space and considerable heights might be required for above-ground systems. Conversely, for underground systems, the land occupation issue is less relevant but investment costs for excavations and site constraints become critical points. In terms of responsiveness and flexibility of discharge time, these systems have great potential thanks to the response time in the order of seconds and to the possible regulation of the discharge velocity of weights. The coordination of multi-weight systems has to be carefully addressed to keep the power under control. The CAPEX reported in the table refers to the Energy Vault tower solution with 35 MWh capacity and 4 MW power, that according to [3.21] it was estimated to be ranging between 200 and 230 \$/kWh. The round-trip efficiency for gravity system is always pretty high and around 80 %, but most of the constructors expect even larger RTEs up to 90 %. Regarding the lifetime of the systems, as cited in the commercial examples, most of the systems have long expected lifetime, always higher than 35 years. Overall, these systems have large potential for storage applications thanks to their low expected maintenance and long lifetime, especially where the visive impact and the large land occupation are not so relevant.



### 3.4 Liquid Carbon Dioxide Energy Storage

The energy storage based on the liquefaction of carbon dioxide is a novel application, similar to the concepts of the liquid air energy storage and compressed air energy storage. The Italian company that commercially proposed this concept is Energy Dome [3.26], which developed two different possible plant schemes: the CO<sub>2</sub> battery and the CO<sub>2</sub> ETCC (Energy Transition Combined Cycle).

The system is based on a CO<sub>2</sub> closed cycle in which the gas is liquified and re-gasified to store and release electric energy. The closed cycle implies that CO<sub>2</sub> has to be stored at gaseous state with ambient pressure and temperature in a large volume dome.

In the CO<sub>2</sub> battery concept, during charge, the system compresses the CO<sub>2</sub> gas from the dome to send it at high pressure (70 bar) towards a heat exchanger. In this heat exchanger, that might be a packed bed thermal storage, the CO<sub>2</sub> is cooled down from the heat gained during compression and the heat is stored for a later use during discharge. After this, a further heat exchanger, linked to a water circuit, cools down the gas up to liquefaction and finally the liquid carbon dioxide is stored in pressurized vessels. Here, the advantage of this technology consists of the liquid storage at near ambient temperature, as it is possible to avoid cryogenic temperatures differently from the liquid air solution. In this case, the input energy during charge comes from the compressor and auxiliaries' power. The scheme of the plant in the charging phase is represented in Fig.80.

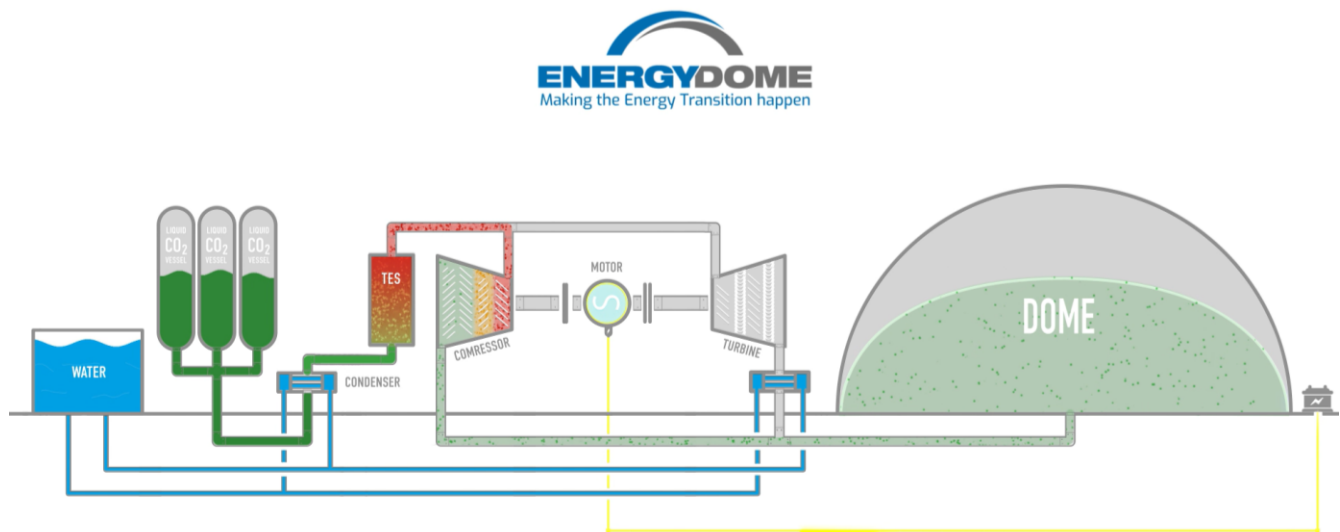


Fig.80 Energy Dome CO<sub>2</sub> battery – Charge phase [3.26]

During the discharge phase, the liquid CO<sub>2</sub> is withdrawn from the pressurized vessels and gasified in the heat exchanger with the water circuit. Then, the gas is superheated thanks to the heat stored in the thermal energy storage and then expanded in the turbine to generate electric energy. Finally, the gaseous CO<sub>2</sub> is returned at ambient pressure and temperature to the dome storage, where it is kept until the next charging cycle. The discharge phase scheme is reported in Fig.81. The battery round trip efficiency should be above 75 % according to Energy Dome.

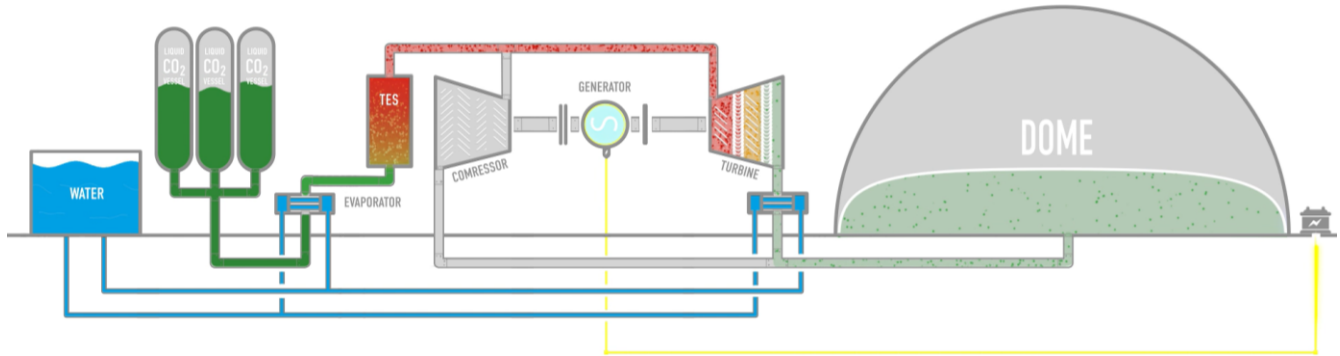


Fig.81 Energy Dome CO<sub>2</sub> battery – Discharge phase [3.26]

A different possible plant scheme is the CO<sub>2</sub> ETCC (Energy Transition Combined Cycle), which is a combination of the CO<sub>2</sub> battery with a gas turbine, to generate a combined cycle. The addition of a gas turbine provides additional power generation, and the waste heat from the turbine discharge can be used directly to superheat the CO<sub>2</sub> or to heat up the thermal energy storage. According to the company, such system could work in four different operation modes: Charging, Boost, Super Boost and Fast Response. The charging mode correspond to the charge of the CO<sub>2</sub> battery. Regarding the Boost operation mode, in this case the plant effectively operates as a combined cycle. The gas turbine is in operation, and the waste heat is directly recovered by the subjected CO<sub>2</sub> cycle. Therefore, the CO<sub>2</sub> cycle operates continuously and not discontinuously as a battery, exploiting the waste heat to improve the efficiency of the plant. Regarding the super boost mode, instead, the CO<sub>2</sub> battery is used in the discharge mode while the gas turbine is in operation providing waste heat. Firstly, the thermal energy storage is exploited and then the heat from the gas turbine. According to the company, this particular operation makes it possible to achieve combined cycle efficiencies above 80% and to generate a power level that is more than double the installed capacity of the gas turbine. This operation mode should be ideal to provide high energy rates during day peaks. The super boost operation mode is represented in Fig.82. Finally, in the Fast response mode, the gas turbine can be kept warm slightly consuming natural gas so that the plant can start the operation in seconds for fast ramp up. Depending on the type of operation and on specific plant configurations, these storage systems should be able to provide different services to the grid including frequency and voltage regulation [3.26].

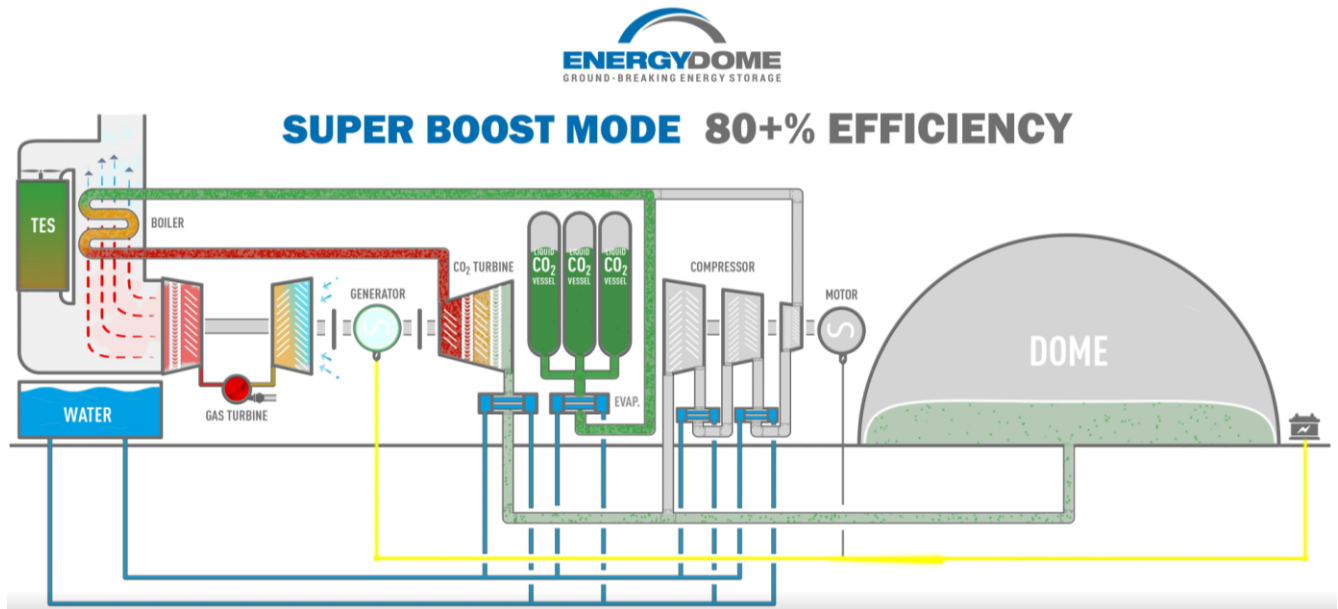


Fig.82 Energy Dome CO<sub>2</sub> ETCC – Super boost mode [3.26]

### 3.4.1 Technical characteristics

According to the company, most of the components for these plants are already available and standardized. They can be combined modularly to get different sizes of storage and power capacity. The proposed solutions are energy storages of 50 / 100 / 200 MWh with possible power output capacity between 10 and 80 MW (Fig.83).

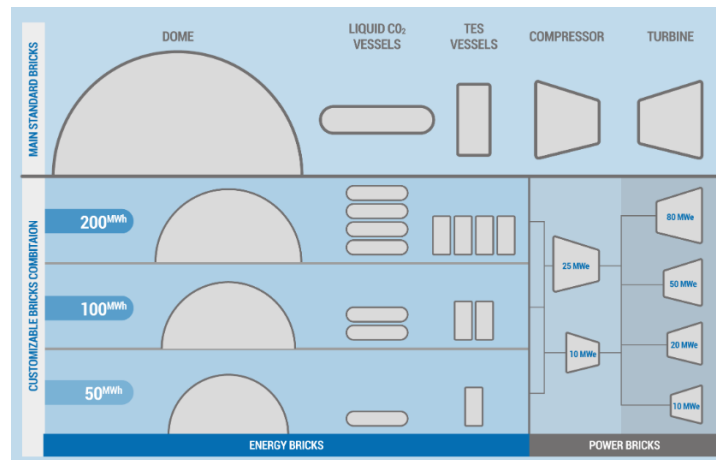


Fig.83 Energy Dome CO<sub>2</sub> components [3.26]

The dome that contains the gaseous CO<sub>2</sub> should be made of two inflatable membranes separated by an air gap, over which a metallic grid should be installed to provide stability and preserve the integrity of the entire structure. The lifetime of this structure is expected to be around 10 years; therefore, this component should be replaced more than one time during the storage lifetime.

### 3.4.2 Commercial Examples

By the end of 2022, the company has only built a pilot plant in Sardinia, Italy (Fig.84). This plant has a power capacity of 2.5 MW and a storage capacity of 4 MWh, with the possibility of storage expansion to 8 MWh [3.27]. The plant has been tested since June 2022 to validate the concept of storing energy through CO<sub>2</sub> and its component's reliability. A new commercial-size plant has been planned in collaboration with the Italian utility A2A: a 20 MW/200 MWh CO<sub>2</sub> battery.



Fig.84 Energy Dome Sardinia pilot plant [3.26]

### 3.4.3 Liquid CO<sub>2</sub> Summary

The great advantage of liquid CO<sub>2</sub> energy storage is the combination of the storage in liquid phase and the near ambient temperature. This allows to achieve high round trip efficiencies (75-80%) and moderately high energy densities, in the order of 66.7 kWh/m<sup>3</sup>. The standardization of the equipment represents another advantage for the system realization. However, the lifetime of the systems is a bit lower than other solutions, and at least two replacements of the dome have to be done before decommissioning, causing additional maintenance costs. The energy storage and power capacity are relevant but limited by the size of the storage. In fact, the main problem of this solution is the size of the dome where the gaseous CO<sub>2</sub> has to be stored. While the liquid CO<sub>2</sub> has high energy density, the gaseous CO<sub>2</sub> storage requires a large footprint: for the standard size of 20 MW and 200 MWh the plant would need almost 5 hectares of footprint. Additionally, also the visual impact is not negligible: the pilot plant had a dome height of 18 m and for the standard size of 20 MW the dome height would reach 40 m. Of course, the combined cycle configuration of the plant presents the disadvantage of relying on fossil fuels and of emitting CO<sub>2</sub>.

Power	Discharge time [3.27]	Lifetime	RTE [3.26]	Energy Density	CAPEX [3.21]
10 - 80 MW	2.5 – 16 h	25-30 years	75 – 80+ %	66.7 kWh/m <sup>3</sup>	2000 - 2250 €/kW

Tab.13 Liquid CO<sub>2</sub> energy storage summary

Overall, while the solution seems to be very promising, the land occupation and the visual impact may jeopardize many of the possible initiatives to adopt this kind of storage solution, especially in Italy, where a lot of attention is put on the landscape preservation. Additionally, the safety of the system has to be assessed in-depth.



### 3.5 Battery Energy Storage Systems

The electrochemical energy storage refers to battery type energy storage: some examples of this application are lead-acid, lithium-ion, vanadium redox battery (VRB). Batteries represent one of the most widespread solutions for electric energy storage nowadays, and they are currently spreading also to the sectors of electric vehicles and stationary energy storage. According to IEA [3.28], the Lithium-ion batteries for stationary applications constitute more than 90% of the new energy storage installations if pumped hydro storage is not considered. Additionally, other types of batteries constitute most of the remaining 10%. According to the Sustainable Development Scenario by IEA, battery storage may reach a total capacity of 550 GW by 2040.

Basically, batteries represent a form of electrochemical storage where redox reactions are used to store and release energy. In particular, the materials involved are able to transfer electrons through an external circuit and to exchange ions inside the battery to maintain overall charge neutrality. The reactions take place at the cathode and at the anode, and the two materials are kept isolated by a separator [3.29]. Inside the cells, an electrolyte allows the transport of ions between the electrodes, while not allowing the electrons transport. In the example figure Fig.85 reported below, a porous insulating membrane, the separator, is placed between the two electrodes and is filled with an ionically conductive salt solution: the electrolyte. The electron flow is collected through an external circuit.

In the case of Lithium-based batteries, during charge the generated lithium ions go from the positive electrode to the negative one, while the opposite happens during discharge. The charging process is generated by the application of a larger voltage to the cathode, while during discharge a larger voltage is applied to the anode. An equal number of charges has to be transferred through the external circuit and the electrolyte.

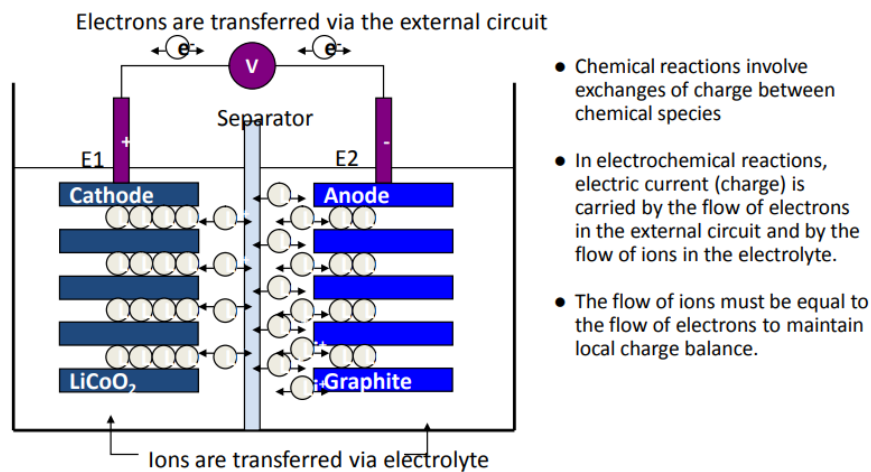


Fig.85 Schematic example of a battery's main elements [3.29]



Stationary BESS require additional components like power converters, which allow to convert AC to DC during charge and vice versa during discharge, but also other components for the balance of plant like protections, controllers, and temperature control systems.

Considering Lithium-Ion batteries, which are the most widespread nowadays, many different chemistries are possible, all of which are based on the transport of lithium ions between the electrodes during operation. The lithium is not kept at its metallic state in the cells, but it is included in composite materials like lithiated metal oxides or phosphates in the cathode, carbon (graphite) or lithium titanate in the anode. According to [3.30], some of the main chemistries used for Li-ion batteries are Lithium nickel manganese cobalt oxide (NMC), Lithium manganese oxide (LMO), Lithium iron phosphate (LFP), Lithium titanate (LTO). Among these, NMC batteries are the most frequently used for stationary storage applications because of their performance in terms of energy, power, cost, and lifecycle. However, some companies are shifting to the Lithium iron phosphate technology, as cobalt represents a critical rare material often extracted in poor countries, where the mining process is related to child labor and human rights abuses.

### 3.5.1 Technical characteristics

Batteries for stationary energy storage applications are typically arranged so that battery cells are packed in modules and installed in racks inside containers or buildings. The cells are configured in parallel into units to achieve capacity targets, while several units in series compose modules. As reported by [3.36], usually modules are composed of 12 units, but the number may vary to 8-10. The series connections of different modules are arranged to achieve voltage levels compatible with the converter, usually around 500 to 800 V. These series may consist of a variable number of modules between 17 and 25. In the end, the batteries series are placed in parallel to meet the capacity requirements. In the following Fig.86, a typical scheme for a large size BESS system is represented. Here, each battery pack is connected to its converter and to the power transformer that connects the plant to the high voltage grid.

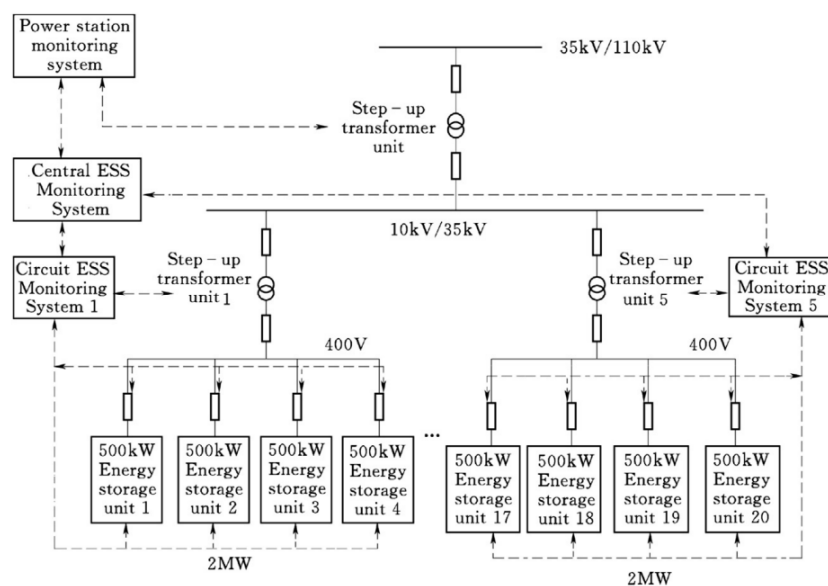


Fig.86 Scheme of a BESS [3.36]

These systems can be used for different purposes, as explained in [3.36]. If connected to wind farms, BESS can limit the fluctuations of the generated power by absorbing and releasing energy, but also stabilize the grid providing the power services. Additionally, BESS are suitable for voltage regulation acting on reactive power absorption or release and for frequency regulation.

BESS systems can discharge over periods that are commonly comprised between 2 and 4 hours, but sometimes they may reach 8 hours duration. Regarding their response time, it is one of the lowest between the energy storage technologies. According to [3.31], the response from 0 to 100% of the power required can be achieved in around 200 milliseconds, and it is expected that it will go down to less than 100 ms by 2030. This makes it possible to use batteries for frequency and voltage regulation in addition to energy shifting. In the case of Sodium batteries, the response time is function of the temperature and can be fast only if the system is already at high temperature. Otherwise, the response time might reach the order of hours. It should also be considered that these storage systems can be installed with relatively short construction times.

Regarding the technical characteristics of battery energy storage systems, the temperature has a large impact on their performance. In particular, there is an effect on their capacity: the lower the temperature, the smaller the battery capacity. This temperature effect can nowadays be seen in electric cars, where the cold temperatures significantly decrease the range of EVs. Lithium-iron phosphate batteries can discharge up to 100% of their rated capacity when their temperature is between 10 and 60 °C, up to 90% when the temperature is -10 °C and up to 70% when -30 °C are reached [3.36]. In BESS systems, a cooling & heating system has to be present among the auxiliaries, as it should keep the batteries around an optimal temperature of 20 °C [3.30]. As an example, according to [3.36], the best operating temperature range for lithium iron phosphate batteries is within 15 to 25 °C. Overall, lithium batteries can work in the temperature range between -20 to 60 °C, and similarly redox flow batteries in the range between 0 and 50 °C. A large difference can be seen in the case of sodium batteries, where the temperature needed for their operation is between 250 and 350 °C [3.31]. This high temperature working condition for Sodium batteries cause complexities in the thermal management and safety issues like fire hazards. Still, also in lithium-ion batteries fire hazard has to be addressed, as under overheating conditions the batteries may produce oxygen, so the thermal management is fundamental.

Differently from the previously analyzed energy storage possibilities, batteries are subject to the self-discharge phenomena. This is due to chemical reactions inside the battery that cause a loss of the stored energy. According to [3.31], for Lithium batteries, the loss of charge is around 2 to 3% per month. Differently, this value is very low for VRF batteries, lower than 0.1% per month and very high for sodium batteries. In lithium iron phosphate batteries, serious over discharge has to be avoided to prevent capacity loss. Therefore, this kind of batteries need to be charged in order to keep the state of charge higher than 80% in long periods of unuse [3.36]. In addition to deep discharges, also overcharge has to be avoided. In lithium iron phosphate batteries, overvoltage during charge has to be avoided as it may cause rapid decrease of performances and even dangerous incidents including burning or explosions.

Regarding the lifetime of batteries, this parameter depends on the type of battery, on its working conditions, and on its frequency of use. In particular, it results to be important the number of

charge/discharge cycles and the depth of discharge to which the battery is subject. According to [3.36], in order to increase the lifetime of batteries both excessive charge and excessive discharge should be avoided by keeping the state of charge (SOC) under control. Additionally, in order to assess the aging performance of batteries, it is defined the state of health parameter (SOH). The SOH parameter is defined as the ratio between the maximum capacity of the battery and its original rated capacity, while the SOC is defined as the ratio between the charge of the system and its rated capacity.

$$SOC = \frac{Q(i)}{Q_{rated}} \cdot 100\% \quad SOH = \frac{Q_{max}}{Q_{rated}} \cdot 100\%$$

Regarding the number of cycles of charge/discharge, this can strongly affect the lifetime of BESS. The total lifecycle of a battery for stationary applications can be considered to be completed when the battery reaches a SOH of 70%. Sometimes the threshold is set to 80% for other applications. As stated by [3.31], batteries for frequency regulation might last just for 3-4 years, while in the case of voltage regulation and domestic batteries the lifetime can reach 15 to 20 years. In terms of cycles, Li-ion batteries are expected to reach 3000 to 10000 cycles, while Sodium batteries should instead reach around 4500 cycles, and redox flow batteries between 15000 and 25000 cycles. Nonetheless, for redox flow batteries the lifetime in terms of years is predicted to be between 11 and 14. Referring to equivalent full cycles with 100% DoD, the lifetime of Li-ion batteries (up to 70% of their initial capacity) should be reached in 4000 to 5000 cycles [3.31].

The depth of discharge (DoD) of batteries is an important parameter that affects the lifetime of the system and its available capacity. As an example, for lead-acid batteries, the depth of discharge is set to 80% when referring to the 100% expected lifetime and if the depth is reduced the lifetime can be significantly increased. If DoD is reduced to 60%, the lifetime can extend to 170%, while reducing it to 25% would increase the lifetime to 375%. Conversely, full discharges (100% DoD) would result in a life reduction to 70% of the initial one [3.36]. For lithium-ion batteries, in order to extend the duration of BESS service, the maximum DoD is set to 90%, with alarms set when the battery is close to reaching the critical value.

In terms of efficiency, the electrochemical storage presents some of the highest efficiencies if compared to the others energy storage technologies. As reported by [3.31], Sodium batteries reach a RTE of around 80%, and redox flow batteries reach RTE of 70 to 80%. Lithium-ion batteries should instead be able to achieve efficiencies of 75 to 90%.

An additional parameter to be defined to describe battery systems is the C-rate. This parameter can be defined as an operative parameter or as a technical specification. As a technical specification, the C-rate represents the ratio between the capacity of the storage and its rated power, so it gives a measure of the duration of the charge and discharge at nominal power. Typically, for stationary applications, batteries with C-rate of 2 or 4 hours are used.

$$C - rate = \frac{P_{rated}}{E_{storage}} = \left[ \frac{W}{Wh} \right] = \left[ \frac{1}{h} \right]$$

Alternatively, the C-rate can be used to describe the battery operation as a normalization of the charge or discharge current on the storage capacity. Once again, it gives a measure of the time needed to charge or discharge the battery.

$$C - rate = \frac{Current}{E_{storage}} = \left[ \frac{A}{Ah} \right] = \left[ \frac{1}{h} \right]$$

In order to control the operation, the safety and the health of batteries, a Battery management system (BMS) is needed. The BMS should be able to control the State of charge (SOC), to estimate the State of Health (SOH) and to protect the system from failures. Based on the size and the structure of the systems, the BMS could control different levels of the plant: at modular, cluster and array level. As an example, a BMS plays an essential role in maximizing the service lifetime by regulating the battery temperature to stop overheating and by distributing the charge evenly across the cells to avoid undercharging or overcharging of individual cells. Additionally, the control system ensures that the battery does not operate outside its safe current, voltage, and temperature limits [3.28]. Considering that each battery cluster is made of hundreds of batteries in series, the performance of each battery influences the whole system. Therefore, the voltage of each monomer should be measured together with the total system voltage. The current during charge and discharge has also to be measured to keep it between the allowable limits and to calculate the state of charge. Finally, the temperature has to be controlled to keep high levels of performance. Regarding the protections, the BMS is also responsible for disconnecting clusters in case of failures and checking for electrical leakages [3.36].

### 3.5.2 Recycling and reusing lithium-ion batteries

One of the weak points of the battery use is the environmental impact that they could cause at the end of their life. Often it is said that they should be recycled or reused, but so far economic viability and market incentives for these options have been limited. However, with the increase of utilization of batteries, a large amount of them should be available for recycling in the future years: IEA [3.28] reports that in the Sustainable Development Scenario around 120 GWh/year of Li-ion batteries would be available by 2030. Therefore, the industry should prepare to be able to process and exploit the resources coming from the used batteries. In particular, the recovery of active materials like lithium and cobalt is critical, even if they are present in batteries in small amounts. One of the main problems in the recycling process is that Li-ion batteries are constructed to not be disassembled, and in stationary applications and electric vehicles the systems present a larger complexity due to the high number of cells, sensors, safety devices, thermal management systems and other circuitry that are present.

Nowadays the main techniques used for battery recycling are Pyrometallurgy and Hydrometallurgy. Pyrometallurgy facilities use high-temperature processes to recover copper, nickel and cobalt through melting of the batteries. This process does not allow for the recovery of organic compounds, plastics, lithium and aluminum. Hydrometallurgical methods consist of chemical leaching, and they are able to recover lithium, differently from pyrometallurgical methods. However, they rely on large volumes of environmentally harmful chemicals. Future perspectives that promise improvements in recycling are generally based on the physical separation of the battery components, for example by crushing the cell

and recovering the materials based on density. These processes might be significantly improved by automation and robotic procedures.

An alternative to recycling is the reuse of batteries. In particular, stationary applications could benefit from the reuse of batteries that are no longer suitable for automotive applications. According to the EU commission [3.31], batteries retired from EV applications, they often still have 70-80% of their initial capacity left. While the reduction of the storage capacity might be a strong penalization for electric vehicles, this might not prevent its possible use in large stationary applications. This possibility may help reducing battery energy storage costs. According to IEA the potential reuse of batteries might lead to a 70% cost reduction compared to 2020 by 2040. Nonetheless, nowadays the use of second life batteries is not fully mature, and the prediction of the remaining lifetime and ageing of batteries represents a critical point for its success.

### 3.5.3 Commercial examples

An example of BESS for large applications is the Megapack by Tesla: a modular solution that has now reached a capacity of 3.9 MWh [3.32]. This product can be used for 2- or 4-hours energy storage, and according to the company it can achieve between 92 and 93.5% round trip efficiency. This solution is represented in Fig.87. An example of application of the Tesla Megapack product is the European largest capacity BESS, which entered operation on November 2022 in northern England. This system is a 98 MW and 196 MWh battery system developed by Harmony Energy [3.33].



Fig.87 Tesla Megapack BESS solution [3.32]

A great example of the scalability of batteries for energy storage is the Moss Landing Battery Storage Project in California, which is currently the largest BESS in the world. This system presents a power of 400 MW and a storage capacity of 1600 MWh after the commissioning of its phase two expansion [3.34]. Additionally, a new large-scale BESS that might become the largest in the world has been planned in Australia: The Waratah Super Battery. This new project should present a power capacity of 909MW and a storage capacity of 1915 MWh, and it is expected to be commissioned in 2025 [3.35]. These examples show how the use of batteries for energy storage is not limited to small systems, but it can reach very large utility size for grid balancing and energy shifting.

### 3.5.4 BESS Summary

Overall, batteries present many features that make them one of the best electric energy storage technologies. Referring to Lithium-ion batteries in particular, as they are the most widely spread, these systems can work above a pretty wide range of temperature conditions (-20 to 60 °C) and are able to respond with full load in a matter of milliseconds. In addition, they are able to store energy with much higher density (500 kWh/m<sup>3</sup>) compared to the previously presented systems. In the end, they present the highest round-trip efficiency, with values that might go over 90%. As a reference given by [3.31], it can be considered a DC/AC (and vice versa) conversion efficiency of 98% and a DC round trip of 95%, resulting in an overall 91% RTE. It should be added also that an improvement on the DC round trip is expected by 2030 towards a 97% value.

Of course, batteries present also downsides like the self-discharge matter, which causes losses of energy while the system is at rest (for amounts variable between 2 and 3% per month). Of great concern is also the lifetime of batteries which is limited because of performance degradation over the years, and which can usually reach 15 years. This lifespan is pretty low compared to other energy assets. In the end, the temperature sensitivity, the risk of fire and the issues related to the use of critical and polluting materials have to be mentioned.

Nonetheless, the possibility of improving the recycling processes and of recovering second life batteries might help mitigate some of the previous issues. Finally, it should be considered that the costs have always represented a large issue for batteries in the stationary energy storage field, but they have undergone across large reductions over the last years. According to [3.30], Lithium-ion battery costs have declined by 80% between 2010 and 2017. IEA [3.28], on the other side, claims that costs between 2010 and 2018 have decreased by 90% for EVs and by around two-thirds for stationary applications. These cost reductions can be explained with new chemistries, improvements on the composition of cathodes, and economies of scale in the manufacturing processes.

Reference values for stationary battery energy storage costs are given by the EU in [3.31]. Battery cells, the key driver for the whole system cost, are currently set between 100 to 200 €/kWh, and it is expected that they might go below the threshold of 100 €/kWh by 2030. Battery packs have a cost of around 250 €/kWh, and the whole storage system should cost between 300 and 400 €/kWh depending on the configuration. In the case of second life lithium-ion batteries from EVs, the costs may go significantly down ranging between 44 to 180 US\$/kWh. In the following, the main characteristics of BESS are summarized in Tab.14.

Power	Discharge time [3.31]	Lifetime [3.31]	RTE [3.31]	Energy Density [3.31]	CAPEX [3.31]
kW to 900 MW	1 - 4 h	15 years – up to 20 >5000 cycles	75 - 90%	500 kWh/m <sup>3</sup>	300 - 400 €/kWh (2020)

Tab.14 Battery energy storage systems summary





## 3.6 Power-to-H<sub>2</sub>

Power-to-X technologies represent a great opportunity for energy storage and for increasing the penetration of renewable energy sources in sectors like the industrial, the residential and the transport one. The Power-to-X applications refer to the shifting of energy from electric energy to a different energy vector, which is frequently a gas or liquid fuel. In particular, most of the Power-to-X applications refer, at least in the first step, to the Hydrogen production. Hydrogen could then be used directly for different final uses or further processed to produce methane, methanol or even ammonia. The large number of possibilities make the hydrogen vector very interesting, as it could reach a large variety of final uses and markets.

### 3.6.1 Hydrogen Characteristics

Hydrogen is the simplest chemical element; its atom is made of a proton and an electron, and its molecule is diatomic with covalent bonding. Hydrogen is colorless, odorless, tasteless, highly flammable, and nontoxic [3.37]. A table with its main characteristics by [3.37; 3.38] is reported in the following Tab.15.

Critical Temperature	33.25 K
Critical Pressure	13.2 bar
Density (gas, 15 °C, 1 atm)	0.0892 kg/m <sup>3</sup>
Density (liquid)	70.79 kg/m <sup>3</sup>
Boiling Point	20.3 K
LHV	119.93 MJ/kg
HHV	141.86 MJ/kg
Energy Density (gas, 15 °C, 1 atm)	10.7 MJ/Nm <sup>3</sup>
Energy Density (liquid)	8491 MJ/Nm <sup>3</sup>
Ignition Range	4 – 77 % by volume in air
Flame Velocity	346 cm/s

Tab.15 Hydrogen vector main characteristics

As it can be seen from the reported data, hydrogen is very light and presents low density values at ambient temperature and pressure. For this reason, in case of hydrogen leaks, the released gas rapidly propagates upwards. This has to be considered for safety reasons in hydrogen systems. Regarding its liquefaction, this gas is the second hardest to liquefy after helium, as its boiling temperature is of 20.3 K (around -253 °C). This constitutes one of the main disadvantages of hydrogen, as in order to achieve liquefaction it is necessary to spend large amounts of energy to reach cryogenic temperatures.

Regarding the energy density of the hydrogen vector, it is one of the highest gravimetric energy densities among fuels. The lower heating value of 119.93 MJ/kg is significantly high. To achieve the same energy content of 1 kg of hydrogen, it would be needed around 2.1 kg of natural gas or around 3 kg of gasoline [3.38]. On the other hand, because of the low density of hydrogen, the energy density by volume is significantly lower. At 15°C and 1 atm, hydrogen contains 10.7 MJ/m<sup>3</sup>, much less than natural gas in the same temperature and pressure conditions, which contains around 36 MJ/m<sup>3</sup>. This lower density implies that large volumes are needed to store energy as hydrogen. For this reason, hydrogen storage is often

performed in gaseous form with high pressure vessels or by gas liquefaction. In fact, in liquid form, the volumetric energy density can reach considerable values. About hydrogen transport and storage, one of the main challenges is the embrittlement, which may cause damages to the infrastructure. As an example, current steel natural gas pipes are not suitable to withstand pure hydrogen with high pressures and high mass flow rates. Therefore, tuned materials would be needed for the hydrogen transport in pipelines. A candidate could be Polyethylene (PE) since it can be extruded and withstand pure hydrogen, preventing any embrittlement problem. Anyway, because of the light weight of hydrogen, diffusion leaks might be relevant. It is estimated that they might be 1.3 to 2.8 times larger than leaks of methane, or 4 times larger than leaks of air in pressurized pipes [1.2]. In the end, it should be highlighted that hydrogen is very flammable. This can be ignited easily with a wide range of flammability: the lower flammability limit is set at 4% per volume in air, while the higher flammability limit is set at 77% per volume. For this reason, safety is one of the most important issues to be addressed in the development of hydrogen applications. Another characteristic of hydrogen combustion is the low radiant heat content of hydrogen flames, which prevents the overheating of the zones close to the flames.

### **3.6.2 Final Uses & Market opportunities**

In the electric energy storage field, the hydrogen production looks very promising for the opportunity of storing energy for long periods of time. From this point of view, hydrogen could be game changing in the seasonal storage field for large quantities of energy, as it does not suffer particularly of self-discharge problems (except for the boil-off in liquid hydrogen storage). In particular, hydrogen could be produced exploiting electrical energy to achieve water electrolysis, to be later used to generate electrical energy once again. This represents a Power-to-Fuel-to-Power application, and hydrogen could even be converted in a different fuel before generating electricity once again. This use of hydrogen as a fuel in electric energy generation is particularly interesting as it could be produced exploiting water and electric energy only, and its use would mainly cause water emissions. This happens because it is a carbon-free fuel, so it does not imply CO<sub>2</sub> emissions. Therefore, it represents a unique possibility as a “clean” fuel, fundamental to reduce greenhouse gas emissions and hazardous local emissions like particulates, which are common in other combustion processes. While the efficiencies of the whole process of fuel production and then conversion back to electrical energy are very low, this possibility is interesting to increase the reliability of the electrical grid with the long-term storage. A first possibility for electric energy generation is given by the use of fuel cells, but hydrogen could also be used in conventional generation plants like combined plants and gas turbines, alone or in combination with other fuels. Regarding gas turbines, hydrogen can already be blended with natural gas in different amounts depending on the equipment compatibility, providing a way to reduce the emissions of the current generation systems, and in the future more turbines fueled by pure hydrogen might be used. Another possibility is given by the co-firing of hydrogen with other fuels like coal and oil to generate steam, which could reduce emissions and even improve the efficiency of combustion. In the end, hydrogen could be converted in other fuels like ammonia or synthetic methane to be used in different power generation systems. In any case, the main downside of hydrogen firing could be the NO<sub>x</sub> generation due to the high temperatures that can be reached by hydrogen flames. For this reason, the temperature should be kept under control and DeNox systems might be required.

In the industrial sector, hydrogen is currently used in oil refining to remove impurities from crude oil, in the ammonia production for fertilizers like urea and ammonium nitrate, in the methanol production, and in steel production [3.37]. In addition to these, it is used in the chemical sector to produce plastics, explosives, synthetic fibers, pharmaceuticals and solvents. As an example, methanol produced from hydrogen could be used to produce dimethyl ether, formic acid, formaldehyde, methyl methacrylate and other solvents. In some regions, methanol could also be used in the methanol-to-gasoline process. In the end, hydrogen could be used as a source of heat in the future for high temperature industrial processes like gasification, drying, melting.

A third important field of application of hydrogen could be the transport sector, where this vector could possibly reach most of the current transport means: cars, trucks, trains, ships and even planes. For cars the use of hydrogen could be in fuel cell vehicles, which are driven by electric energy generated through the hydrogen vector. Another possibility might be the direct use of hydrogen in internal combustion engines tuned for its use as pure gas, or as a blend with other common fuels to reduce their emissions and to improve combustion. Once again, in case of hydrogen combustion, the topic of NO<sub>x</sub> emissions should be carefully addressed. An example of already existing fuel cell car is the Toyota Mirai. The fuel cell technology could be particularly interesting for fuel cell electric buses and trucks, which could take advantage of large hydrogen tanks and use lower storage pressures, around 350 bar. This might be an improvement compared to electric heavy transport thanks to the faster refueling times, greater autonomy and lower weight of the energy storage system [3.37]. Regarding the rail transport, the use of the hydrogen vector and fuel cells could represent a green solution to decarbonize the non-electrified railways, that are mostly served by diesel-powered trains. In particular, it might represent an optimal solution for railways where direct electrification might be too complex or costly. Hydrogen fueled trains have already been developed and are commercially available, as it is demonstrated by the company Alstom [3.42], which deployed the first train in Germany in 2018. Regarding naval applications, hydrogen could be used in fuel cells for small ships, or through synthetic fuels like methane and ammonia for larger applications. Tanker ships represent another possibility, as they could transport liquid hydrogen for international trades, and part of it might be used as a fuel, as it is already done with liquified natural gas. An example is given by the Susio Frontier, the first ship of its kind, which entered operation in 2022 for liquid hydrogen trade between Australia and Japan [3.43]. In the end, in the aviation field the use of hydrogen seems to be more challenging, but still possible with synthetic fuels or with its direct combustion in aeronautical turbines.

A fourth field of application for hydrogen is the residential one, where this vector could serve as a partial or total replacement of methane in the supply of heat and domestic hot water. In the Power-to-methane, process, synthetic methane could be produced to be later used with current devices, or blends of natural gas with small amounts of hydrogen could be possible. In particular, blends between 2 and 10% of hydrogen have been demonstrated to be possible depending on the natural gas grid conditions. A different possibility might be the use of a dedicated infrastructure for the distribution and use of pure hydrogen. An example of pure hydrogen use is the boiler developed by Baxi [3.44].

Currently most of the hydrogen globally produced comes from fossil fuel processing. Some of the main methods are the Steam Methane Reforming, which exploits natural gas, Partial Oxidation of oil and coal Gasification. All of these methods imply carbon emissions during the production process, and their effect can be mitigated with carbon capture mechanisms. In case of hydrogen production by natural gas reforming with carbon capture and sequestration, the hydrogen is commonly defined as “blue” hydrogen. While the objective is to decarbonize the hydrogen production, the use of carbon capture technologies is expected to be a step in the transition to renewable energies. In fact, CCS allows to reduce CO<sub>2</sub> emissions up to 90% [3.38].

Hydrogen can also be produced with renewable energy sources, as an example by water electrolysis performed with renewable electric energy. In addition, renewable hydrogen can also be produced with biomass gasification processes. In this case, biomass gasification implies carbon emissions, which are considered to be not impacting on the greenhouse effect mechanism as plants absorb carbon during their lifetime. This process is therefore considered to be CO<sub>2</sub> neutral. Moreover, thermochemical processes exploiting solar thermal energy and photobiological processes can be considered for renewable hydrogen production. For large scale production, the most interesting one is the production via water electrolysis, which in the future might exploit the excess renewable energy. The hydrogen produced by exploiting renewable energy sources is often called “green” hydrogen. For the scope of this analysis, the production of hydrogen via water electrolysis was the one of major interest, as it would allow to store the electric energy generated by the wind farm for a later use or for a different type of use. Therefore, in the following the main characteristics of the electrolysis process are studied.

### **3.6.3 Electrolyser**

Water electrolyzers are electrochemical devices used to split water molecules into hydrogen and oxygen by exploiting electric energy. Most of the information about these devices was gathered up by the IRENA report [3.39]. The electrolysis process takes place in electrolytic cells, which are commonly made of two electrodes (an anode and a cathode), an electrolyte (which can be liquid or solid), two porous transport layers and bipolar plates that provide mechanical support and distribute the flow. Among the current electrolysis technologies, four main types of electrolyzers can be identified. The Alkaline electrolyzers and the Proton exchange membrane electrolyzers (PEM) are the two commercially available systems nowadays. The other technologies that have yet to become ready for commercial deployment are the Anion exchange membrane (AEM) electrolyser and the Solid Oxide electrolyser. The schematic operation of the cells of each of these types is reported in Fig.88.

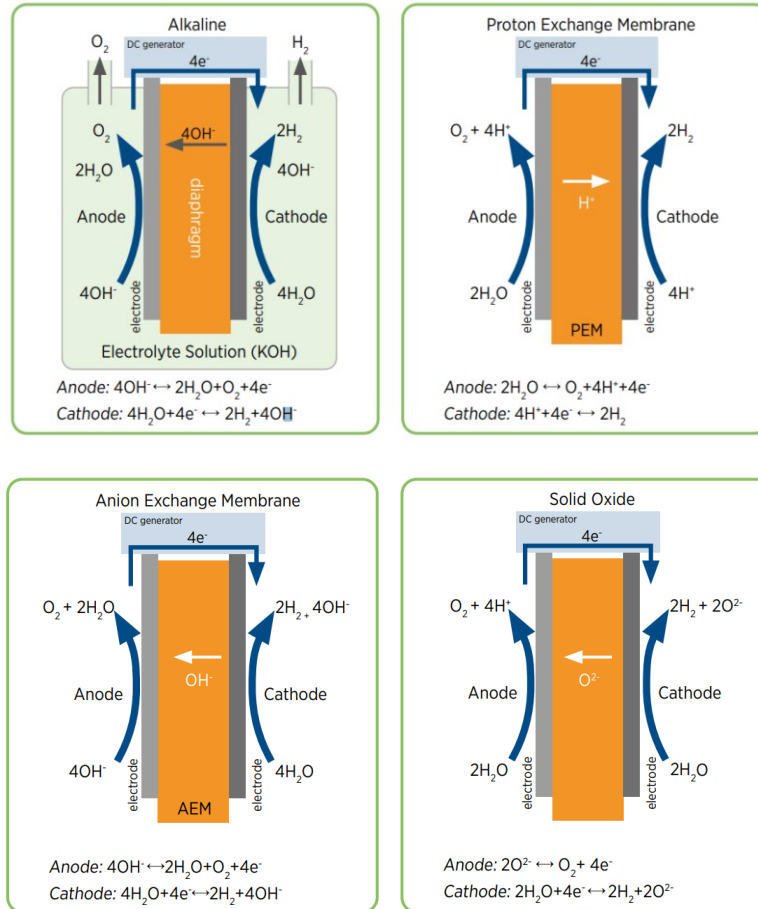


Fig.88 Schematic operation of the different electrolytic cells [3.39]

The electrolysis reaction takes place at the electrodes, where reduction and oxidation reactions take place and oxygen and hydrogen gases are produced. The electrolyte separates the electrodes and is used to transport the ions generated during the reactions from an electrode to the other one, so as to balance the net charge.

In the case of the Alkaline cells, the electrolyte is a basic liquid solution, typically with concentrated KOH or NaOH, which allows for the transport of OH<sup>-</sup> anions to the anode. In addition, in alkaline electrolyzers, a porous separator (or diaphragm) is inserted between the electrodes. This component allows the transport of anions as it is permeable to the electrolyte, while preventing the mixing of the hydrogen and oxygen gases generated, which may otherwise create explosive mixtures. However, the permeability of the separator to water and KOH may cause some mixing of the gases, therefore particular attention has to be paid to the thickness of the separator. In fact, the separator thickness determines also the resistance to the transport and therefore it could penalize the process efficiency. To further avoid the mixing, in some cases spacers are added between the separator and the electrodes. Generally, alkaline cells work at temperatures ranging between 70 and 90 °C.

In the other electrolyser technologies, the electrodes of the cells are separated by a solid electrolyte (instead of a liquid one), which simultaneously allows for the transport of ions and the separation of the gases produced during operation.

In Polymer Exchange Membrane cells (or Proton Exchange) the solid electrolyte is a thin perfluorosulfonic acid (PFSA) membrane, which is chemically and mechanically robust, which allows for pressure differentials between the oxygen and the hydrogen side. For this reason, in PEM electrolyzers, it is possible to generate hydrogen at high pressure (up to 70 bars) while keeping the oxygen at ambient pressure. PEM cells typically operate at temperatures between 50 and 80 °C. Overall, PEM cells are simple and very efficient. Among the downsides of PEM electrolysis, there is the use of noble metals and titanium-based materials, which make the stacks more expensive than alkaline ones. In addition to this, the cells are very sensitive to the presence of impurities in the water fed. The name of the PEM is due to the capability of transport of  $H^+$  ions of the membrane.

In Anion Exchange Membrane cells (AEM), the membrane allows for the transport of  $OH^-$  anions, differently from the PEM. These cells should not require rare and noble materials and should allow for differential pressure operation like PEM electrolyzers. The operative temperature range of these cells are nowadays between 40 and 60 °C. Overall, these systems should be simple and efficient, however, the poor stability of the membrane make their lifetime low and difficult to predict. For this reason, further developments are needed before the commercialization of these kind of products.

In the end, regarding Solid oxide cells (SOEC), they work at high temperature levels, ranging between 700 and 850 °C. The high operative temperature is favorable for the reaction kinetics and therefore allow for the use of cheaper materials like nickel electrodes. In addition, as part of the energy is provided as heat, the electrical energy requirement for electrolysis is lower. On the other hand, the working conditions lead to faster degradation (with ramping and shutdown), shorter lifetimes, contaminations and challenges related to sealing.

Given the current unreliability of AEM and SOEC systems, they were not considered as valid possibilities for a possible hydrogen production coupled to the offshore wind farm.

Each electrolyser is composed of stacks, which are made of multiple cells connected in series. The stacks include spacers which add insulation between the electrodes with opposite charges, and also seals, frames that provide mechanical support and the end plates that collect the fluids. However, the whole electrolyser facility goes beyond the stacks, and comprises other equipment necessary for the operation like power supply, water supply and purification, compression, cooling and hydrogen processing. The power supply system includes transformers and rectifiers to provide the DC electricity input, while the water supply system provides the purification and supply of deionized water with circulation pumps. The removal of oxygen is also necessary, while in the hydrogen processing purification steps should be present in addition to the compression. Moreover, some buffers of hydrogen or electrical energy might be present. A general schematic of an electrolyser plant is shown in [Fig.89](#).

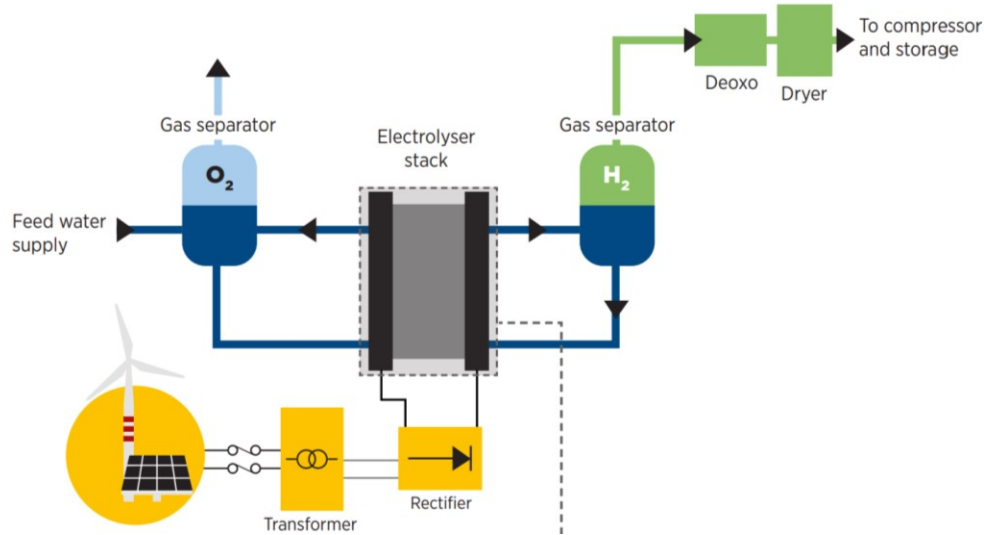


Fig.89 Simplified electrolyser scheme [3.39]

At system level, the alkaline electrolyzers require a recirculation of the basic electrolyte in and out of the stacks. The electrolyte exiting from the stacks carries also the gases produced during operation, and therefore gas separation units are exploited both on the oxygen and on the hydrogen side. After the separation, the electrolyte can be sent back to the stacks together with the deionized water. In these systems the operation could be carried out under pressure up to 200 bars, but not with differential pressure between the oxygen and hydrogen sides. A more detailed plant scheme of an alkaline electrolyser system is presented in Fig.90.

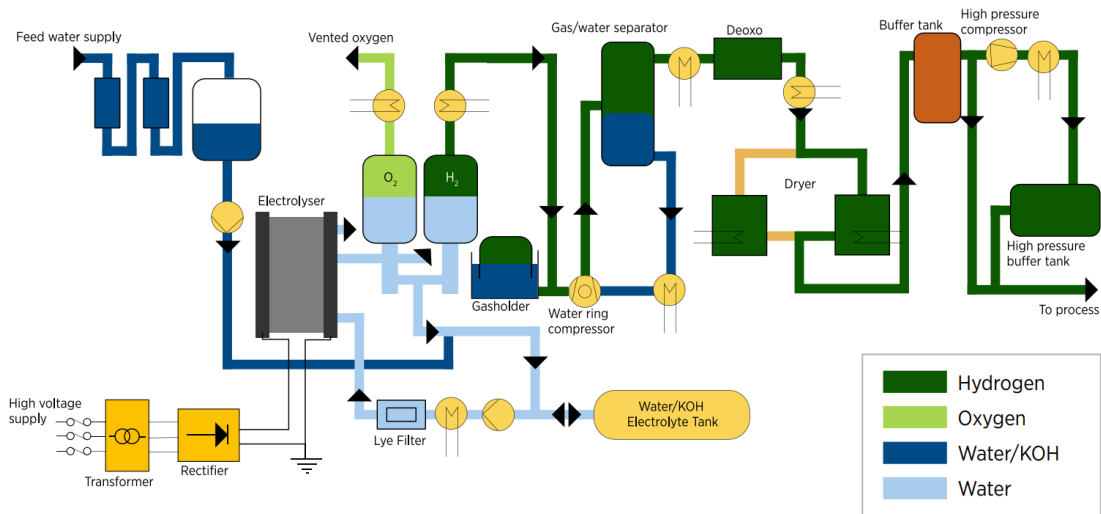


Fig.90 Alkaline electrolyser system scheme [3.39]

In PEM systems, water is typically sent to the stacks through circulation pumps and recirculated to extract the hydrogen and oxygen gases in the water-gas separators. On the hydrogen side, the gas is processed to remove the remaining oxygen with a Deoxo reactor and to remove the remaining water with a dryer. Regarding the operative pressure, this depends on the design, as these systems can work at atmospheric



or differential or balanced pressure. In case of differential pressure, the membrane has to be dimensioned correctly, and pressures can reach 30 to 70 bars. A PEM system scheme is reported in Fig.91.

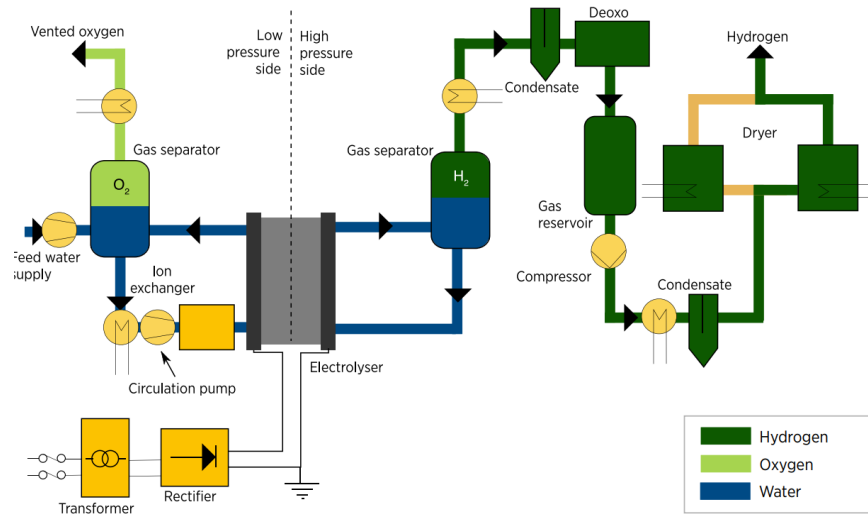


Fig.91 PEM electrolyser system scheme [3.39]

The efficiency of electrolyzers could be defined at different levels as voltage efficiency or DC efficiency. The system efficiency is measured as the ratio between the energy content of the hydrogen produced and the electrical energy input needed to generate it. However, for this efficiency it is necessary to define clearly the boundaries of the system considered, as it might not be comparable with other plants. In particular, rectifiers, transformers, cooling, water pumping might be included or not.

$$\eta_{electrolyser} = \frac{m_{H_2} \cdot HHV \text{ (or LHV)}}{\text{Electric energy input}}$$

The input energy takes into account the energy consumption of the power supply, the cooling system, the purifiers, the water treatment, the pumping and compression phases in addition to the stacks. The ensemble of these elements is called Balance of Plant (Bop). Usually, the rectifiers are key elements in the Bop, in particular at low loads, where they have very low efficiency. At loads higher than 15-20%, the efficiency of rectifiers rapidly increases, remaining than at high levels. For this reason, too low load levels should be avoided for electrolyzers. However, the efficiency of these systems decreases beyond 30% load level and towards the nominal power.

Alkaline electrolyzers show system efficiencies ranging between 50 and 78 kWh/kgH<sub>2</sub>, and similar values are achieved by PEM systems with efficiencies between 50 and 83 kWh/kgH<sub>2</sub>. AEM and SOEC systems show potentials for efficiency improvements in the electrolysis, but yet technical problems have to be solved. AEM systems, should be able to achieve lower consumptions, between 57 and 69 kWh/kgH<sub>2</sub>. SOEC systems, instead, could reach the lowest electrical consumptions: between 44 and 55 kWh/kgH<sub>2</sub>. However, it should be remembered that part of the energy is provided as thermal energy in SOEC systems, and therefore the overall efficiency of these systems would be lower than the apparent.

Regarding the lifetime of the electrolyser stacks, the PEM has values ranging between 50000 and 80000 hours, while for Alkaline electrolyzers the expected life is of 60000 hours. Nonetheless, Alkaline typical designs are known to be robust, and some systems have exceeded 30 years of lifetime.

In terms of hydrogen purity, both Alkaline and PEM electrolyzers can produce hydrogen with purity above 99.9%. However, PEM systems are typically able to reach higher purity levels, up to 99.9999%. About the dimensions of the stacks, one of the advantages of PEM systems is the compactness, due to the higher levels of current density, which are often comprised between 1 and 2 A/cm<sup>2</sup>. Differently, Alkaline systems adopt lower current densities, varying between 0.2 and 0.8 A/cm<sup>2</sup>, and occupy therefore a larger volume because of the larger electrode area needed.

Regarding the flexibility of electrolyzers, it is reported that alkaline and PEM stacks should be able to follow the fluctuations of wind and solar power sources. In fact, both Alkaline and PEM electrolyser systems have been certified to be able to provide primary reserve services. However, the flexibility of the systems could be limited by the other components of the balance of plant, like compressors, and this might affect the design of these components to reach the required level of flexibility. In particular, pressurized operation might prevent the hydrogen compression process from becoming the bottleneck for the flexibility of the whole electrolysis system. Generally, ramping up and down to change the consumption of electricity is guaranteed to be completed in less than one second during operation. Regarding the cold start, instead, PEM electrolyzers could achieve it in less than 5 minutes (up to 20 minutes), while for Alkaline facilities it could take up to 50 minutes. Shutdown instead could be done in the order of few seconds for PEM.

About the water use of electrolysis facilities, this has to be considered as it is a key input of the system, and large flow rates might be required. The minimum amount of water theoretically required to produce 1 kg of H<sub>2</sub> is 9 kg of water. However, taking into account the process of water demineralization, with typical water consumption, the water needed can vary between 18 kg and 24 kg per kg of hydrogen. For this reason, the water availability should be assessed in places with water stress. In case of seawater availability, desalination could be considered with a limited impact on the cost and on the system efficiency. In terms of costs, the purification of desalinated sea water has a marginal importance, as it should be well below 1 USD/ m<sup>3</sup>. However, other additional treatments could add significant costs, like water deionization. In general, these costs affect the hydrogen production with less than USD 0.01/kg H<sub>2</sub>. An interesting option in stationary applications would be the recovery of ultra-pure water produced by the hydrogen use in fuel cells.

The costs of electrolyzers are very variable, and difficult to frame in a narrow range. Generally, PEM systems are more costly than Alkaline ones, with 50-60 % higher investment cost. Looking at the whole systems rather than the stacks only, PEM electrolyzers costs range between 700 and 1400 USD/kW. Alkaline systems instead range between 500 and 1000 USD/kW. For both types, large potentials of cost reductions are expected.

### 3.6.4 Hydrogen Storage

After the hydrogen production process, the gas has to be treated for transport or storage, depending on the application. Commonly, this vector can be stored in the form of compressed gas at high pressure, or liquified, or even converted in a different energy carrier.

Hydrogen could be compressed to different pressure levels depending on the application. As an example, pressures up to 1000 bar are used for storage in tanks, to reduce its volume by 625 times compared to atmospheric pressure. In transmission lines instead, pressures of around 70 bar could be applied, with a 65 times volume reduction. For vehicles fueling, hydrogen could be pressurized between 350 and 700 bar. Hydrogen liquefaction, instead, could allow a volume reduction of a factor of 870. Hydrogen compression could be partially performed in the electrolyser, with relatively low penalties on efficiencies and additional costs, or after the hydrogen production with separate compressors. Starting from atmospheric pressure, the electric energy needed to compress to 30 bar would be equivalent to 3.5 to 4% of the hydrogen lower heating value [3.39]. Optimization of the choice of how to compress hydrogen would be required to improve the efficiency of the whole facility. An estimation of the electric energy needed for the hydrogen compression is provided in the following Fig.92 by IRENA.

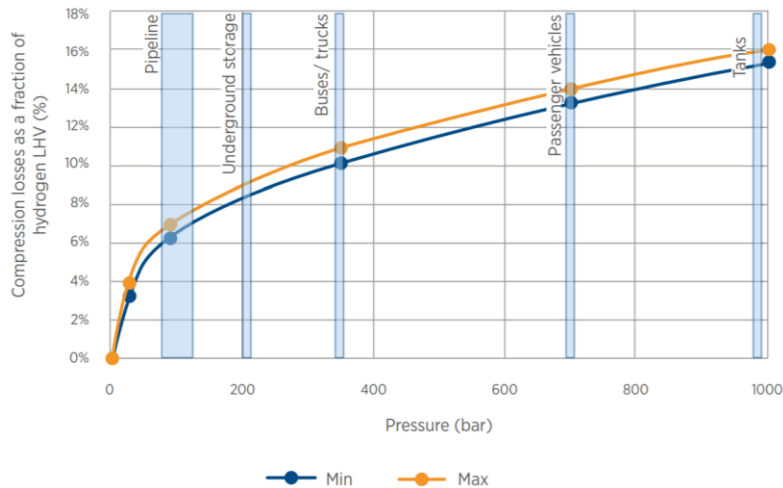


Fig.92 Compression losses as fraction of the hydrogen LHV for different pressure levels

Regarding the physical storage as compressed gas, there are different types of possible vessels, as explained by [3.40]. For stationary uses in the industry field, typically steel vessels (type 1) are used for pressures up to 200-300 bar. Alternatively, type 2 lighter composite cylinders are available. Type 3 vessels are fully wrapped composite cylinders with an aluminum liner on the inside, which is used as a hydrogen permeation barrier, preventing embrittlement, and contributing to mechanical resistance. These vessels can be used with pressures up to 450 bar and offer larger storage possibilities. In the end, type 4 vessels are still composite cylinders which use a plastic liner like high-density polyethylene once again as hydrogen permeation barrier. These last vessels could be used for pressures up to 1000 bar. Both type 3 and 4 types could be used for transport applications, as the pressure range needed is between 350 and 700 bar. Generally, the storage of hydrogen as a compressed gas is complex because of the cost and

heaviness of cylinders, and because of the low energy density. Additionally, there are safety concerns because of the very high-pressure levels and because of the easy leaks of hydrogen.

Compared to the compressed hydrogen storage, the liquid hydrogen option represents a much more compact solution, with lower safety issues thanks to the absence of high pressures. However, the main disadvantage of hydrogen liquefaction is the energy consumption needed to reach cryogenic temperatures. In fact, the critical temperature of hydrogen is  $-240^{\circ}\text{C}$ , while the boiling point at atmospheric pressure is  $-252.9^{\circ}\text{C}$ , a very challenging condition to reach. The cooling process for hydrogen liquefaction could require between 25 and 40% of the hydrogen energy content according to [3.40]. Vessels for storage of liquid hydrogen need to be highly insulated, typically with double walls with vacuum conditions in between. However, because of the unavoidable heat transfer from environment, the boil-off is present, as part of the hydrogen is able to evaporate. The boil-off rate could reach 0.4% per day in small vessels, and for this reason a recirculation of the hydrogen to liquefy it again would be needed. In addition to the energy loss, the boil-off may represent a safety issue if uncontrolled, as it might cause pressure increase. Generally, because of the system cost, complexity, energy losses and boil-off risks, the use of liquid hydrogen is limited to applications where high energy densities are necessary and where the hydrogen is used within a short period. Some examples are large scale transports like trailers (which can transport 4000 kg of liquid  $\text{H}_2$ ) and ships for international trades.

An alternative storage could be the cryogenic-compressed storage. The combination of the abovementioned storage technologies could provide higher energy densities and lower boil-off losses, providing a better solution also in terms of safety. This kind of storage should be kept at cryogenic temperature and pressures typically lower than 300 bar. Hydrogen density and energy densities are reported for some of the different storage options in Tab.16.

	Thermo-physical properties Hydrogen			
	Density ( $\text{kg/m}^3$ )	LHV ( $\text{MJ/kg}$ )	LHV ( $\text{MJ/l}$ )	LHV $\text{kWh/m}^3$
<b><math>\text{H}_2</math> (1 atm)</b>	0.082	119.6	0.00981	2.72
<b><math>\text{H}_2</math> (350 bar)</b>	23.30	119.6	2.79	774
<b><math>\text{H}_2</math> (700 bar)</b>	39.30	119.6	4.70	1305
<b>Liquefied <math>\text{H}_2</math> (1 atm)</b>	70.80	119.6	8.47	2352
<b>Cryo-compressed <math>\text{H}_2</math> (240 bar)</b>	87	119.6	10.40	2890

Tab.16 Hydrogen energy density in different states

Alternatives to the hydrogen compression and liquefaction are solid state storage technologies like physisorption and chemisorption. A first possibility is given by the adsorption of hydrogen, where the gas molecules are bond to the surface of specific materials thanks to van der Waals forces. With this kind of storage, the adsorption and desorption are completely reversible and the reaction kinetics is fast. In addition, the stability of these process us high. However, due to the low interaction forces, frequently high pressures and cryogenic temperatures are needed [3.40]. In fact, if physisorption is carried out at ambient temperature and pressure, the storage capacity would be very low usually with hydrogen content lower than 1% by weight.

Regarding chemisorption technologies, they involve the formation of strong chemical bonds between the hydrogen and the storage material molecules. These processes are typically performed at specific pressures and low temperatures and provide solid compounds of metal-hydrogen: metal hydrides. After the absorption process, the hydrogen can be released with a temperature increase or a pressure decrease [3.41]. In this case, the hydrogen content can be higher than with physisorption, but at the expense of lower reaction kinetics, partial irreversibility and higher temperatures needed for hydrogen release. In addition, another weak point about metal hydrides storage regards the system weight that is typically very high, making it less suitable for transport applications. A lot of research has been done to improve the weak points of this technology, so as to achieve a safe storage technology with high hydrogen storage capacity. The materials used in this chemical sorption storage type are mainly classified in intermetallic hydrides, binary hydrides, and complex metal hydrides [3.40]. Intermetallic hydrides are considered low-temperature hydrides, and their hydrogen content is usually limited to less than 3% by weight. Nonetheless, intermetallic hydrides that store hydrogen in interstitial sites show relatively fast hydrogen absorption/desorption kinetics. Then, among binary hydrides there is Magnesium hydride, which is one of the most interesting materials because of its high theoretical hydrogen storage capacity by weight (of 7.6% by weight) and by volume ( $110 \text{ kg/m}^3$ ). In addition, it is a light, abundant and low-cost material. However, the reaction kinetics of this hydrogen storage are slow, and to release hydrogen temperatures above  $300^\circ\text{C}$  would be needed. In the end, complex hydrides are interesting thanks to their high storage capacities for hydrogen uptake. The main problem about this last group of materials regards their stability which affects the reversibility of the processes and the temperatures needed to release the stored hydrogen. Metal hydride technologies represent a huge possibility for hydrogen storage, and for stationary storage because of their weight. This thanks to their intrinsic safety and high hydrogen storage capacities. Nowadays metal hydrides are seeing some of the first commercial applications, that in the future might rapidly scale up.

### 3.6.5 Fuel Cell

Fuel cells are devices used to generate electricity from fuels like hydrogen. These devices are based on electrochemical reactions and could be able to exploit hydrogen or its derivatives like methanol and ethanol to directly generate electric energy [3.45]. For hydrogen, the reaction is opposite to the one of electrolysis and consists of the combination of oxygen and hydrogen to produce water, heat and electricity. Similar to electrolyzers, a fuel cell is made of an anode, a cathode, an electrolyte, and the external circuit. Once again, the reactions take place at the electrodes, and not directly between fuel and oxidant. The hydrogen is meant to be oxidized at the anode, generating electrons and protons. The first ones are transferred through the external circuit to the cathode, while the second ones might be transferred by the electrolyte. Depending on the electrolyte type, this might transport protons or oxygen ions, closing the reaction with water formation and heat generation as a byproduct. Among the possible electrolytes there are acidic and non-acidic ones. In acidic electrolyte fuel cells, the protons are transported from the anode to cathode, while in nonacidic electrolyte fuel cells, the oxide ions travel from the cathode to anode.

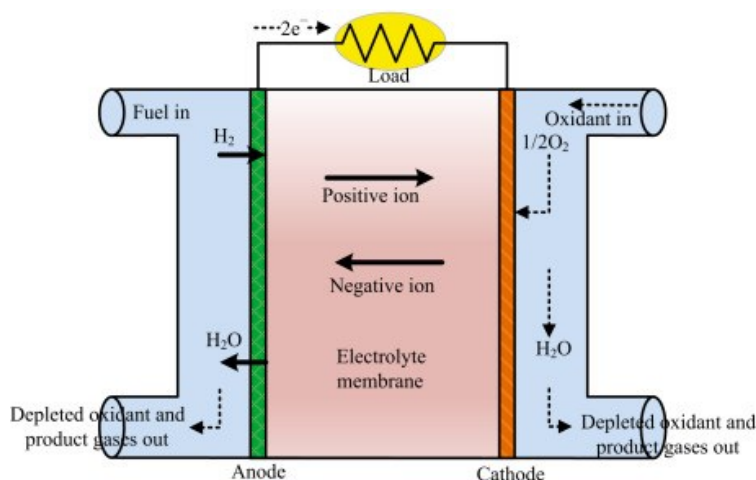


Fig.93 Schematic of a fuel cell operation [3.45]

In fuel cells, both the distance between the electrodes and the contact area between electrodes and the electrolyte is small. For this reason, to improve the electricity generation efficiency and to increase the surface area, flat and porous electrodes are used, and the electrolyte is set as a thin layer. As for electrolyzers, the cells are connected in series as stacks meaning that the anode of one cell is linked with the cathode of the next cell. The fuel cells can be classified as Solid oxide fuel cell (SOFC), Molten carbonate fuel cell (MCFC), Phosphoric acid fuel cell (PAFC), Alkaline fuel cell (AFC), Proton exchange membrane fuel cell (PEMFC), Direct methanol fuel cell (DMFC).

The solid oxide fuel cells have an electrolyte made of a mixture of zirconia ( $\text{ZrO}_2$ ) and yttria ( $\text{Y}_2\text{O}_3$ ), and work at very high temperatures, around  $1000^\circ\text{C}$ . These fuel cells are able to work with hydrocarbon-based fuels, as they are able to reform the fuel into hydrogen and carbon monoxide. Molten Carbonate fuel cells, instead include a mixture of molten carbonate salts as electrolyte and non-noble metal as electrodes. These fuel cells work at high temperatures too, in the order of  $600^\circ\text{C}$ . As for SOFC, they are able to operate with some hydrocarbon fuels like methane. Regarding Phosphoric Acid fuel cells, they use highly concentrated liquid phosphoric acid ( $\text{H}_3\text{PO}_4$ ) as electrolyte and porous carbon-based electrodes for anode and cathode. Their operation is constrained between  $150$  and  $220^\circ\text{C}$  to increase the ionic conductivity in the electrolyte.

Alkaline fuel cells, as alkaline electrolyzers, use alkaline solutions like  $\text{KOH}$  as electrolyte. These fuel cells operate with pure hydrogen at temperatures between  $20$  and  $90^\circ\text{C}$ . These systems have several advantages, like the fast startup and response time, the low-cost catalysts and electrolyte, the high efficiency, and low-temperature operation. In the end, PEM fuel cells use a solid polymer electrolyte and platinum as a catalyst. As alkaline cells, they work at relatively low temperature, between  $60$  and  $100^\circ\text{C}$ . Their efficiency increases with temperature because of the reaction rate but dehydration of the membrane might represent an issue. Generally, the electrical efficiency of PEM fuel cells is comprised between  $40$  and  $50\%$ . The advantages of these systems are the fast startup, the compact design, the low weight, the low cost, and the solidity of the electrolyte.

### 3.6.6 Commercial examples

Hydrogen is currently developing its role in nowadays economy, and therefore few large plants for renewable hydrogen production and use are available. Nonetheless, many projects are being developed or have been planned. A first example could be the SEMREV project, developed by Lhyfe, BW Ideol, Centrale Nantes, which is the world's first renewable hydrogen floating offshore production facility [3.46]. This first plant entered operation at the end of 2022 as a demonstration of the feasibility of performing electrolysis offshore by using seawater and energy generated by offshore wind. Another theoretical example of the possible investments in hydrogen production is the project by Aquaterra and Seawind [1.7], which planned 1 GW of hydrogen production facility coupled with an offshore wind farm. About other relevant experimental projects on hydrogen, there is the Brande Hydrogen project by Siemens Gamesa [3.47]. This last project consisted of a 3 MW onshore wind turbine coupled with a 400-kW electrolyser supplied with water from the mains and with a 560 kWh BESS. The presence of the battery, in this case, was used to stabilize the grid with fast response and to assure stable working conditions to the electrolyser, avoiding any fluctuation of the wind power.

### 3.6.7 Power-to-H<sub>2</sub> Summary

Overall, hydrogen represents an interesting energy vector and product for the variety of its possible uses, which are not strictly linked to the form of energy storage. Referring to its use as energy storage, its main characteristic is the possibility of storing energy for long periods of time without energy loss over time, making it possible to shift energy over time. However, its main disadvantage is related to the chain of losses in the power-to-power, that would lead to very low round trip efficiencies (in the order of 20 to 30%). Additionally, the currently high costs of the equipment needed to produce and store hydrogen would affect the hydrogen cost, together with the cost of the electric energy. Nowadays renewable hydrogen cost is still quite high and not competitive with hydrogen production via steam methane reforming, but it is expected that with the growing hydrogen economy and with price reductions due to scale effects and efficiency improvements, the costs will become comparable with the one of fossil origin. Regarding the energy density of hydrogen, as it was previously explained, it depends on the form in which it is stored. In case of liquid hydrogen storage, the energy density is very high, but the extreme thermodynamic conditions make it difficult and energetically expensive. Conversely, in gaseous form the energy densities are low, and very high-pressure levels are needed to make it acceptable.



### 3.7 Choice of the Storage System

After the review on energy storage technologies was carried out, the different solutions were compared to identify the one to further investigate for a possible investment by the company.

Regarding compressed air energy storage systems, this kind of solution was very interesting for the large-scale storage possibilities and for the long lifetime of the assets. However, these solutions typically have relatively low efficiencies both for the Diabatic and Adiabatic solution. In addition, their energy density is very low, and it would require large volumes. Also, considering the location in Calabria, it would be difficult to find available existing spaces to be used as compressed air storage. Alternatively, the artificial construction of a reservoir underground might be very costly, and it might be not well accepted by the local community. For these reasons the CAES systems were not considered as a valid option, also considering the relatively low spread of these systems and frequent unfinished projects.

Regarding the liquid air energy storage systems, they were considered to be interesting for their long lifetime and for their relatively higher energy density. However, the complexity of cryogenic storage and the low efficiencies were considered as weak points for this technology. Also, these solutions are scaling up recently, and the experience on these kinds of solutions was not considered to be sufficient to convince the investors.

About gravity-based storage solutions, the key parameters in favor of this technology were their simplicity and their high efficiency. However, these solutions suffer of very low energy densities, and therefore large volumes would be needed to satisfy the storage need. In case of aboveground storage, large heights should be needed, with consequent damages to the landscape in Calabria and probable authorization problems. Underground storages could be feasible, but as for CAES systems, existing mines would be needed to avoid relevant excavation costs.

Then, the liquid CO<sub>2</sub> energy storage was confirmed to be one of the most interesting new solutions, thanks to the relatively long lifetime, low costs, high efficiency, safety. Also, one of these plants already exists in Italy, proving the feasibility of such systems. However, for larger storage solutions, the low-pressure reservoir would require very large volumes, with consequent difficult authorization processes due to the impact on the Italian landscape. Therefore, this solution was marked as feasible but with the limitation of relatively low size.

Talking about hydrogen, this represents an opportunity thanks to the ongoing momentum to develop the supply chain and its final uses. However, still many uncertainties are present and investments on hydrogen might be considered to be risky. Low efficiencies, high costs, safety issues, storage and transport complexities make hydrogen a challenging vector to be produced and used. Therefore, its application was considered to be useful only at experimental level due to the lack of knowledge in the company. While hydrogen might be very important in the future, as stated by many forecasts, this storage option was not suggested for the wind farm case.

In the end, the choice of the company for a possible investment on an energy storage technology was on battery energy storage systems. This choice was done considering the high energy density and relatively

low visual impact, the highest efficiency among the presented technologies, the scalability, and the cost reductions that have occurred in the recent years. In addition, the widespread application of BESS and their safety, made this choice preferable also for the search of possible investors. The only risk to be considered was the low lifetime of these systems, which was compensated by the system flexibility by the way, which made it possible to evaluate the operation to provide different services. For this reason, the system simulation was centered on BESS as the most suitable technology.

Another reliable solution would have been the pumped hydro energy storage, which was anyway excluded from this analysis due to the already existing knowledge of this technology inside the company.

## 4 Connection to the Local Grid

### 4.1 Local Energy Demand

In order to understand the size of the energy storage needed to provide the services to the grid and to limit the wind power curtailment, data about the local grid nodes were requested to Terna, the Italian TSO. The provided data refer to a portion of the province of Crotone, where the offshore wind farm in Calabria should be connected. The data refer to the year 2019. In particular, the imports and exports of active power every 15 minutes were received for 5 different nodes. The total imports and exports of power of the load island were estimated as the sum of the power fluxes of all the nodes. Negative power fluxes show an export condition, while positive power fluxes refer to import conditions. In the following it is reported the total power flow of the load island near Crotone ([Fig.94](#)).

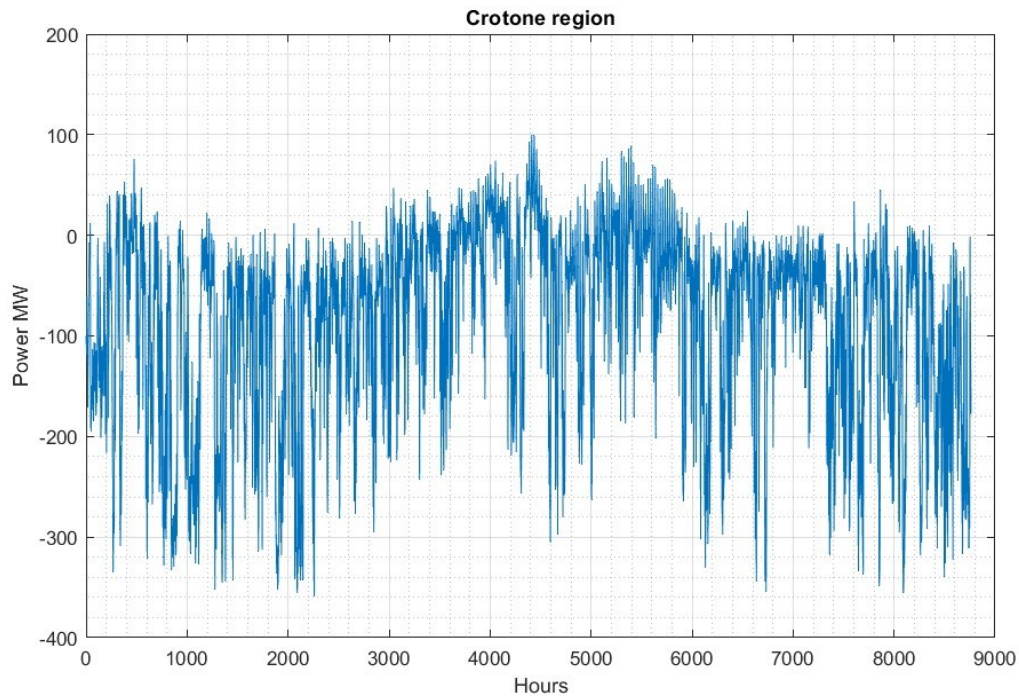


Fig.94 Crotone load island import/exports of power

It is possible to observe how the zone is exporting power for most of the year as most of the values are negative. In particular, the maximum power exported is equal to 358.89 MW, while the maximum import is equal to 100.10 MW. If the wind farm was connected to this portion of the grid, it would further provide power, partially solving the import needs and partially increasing the export to the adjacent zones in Calabria and to the South of Italy. The large size of the wind farm might cause overloading problems in the existing lines. Starting from the overall data of the zone, a power duration curve of the export was built by using MATLAB. In particular, for each power level, the number of hours in which the power exported was equal or higher was counted to determine values on the x axis. The Grid duration curve is reported in the following [Fig.95](#).

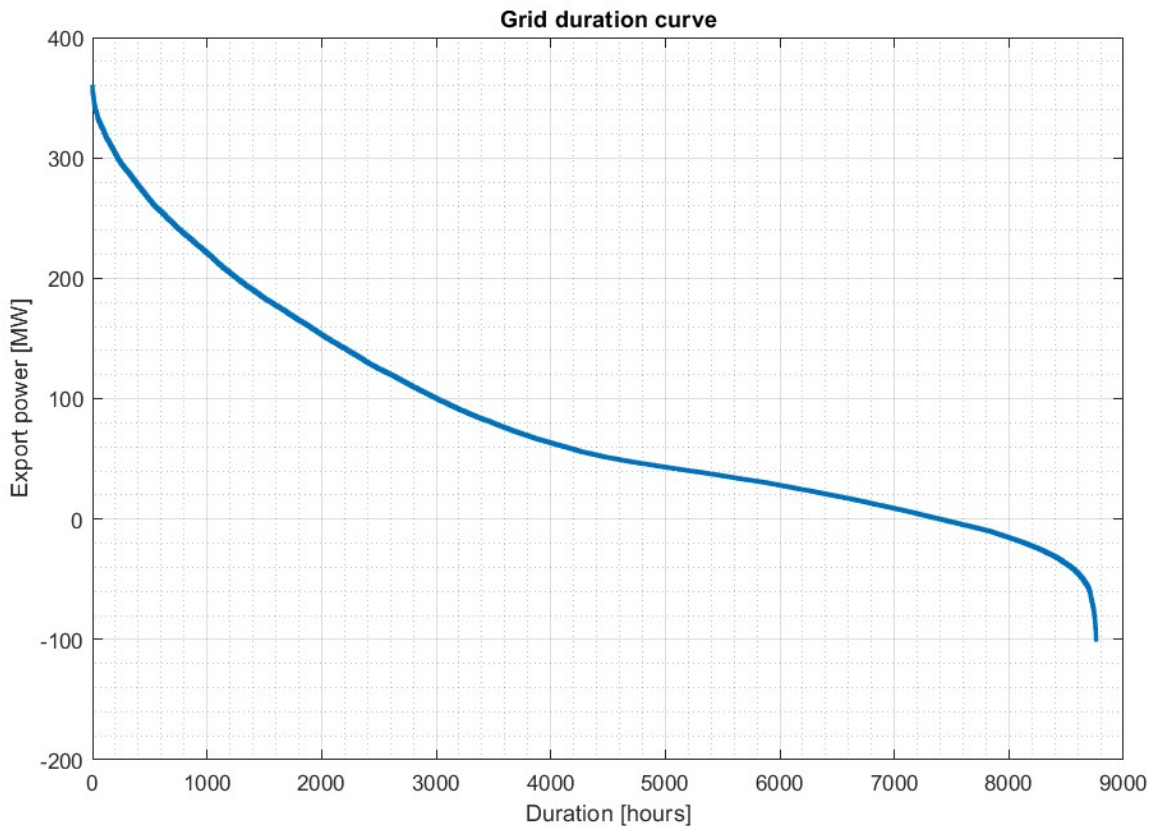


Fig.95 Electrical grid power duration curve

Observing the above duration curve, it is possible to see that the zone did export energy for 7395 hours in 2019, while for the remaining 1365 hours it imported energy. This is reasonable as the province has an energy demand that is much lower compared to its energy generation. Looking at Terna's statistical data [4.01], it is possible to see that in 2019 the whole province consumed a total of 426.3 GWh and produced a total of 4515.1 GWh: a ratio generation/consumption of 10.5. In terms of installed capacity of the province in 2019, 884.4 MW of thermoelectric capacity were present, together with 406.4 MW of wind, 229.2 MW of hydro and 36.2 MW of solar. Most of the energy generated in the province came from thermoelectrical power stations (71.6 % in 2019 corresponding to 3235.1 GWh) and therefore we could imagine that this amount could be reduced by modulation of the combined plants while increasing the renewable generation thanks to the new offshore wind farm. However, while this might be true on the province level, the local generation is unknown and therefore it must be considered as impossible to modify it, as it might include relevant amounts of not programmable renewable energy. Just referring to yearly energy values, considering the estimated P50 of the wind farm of 1440 GWh/year, wind energy could ideally substitute 45% of the thermoelectric energy exploited by the province. In practice, considering non-simultaneous generation and demand, increase of the electric energy demand and other losses, the thermoelectric generation reduction would be lower. The following storage simulation should provide data about the dimensioning of the required storage and the economic feasibility of the project, based on wind and market data.

## 5 Coupling the Storage with the Wind farm

### 5.1 Battery Energy Storage System Simulation

To assess the economic feasibility of a BESS coupled to the wind farm, it was simulated its operation during a year by using the software MATLAB. The objective of the simulation was both to assess the economic feasibility of a storage system and its suggested size. The main inputs of the simulation were the electrical grid data, the market prices trend, and the wind farm power profile. All of these inputs were discussed in the previous chapters. The wind farm power profile was calculated as explained in Chapter 1, while market prices were extracted from historical data of GME as reported in Chapter 2. Regarding the electrical grid data, they were provided by Terna, and they were presented in Chapter 4.

Regarding the battery data, the Tesla Megapack product was used as a reference product. This was done to use reliable commercial data, which are publicly available. In particular, the Tesla website [5.01] provided the main specifications of the battery packs as well as their investment and maintenance costs. The single Megapack unit can be sold with two possible C-rate variants according to company. The first one refers to a discharge time of 2 hours (C-rate = 0.5), while the second one refers to a discharge time of 4 hours (C-rate = 0.25). Typically, energy storage units in Italy are designed with a 4-hours duration of discharge, but for grid services the C-rate used might be lower. Each unit of the 4-hour Megapack presents a storage capacity of 3.916 MWh and a rated power of 970 kW, while for the 2-hour Megapack unit their capacity is slightly lower with a total of 3.854 MWh and with a rated power that is almost double: 1.927 MW. The modularity of these BESS makes it possible to evaluate different sizes of the storage plant simply by adding more Megapack units. For this reason, it was decided to repeat cyclically the simulations with different numbers of storage units, so as to compare the results and get some indications about the needed storage size. According to the data from the Tesla website, the 4-hour product presents a round trip efficiency of 93.5% while the 2-hour one presents a round trip efficiency of 92%. These values include both the charge/discharge phases and the conversion from AC to DC and vice versa. Instead, transformation losses from Low to High voltage and vice versa were not included in this round-trip efficiency, and they had to be considered separately.

The CAPEX and OPEX of the BESS system by Tesla were extracted from the website [5.01]. Here, the investment cost needed to buy and install the Megapack units is defined as a function of the number of units required. This tool provides a realistic prediction of the capex expenses, as it also takes into account the price reduction due to the increasing size of the project. Discrete data from the site were manually extracted and then interpolated to generate a price curve linking the number of units to the corresponding CAPEX. The plot of this curve is shown in Fig.96. In addition, it was evaluated the specific CAPEX as the ratio between the CAPEX and the corresponding energy storage capacity. Looking at the specific CAPEX, it is possible to observe the previously cited price reduction that occurs with the increasing size of the storage system. The data were expressed in US Dollars, as the product is mainly sold in the American market, so a conversion factor was applied to calculate corresponding European price. As by January 2023, the USD/Euro change considered was 1.07.

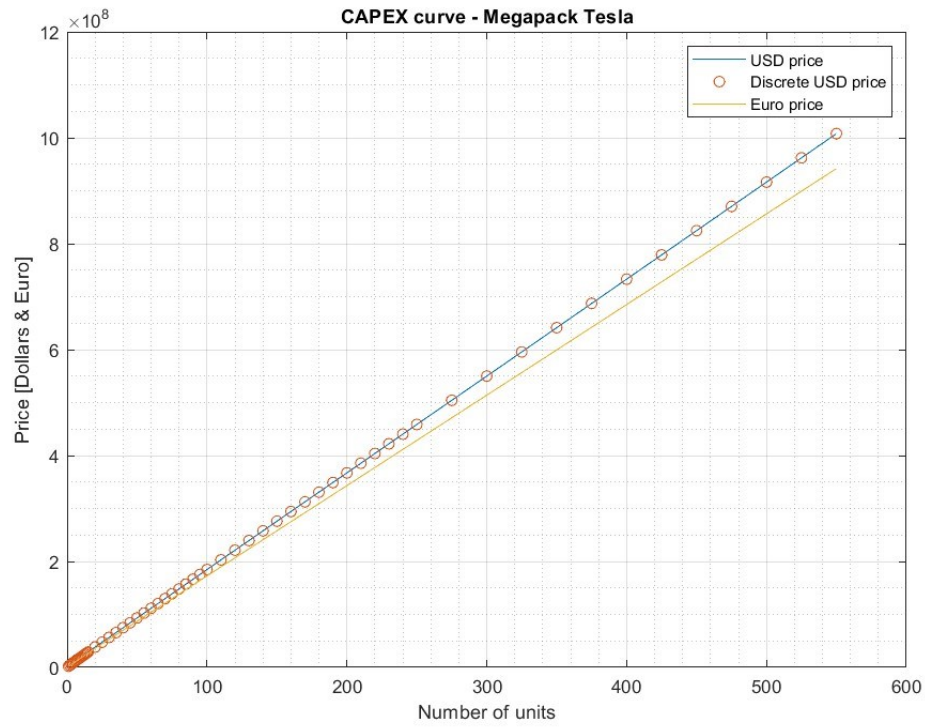


Fig.96 Capex as function of the number of Megapack units (C-rate 4 hours)

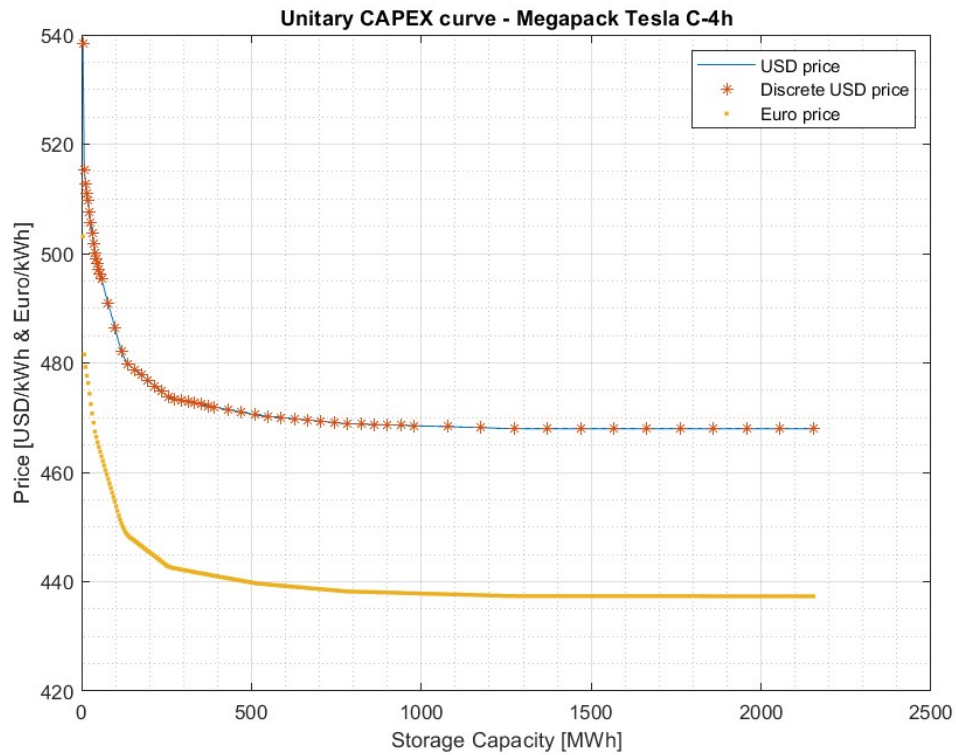


Fig.97 Specific Capex as function of the number of Megapack units (C-rate 4 hours)

In addition, the company's design tool provides data about the yearly maintenance expenses for the first year as a function of the number of units. This was therefore used as an estimation of the yearly OPEX of the BESS. As it was done with the CAPEX, the data for the same number of units were extracted and then interpolated with a spline function to generate a yearly OPEX curve. The values from this curve were used to estimate the lifetime OPEX of the system, given that the company precises that the annual maintenance cost increases by 2% per year. In the following [Fig.98](#), the estimation of the first year – OPEX curve is plotted as function of the number of units.

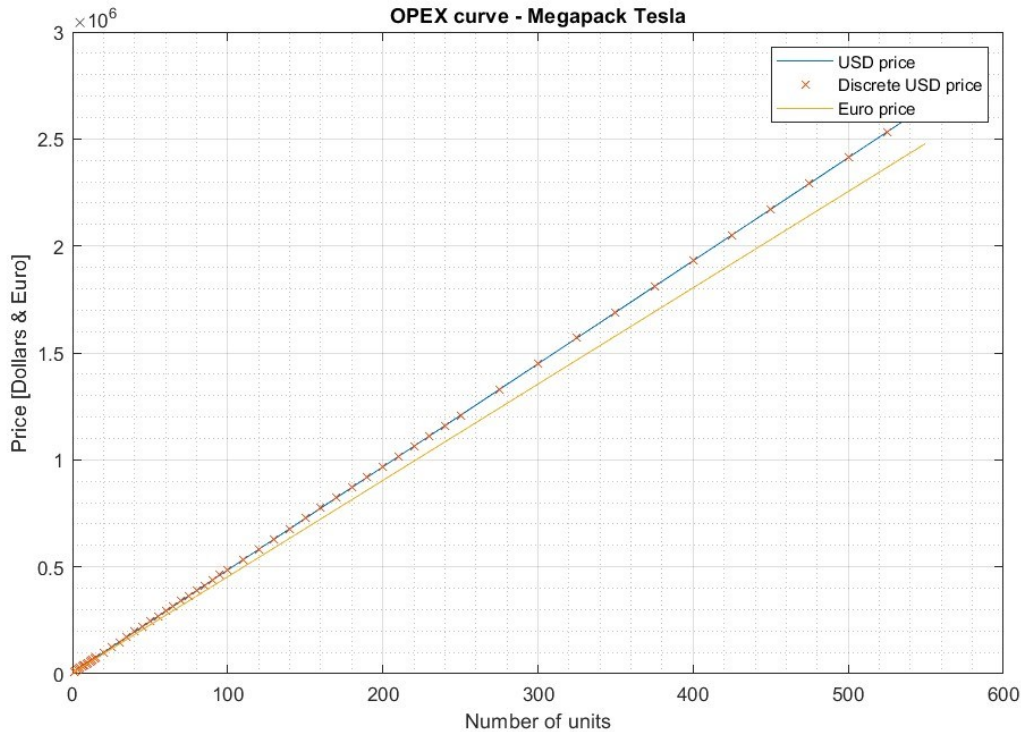


Fig.98 First year - Opex as function of the number of Megapack units (C-rate 4 hours)

It should be noticed that BESS costs have increased over the recent years, partially moving against the cost decrease over which batteries underwent in the last decade. This can be noticed looking at specific CAPEX values, which are now in the range 510 – 470 kUSD/MWh for the 4-hour Megapack and between 680 and 480 kUSD/MWh for the 2-hour Megapack. The previous Megapack version, proposed by Tesla in 2021 [5.02], consisted of a 3 MWh capacity storage per unit. The specific price of this previous model was significantly lower, as it ranged between 406 and 278 kUSD/MWh. This price increase can be explained by the problems in the materials supply chain that occurred between the end of 2021 and 2022, that caused a spike on the prices of many resources and on final products. In addition, a further price increase could be explained by the change in the battery technology used by the Megapack product, which now uses LFP battery cells. In the following, the Capex, Opex and specific Capex curves are presented also for the 2-hour Megapack product.



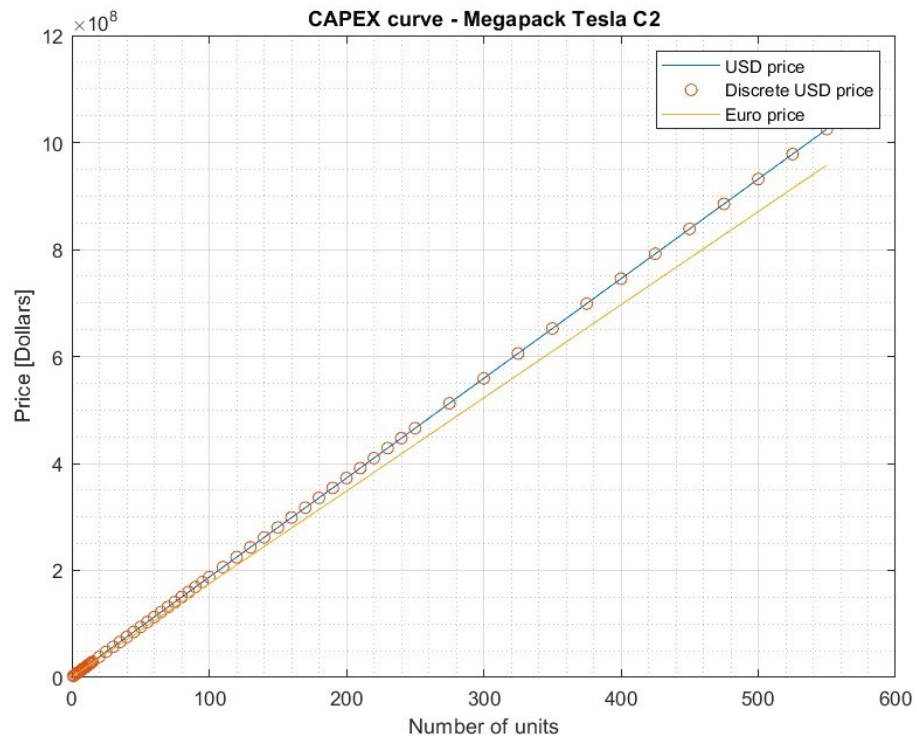


Fig.99 Capex as function of the number of Megapack units (C-rate 2 hours)

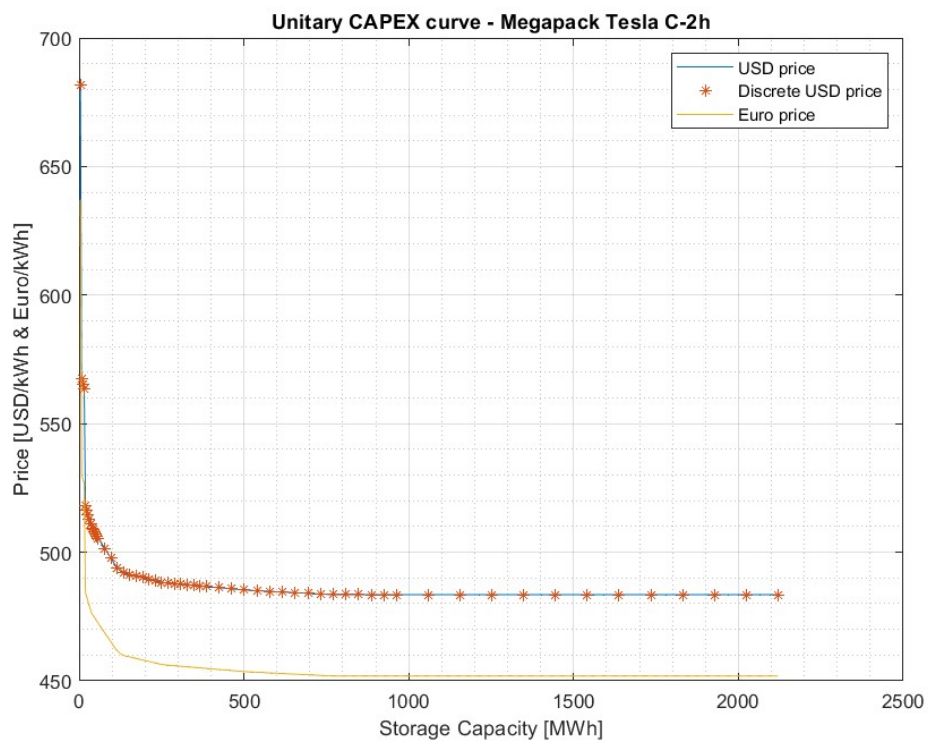


Fig.100 Specific Capex as function of the number of Megapack units (C-rate 2 hours)



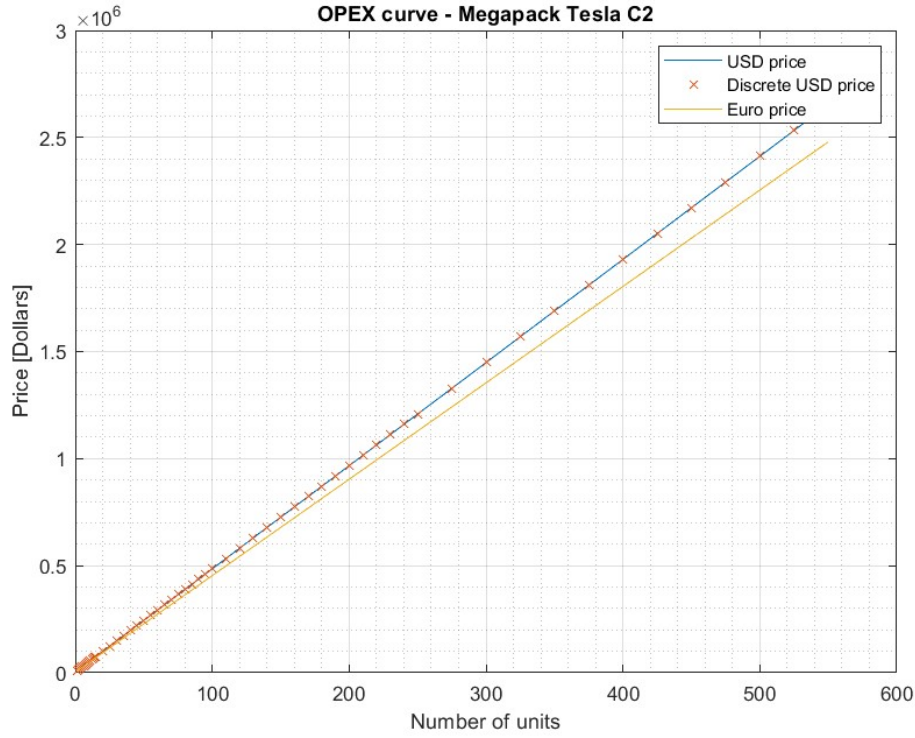


Fig.101 First year - Opex as function of the number of Megapack units (C-rate 2 hours)

### 5.1.1 Operation of the Battery System

In the simulation of the storage, some constraints and characteristics were defined to describe its operation. As a simplification, the BESS was operated as a unique black box, characterized by its capacity, power, efficiency and by its state of charge. It was then assumed that in real operation the BMS would have optimized the operation of each battery pack.

As previously mentioned, the data about the efficiency, power and storage capacity were taken from the Tesla Megapack product characteristics. Starting from the efficiency of the system, in the model the transformer losses were included both during charge and discharge. In particular, as it was done in the wind farm power profile generation, it was cautiously considered a transformer efficiency of 98%. Therefore, if added to the 93.5% round-trip efficiency of the AC/DC conversion and battery charge/discharge, the complete AC-AC cycle for the 4-hour Megapack accounted for a round-trip efficiency of 89.79%.

$$RTE_{4hour} = \eta_{transformation} \cdot \eta_{BESS} \cdot \eta_{transformation} = 0.98 \cdot 0.935 \cdot 0.98 = 89.79 \%$$

It was assumed to equally distribute half of the losses to the charging phase and the other half to the discharging phase. During the charge phase it was assumed a charge efficiency of 94.78%, and similarly during discharge it was assumed a discharge efficiency of 94.78%. These values, if combined, give the previous result of 89.79% of total round-trip efficiency. The round-trip efficiency for the 2-hour Megapack was calculated in the same way:

$$RTE_{2hour} = \eta_{transformation} \cdot \eta_{BESS} \cdot \eta_{transformation} = 0.98 \cdot 0.92 \cdot 0.98 = 88.35 \%$$

Then, once again, the efficiency was equally distributed on the charge and discharge phase by assumption with a 94% value for each phase. These efficiency values were used to determine the amount of energy charged and discharged from the storage, as well as the power absorbed and injected on the DC and AC sides. In particular, the “AC” side considered was the one on the High voltage level of the connection between the storage plant and the national grid; while the “DC” side was the one after the converter and it ideally accounted for the power fluxes directly entering or exiting from the battery. The charge and discharge efficiencies were used to determine the effective amount of energy charged and the effective amount of energy sold, compared to the energy purchased and to the energy discharged. The equations considered are here shown.

$$Power_{charged} = Power_{purchased\ AC} \cdot \eta_{charge} \rightarrow Power_{charged}$$

$$Power_{discharged} = \frac{Power_{sold\ AC}}{\eta_{discharge}} \rightarrow Power_{sold\ AC}$$

In order to estimate the lifetime of the BESS, various degradation models have been developed over the years. However, these models are often related to experimental data and require deep knowledge of the operative conditions of the BESS. As explained in Chapter 3, batteries' lifetime is influenced by the temperature of operation, by the depth of discharge, by the overcharge level, by the speed of charge and discharge and therefore by voltage and current levels, and in the end by the number of cycles. Since the battery type considered for this simulation has a C-rate of 4 or 2 hours, the ageing mechanism related to fast charge and discharge was considered to be negligible. Regarding the operational temperature, it was supposed to be able to keep the battery in optimal conditions thanks to the thermal management. In addition, considering the location in the south of Italy, it was supposed to be able to avoid critical low temperatures thanks to the relatively hot climate. In order to ensure a long lifetime of the system, as it is usually done with lithium batteries, it was supposed to limit the storage operation with a maximum Depth of Discharge of 80% (corresponding to a 20% SoC) and with a maximum State of Charge of 90% to prevent overcharge. In the end, to evaluate the duration of batteries, it was decided to count the number of equivalent cycles of operation. The number of equivalent cycles was used to estimate the portion of life of the battery system exploited during the year, and therefore to estimate the remaining years of life. The number of equivalent cycles ( $N_{eq}$ ) was evaluated considering all the charge and discharge variations of the State of Charge of the battery. Each charge variation of full charge or full discharge (100% to 0%) accounted for half cycle, as shown in the following equation.

$$N_{eq} = \sum \frac{|\Delta Soc|}{2}$$

As explained in Chapter 3, Li-ion batteries have a variable lifetime from 3000 up to 10000 cycles in particular conditions [3.31]. Typically, for stationary applications, the same source estimates a lifetime of 4000 to 5000 cycles with 100% DoD operation and with a lifetime limit of 70% of the initial storage capacity. Considering that LFP batteries have one of the highest lifetimes between Li-ion batteries, the

number of cycles could be even higher. This is shown by [5.03], which estimates that LFP batteries can achieve lifespans of 2500 to 9000 cycles over a range of different conditions. In this case, the lifespan limit was set when the degradation process led to 80% of the initial capacity. Some of the results of the paper are shown in Fig.102, where it is possible to observe that with a DoD of 100% and C-rate of 2 hours (0.5C) the individual cells should be able to withstand more than 6000 cycles. Therefore, with a C-rate of 0.25 and operation limited in the range 20-90% SoC, the number of full equivalent cycles expected to reach 70% of the initial capacity could be reasonably set between 6000 and 10000 cycles.

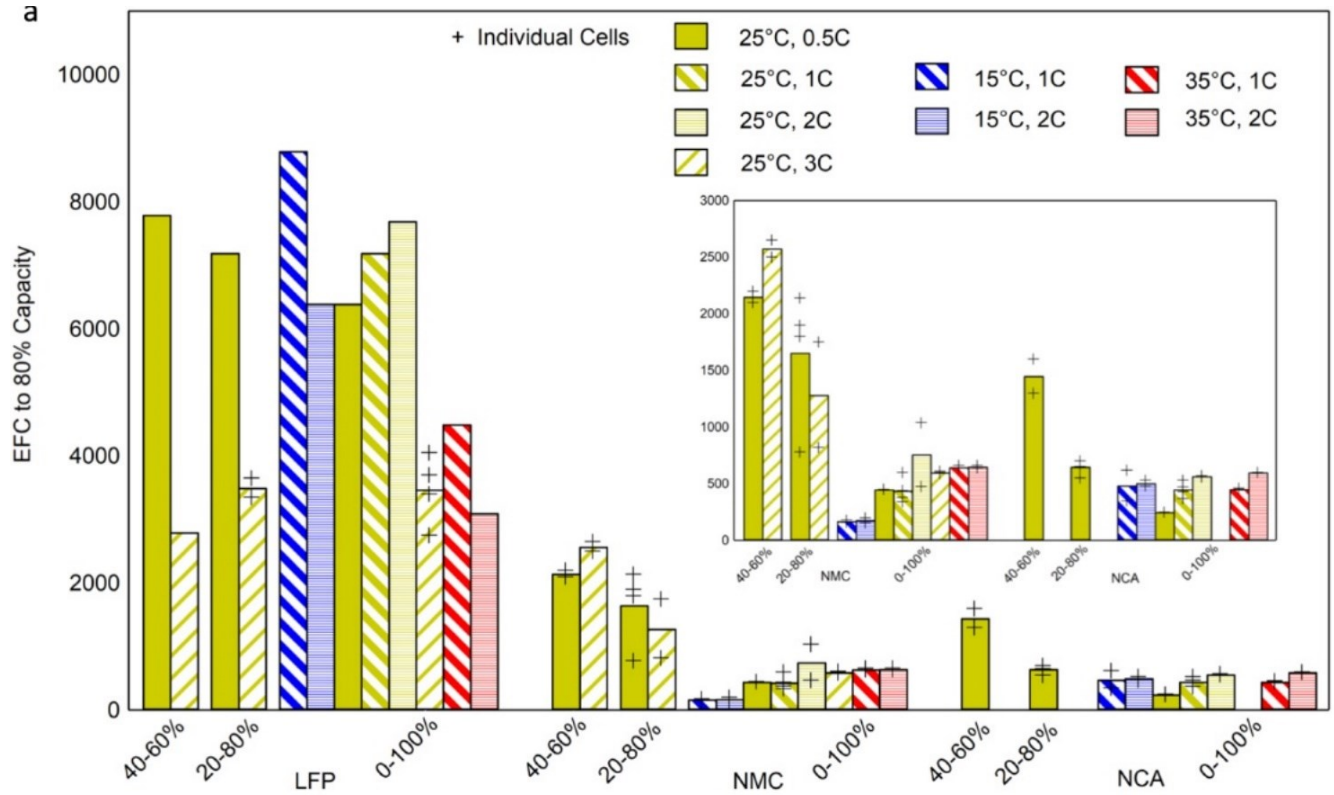


Fig.102 Equivalent full cycle (EFC) count at 80% capacity for different cells and cycling conditions [5.03]

Regarding the self-discharge mechanism, it was supposed a discharge rate of 3%/month, as the typical values range between 2 and 3%. The self-discharge rate was applied only in periods of resting of the storage, where no charge and discharge schedules were present. The following equation allowed to determine the velocity of self-discharge referred to the quarter of hour time step of the simulation.

$$\text{Self - Discharge rate} = \frac{0.03 \cdot \text{Storage Capacity}}{\frac{365}{12} \cdot 24 \cdot 4} \left[ \frac{\text{MWh}}{\frac{1}{4} \text{ hour}} \right]$$

### 5.1.2 Energy Storage Simulation

At first, the company asked to study the feasibility of using a battery energy storage system to overcome the inadequacy of the grid. In this scenario, the offshore wind farm would have been connected to the Crotona region without any grid improvements. This might represent a possible scenario under which Terna might not be able to guarantee the grid adequacy due to the too fast renewable growth in the south. As explained in Chapter 4, the maximum export from the Crotona region registered in 2019 was around 360 MW, therefore it was assumed that the maximum export capacity of the zone was of 400 MW, which might be reasonable considering that most of those data refer to the 150 kV grid. Therefore, we would have a bottleneck in the export from Crotona towards the other portions of Calabria and towards the other regions. For this reason, it was assumed to use a BESS to time shift the wind power generated from the wind farm to allow the respect of the transmission capacity and reduce the curtailments. Considering that the wind farm would have a rated power of 495 MW and that the region is already frequently in export conditions, a bottleneck of 400 MW in the export power would be very dangerous for the plant operation. In fact, the TSO might need to disconnect the plant from the grid to preserve the safety of the system, preventing the injection of wind power and mining the revenues and economic feasibility of the wind farm. In order to simulate the operation of a storage, the previously generated wind profile was summed to the grid load data, so as to identify periods of overload for the grid. Then, it was supposed to operate the storage by participating in the MSD market, providing services to the grid and solving the congestions. The participation to this market with the storage system as standalone was chosen, rather than a direct connection with the wind farm, because it was expected that the wind farm would be able to receive an incentive that would assure a fixed sale price, independently from the PUN value. Therefore, the injection of wind power directly in the BESS rather than in the national grid would have caused the loss of the possibility to sell that energy at the fixed price of 185 €/MWh. Differently, the injection on the local grid and the purchase with a separate storage could have been more economically interesting for the company, lowering the risk for the wind farm and making it possible to operate the storage with market prices. The historical results of the MSD and MB volumes elaborated in Chapter 2 were not considered in this case, as the requests to increase or decrease power would have been linked only to the local grid and wind farm. However, to provide data about the economic operation of the system, the historical hourly prices “up” and “down” previously calculated in Chapter 2 were used for the simulation, referred to years from 2018 to 2022. As it was decided to operate in the MSD market, it was considered to not be able to schedule the battery operation in advance, as the results of the bidding system are typically available very close to real-time. It should be noticed that the addition of a large wind farm in Calabria could have a strong influence on the region, lowering the energy price of the market in periods of abundant production, both on the dispatching services market and on the MGP market. However, the forecasting of prices would be difficult, therefore it was supposed to use the historical data as they are, without studying the wind farm effect on the market.

To determine the size of the storage it was decided to make iterative calculations, varying the storage size by increasing the number of Megapack units considered. By varying the storage size, the BESS power capacity would be varied and therefore its capability to operate on the market and to solve the congestions would have been affected too. This should have provided useful information about the

storage size effectively needed for the case considered. In addition, the variation of number of battery units, would have changed the investment costs and the operative costs. The respective CAPEX and OPEX were calculated from the curves defined at the beginning of this Chapter. In particular, for the OPEX, it was considered the 2% increase of expenses per year, considering the 15-year lifetime guaranteed by Tesla.

$$CAPEX = Capex(N_{units})$$

$$OPEX_{lifetime} = Opex(N_{units}) \cdot \sum_{n=1}^{15} 1.02^{n-1}$$

In order to understand when it would have been economical to operate the storage, it was supposed to try different levels of price for the offers to buy and to sell energy for each storage size. Considering that Terna accepts the best offers not only in terms of price but also in terms of adequacy to solve the grid issues, the outcome of the participation to the MSD market would be very difficult to predict with sufficient certainty. However, given the particular condition described by this first scenario, it was supposed to be the only local operator able to solve the congestions, and therefore the rule to decide whether the offers would have been accepted or not was based only on the prices offered. For periods of congestion, the offers “down” were considered to be accepted in case the price offered to buy energy was higher than the historical average values accepted in the considered hour in Calabria. On the other hand, for periods of low grid load, the offers “up” were considered to be accepted in case the price offered to sell energy was lower than the historical average values accepted. It was assumed to be unrealistic and excessively optimistic to be able to be rewarded with the hourly average price values of the market.

Given the large variability of historical prices along the years, it was supposed to carry on a price optimization iteration year by year to define the best range of prices to be offered to maximize the revenues for each storage size. This was done by performing iteratively yearly simulations with constant price offers both to buy and to sell in the MSD market. To do this, a double cycle was performed, of which one fixed the maximum purchase price (equal to the constant offer to buy/charge) and the other one fixed the minimum sale price (equal to the constant offer to sell/discharge). By trying different combinations of prices, then the best result in terms of simplified yearly return of the investment was chosen as the optimal one for the storage size considered. In this simplified estimation of the ROI, the net revenue of the year was calculated as the difference between the revenues for selling energy and the expensed for the purchase of the excess energy. This net revenue was then divided by a first estimation of the investment needed, including the system cost, the installation cost and the maintenance cost (for the 15-year lifetime).

$$Return\ on\ Investment = \frac{Yearly\ Net\ Revenue}{CAPEX + OPEX_{lifetime}} = \frac{(Revenue_{sale} - Expense_{purchase})_{year}}{CAPEX + OPEX_{lifetime}}$$

The final results of the simulations consisted of the optimal results in terms of ROI for the different storage sizes for the considered year. Summarizing, the yearly simulation was included in a triple cycle, one controlling the storage size, and the other two the prices to be offered in the market sessions.

### 5.1.3 Simulation 1 – Control Strategy

In the first simulation, it was evaluated the possible bottleneck issue on the export grid, therefore the simulation was based on the local grid data about the Crotona zone by Terna (referred to year 2019). These data were considered as a picture of the local grid condition and were used also in the simulation of the other years (2018-2022). Equally, the same wind power profile was considered for the simulation of all years. The only difference between these local simulations was on the prices “up” and “down”, which were linked to the historical data, and which influenced the BESS behavior and the economic results. The wind power profile and the grid data were compared by summing them. In case of existing export for the grid data (considered as positive in the simulation), the sum of the already present power fluxes and the wind power provided a total theoretical export flux. Similarly, in case of grid import (considered as negative in the simulation), the sum between import required and the wind power generated (positive) provided a theoretical excess power flux to be exported from the local region or an import power flux. The resulting export fluxes were then compared to the bottleneck threshold to determine whether the wind farm could have operated normally or whether the plant had to be stopped or disconnected. The possible conditions identified are here analyzed.

#### 1) Export condition & Wind power excess – [Charge 1]

The wind power excess condition was identified evaluating when in the considered timestep the sum of the wind power and the export power flux was higher than the export capacity of the grid.

$$P_{wind}(i) + P_{grid\ export}(i) \geq Threshold$$

The excess power was evaluated as the difference between the wind power profile and the export power flux.

$$Excess\ power(i) = P_{wind}(i) + P_{grid\ export}(i) - Threshold$$

In this condition, the export towards the surrounding zones was limited by the transmission capacity, and the wind farm would have been partially disconnected or fully stopped to avoid overloads. For this reason, it was evaluated the possibility of charging the energy storage with the excess wind power production, so as to allow the operation of the wind farm without overloading the transmission lines. At this point, the choice on whether charging the storage or not was based on the market data. For the considered timestep, the price down in the MSD & MB was compared to the maximum price level chosen before the simulation. In case of a market price lower than the upper threshold, it was configured the possibility to buy the available energy. Otherwise, in case of higher price or non-defined price down (price = 0 in case of no offers accepted) it was decided to keep the BESS in a stand-by mode.

$$Price_{down}(i) \leq Max\ purchase\ price\ threshold \rightarrow charge\ condition$$

$$Price_{down}(i) > Max\ purchase\ price\ threshold(i) \quad or \quad Price_{down}(i) = 0 \rightarrow standby\ condition$$

In the case of the standby mode, only the self-discharge rate was applied to the storage system. Conversely, in the case of the charge mode, the state of charge of the battery at the given timestep was evaluated so as to determine the charge possibilities. The three constraints to be addressed were the limits to the state of charge and the capacity of the storage, and also its rated power. In particular, the general conditions to charge the excess power from the grid are here reported:

$$SoC\ constraint \rightarrow SoC(i) < Max\ charge\ level$$

$$Capacity\ constraint \rightarrow SoC(i) + Excess\ energy \leq Max\ Energy\ level$$

$$Power\ constraint \rightarrow Excess\ power \leq Rated\ Power$$

Regarding the capacity constraint, it was also considered the charge efficiency of the system, as the power absorbed from the grid would have been higher than the one effectively charging in the storage. In addition, the upper limitation of the storage capacity was introduced. Therefore, the complete capacity constraint was:

$$Energy\ stored(i) + Power_{charge\ AC}(i) \cdot timestep \cdot \eta_{charge} \leq (Max\_charge \cdot Storage\_Capacity)$$

Similarly, regarding the power constraint, the charge efficiency was once again considered to determine the power flux that would have been effectively reaching the battery during the absorption of the excess wind power.

$$Power_{charge\ AC}(i) \cdot \eta_{charge} \leq Rated\ Power\ DC$$

By evaluating these constraints for the charge mode, the following resulting possible conditions were identified.

- a. Storage fully charged.

The first case defined was the condition of storage already fully charged, to which was applied the standby condition. In this case, the power generated by the wind farm could not have been injected in the electrical grid, and then it would have been curtailed. The following conditions refer all to not fully charged storage.

- b.  $SoC + Energy\ Charged \leq Max\ capacity \ \& \ Power\ required\ DC > Storage\ rated\ power\ DC$ .

In this second condition it was found that the energy to be absorbed by the grid could be accepted in the storage, but the excess wind power was higher than the rated power of the storage system. Therefore, for this condition it was decided to apply a charge mode at full power for the storage in the considered timestep. The remaining excess power would then be curtailed because of the storage unavailability.

- c.  $SoC + Energy\ Charged \leq Max\ capacity \ \& \ Power\ required\ DC \leq Storage\ rated\ power\ DC$ .



In this third case, both the capacity and the power constraints were satisfied, and it was possible to charge the storage with the excess power from the grid, fully avoiding the curtailment.

d.  $SoC + \text{Energy Charged} > \text{Max capacity}$ .

In the fourth case, the storage capacity constraint was not satisfied, therefore it was not possible to accumulate all the excess power from the wind farm. The charge power to be absorbed was then modulated so as to not exceed the storage maximum capacity constraint.

$$Power_{charge\ AC}(i) = \left( \frac{(Max\_charge \cdot Storage\_Capacity) - Energy\ stored(i)}{timestep \cdot \eta_{charge}} \right)$$

This partial charge condition would still be subject to the rated power constraint. Therefore, in case this new power was higher than the rated one, the charge phase was performed at rated power. In case of charge power lower than the rated one, an additional constraint was added to prevent operation at excessively low load. In particular, it was set that for charge power required lower than 20% of the rated power, the battery system would not have entered operation by adopting a standby mode. Otherwise, the BESS would have operated with a partial load charge.

Under all these conditions of “charge”, the simulation would have then evaluated the charge power, the new state of charge of the system, the expense to buy the energy, and eventually the amount of energy curtailed.

$$Expense = Power_{charge\ AC}(i) \cdot timestep \cdot Price(i)$$

## 2) Export condition & Low Grid Load - [Discharge 1]

This second condition was identified by evaluating when in the considered timestep the sum of the wind power and the power already in export from the zone was lower than the export threshold.

$$P_{wind}(i) + P_{grid\ export}(i) < Threshold$$

In this case, it was identified an opportunity to release energy and export to the national grid from the zone.

$$Possible\ power\ transmission(i) = Threshold - (P_{wind}(i) + P_{grid\ export}(i))$$

In this condition, the wind power did not overload the zone, and it was considered the possibility of discharging the storage to sell to the adjacent regions and to empty the storage for a future charge. Once again, the choice was on the market prices, that had to be analyzed to decide if it was worth to sell the stored energy or not. Therefore, for the timestep considered, the price up in the MSD & MB was compared to the minimum price level at which energy could be sold. This minimum price was determined as the sum of the maximum purchase price and the minimum price difference set.

$$Minimum\ sale\ price = Max\ purchase\ price\ threshold + \Delta price$$

If the market price was higher than the threshold, it was possible to evaluate the possibility of discharging the storage. Conversely, if the price up was too low or non-defined (price = 0 in case of no offers accepted), the storage was set to keep the charge and apply the standby mode.

$$Price_{up}(i) \geq \text{Minimum sale price} \rightarrow \text{discharge condition}$$

$$Price_{up}(i) < \text{Minimum sale price} \quad \text{or} \quad Price_{up}(i) = 0 \rightarrow \text{standby condition}$$

Once again, in case of standby operation, the self-discharge only would be considered. Otherwise, in case the prices were favorable for energy sale, the constraints of operation were evaluated as for the charge phase. The constraints still referred to the level of charge, to the capacity and the rated power of the system. The general constraints are here reported.

$$SoC \text{ constraint} \rightarrow SoC(i) > \text{Min charge level}$$

$$Capacity \text{ constraint} \rightarrow SoC(i) - \text{Energy request}(i) \geq \text{Min energy level}$$

$$Power \text{ constraint} \rightarrow \text{Power request}(i) \leq \text{Rated Power}$$

As it was done for the excess of wind power, both the discharge efficiency and the minimum energy stored threshold were considered in the capacity constraint. It was considered that to meet the grid power requirement it was necessary to discharge a larger power from the battery, as there were losses during the discharge, the conversion and the transformation.

$$\text{Energy stored}(i) - \frac{\text{Power}_{\text{discharge AC}}(i) \cdot \text{timestep}}{\eta_{\text{discharge}}} \geq (\text{Min\_charge} \cdot \text{Storage\_Capacity})$$

Regarding the rated power constraint, the same concept related to the efficiency was added.

$$\frac{\text{Power}_{\text{discharge AC}}(i)}{\eta_{\text{discharge}}} \leq \text{Rated Power DC}$$

Evaluating these constraints for the discharge, the following resulting possible cases were identified.

- a. Storage fully discharged.

In this first case, the constraint of availability of energy was not satisfied, as the level of charge was equal or lower than the minimum threshold, and the BESS was therefore not able to provide energy to the grid. In this situation, it was decided to apply the standby condition waiting for a power excess condition to recharge the system.

- b. SoC - Energy Discharged > Min capacity & Power required DC > Storage rated power DC.

In this second case, the storage would be able to discharge without trespassing the threshold of the minimum energy stored, but it would be possible to apply a discharge power higher than the nominal

one. Therefore, for this condition it was decided to apply a discharge at full power in the considered timestep.

c. SoC - Energy Discharged > Min capacity & Power required DC ≤ Storage rated power DC.

In the third case, both the constraints were satisfied: the storage would be able to discharge without trespassing the threshold of the minimum energy stored and the power required could be fully provided by the BESS.

d. SoC - Energy Discharged < Min capacity.

In the last case, the capacity constraint was not satisfied, and the storage would have been required to discharge below its minimum energy stored level. Therefore, it was decided to apply a partial discharge that would lead the storage exactly to its minimum energy stored level.

$$Power_{discharge\ AC}(i) = \left( \frac{Energy\ stored(i) - (Min\_charge \cdot Storage\_Capacity)}{timestep} \right) \cdot \eta_{discharge}$$

This partial discharge condition was still subject to the rated power constraint. Therefore, in case this new discharge power was higher than the rated one, the discharge phase was performed at rated power. Conversely, in case of possible discharge power lower than the nominal one, the discharge was performed with partial load discharge.

Under all these conditions of “discharge”, the simulation would have then evaluated the discharge power, the new state of charge of the system and the revenue for the energy sale.

$$Revenue = Power_{discharge\ AC}(i) \cdot timestep \cdot Price(i)$$

### 3) Import condition & Wind power excess - [Charge 2]

In this third condition, it was found an import power condition on the grid with wind power overgeneration. The excess of wind power was once again calculated with the difference between the residual wind power and transmission capacity threshold. Here, the residual wind power was calculated as the sum of the wind power to the land and the (negative) import required. The check to identify the overgeneration and the estimation of the excess wind power equations are here reported.

$$P_{wind}(i) + P_{grid\ import}(i) \geq Threshold \quad \text{where} \quad P_{grid\ import}(i) < 0$$

$$Excess\ power(i) = P_{wind}(i) + P_{grid\ import}(i) - Threshold$$

Under this condition the import was fully covered by the wind power, and the excess energy might have been curtailed. In order to avoid this, it was evaluated the possibility to charge the storage with the excess power, as it was done in condition 1).

#### 4) Import condition & Low Grid Load - [Discharge 2]

In this final import condition, the wind power did not cause any local overload, and the transmission was able to export some energy to sell in the adjacent markets. The space available for power transmission out of the zone was calculated once again as the difference between the transmission capacity threshold and the sum of wind and local power generation.

$$P_{wind}(i) + P_{grid\ import}(i) < Threshold \quad \text{where} \quad P_{grid\ import}(i) < 0$$

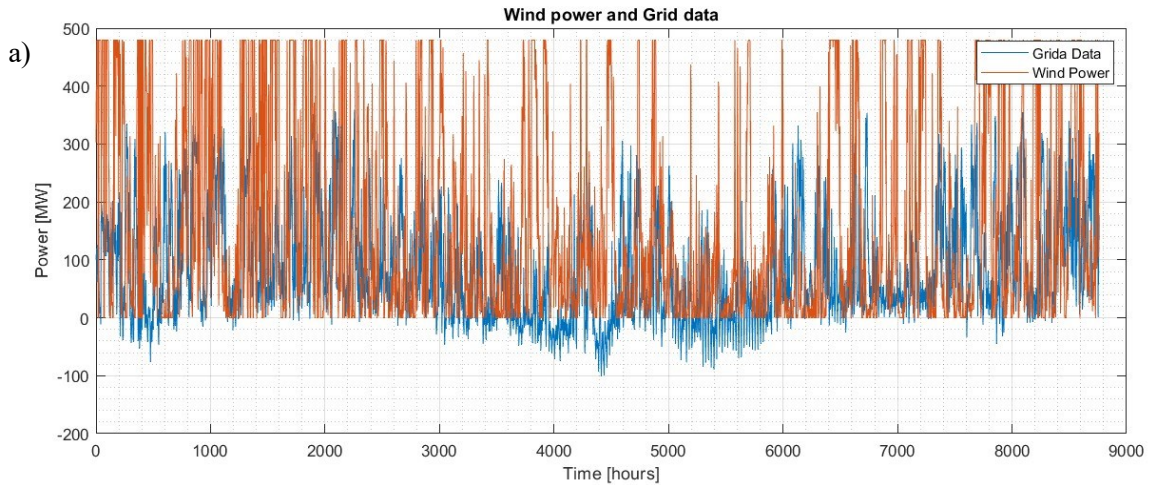
$$Possible\ power\ transmission\ (i) = Threshold - (P_{wind}(i) + P_{grid\ import}(i))$$

For this condition, it was decided to evaluate the possibility of selling as much as possible of the energy previously stored in the BESS. The process was then identical to condition 2).

### 5.1.4 Simulation 1 – Results

#### Single Cycle Results

To show how the storage model works, some plots related to a single cycle of the year 2018 simulation are represented in the following as an example. Particularly, these plots refer to the simulation of a BESS made of 50 megapack units with c-rate 4 hours (195.8 MWh) with market prices of 2018, maximum purchase price set to 50€/MWh and minimum sale price set to 100€/MWh.



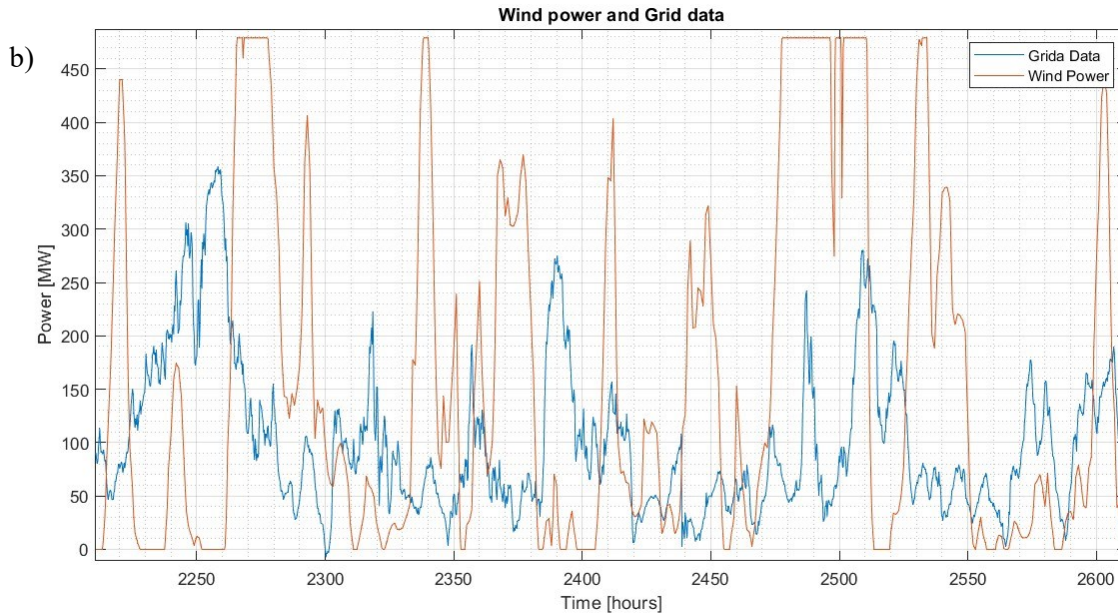


Fig.103 Wind power profile and Local grid data - (a) year – (b) detail

Firstly, in [Fig.103](#) , it is possible to observe the superimposition of the wind power profile with the Crotona grid data by Terna, both for the whole year and with more detail for a period of time of about two weeks. Clearly, it is possible to see that the wind farm alone would exceed the transmission capacity of 400 MW, and that for most of the time the zone was already in export conditions, with the blue curve frequently above zero.

Secondly, in the next plots the storage behavior can be seen. In the first plot [Fig.104](#) it can be seen a portion of the year, where the state of charge, the power absorbed and the power injected are shown. In the second plot, instead, the state of charge during the whole simulated year can be observed. It should be noticed the presence of the upper and lower limits of the SoC, set at 90% and 20% respectively, together with the self-discharge phenomena, which can be seen during stand-by periods.

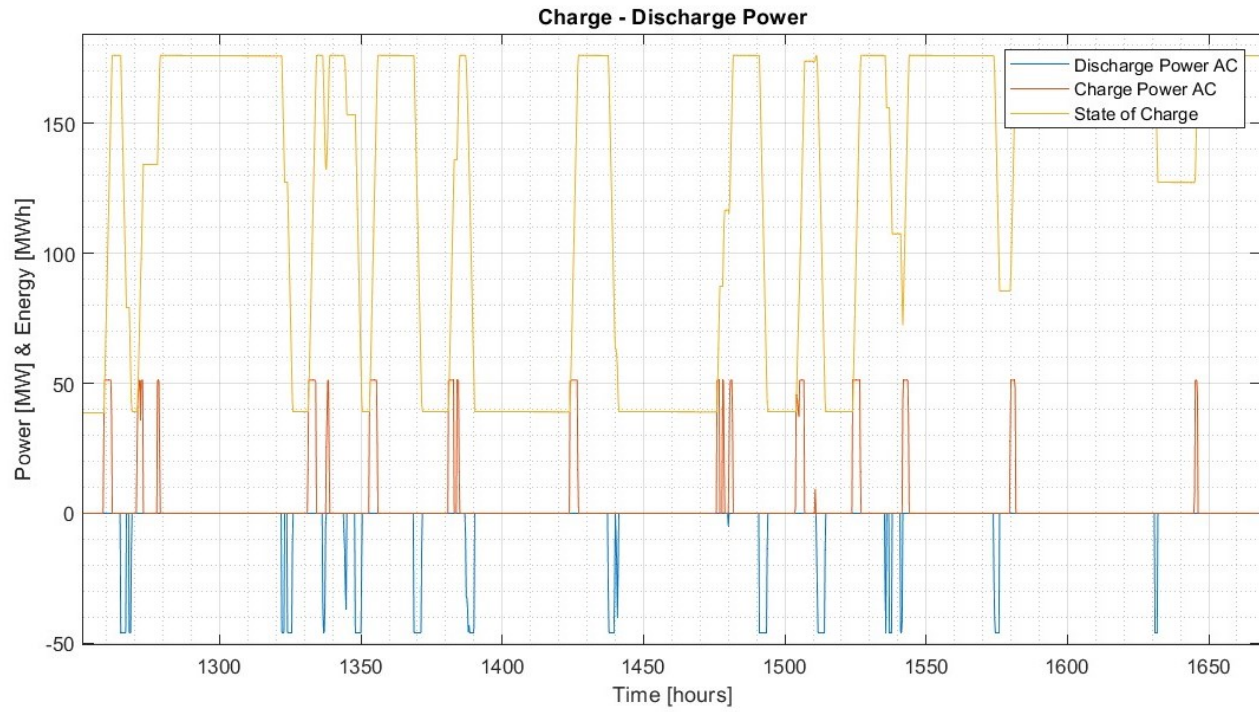


Fig.104 Example - Detail of operation for a storage

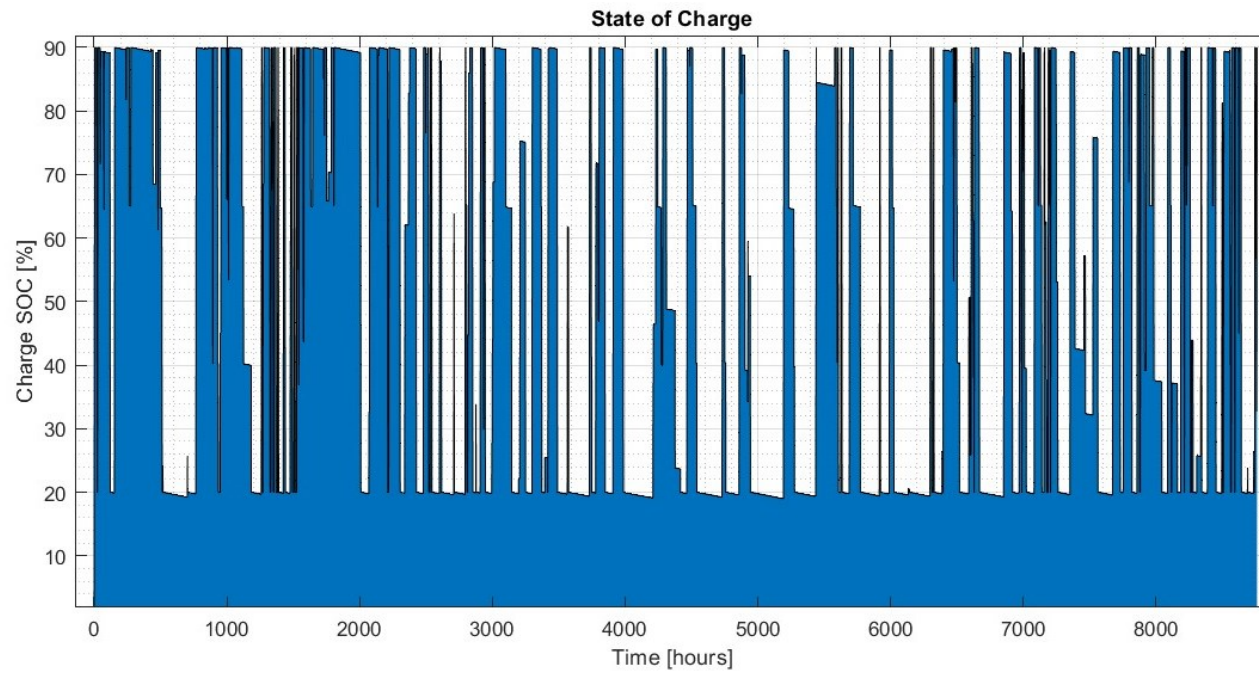


Fig.105 Example - Yearly trend of the State of Charge



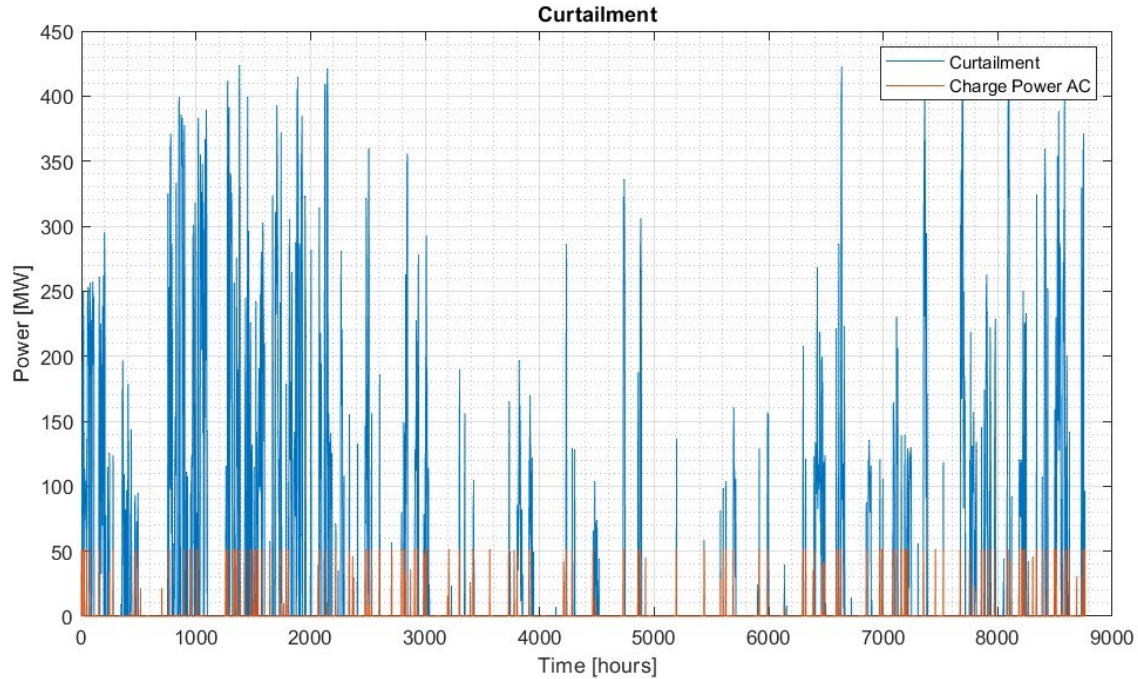


Fig.106 Example - plot of the Curtailment not avoided and of the Power absorbed by the grid

For the same example case, it is shown the curtailment that would happen to prevent the overloads (unavoidable even with the storage), together with the energy absorbed by the storage which corresponds to the curtailment avoided. Of course, for the considered example the rated power was 48.5 MW, and therefore it was not possible to absorb most of the excess wind power.

### Fixed price difference / variable storage size & variable purchase price - Results

These results show the storage behavior if the price difference is kept fixed (in the example at 50€/MWh) and different purchase price offers are evaluated in the yearly operation of different sizes of the BESS. In the following are reported the number of full equivalent cycles of the system during the simulated year (2018). It can be seen that the smaller the storage the higher the probability of being able to exploit more the storage with more cycles during the year. However, the choice of the purchase price is relevant, as it determines the amount of offers to charge that might be accepted. In addition, given the fixed price difference, the purchase price also determines the sale price, which should not be too high to avoid a lower number of accepted sales offers. In the example presented, offers to buy energy in the range between 25 and 40€/MWh (and to sell between 75 and 90€/MWh) provide optimal results in terms of cycles, but also in terms of revenues, as it can be seen in the following plots in [Fig.107](#) and [Fig.108](#). Regarding the net revenues, higher values can be obtained with larger storages, as they are able to store and sell more of the excess energy, however they would need much larger investments. Finally, it is also shown the plot of the wind power curtailment in [Fig.109](#). It can be seen that in the example with a large storage (almost 2 GWh) and with the correct price offer choice, it could be possible to avoid the curtailment of 100 GWh.

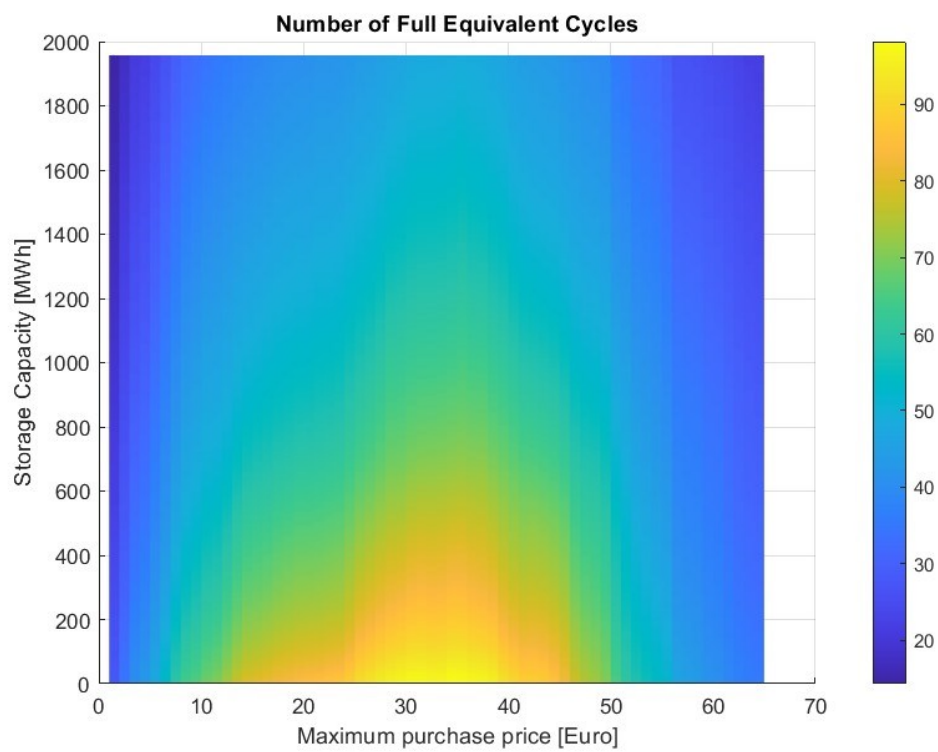
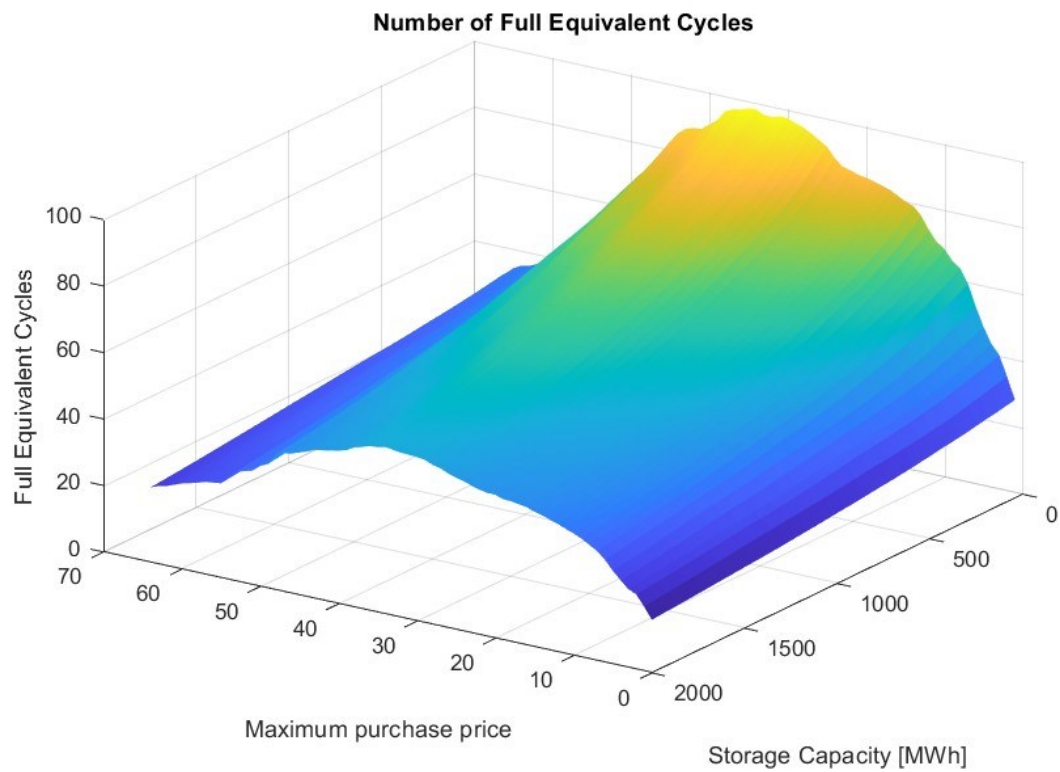


Fig.107 Example - Number of full equivalent cycles plot as function of the storage capacity and purchase price choice



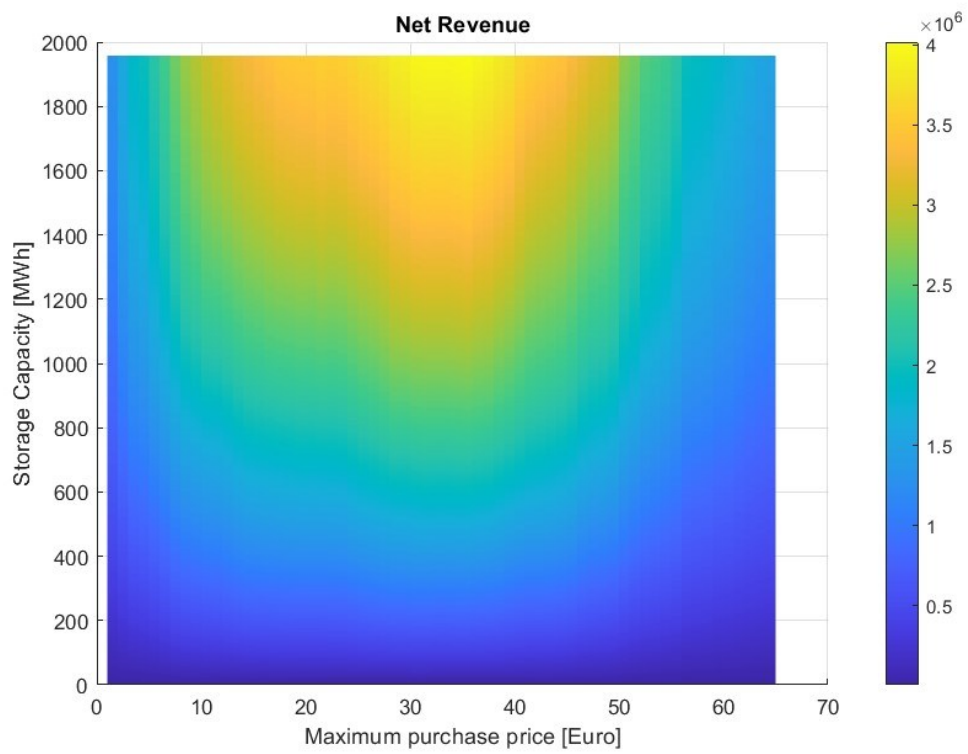
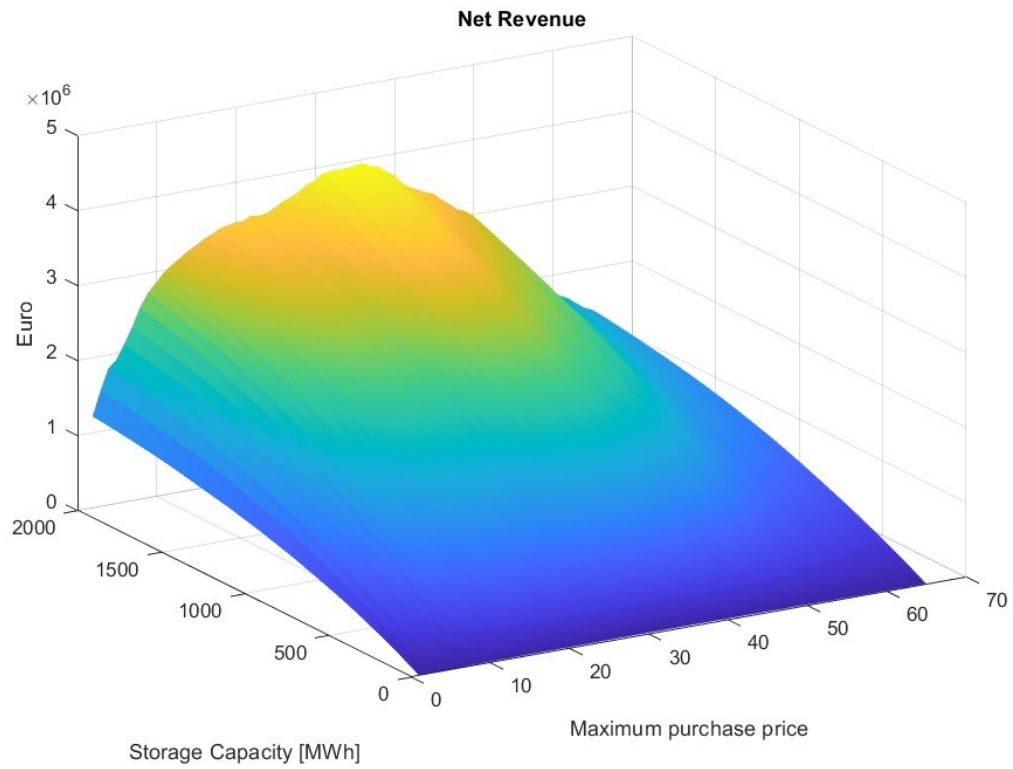


Fig.108 Example - Net Revenue plot as function of the storage capacity and purchase price choice

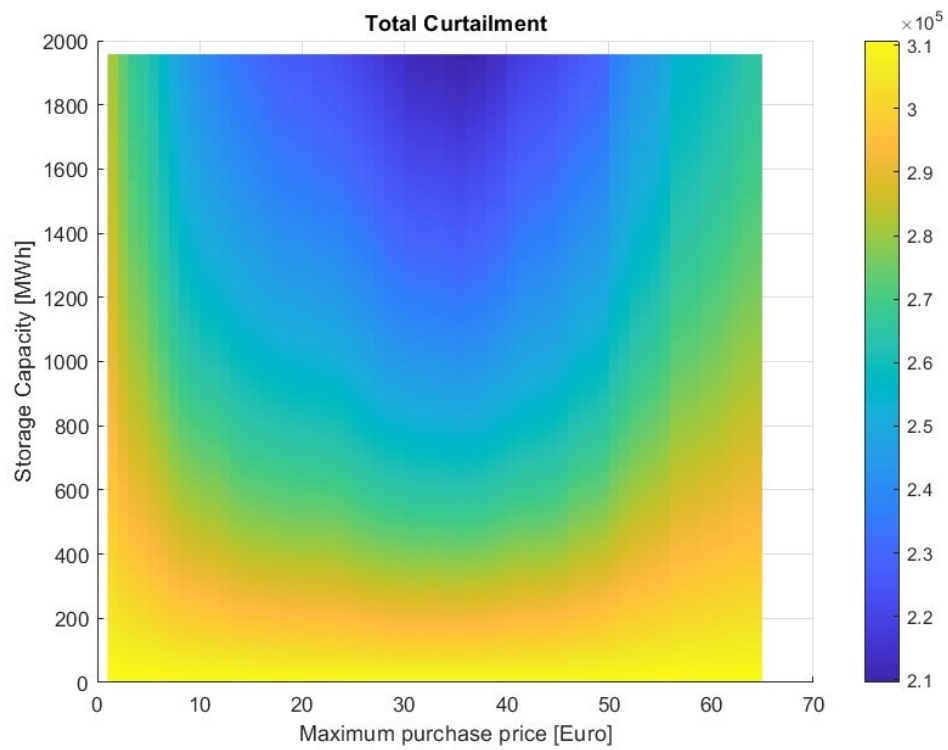
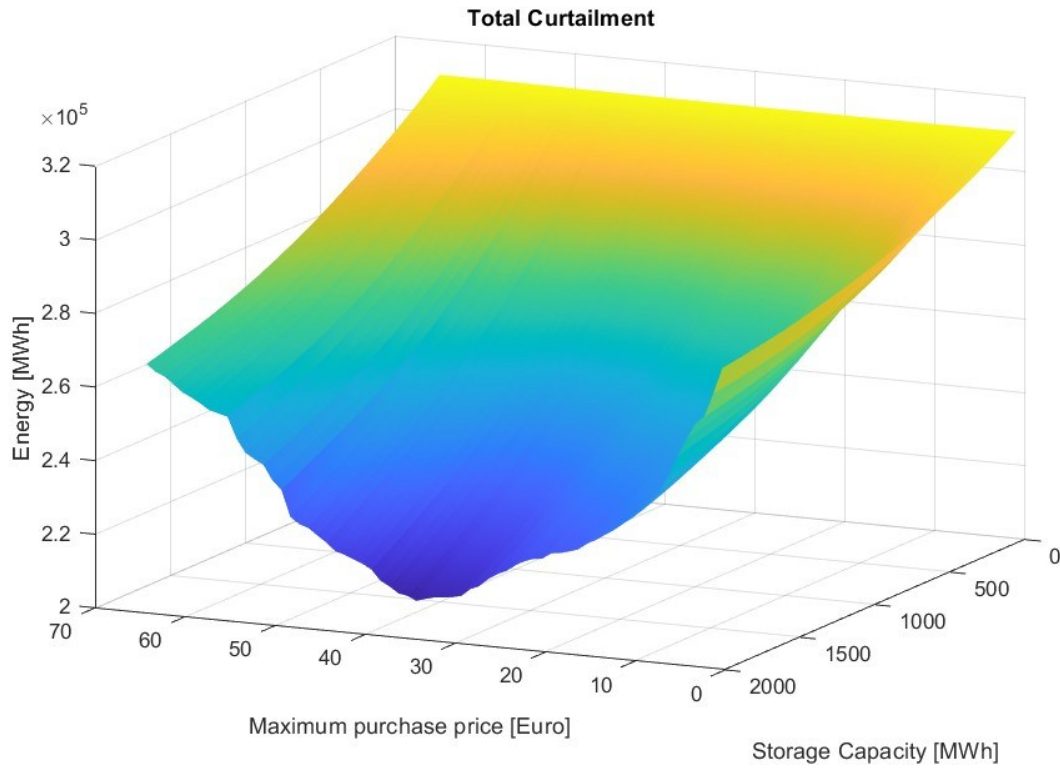


Fig.109 Example - Curtailment plot as function of the storage capacity and purchase price choice

### Fixed storage size / variable price difference & variable purchase price – Results

In this case, some examples of the price offer optimization are shown. Here, the storage size was kept fixed and the simulations were cyclically performed with different constant offers to buy and to sell energy. In the examples here reported, the simulation was performed with 50 megapack units with C-rate 4 hours (195.8 MWh) with market prices of 2018.

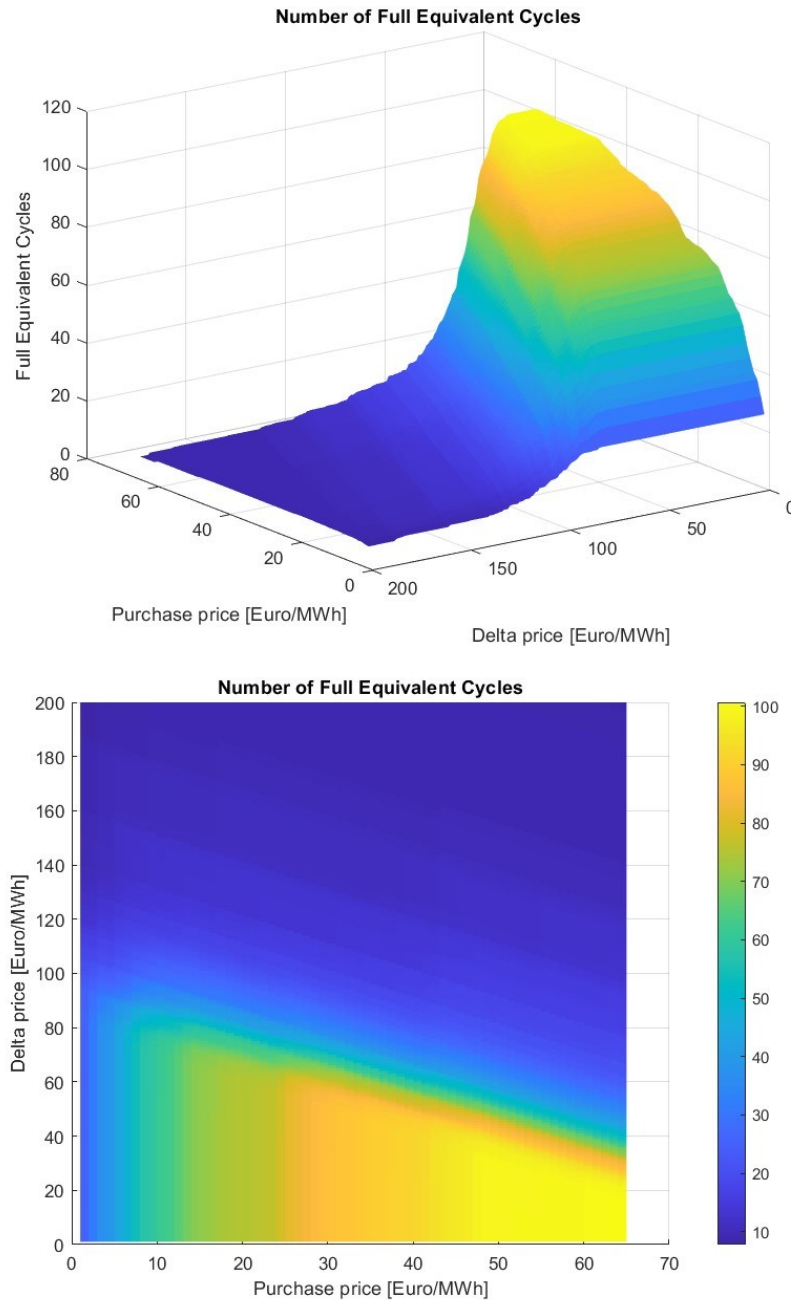


Fig.110 Example - Number of full equivalent cycles plot as function of the combination of purchase price and sale price (delta price)

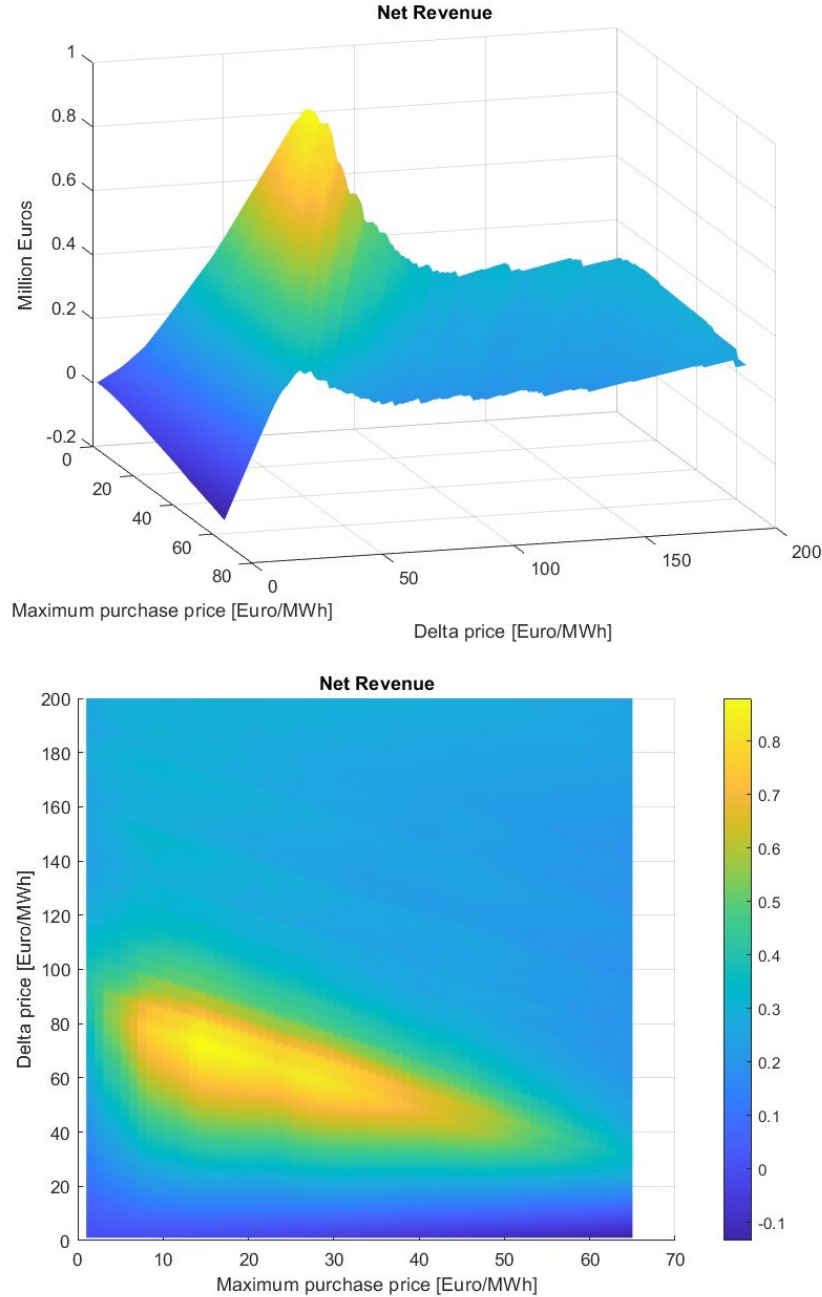


Fig.111 Example - Net revenue plot as function of the combination of purchase price and delta price

From the previous plots (Fig.110; Fig.111) it can be seen how the choice of the combination of offers to purchase and sell electricity strongly affects both the number of cycles that the storage would be able to perform and the revenues that could be achieved. In terms of cycles, while higher offers to buy energy would generally lead to more charge phases, excessive delta prices would lead to the impossibility of discharging the system enough. Looking at revenues, instead, we can see that the maximum values do not necessarily correspond to the combination that gives the highest number of cycles. Instead, it would be preferred a lower operation with better price combinations.

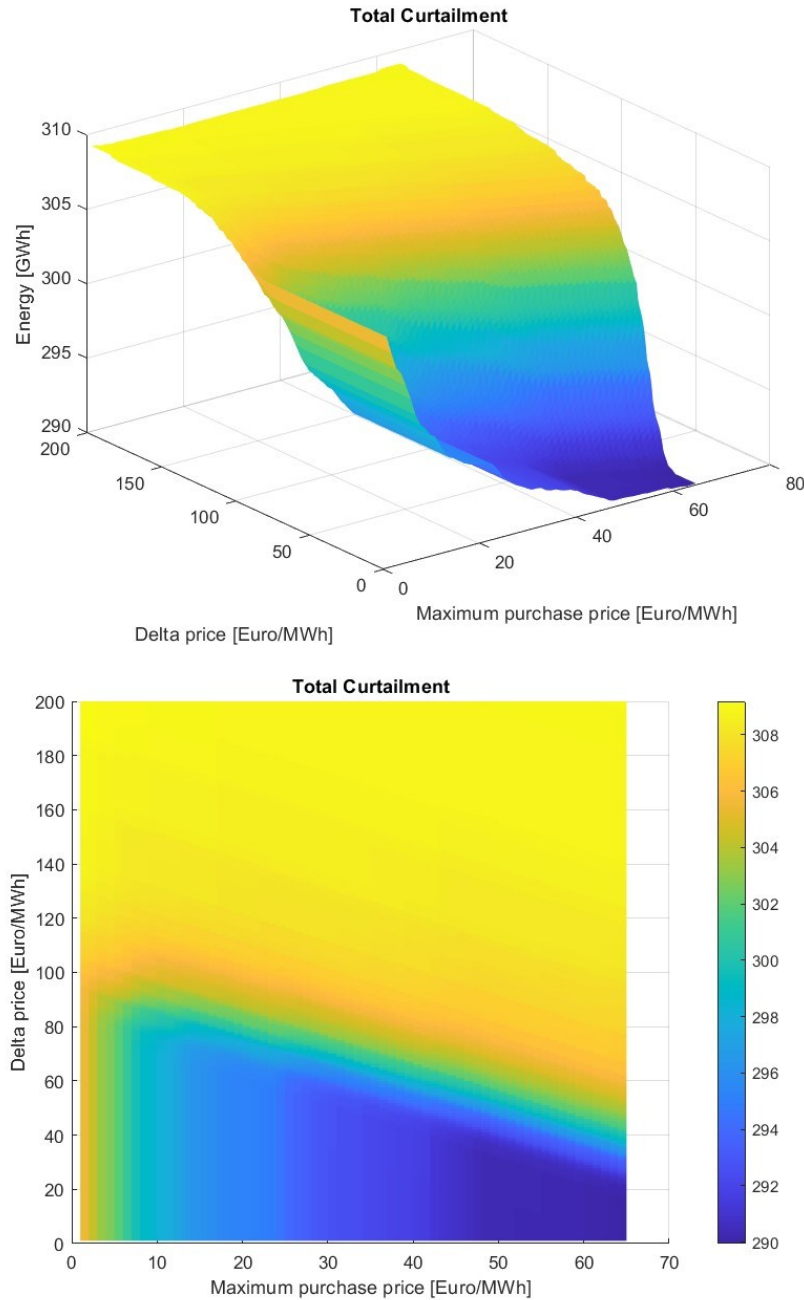


Fig.112 Example - Curtailment plot as function of the combination of purchase price and delta price

In the end, looking at the curtailment plot (Fig.112), we can see that it is complementary with the number of equivalent cycles. In fact, the higher the number of cycles performed, the higher the curtailment reduction would be. However, looking at the economic result of the battery alone, we can see that the maximum curtailment avoided case would correspond to an economic loss for the battery. In fact, to make the BESS work as much as possible, the system would need to buy energy at high prices and then sell it with too low price-difference.

## Simulation 1 – Final Results

In the following are reported the plots resulting from the optimal operation in terms of ROI for each storage size considered. The results refer to year 2020 and megapack units with C-rate 4 hours. Each point of the curves represents the yearly operation data about a different size of storage, operating with the best combination of purchase and sale price in terms of return of the investment.

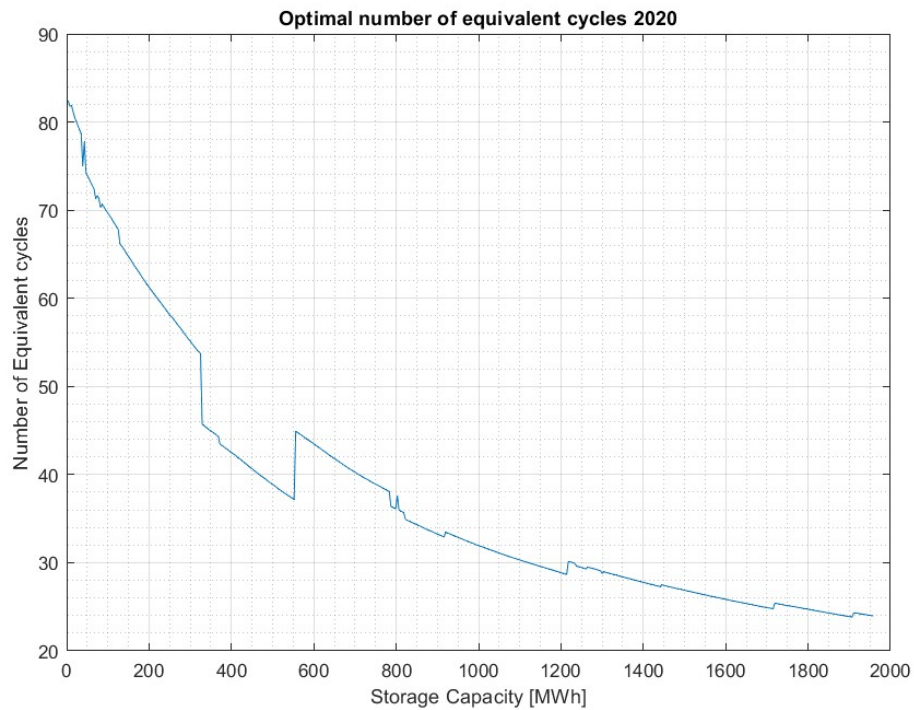


Fig.113 Number of full equivalent cycles in 2020 for different storage sizes



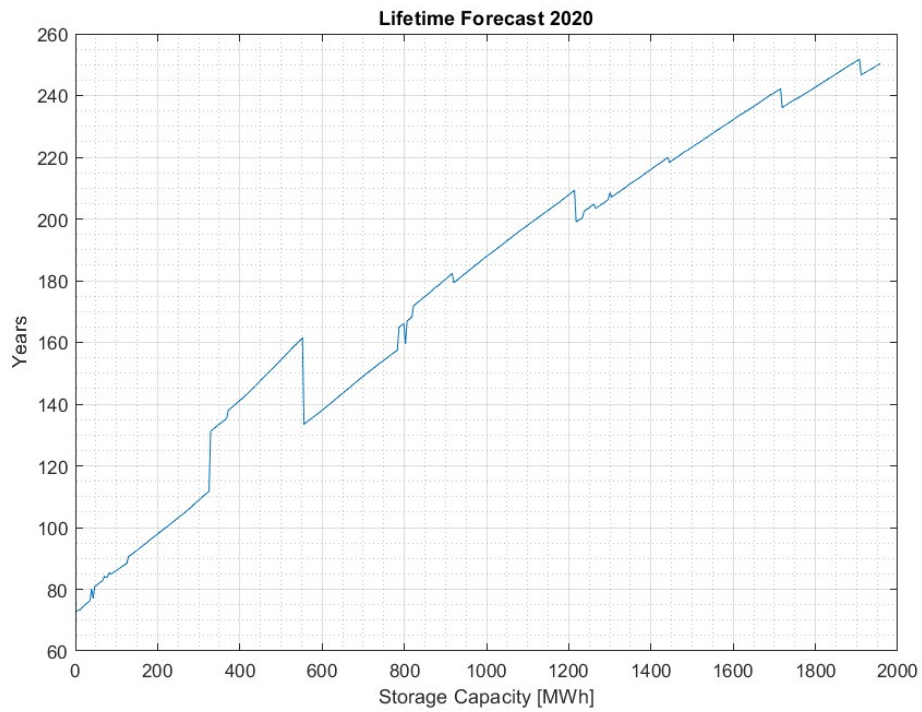


Fig.114 Lifetime forecast based on the equivalent cycles for different storage sizes.

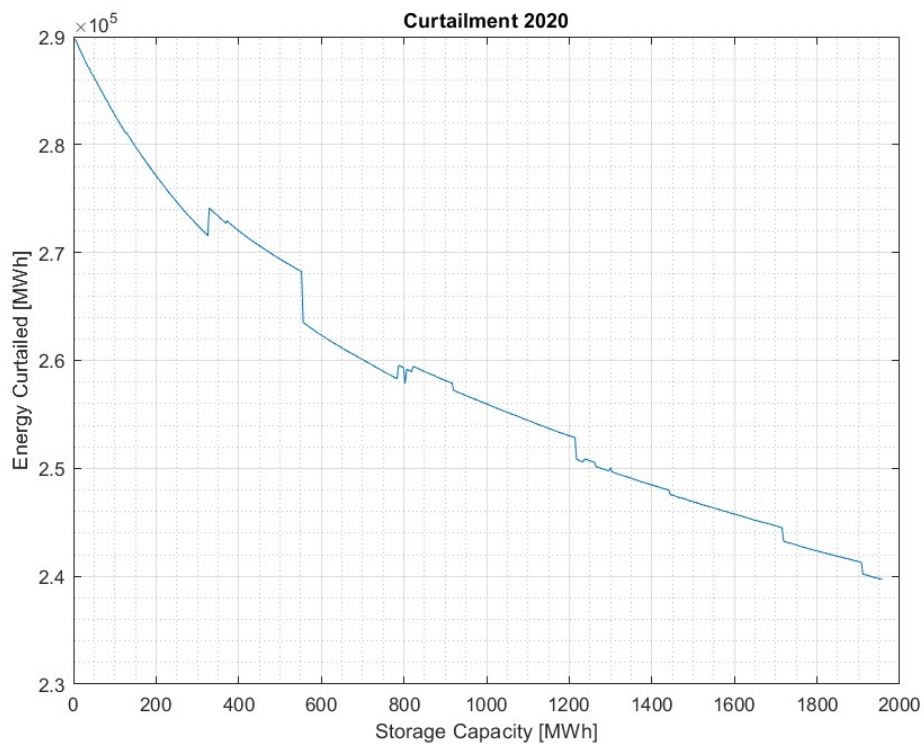


Fig.115 Wind energy curtailed for different storage sizes.



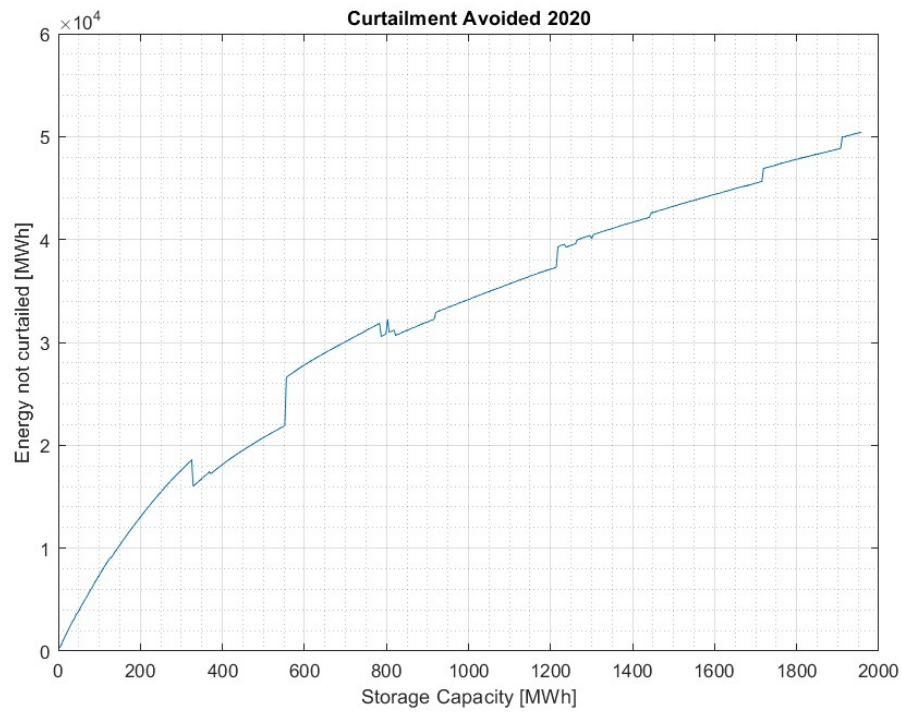


Fig.116 Curtailment that could have been avoided for different storage sizes.

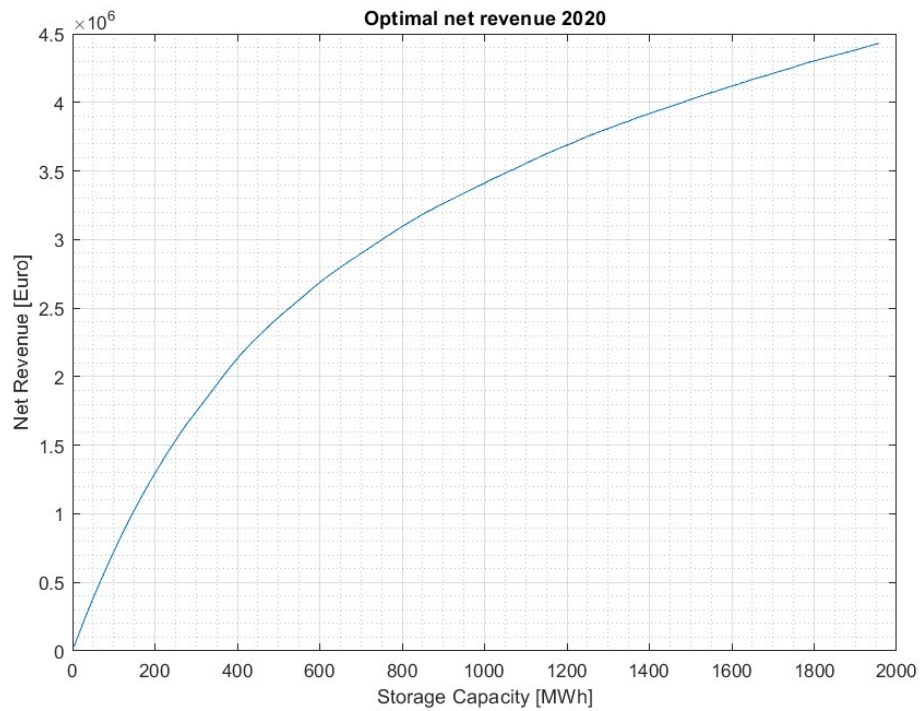


Fig.117 Optimal net revenue in 2020 for different storage sizes.

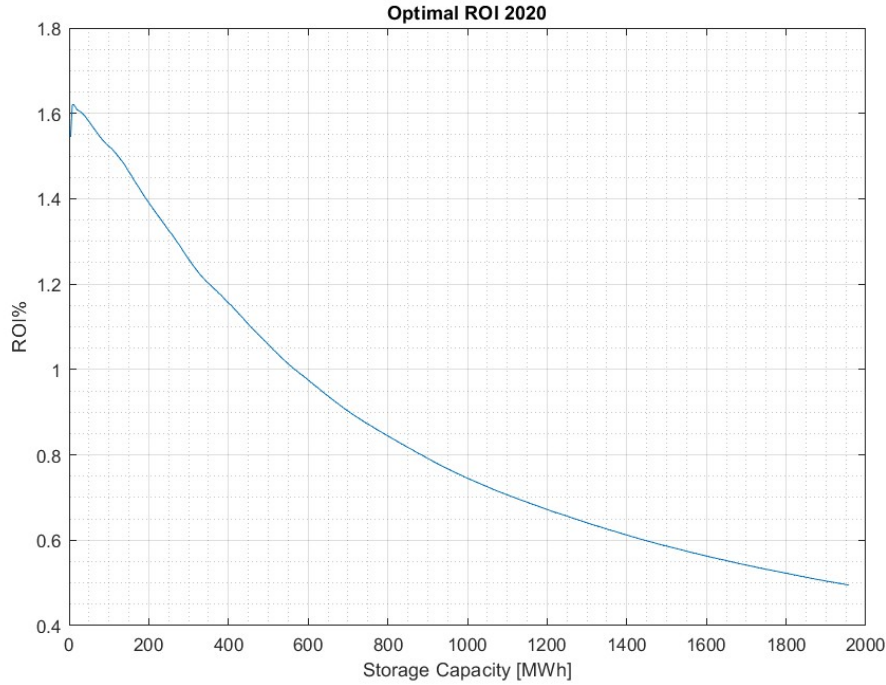


Fig.118 Optimal ROI values in 2020 for different storage sizes.

As it can be seen for the 2020 & C-rate 4 hours simulation, a storage system operating in this scenario with the described conditions would not be able to work enough. In fact, looking at the number of full equivalent cycles (Fig.113), they would be too low even in the case of small size energy storages. This could be partially due to the relatively low historical local demand for services, that causes some offers on the market to not be accepted, even if the services might be needed with the new introduced congestions. However, the main problem might be seen on the low transmission capacity combined with the high energy production of the plant, that could keep the storage frequently charged and not allow for a sufficient discharge time. In this scenario, it might be possible to not consider the operation of the BESS on the market, but the optimization of the wind farm together with the storage as a unique virtual unit. As it can be seen from the forecasted lifetime plot (Fig.114), estimated as the ratio between the number of cycles to the end of life and the yearly cycles performed, the systems would ideally last for very long times. In practice, however, the lifetime of batteries is comprised between 10 and 20 years, and therefore any value above these should be considered as unfeasible.

$$Expected\ lifetime = \frac{6000\ cycles}{N\ cycles/year}$$

Of course, this lifetime forecast represents only a simple estimation, and for a precise forecast more complex models would be needed to evaluate the state of health of the batteries. Looking at the curtailment (Fig. 115), we can see that without a storage solution, for the considered scenario, around 300 GWh could be curtailed. Such value would definitely mine the feasibility of the wind farm project, considering that the productivity of the system is estimated to be 1440 GWh/year. Using the incentive

value of 185 €/MWh as a reference to evaluate the value of the curtailment, the absence of the battery could cause a loss of possible earnings of around 55 million € for this scenario. The addition of the BESS in this scenario could have allowed a curtailment reduction of up to 50 GWh ([Fig.116](#)), corresponding to a value of 9.25 million € of wind energy. On the other hand, due to the low number of cycles per year, the storage would have had net revenues up to 4.5 million € (for the largest storage size as it can be seen in [Fig.117](#)). These revenues could have never covered the investment costs for the storage, as the ROI values were between 1.6% and 0.4% for all the possible storage sizes ([Fig.118](#)). The ROI results were higher for lower storage capacities, but the adoption of small storage capacity would have strongly penalized the curtailment savings. These results led to similar conclusions also for the other years simulated. The plots of the other simulations are reported in [Appendix A](#). Given the results of the C-rate 4 hours, it was decided not to investigate further this scenario with the C-rate 2 hours. In the end, this simulation proved that in this scenario the curtailment would have significantly affected the revenues of the wind farm. The addition of any size of energy storage would have partially reduced the curtailment but it would have not solved the problem, and the storage solution would not have sustained itself economically even by participating to the MSD and supposing all adequate offers to be accepted. For this reason, it was concluded that a relevant bottleneck could have mined the feasibility of the whole project, and a new scenario was considered for the following simulation.

### 5.1.5 Simulation 2 – Control Strategy

In the second simulation, it was supposed to be able to connect the wind farm to the local grid without any grid adequacy issue. In this scenario, Terna managed to improve the grid stability and capacity, so as to be able to export all the incoming power fluxes towards the Centre-South regions and towards Sicily. Therefore, in this scenario no bottleneck was considered at local level. However, the injection of additional power due to the wind farm might have caused other issues on the grid because of its variability or because of other congestions on other portions of the national grid. For this reason, it was still evaluated the possibility of applying a BESS in the region. This time, the storage would not have solved only the congestions due to the presence of the wind farm, but it could have provided services to the whole region of Calabria and to the adjacent zones. In particular, the storage could have still solved congestions but also could have contributed to the frequency and voltage regulation, as well as load and demand balancing.

Once again, the wind farm realization was bound to the access to the fixed price incentive of 185 €/MWh. For this reason, the storage was still considered to be a standalone system that would have operated on the markets independently from the wind farm. The correction of the wind farm imbalances before the meter was not considered, as the imbalance charge value is very low (typically lower than 2€/MWh) and the company considered it not to be relevant. Nonetheless, the wind farm power profile was considered to estimate a possible change in the grid power request both as increase and decrease of power injection. In this case, the local grid data were not used. Instead, the historical volumes of MSD ex-ante and MB were considered to define the demand of services “up” and “down”. As the storage would have operated no more at local level, the data about the whole Centre-South of Italy were used, so as to simulate the possibility of intervention to solve congestions with the other zones and to correct imbalances present in the South. Given that the Crotona data by Terna would not have been used, the new simulation was set to work on hourly level, differently from Simulation 1, where the timestep considered was of 15 minutes in accordance with the data.

In order to combine the historical data with the ideal integration of the wind farm on the grid, it was supposed that the additional wind power would have influenced both the demand for services “up” and “down” on the MSD. As load and demand balancing and frequency regulation is mainly based on injection or absorption of active power, the new wind power injected on the grid would have contributed to the decrease of the demand to increase the power injection. For this reason, the new demand of services “up” was calculated as the difference between the historical volumes “up” and the wind power to the land.

$$Volume_{up\ new}(h) = Volume_{up}(h) - P_{wind}(h) \leftrightarrow \text{if } (Volume_{up}(h) - P_{wind}(h)) \geq 0$$

In case this reduction led to a negative value, that was considered as an increase of the demand for services “down”.

$$Volume_{down\ new}(h) = Volume_{down}(h) + (Volume_{up}(h) - P_{wind}(h))$$

$$if (Volume_{up}(h) - P_{wind}(h)) < 0$$

The modified historical MSD & MB volumes were then used in the second simulation as demand for services to be provided by the storage. The control system used to simulate the possible storage operation was very similar to the one used in Simulation 1. The main difference consisted of the initial conditions to identify a possible charge or a possible discharge period. While this distinction was made in Simulation 1 based on the transmission capacity threshold, in this case it was based on the historical market volumes. The large portion of the market considered led to the contemporary coexistence of demand for injection and absorption of power. In real applications, the plant is controlled remotely by Terna for voltage and frequency regulation, while dispatching orders are received in advance in case of tertiary reserve. Generally, the choice of operation does not depend on the plant owner, but it relies on the TSO. To simulate the best possible operation of the plant, it was arbitrarily decided to be always rewarded with the possibility of operating in case the offers were competitive with respect to the weighted average historical values, similarly to what it was done in the first simulation. Then, to choose whether it was worth to provide services injecting or absorbing energy from the grid, it was arbitrarily chosen to prefer the charge possibility in case the state of charge of the battery was lower than 55%. Otherwise, in presence of both demands, the BESS control system would have preferred the discharge mode.

### 1) Charge Demand

The first condition to identify a demand for charge, as previously introduced, was based on the presence of a request for power reduction in the zone considered together with a relatively low state of charge of the battery. The state of charge condition allowed to give a preference to the charge mode in case of contemporary demand for charge and discharge on the market.

$$Volume_{down\ new}(h) > 0 \quad \& \quad SOC < 55\%$$

Then the possible charge power would have been identified as the power down requested.

$$Excess\ power(i) = Volume_{down\ new}(h)$$

Then, the remaining part of the control strategy was equal to the one described in point 1) of Simulation 1.

### 2) Discharge Demand

In case the charge mode was not preferred, the presence of historical market volumes to provide services “up” would have been considered.

$$Volume_{up\ new}(h) > 0$$

Then the possible discharge power would have been identified as the power up required by the zone.

$$\text{Power injection Demand}(h) = \text{Volume}_{up\ new}(h)$$

After this, also in this case the control strategy adopted was the same as described in point 2) of Simulation 1.

### 3) Stand-by

In case both the market demands were null, the system would have adopted the stand-by mode, without any charge or discharge except for the self-discharge.

## 5.1.6 Simulation 2 – Results

### Single Cycle Results

As an example, in the following are reported some plots that show some results from the simulation of the operation of a storage system made of 100 megapack units with C-rate 2 hours (385.4 MWh & 192.7 MW) that would have operated in 2018 with constant offers of purchase price set to 40€/MWh and sale price set to 156 €/MWh. Looking at the charges and discharges in [Fig.119](#), it is possible to see that in some cases with high demand for power injection and absorption, the BESS would operate continuously charging and discharging the battery. In real applications, however, this might not be realistic and the TSO might require a full charge or full discharge of the system.

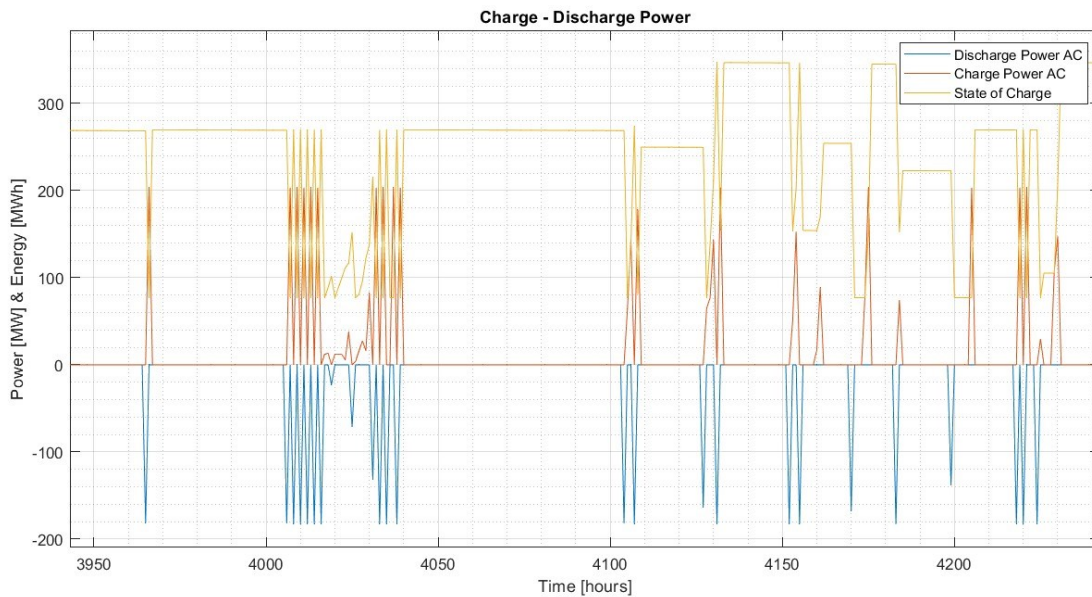


Fig.119 Example - Detail of operation for a storage with C-rate 2 hours

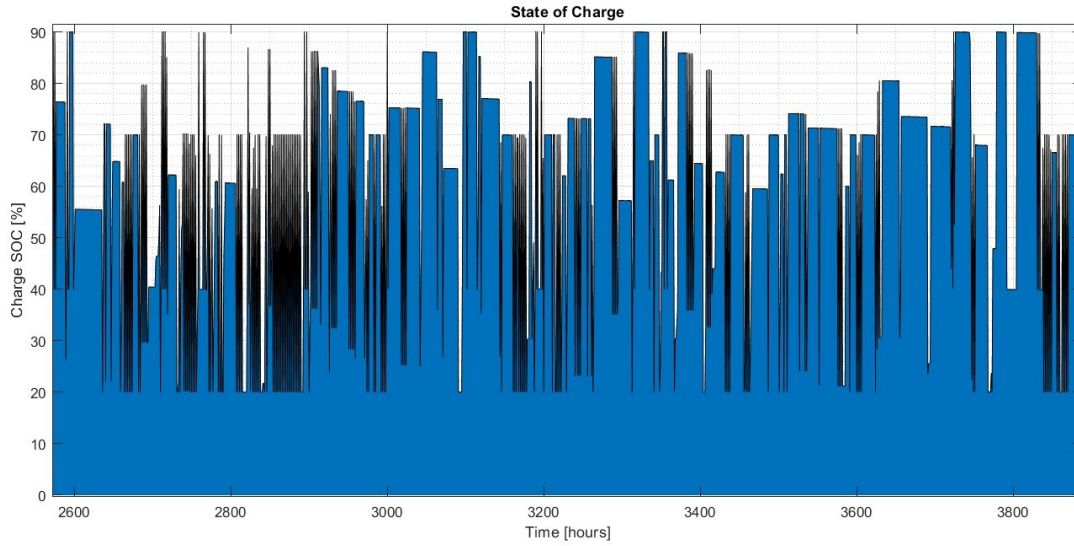


Fig.120 Example - Trend of the State of Charge for a storage with C-rate 2 hours

### Simulation 2 – Final Results

The final results of the simulations show that the solution with C-rate 2 hours would be more profitable than the one with C-rate 4 hours. Therefore, in the following are reported some results of the simulation with C-rate 2 hours in 2020. Among the yearly simulations, 2020 allowed for the best result. The results of all the simulations both for C-rate 2 and 4 hours are reported in [Appendix B](#).

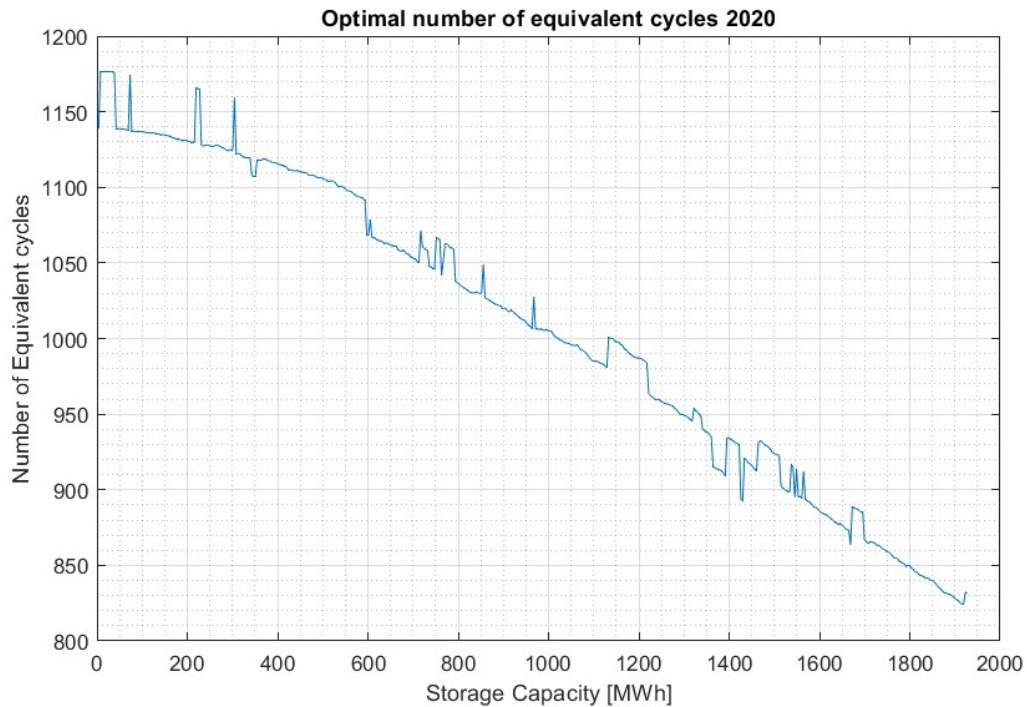


Fig.121 Number of full equivalent cycles in 2020 for different storage sizes with C-rate 2 h.



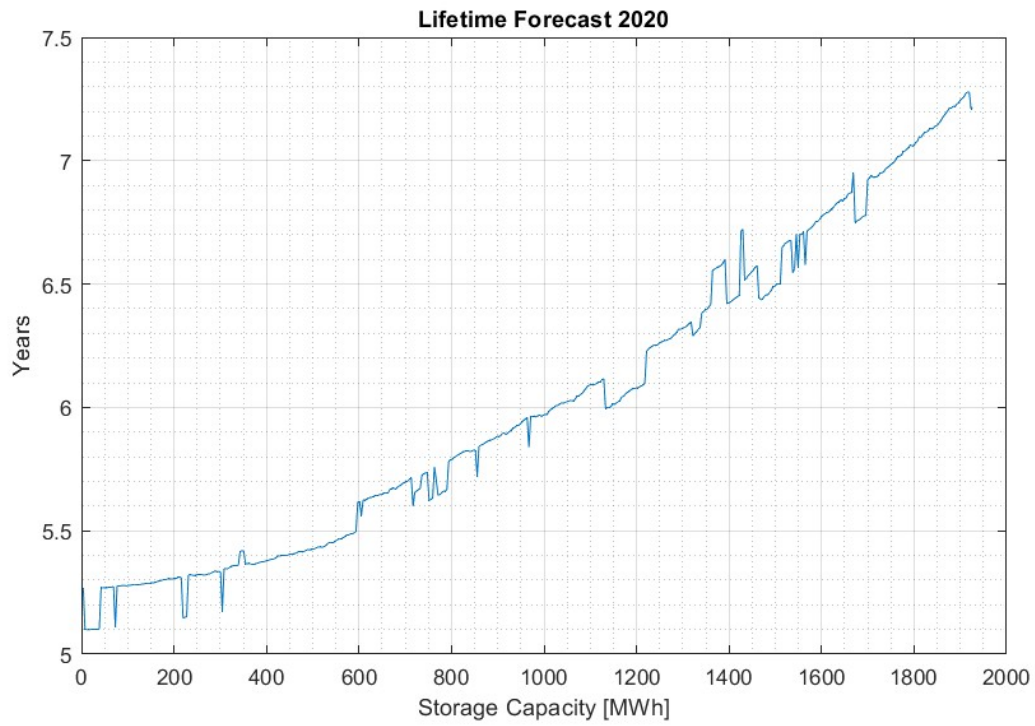


Fig.122 Lifetime forecast based on the equivalent cycles for different storage sizes with C-rate 2 h.

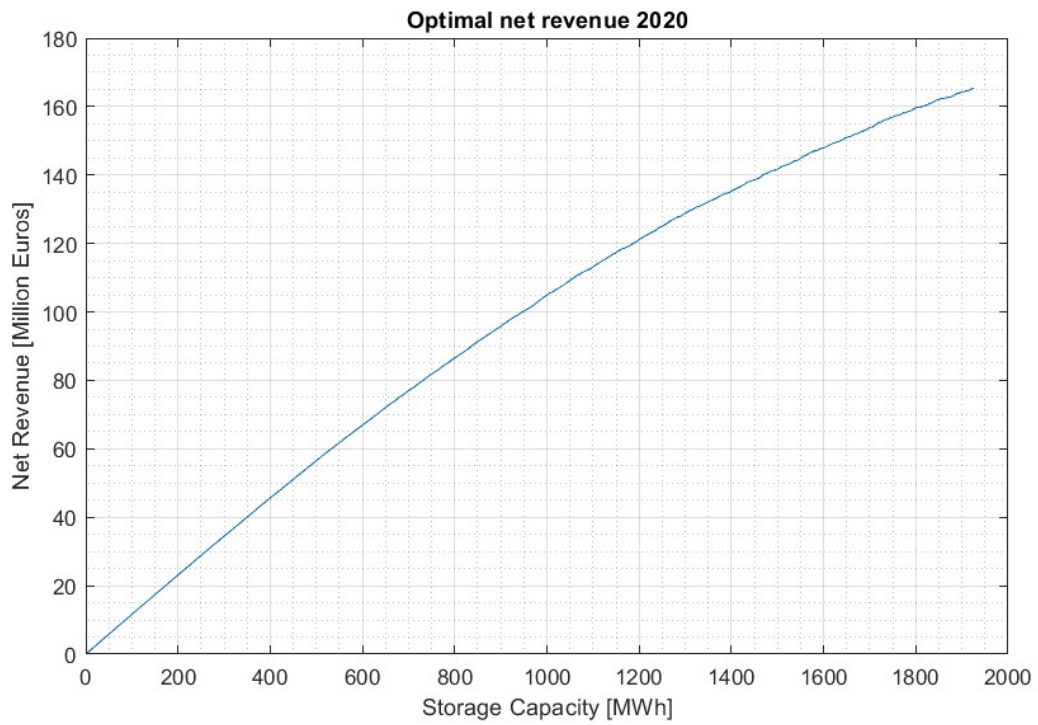


Fig.123 Optimal net revenue in 2020 for different storage sizes with C-rate 2 h.

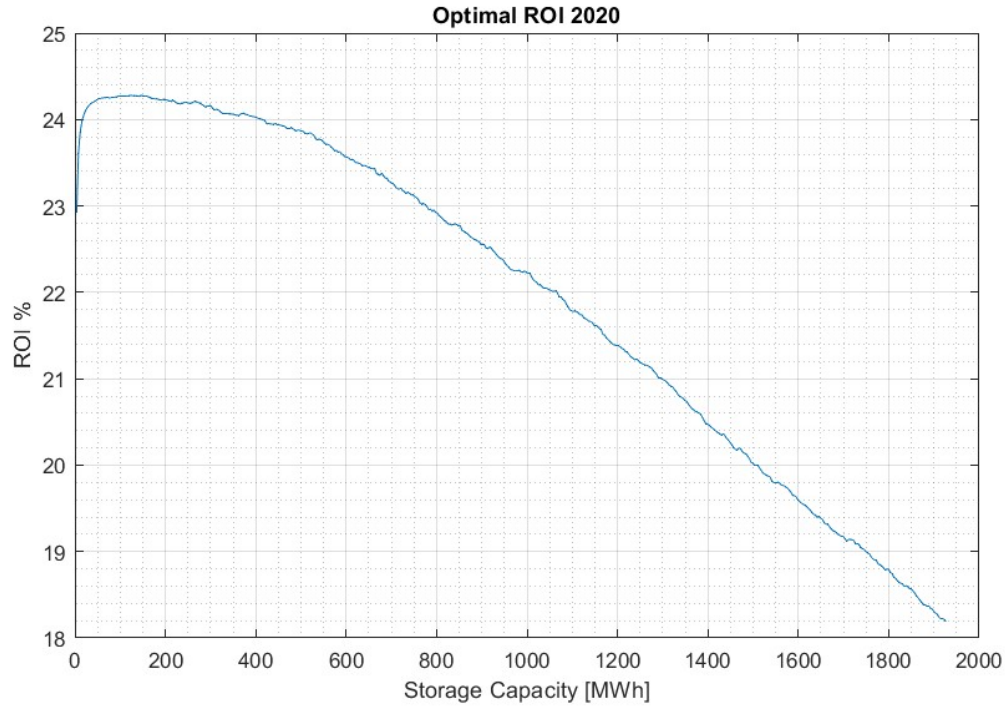


Fig.124 Optimal ROI values in 2020 for different storage sizes with C-rate 2 h.

From the results of the simulations, it is possible to see that the larger portion of the market considered gives much more opportunities for the storage system to operate. Still with the hypothesis of being awarded with all the offers presented with competitive prices, the BESS would be ideally able to reach very high number of cycles, almost 1200 in some cases. The trend is the same previously presented in simulation 1 results, as the number of equivalent cycles simulated decreases with increasing storage size. Year 2020 presented the largest opportunity for storage operation, with the highest revenues and number of cycles between the considered years. For C-rate 2-hours systems, the number of cycles that could be performed over a year result to be higher than for the C-rate 4-hours option. Referring to year 2020, C-rate 2 hours BESS could have performed between 820 and 1175 cycles (Fig.121), while C-rate 4 hours BESS could have performed between 510 and 580 cycles. The larger opportunity is probably due to the higher power, which allows for faster charge and discharge phases. The lower efficiency and higher cost of the C-rate 2 hours solution, however, does not counterbalance the larger number of operation opportunities. In fact, the possible economic results and return on investment are generally higher than the 4-hour solution. Looking at the simplified lifetime forecast based on the number of cycles (Fig.122), it can be seen that the lifetime span would be relatively low in 2020 due to the frequent cycling. However, this is not necessarily a disadvantage, as the frequent operation might allow for a fast return of the investment. In addition, in this second simulation, the lifetime forecast is mostly lower than 15-20 years and therefore reasonable for a BESS, differently from the results of simulation 1. The only exception is for year 2022, when both for the C-rate 4 and 2 hours, the number of cycles is lower, and less acceptable for some storage sizes. This different result is due to the trend of prices during that year, that affected the simulation performed with a unique combination of optimal prices. A variable price should have been

adopted during 2022 to correctly manage the BESS also during the periods of price peak. Looking at the ROI values (Fig.124), the parameter allows to identify the best range of storage sizes, which could operate enough to cover the investment costs relatively fast. Year 2020 presented the best ROI values among the years, with a peak at around 24% of estimated Capex and Opex. For the C-rate 2 hours, the best storage sizes would have been between 20 and 400 MWh in 2020, as seen in the previous plot. Regarding the other simulated years, the best size ranges are reported in the following tables [Tab.17](#) and [Tab.18](#), with the corresponding minimum ROI threshold to identify the peak. In addition, the ROI results of all the simulations are plotted together in [Fig.125](#) and [Fig.126](#).

Year	Peak ROI	Optimal range [C-rate 2 hours]
2018	>19 %	7.7 – 84.7 MWh
2019	>20 %	27 – 192.7 MWh
2020	>24 %	19.7 – 412.4 MWh
2021	>18 %	3.85 – 312.2 MWh
2022	>13 %	3.85 – 96.3 MWh

Tab.17 Optimal results based on ROI from the yearly simulations (C-rate 2 hours)

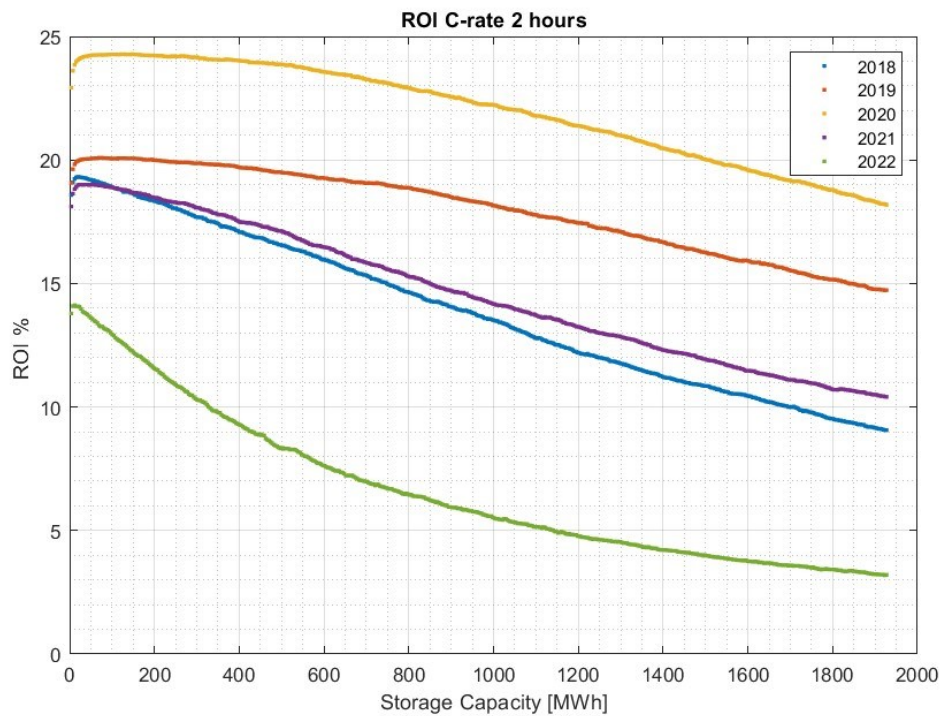


Fig.125 Optimal ROI results from the simulations for the C-2 hours case

Year	Peak ROI	Optimal range [C-rate 4 hours]
2018	>9.5 %	11.75 - 560 MWh
2019	>10.4 %	180 – 614.8 MWh
2020	>12.5 %	160.5 – 924.2 MWh
2021	>9.8 %	113.5 – 379.85 MWh
2022	>7 %	7.8 – 168.4 MWh

Tab.18 Optimal results based on ROI from the yearly simulations (C-rate 4 hours)

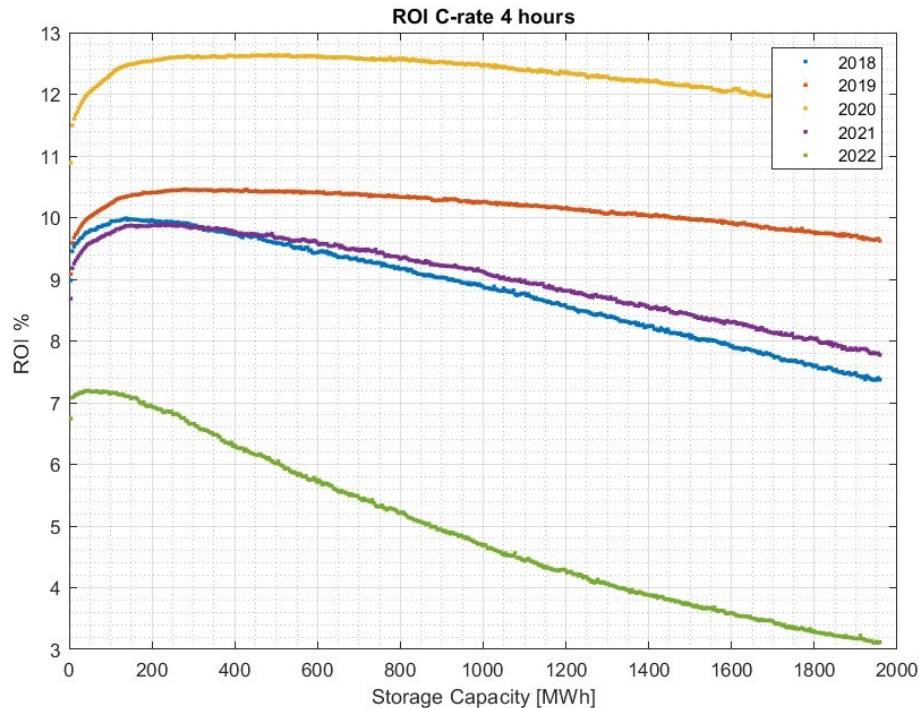


Fig.126 Optimal ROI results from the simulations for the C-4 hours case

From the ROI values, it is clear that the C-rate 2 hours solution would be economically the best. In addition, it can be noticed that generally the storage sizes that allow for a better economic result are higher for the C-rate 4 hours if compared to the C-rate 2 hours. This might be explained by the higher power reached with larger C-4h BESS, or by the fact that for C-rate 2 hours BESS would not need large storage capacity as they would rapidly charge and discharge to provide the services needed. By summing the ROI values over the years, it was possible to identify the storage size that ideally would have operated with the best economic result. Considering all years, the best size with C-rate 2 hours would have been the one with 6 units, for a total of 23.12 MWh and 11.5 MW. However, given the particular results of 2022, if only years from 2018 to 2021 were considered, the best result would have been the one with 10 units, for a total of 38.54 MWh and 19.7 MW. In Fig.127 it should be noticed that the range of optimal values was quite wide, with relatively small variations of ROI. Looking at the detail of the sum of the curves without considering 2022, storage sizes up to 300 MWh could have provided a theoretical total ROI value higher than 80%.

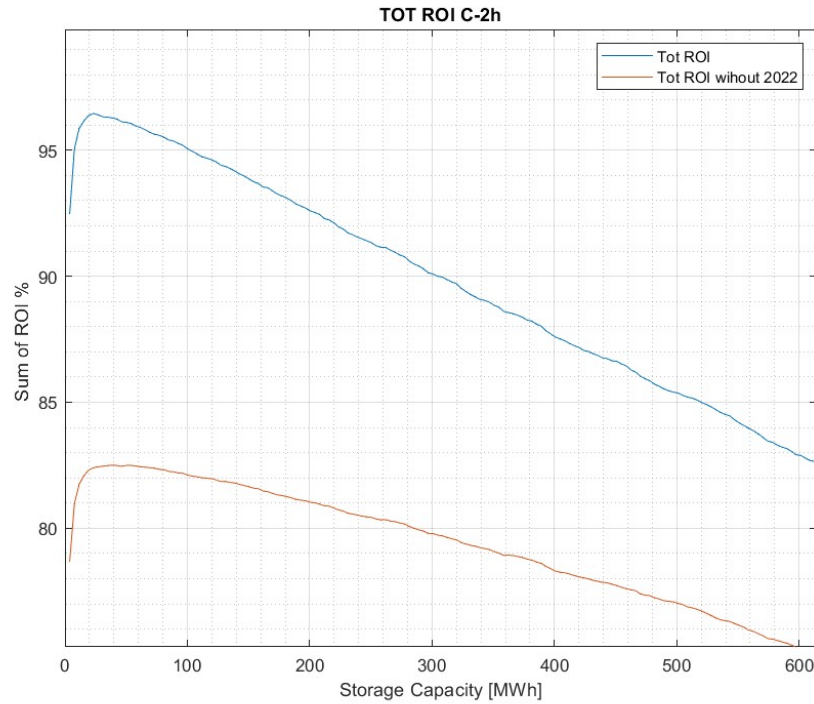
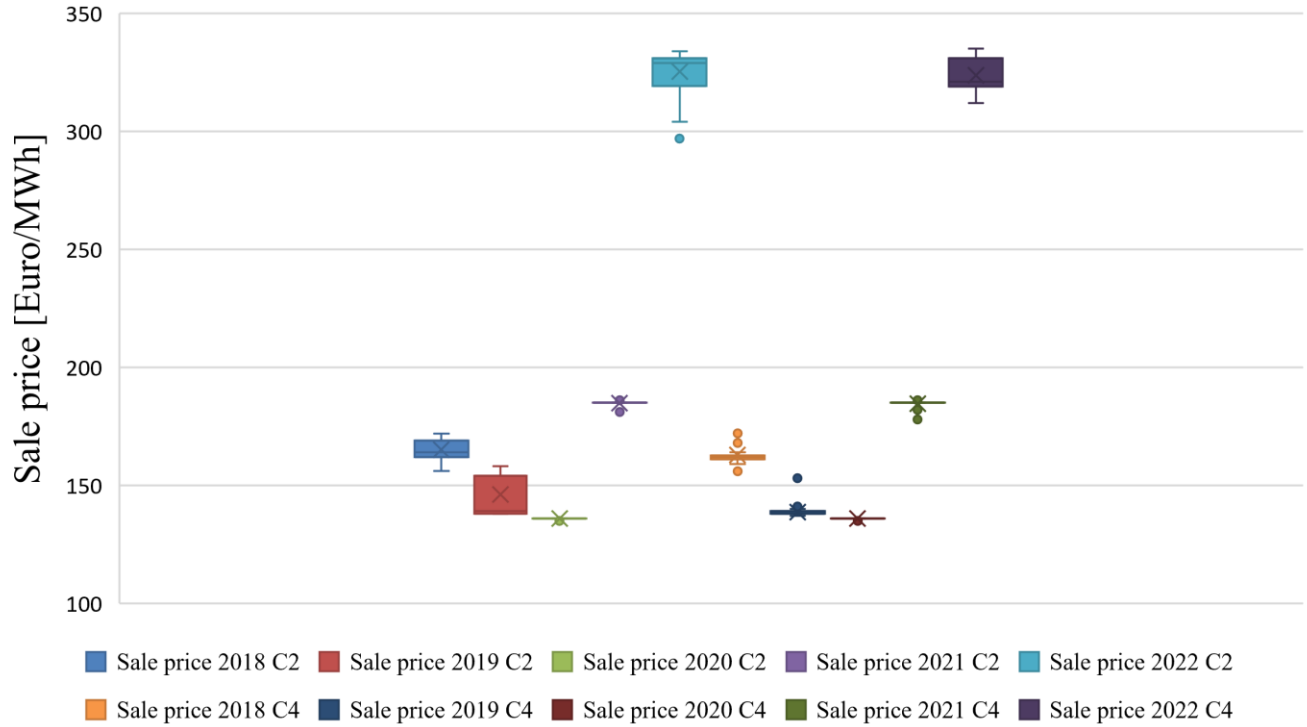


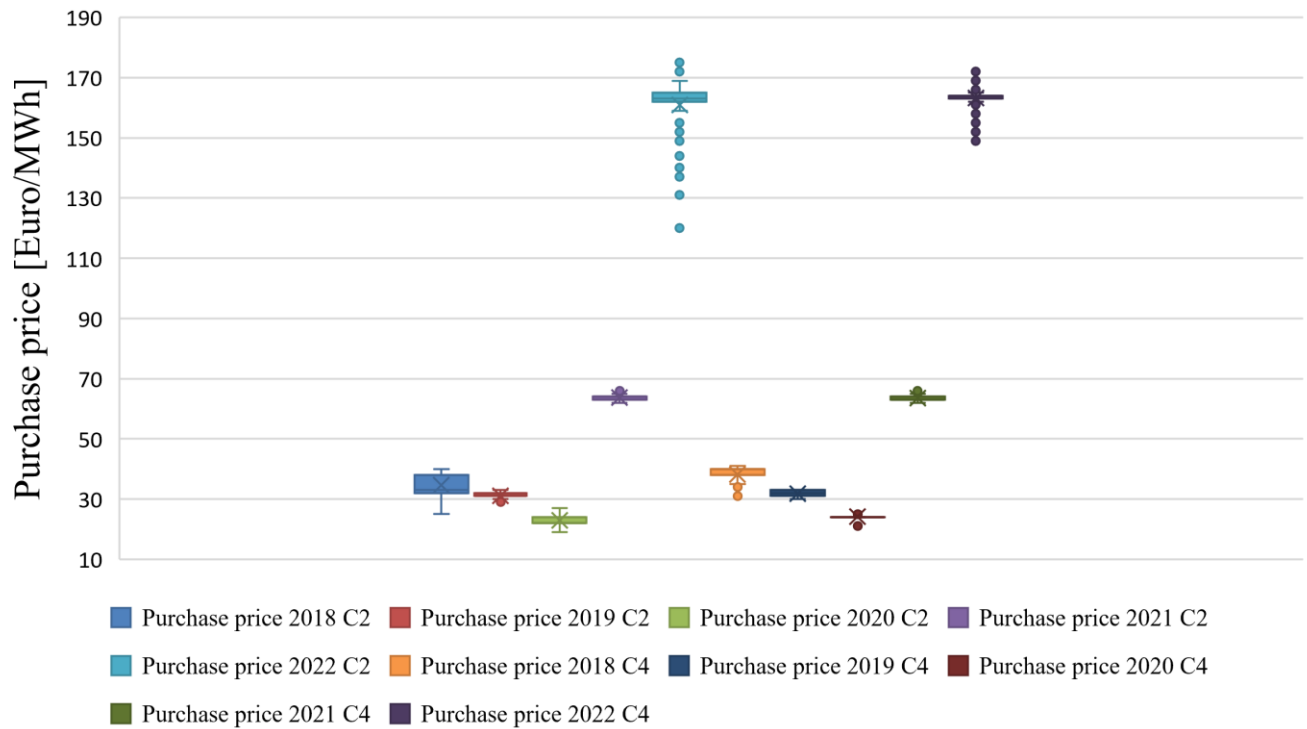
Fig.127 Sum of optimal ROI results for the C-2 hours case

Regarding the choice of combination of price offer to buy and to sell energy on the market, the plot of the optimal results is reported in the following [Fig.128](#). As it is possible to see the ranges of purchase and sale prices are pretty narrow for each year considered, both for the C-4 and the C-2 hours solution. In both cases, the values of 2022 are very different from the ones of the previous years, due to the large price variations that occurred in the year. Even year 2021 presents higher prices, but still within an acceptable range. Comparing the C-2 and C-4 results, some variations can be noticed, but overall, the optimal offers are always in the same range. About optimal purchase prices, they are typically between 20 and 40 €/MWh considering 2018-2020, with an increase to 60 €/MWh for 2021. Looking at sale prices instead, the best range is between 135 and 165 €/MWh in years between 2018 and 2020, while for 2021 the optimal value increases up to 180-185 €/MWh.

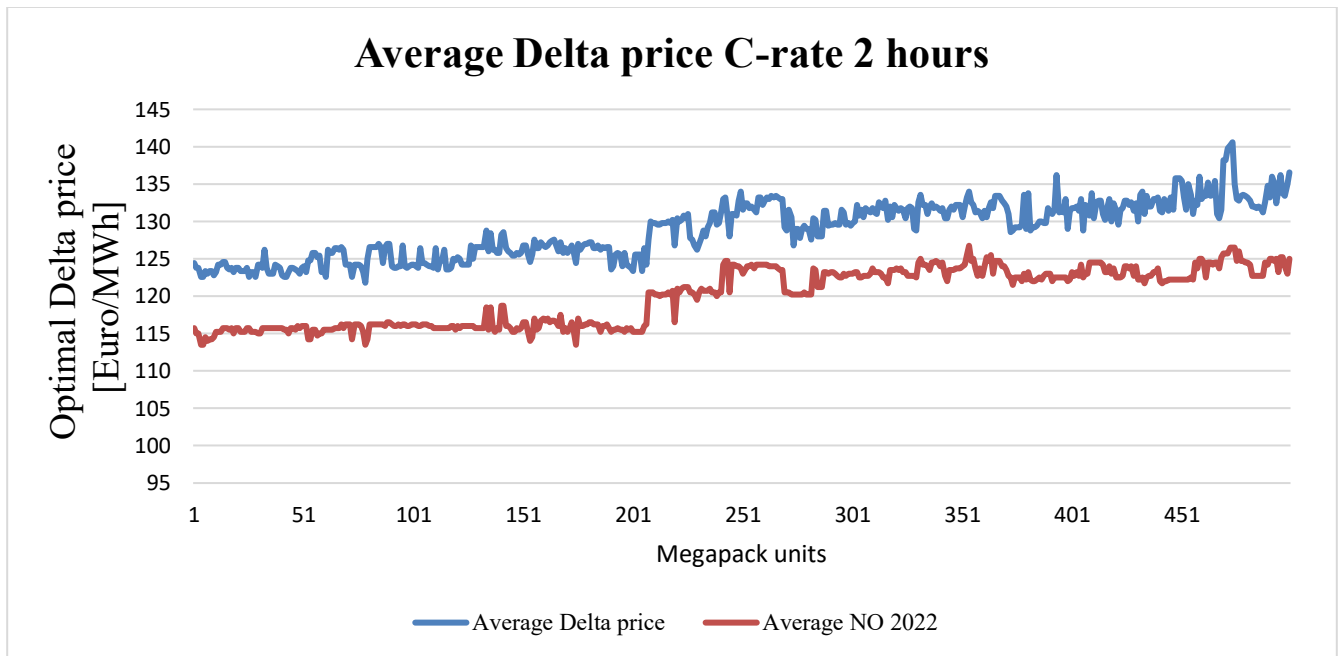
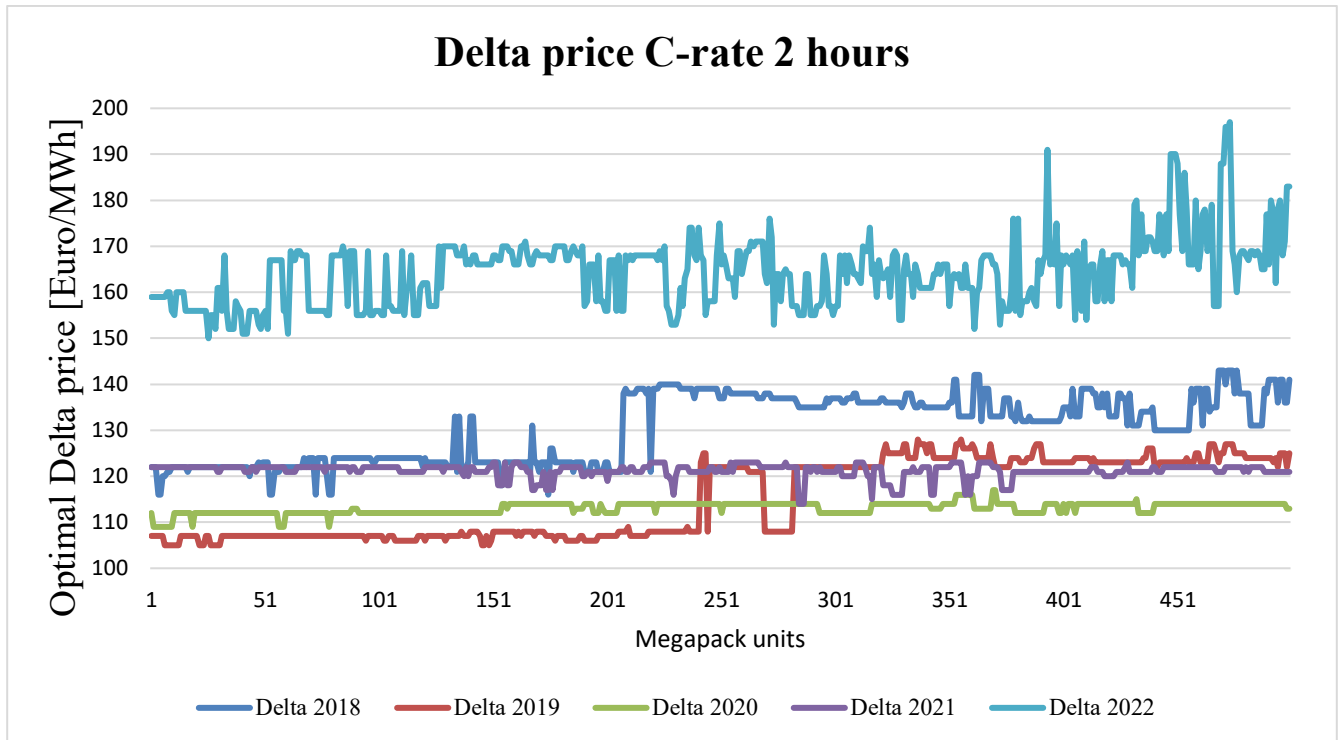
## Optimal Sale price



## Optimal Purchase price







Here are shown the plots of the price difference between the optimal values of the sale and purchase price offers for the C-rate 2 hours solution. In the first plot (Fig.129), the delta price is plotted for the whole singular yearly simulation results, and it is possible to see that typically the delta price is between 105 and 125 €/MWh, except for year 2022 and for part of the results of 2018. Looking at average values (Fig.130), it was decided to exclude 2022, because of the strange results that would have affected the whole average shifting it towards higher values. The average price difference between 2018 and 2021 shows optimal values in the range 115 to 125 €/MWh.



## 6 Business Plan

### 6.1 Business Plan for the Electric Energy Storage

In order to evaluate the feasibility of a BESS, a business plan was prepared by exploiting an economic model typically used by the company. Given the results of the Simulation 2, the company decided to focus on a BESS solution with C-rate 2 hours, made of 52 Megapack units, for a total storage capacity of 200.4 MWh and 100.2 MW. This choice was done mainly to provide enough power capability to absorb the power generated by the wind farm if required, even if the optimal results did show that lower storage sizes could have been more economically interesting. In addition to the size, the inputs used for the business plan were the number of cycles performed by the storage, the percentage of offers accepted, and the average prices of purchase and sale of energy. Both the prices and the number of equivalent cycles per year were taken from the simulation 2 results.

On average, a 200 MWh system, between 2018 and 2022 would have performed a maximum number of 837 full cycles per year. However, if 2022 was excluded from this average, the number of full equivalent cycles per year could have increased to 933 cycles. Given the extraordinariness of year 2022 in terms of prices, it was decided to not consider its results for the storage sizing and for the inputs of the business plan. In fact, the inclusion of that year would have led to a decrease of cycles and a significant increase of prices.

Regarding the prices used to simulate the economic performance, it was calculated the average of optimal purchase and sale prices from the simulation results, still excluding 2022. The average purchase price considered was 39 €/MWh, while the average sale price was 155 €/MWh, for a total price difference of 116 €/MWh. If 2022 was included, both prices would have been higher: 64 €/MWh for the purchase and 187 €/MWh for the energy sale, thus this justifies the exclusion of that year from the average calculation. The results of the simulation used for the economic evaluations are here reported in Tab.19.

<b>Input Data from the Simulation 2 results</b>	
Megapack units (C-rate 2 hours)	52
Storage Capacity	200.4 MWh
Rated Power	100.2 MW
Megapack System Cost + Installation Cost	91565300 €
Megapack Yearly Maintenance	237398 €
Max Number of full eq. cycles	933
Average Purchase price	39 €/MWh
Average Sale price	155 €/MWh

Tab.19 Business Plan input data

Given that the simulation results were referred to a case where all the competitive offers were considered as accepted by Terna, to simulate the real economic result of the system over the years it was necessary to introduce a reduction of the number of accepted offers. It was therefore introduced an offer acceptance ratio, supposing that a given percentage of offers accepted would have directly affected the number of

cycles performed per year. Once fixed this acceptance ratio, the effective number of cycles was considered to be constant over the years, until the end of life of the system.

$$N_{cycles\ effective} = Acceptance\ ratio \cdot N_{cycles\ max}$$

Then, in order to evaluate a realistic performance of the storage system, it was considered a degradation factor, simulating a linear decrease of the storage capacity over the years. Based on the observations from [5.03], it was firstly supposed a degradation from 100% to 80% of the storage capacity over 6000 cycles. However, it was supposed to be able to operate with the storage until the maximum storage capacity would have reached the 70% of the rated capacity. This would correspond to a theoretical 10000 cycles of lifetime of the battery, which is a rather optimistic assumption.

$$Degradation\ rate = \frac{(100 - 80)\%}{6000} = 0.003\%/cycle$$

Given the number of effective cycles performed every year, the capacity lost over the time was calculated for every year and considered for the following ones, affecting the amount of energy that could be theoretically bought and sold. In particular, for every year  $n$  it was considered the degradation at the beginning and at the end of the year, as a percentage lost from the initial capacity. Then, to estimate the amount of energy bought and sold, an average degradation for the year was considered, so as to use an average storage capacity available.

$$Degradation\ (year\ n) = N_{cycles\ effective} \cdot Degradation\ rate$$

$$Cumulative\ degradation\ (n) = Cumulative\ degradation\ (beginning\ n) + Degradation\ (n)$$

$$Average\ degradation(n) = \frac{Cumulative\ degradation\ (n) - Cumulative\ degradation\ (n - 1)}{2}$$

$$Storage\ Capacity\ (n) = Storage\ Capacity_{rated} \cdot Average\ degradation\ (n)$$

The amount of energy purchased was calculated through the number of cycles, the effective storage capacity and the efficiency of the system, equal to the one previously assumed in the simulations (94% for C-rate 2 hours). Then, the energy sold was calculated considering the energy purchased and the round-trip efficiency of the system (94%·94% = 88.36%).

$$Energy\ purchased = \frac{N_{cycles\ effective} \cdot Storage\ Capacity(n)}{\eta_{charge}} [MWh]$$

$$Energy\ sold = Energy\ purchased \cdot RTE_{BESS} [MWh]$$

Given the estimation of the amount of energy bought and sold for every year, it was also calculated the estimation of expense and revenues from this activity. The average prices from the simulations were used for this calculation.

$$Energy\ purchase\ cost = Energy\ purchased \cdot 39€/MWh$$

$$\text{Energy sale revenue} = \text{Energy sold} \cdot 155\text{€/MWh}$$

Then, the capex was estimated, starting from the system and installation cost from the Tesla product. The estimation of the total capex included also the civil works (200 k€), the electrical works (2 M€), and an additional 2% of contingencies (1.875 M€). The sum of all these components led to a CAPEX of 95.641 M€. Regarding the operating costs, its main component was the maintenance estimated from the Tesla data. In addition to this, it was added an additional component of extra maintenance (5 k€/year), the land lease component (25 k€/year) and the insurance component (50 k€/year). It was supposed that no personnel were needed for the plant operation, and therefore this cost was neglected. Overall, the total annual operating cost was 327.4 k€. During the calculations of the model, this amount was increased due to inflation by about 2% per year.

Regarding the project financing, it was supposed to use 25% of the capital from the equity and 75% from bank loans. The interests to the bank were considered to be 5% per year, which is a typical value for this period of time. It was supposed to start the financing of the project in 2024, with the plant starting its operation in 2025, and being able to operate for 60% of the starting year.

At this point, the behavior of the project was evaluated considering the economic parameters resulting from different values of the offer acceptance ratio. In fact, it is unknown how many offers the TSO will accept and therefore how much the system will be effectively operating in the future. In fact, this depends on the type and number of services required by the grid that could be solved by the system, together with the competitiveness in the market. For this reason, the variation of this parameter was used as a sensitivity analysis, to show which range of accepted offers would allow a satisfactory economic operation. An example of the acceptance ratio could be seen in the analysis reported in [6.04], where for a case in the south zone of the market, it was reported that 38% of the offers “up” and 58% of the offers “down” were accepted in 2018. While the increase of renewable intermittency might increase the demand for this kind of services, the increase of the competition due to the new storage might balance it. Therefore, a good objective might be to prove the feasibility in this range of accepted offers.

For each offer acceptance value established in the business plan, the number of cycles performed every year varies, and therefore also the lifetime of the system. For this reason, based on the calculated lifetime, it was supposed to vary the length of the financing so as to keep it one year shorter than the years of operation of the system. The length of the financing would have affected both the total amount of interests to be given and the yearly repayment needed. The main indexes used by the company to evaluate the investment were the DSCR and the IRR.

The IRR is the internal rate of return, which is defined as the discount rate that makes the Net Present Value equal to zero. This index is calculated iteratively and allows to determine if the investment might be convenient enough, providing an estimation of the return on the investment. In this case, in the business plan it was mainly considered the levered IRR, which refers to a case in which the cost of debt financing was accounted. This was done considering that a large investment on a storage system wouldn't have been made without the access to bank loans. An unlevered calculation, instead, would not have

considered the use of debt but equity capital only. The company established that a solution would have been considered as sufficiently convenient only if the levered IRR would have overcome the 8.5% value.

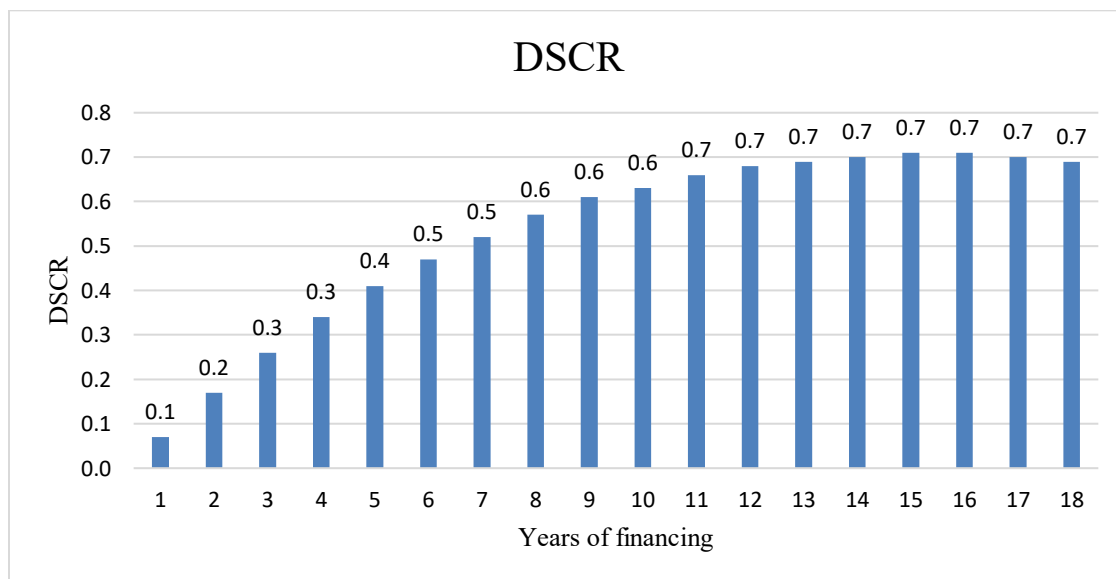
The DSCR (the Debt Service Coverage Ratio) is an index used to evaluate the financing sustainability, showing if it will be possible to cover the costs related to the debt. The index is calculated as the ratio between the operative positive cash flows and the negative cash flows related to the debt, like debt repayment and interests on debt.

$$DSCR = \frac{EBITDA + Taxes}{Debt\ repayment + Debt\ interests}$$

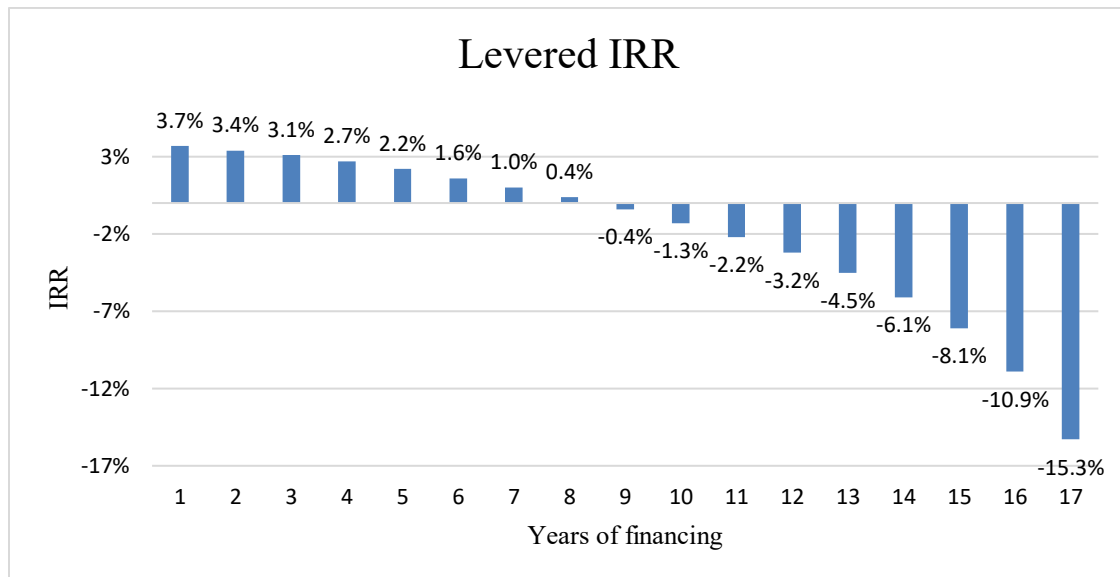
Here, EBITDA represents Earnings Before Interests Taxes Depreciation and Amortization, which corresponds to the gross operative margin achieved. The DSCR value should typically be higher than 1.2 or 1.3, showing that the project would be able to generate enough value to cover the financial costs. A DSCR value lower than 1 would demonstrate that the project would not be able to sustain the debt repayment. In the business plan, the DSCR value was calculated for every year and then averaged, so as to evaluate the overall performance over the lifetime of the project.

### Financing length variation

To show the effect of the variation of the length of the financing, in the following are reported as an example the levered IRR (Fig.131) and the DSCR (Fig.132) values for a case with 50% accepted offers (and therefore 466 cycles/year) with different lengths of financing.



From the above results it can be seen that increasing the length of the financing, it would be easier to cover the yearly repayment of financial costs, and therefore DSCR values would be higher. However, for the considered case, the DSCR value would never be acceptable, always being lower than 1.2.



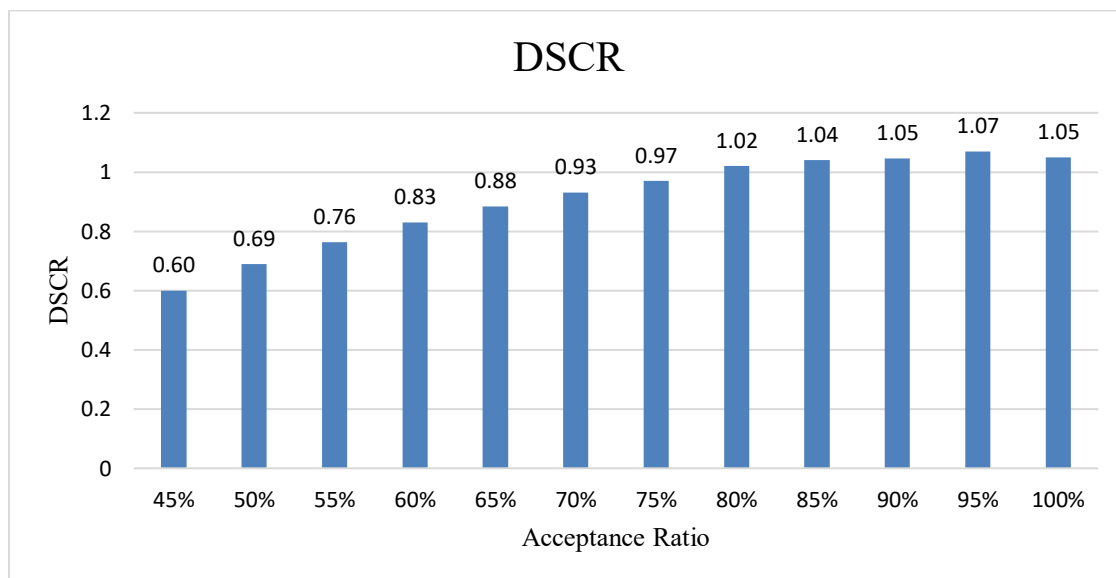
Regarding the IRR value, instead, it can be seen that a longer financing period would mean a larger amount of interests to give back to the bank, which might penalize the economic result. In this particular case, the IRR value would never be satisfactory, even reaching negative values. The two parameters should be balanced to find the right solution, providing a good economic return on the investment and appropriately covering the loan costs. Overall, this shows that the 50% offer acceptance ratio condition would never make the project economically feasible.

## 6.1.1 Business plan results

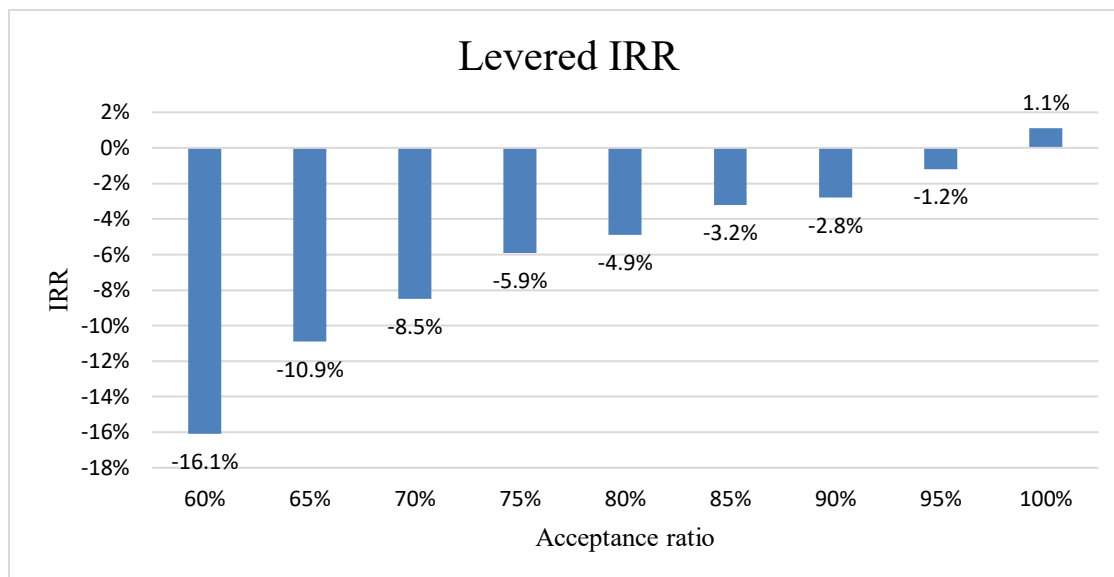
### CASE 1) - Offer acceptance variation

In the following are reported the results obtained for different offer acceptance ratio values. Starting from a 100% acceptance of the offers on the market, the offers accepted (and therefore the number of cycles) were decreased with steps of 5%. For each condition considered, the financing length was adjusted to be 1 year lower than the storage lifetime. In the following are reported the DSCR ([Fig.133](#)) and IRR values ([Fig.134](#)) resulting from each supposed condition.

Looking at the DSCR values, it can be seen that they would never be satisfactory, always being lower than 1.2. By decreasing the number of cycles, the system would increase its lifetime, and therefore it would be possible to perform a longer period of financing. However, due to the lower system operation, the yearly revenues would be lower, making it more difficult to cover the financing repayments. While the longer financing period positively affects the DSCR, it seems that the lower revenues would have a stronger effect on this parameter, making it lower and lower. Overall, with this kind of investment, it seems that it would be difficult to be able to sustain the financing costs.

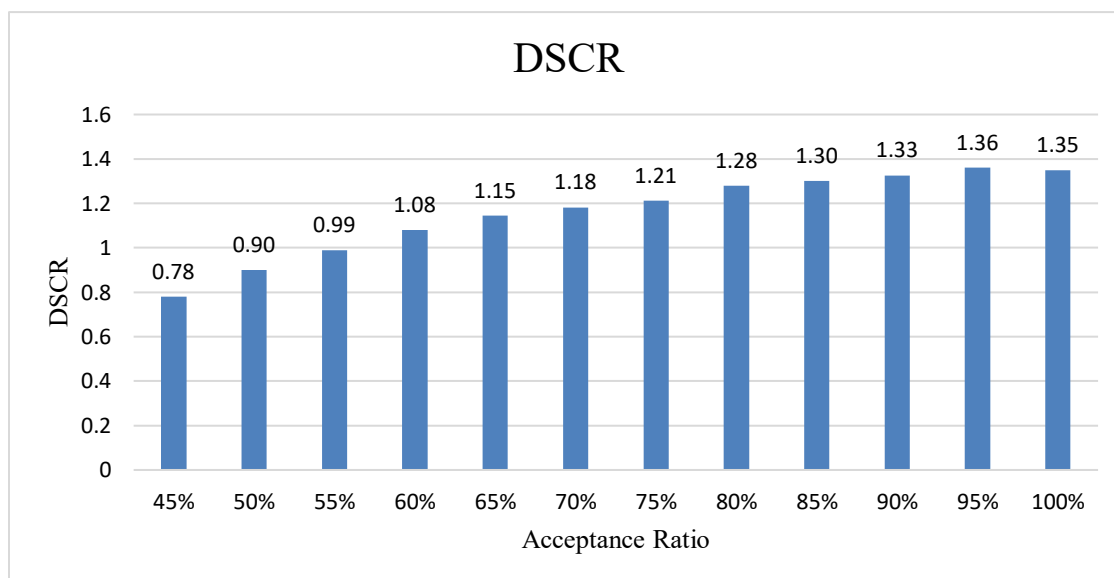


About the levered IRR, it is clear that the investment would not be able to repay itself through a financing, as it would be negative in most of the cases, far from the objective of the company of 8.5%. It should also be considered that reaching the high values of accepted offers shown is highly improbable, due to market dynamics. In addition, it would be very difficult to convince the equity to invest such a large amount of money in such a risky investment. For this reason, it was concluded that the examined project would not be feasible.

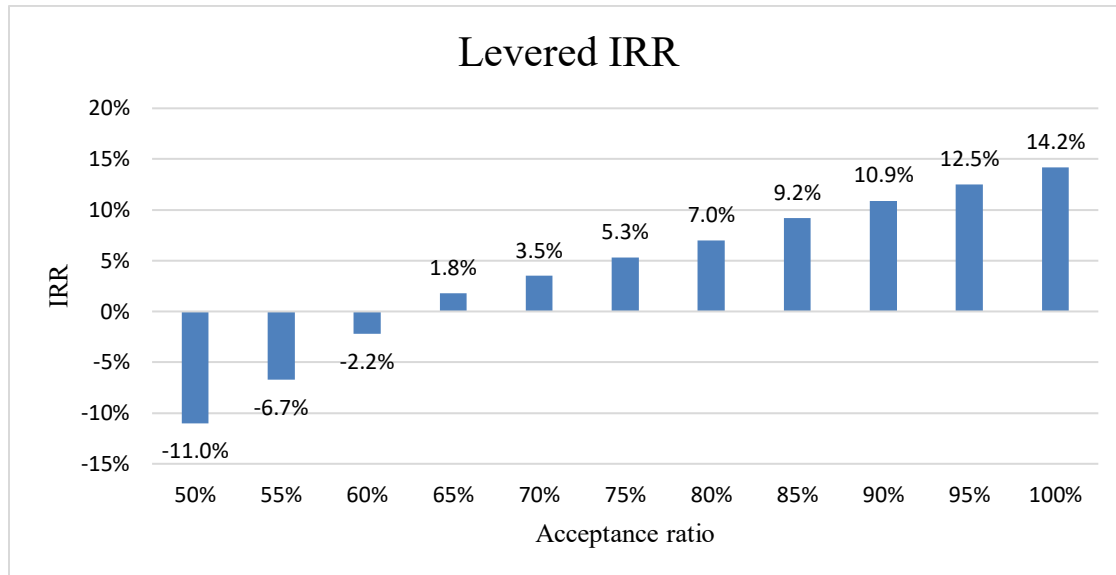


## CASE 2) - CAPEX variation [350 k€/MWh]

Given the results with the Megapack product, it was deduced that the main factor negatively influencing the economic results was the investment cost of the batteries, which led to a very high CAPEX. In particular, the product by Tesla had a specific cost of 457 k€/MWh. Therefore, it was performed another analysis, considering to be able to achieve a lower cost of batteries and installation like 350 k€/MWh. Such value was provided by other works and studies made by the company. By modifying this parameter, the total CAPEX reached 73.790 M€, about 20 M€ lower than the previous case. The other costs were supposed to be equal to the previous case, including the estimation of the maintenance costs, which was originally referred to the Tesla batteries. Moreover, the characteristics of the BESS were considered to be equal, including the rated power, the storage capacity and the system efficiency. Then, as it was previously done, the acceptance ratio was varied to evaluate the possible results. The plots in the following show the main parameters resulting.





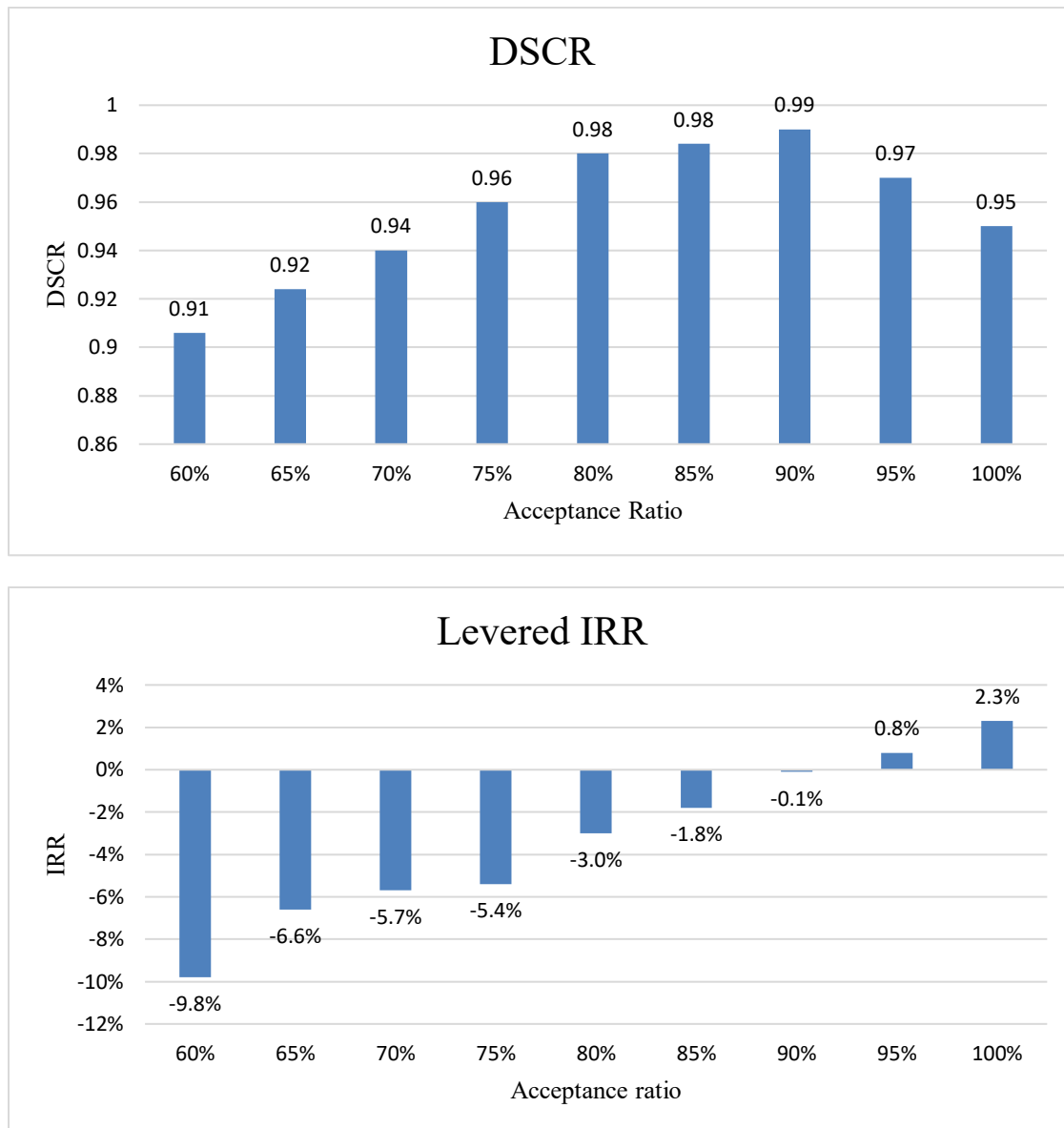


In this case it can be seen the positive effect of decreasing the initial investment cost. Both the DSCR (Fig.135) and the IRR (Fig.136) would be positively influenced by the lower annual financial repayment and interests. Looking at the DSCR values, the financing would be sustainable for the project for acceptance ratios above 65%. Of course, this would still not be completely satisfactory, as for lower numbers of offers accepted the coverage of financial costs would not be assured and being able to work on MSD with more than 600 cycles per year might seem improbable. Looking at the IRR plot, instead, the objective of 8.5% would be achieved only with more than 85% of the offers accepted, corresponding to almost 800 cycles per year. For lower acceptance ratio values the IRR would become lower and lower, still showing the project unfeasibility, also considering that the probability of getting the offers accepted would range between 30 and 60% of the presented one. Overall, this shows that the capex decrement would improve the economic feasibility of the project, but still, it would represent a risky business.

### CASE 3) - CAPEX & Degradation variation [350 k€/MWh & 6000 cycles]

In addition to the capex reduction, the analysis was once again performed considering a less optimistic lifetime of 6000 cycles so as to see the impact of this factor on the economic feasibility. Therefore, the degradation rate was increased as reported.

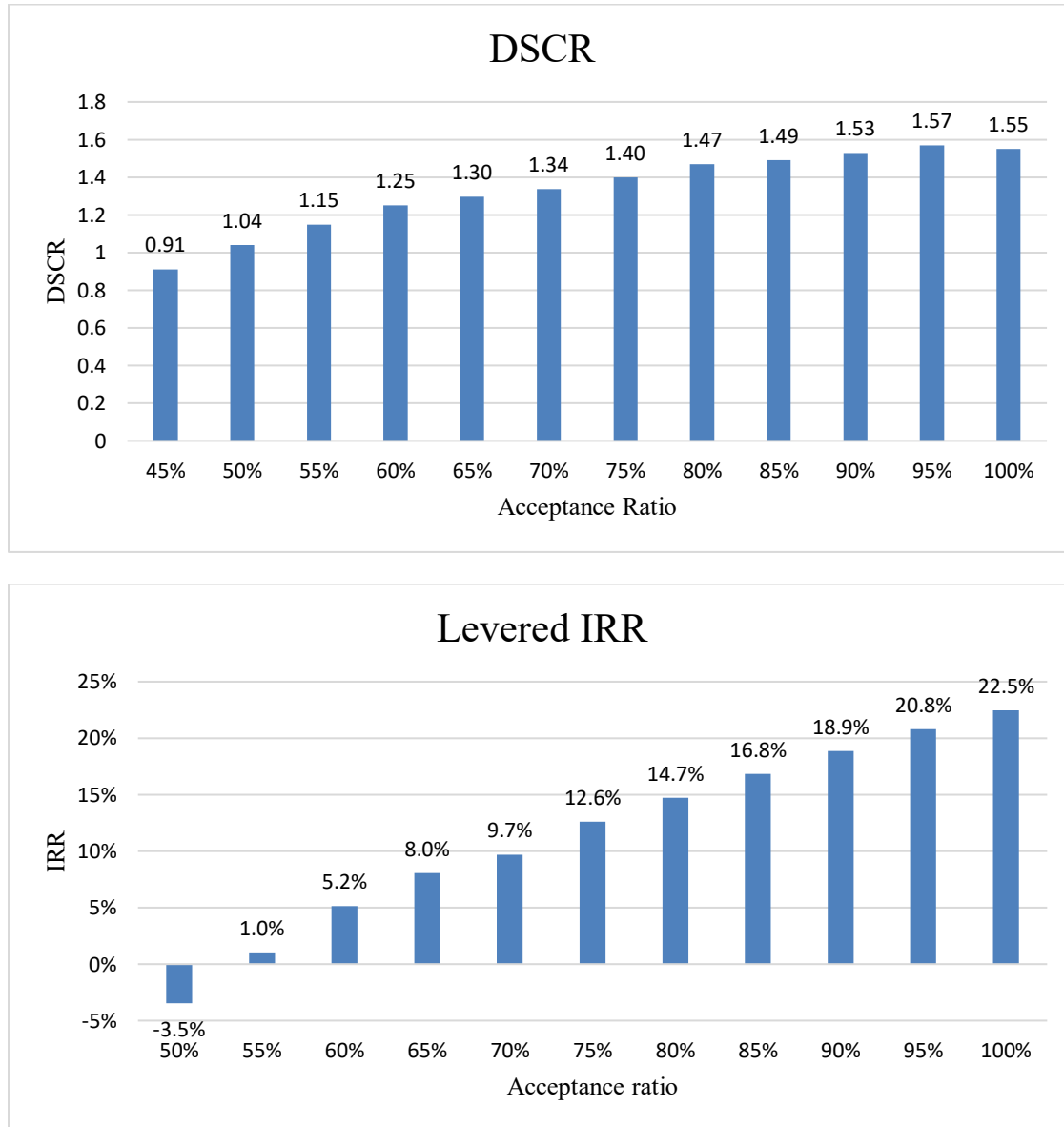
$$\text{Degradation rate} = \frac{(100 - 70)\%}{6000} = 0.005\%/cycle$$



As expected, a faster degradation of the system would lead to a premature end of life of the system, affecting the economic performance of the project. Still considering the 350 k€/MWh cost variant, both the IRR (Fig.138) and DSCR (Fig.137) would become unacceptable under any offer acceptance ratio condition. The lower lifetime would reduce the revenues because of the lower number of years of operation, because of the lower storage capacity available, and also because it would also reduce the financing duration. The shorter financing period would decrease the total interests to give back to the banks, but it would also increase the annual repayments of the invested capital, significantly decreasing the DSCR. Therefore, both parameters would be negatively affected by the higher degradation rate. This analysis shows how this kind of investment might be very risky due to the degradation phenomena, which might jeopardize the whole economic feasibility. For this reason, an accurate estimation of the lifetime cycles that could be sustained by the system would be needed before the project realization.

#### CASE 4) - CAPEX variation [300 k€/MWh & 10000 cycles]

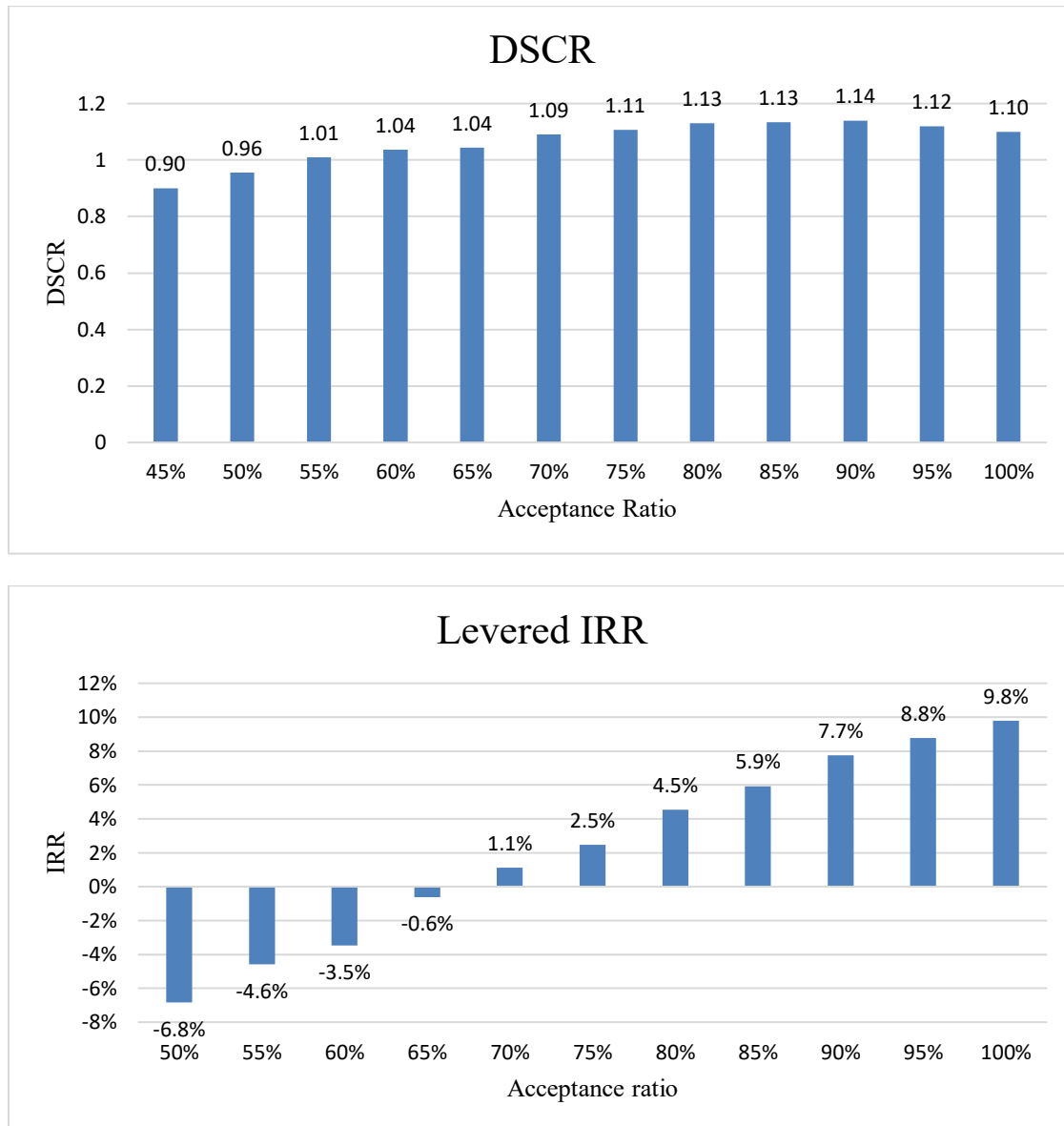
To further investigate the feasibility of a BESS operating on the market, it was analyzed a case with a cost of batteries and installation of 300 k€/MWh, a value that could have been achieved according to pre-crisis estimations in 2020.



In this case, the even lower investment cost would have positively affected the economic feasibility. In terms of DSCR (Fig.139), the project would have been able to comply with financing costs for acceptance ratios higher than 55%. Instead, the IRR values (Fig.140) would have been satisfactory for acceptance ratios higher than 65%. The range of acceptable results obtained was larger than the previous case with 350 k€/MWh cost, but it still would have not reached the target of feasibility in the 30 to 60% range of acceptance ratio.

### CASE 5) - CAPEX & Degradation variation [300 k€/MWh & 6000 cycles]

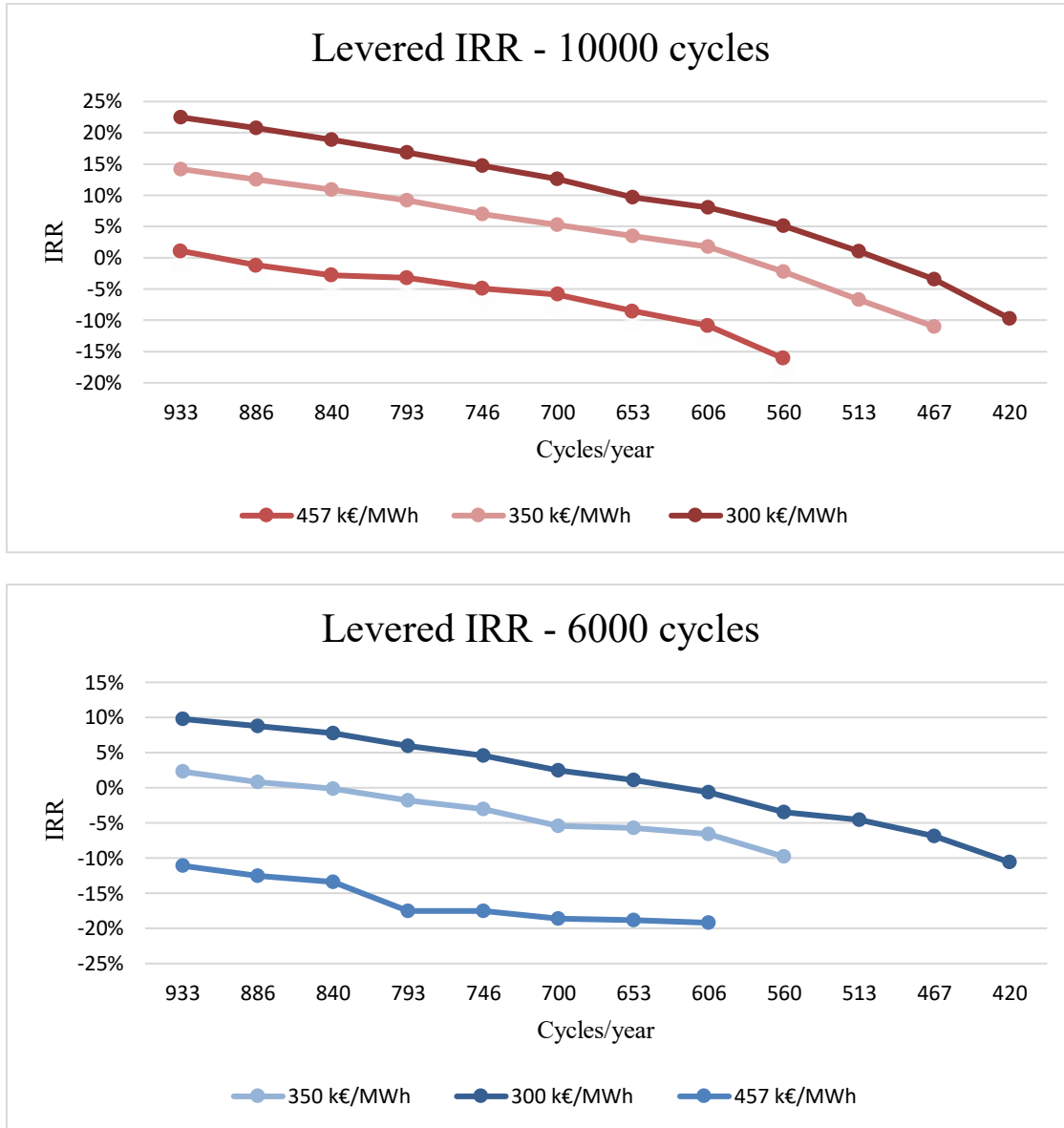
In the end, as it was previously done, it was also considered the conservative hypothesis of end of life of the system over 6000 cycles for the 300 k€/MWh case.



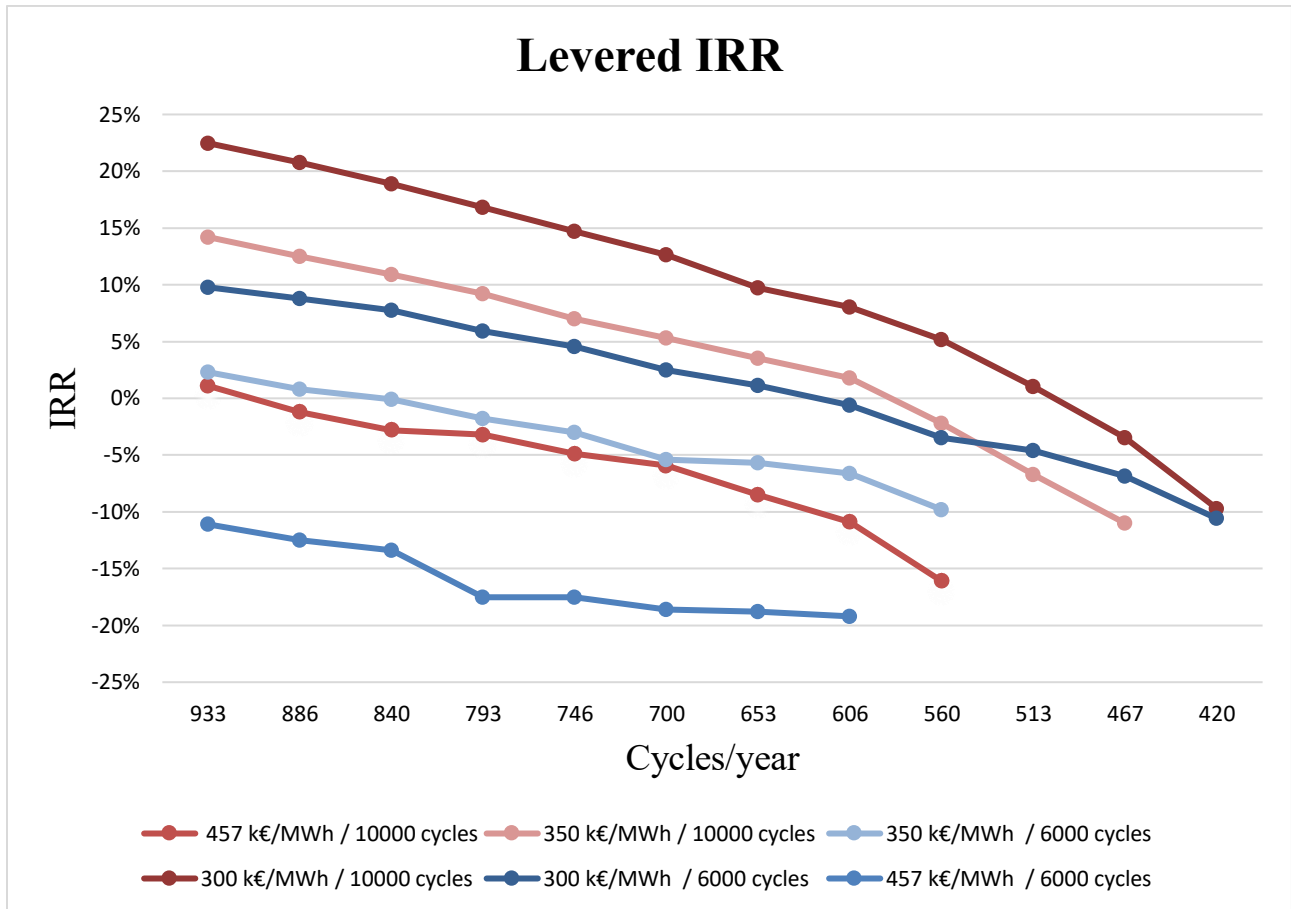
As in the other case with 6000 cycles over the system lifetime, the DSCR (Fig.141) and IRR (Fig.142) values were lower because of the lower earnings and higher annual repayments to give back to the banks.

## 6.1.2 Comparison of the CASES

The different cases were compared to graphically observe the effects on the feasibility of the system. In the following the IRR results are grouped in cases with a system life of 10000 ([Fig.143](#)) and 6000 cycles ([Fig.144](#)).



Here, the x-axis reports a decreasing number of cycles, which is equivalent to a decreasing percentage of accepted offers. Once again it can be seen how the decreasing the cycles, and therefore the system operation, the rate of return decreases, reaching unacceptable values. The CAPEX plays an important role, as we can observe a shifting of the curves upwards with the decrease of initial investment cost. In the above plots, the 457 k€/MWh lines represent the Megapack product by Tesla, in accordance with the price estimation made for the simulations. All the curves are then shown in the following plot in [Fig.145](#).



### 6.1.3 D.Lgs. 210/21

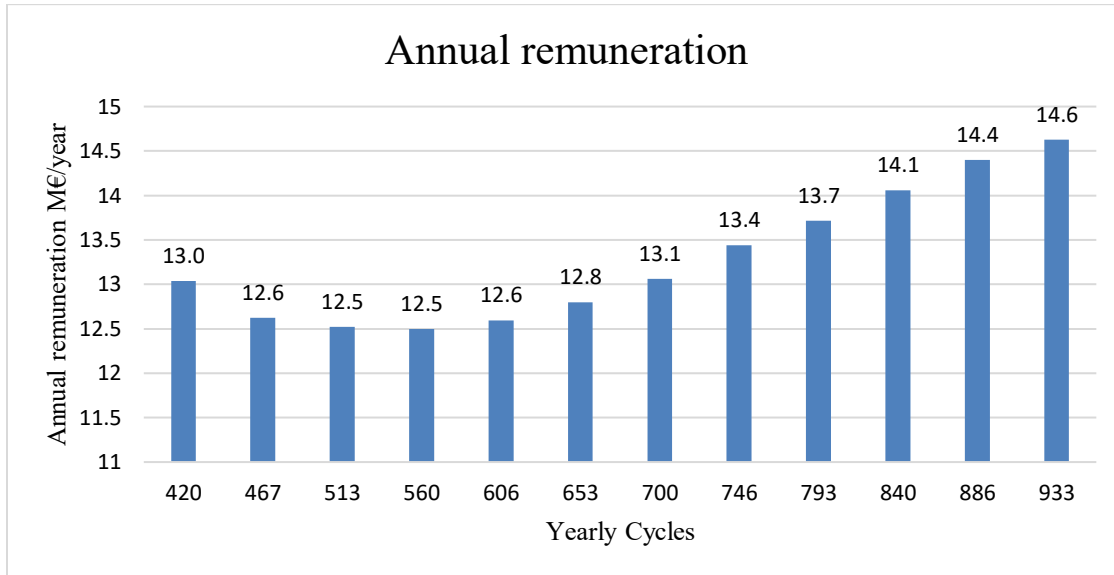
Given the economic results of the business plan, it was proved that operating on the MSD market only would not be feasible due to the high uncertainty on the effective operation of the system, which is dependent on the choices of the TSO and on the competitiveness of the market. For this reason, it would be needed to operate also on other markets like MGP and MI, together with MSD for a higher certainty of operation. However, the price differences achieved on the other markets would typically be smaller, leading to lower incomes. Overall, operating a storage system standalone on the market might be very risky, due to the uncertainties on prices, on the effective volumes bought and sold, and on the degradation of the system. For these reasons, it is presented an alternative that might be interesting for future investments on this field. In 2021, as an actuation of the European Directive UE 2019/944, Italy issued the legislative decree 210/21 [6.01]. In article 18 of this decree, some measures were proposed for the development of the storage capacity needed by the country through bids. This legislative decree was made to assure the future adequacy of the Italian electric system, that will have to withstand renewable overgeneration, more frequent congestions, lower programmable generation, larger price volatility. Then, receiving the instructions from the d.lgs. 210/21, in 2022 ARERA published the document for consultation 393/2022 [6.02]. This document was made to define the introduction in the Italian energy market of the new mechanism for term supply of energy storage resources. Even in this document, it is highlighted how investments on energy storage technologies in a market energy only are very risky because of high fixed costs and high uncertainties. In the d.lgs.210/21 it was established that Terna will have to provide a progression plan of the storage capacity needed, defining the types of storage required and the geographical area specific needs. On the other hand, it was established that the Authority ARERA will have to define the base conditions that Terna will have to comply with in the definition of the discipline for the storage long term supply competitive bids. As result of these bids, the new storage capacity awarded will earn the right to receive an annual remuneration for the period of the contract, while complying with the obligation of making the storage capacity available to third parties for the participation to the energy markets. The annual remuneration for the capacity will contribute to cover the investment costs, moving the risk to the TSO, which establishes the minimum storage resource required. The contracts for the supply of the energy storage resource will define the time length of the contract, the period of delivery, the storage duration, the storage cyclicity, the delivery place and other minimum requirements. These kinds of contracts could be done both for battery energy storage systems and pumped hydro, with appropriate contract differences related to the different technology characteristics. Regarding the obligations for the owners of the awarded storage, they will have to make the system available to third parties to provide time shifting products in the market, and to Terna to operate on the MSD market. In the case of time shifting products, the storage will be used to move energy from low price periods to higher price periods, making possible for the third parties that bought the right to manage a storage to make profit on the price differences in the energy markets. Instead, in the case of the MSD participation, the storage will have to be available for Terna to provide ancillary services. For this service, the participation to MSD will be reserved to the owners of the storage systems, as it will be required to know their availability and effective state. However, in order to avoid over-remuneration of the capacity, some economic constraints on the offers on MSD will be introduced for the capacity under contract according to the consultation document. In particular, the prices for the offers “up” on the market will be



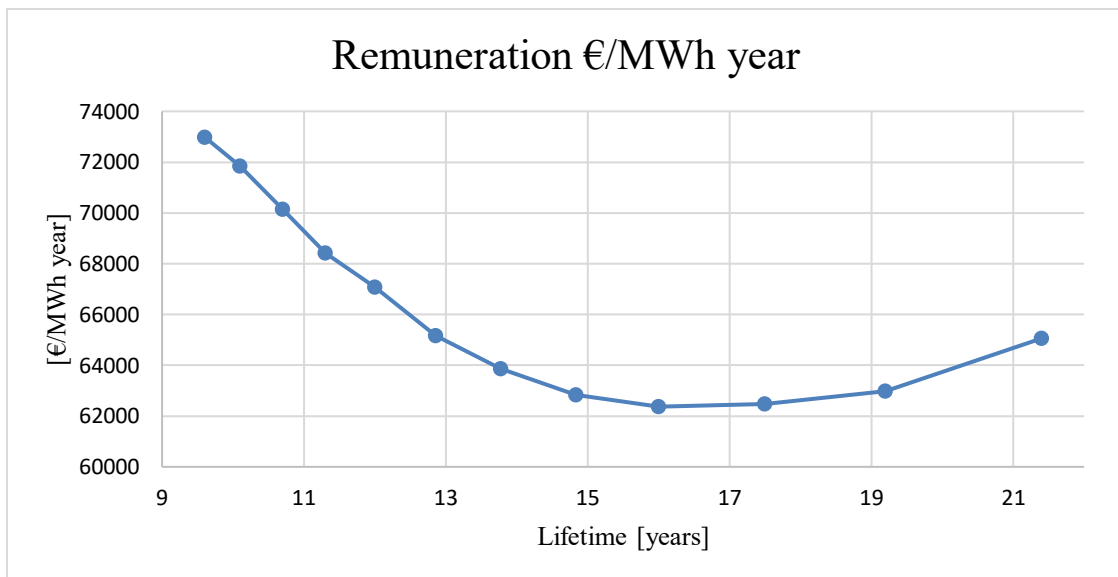
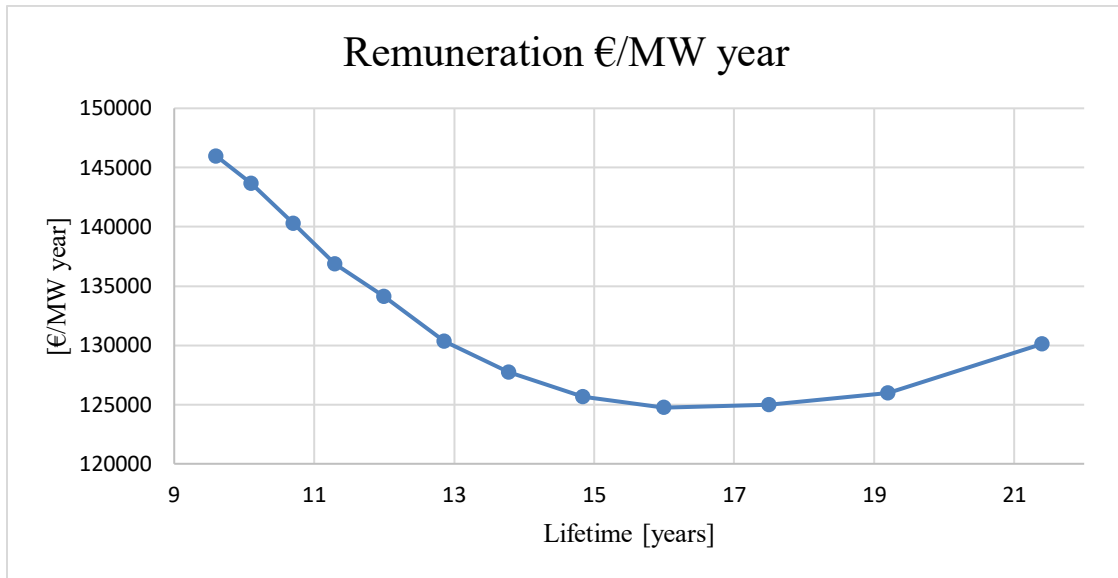
limited to the average of the peak prices on the MGP in a limited period before the time to which is referred the offer. The prices for the offers “down”, instead, will be limited to the minimum between the product between the price “up” and the storage efficiency, and the average of prices on MGP in a period of low price. However, according to this first draft, any positive margin from the operation on the MSD market should be given back to Terna, so as to reduce the fee needed to finance this mechanism. This means that the investment, operation and adequate remuneration will be covered only by the fixed annual remuneration by Terna. The storage owner will be considered as an MSD operator and will have to comply with the dispatching orders and face imbalance charges and eventually fees for the non-compliance of orders. Regarding the bidding process, the participants will be able to offer their capacity, and the award will be expressed as a prize in €/MWh/year or €/MW/year. Given that the document by ARERA is still not definitive, some observations were presented by Elettricità futura [6.03] and they might reflect future modifications. In particular they highlighted how the constraints on the prices of offers on MSD might cause market distortions, potentially affecting the revenues of other operators of the market that are based on initiatives external to this mechanism of capacity supplying. In addition, these constraints might not stimulate the use of best technologies in the project phase and the high efficiency maintenance during the management of the plants. For these reasons the constraints might be modified: a first proposal by Elettricità futura would be to apply price limits similar to those of the capacity market and thus permitting positive margins for the operators, which could stimulate the optimal use and management of the assets. Alternatively, a second proposal would be to calculate and corresponding to the storage owners a percentage of the margins achieved operating freely on the MSD without price constraints. A further revenue stream could come from the furnishing of additional performances compared to the ones required from the bids. It is still uncertain how these extra performances will be evaluated in the bids and then remunerated. Elettricità Futura’s proposal was once again to make possible for the storage system to offer their performance freely on the markets allowing positive margins, rather than adding a component to the annual remuneration of the system. As previously explained, the normal participation to the markets should limit the distortions due to the capacity supply mechanism.

Overall, for our purposes, this mechanism might be interesting as it would relieve the risk related to the uncertainties of the revenues of a storage system. It might be possible to invest on the realization of a storage with the certainty of being able to cover the costs and to achieve some remuneration of the invested capital. On the other hand, the participation to the markets would be limited for the plant owner, if not through a portion of the capacity external to this mechanism or through the new mechanism of time shifting products (if the mechanism was not modified). Based on the information on the first document by ARERA, it was decided to include in this business plan the possibility of participating to the mechanism. In particular, the expenses and revenues from the market participation were removed, and instead it was added an annual remuneration. It was supposed that the annual remuneration would have been given for the whole lifetime period of the system. Therefore, as it was done previously, the number of cycles per year was varied, so as to determine the influence on the lifetime of the system and therefore on the financing. This time, it was decided to directly avoid considering the Tesla product prices, and for this reason it was used the hypothesis of 350 k€/MWh for battery and installation cost. For each lifetime

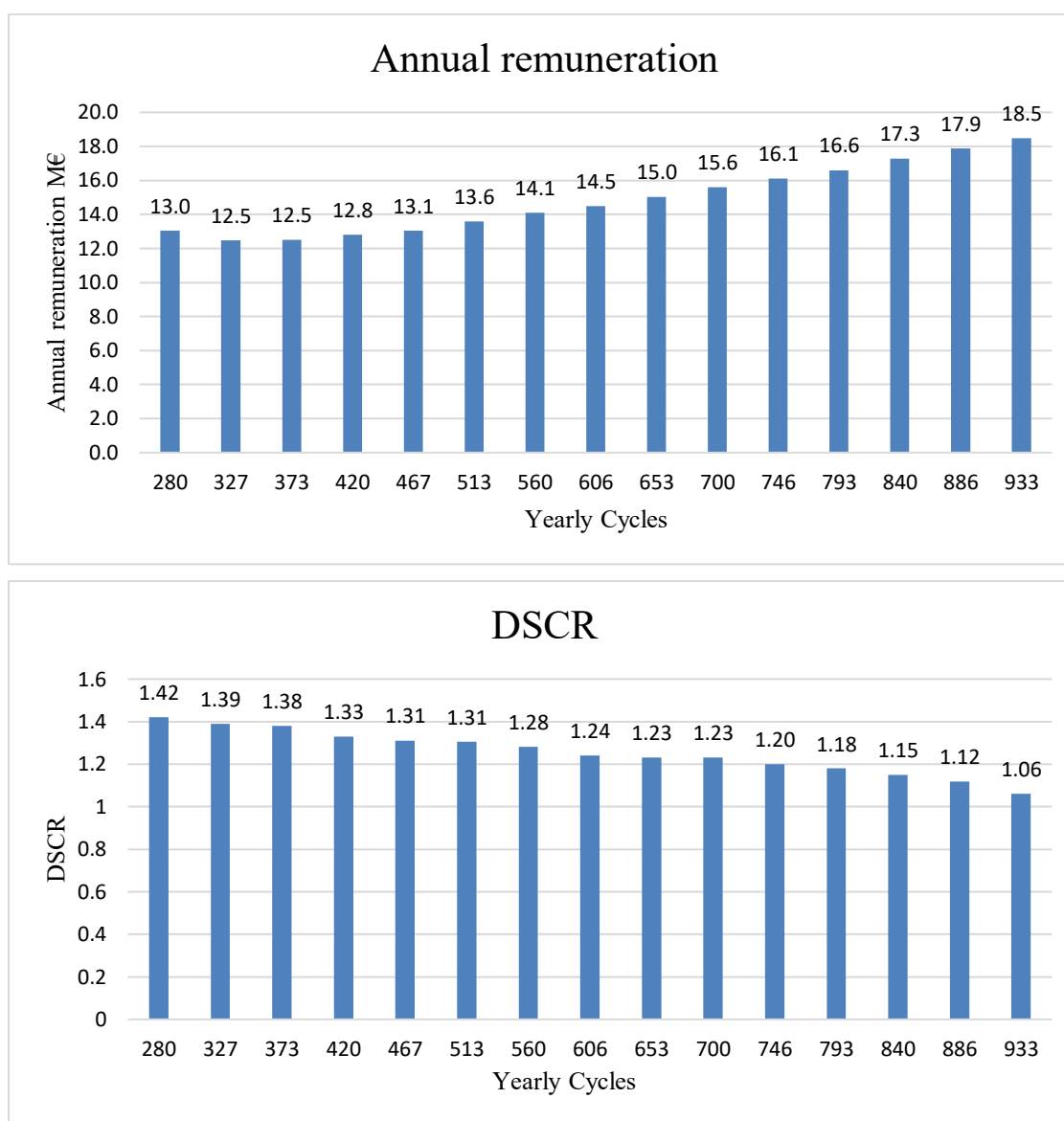
and financing duration, it was calculated the annual remuneration that would have been needed to achieve a levered IRR of 8.5%. In a first case, it was considered the optimistic system duration of 10000 cycles (from 100% to 70% of the initial storage capacity available). Here in the following are reported the resulting annual remunerations that would be required to achieve the objective of 8.5% levered IRR (Fig.146).



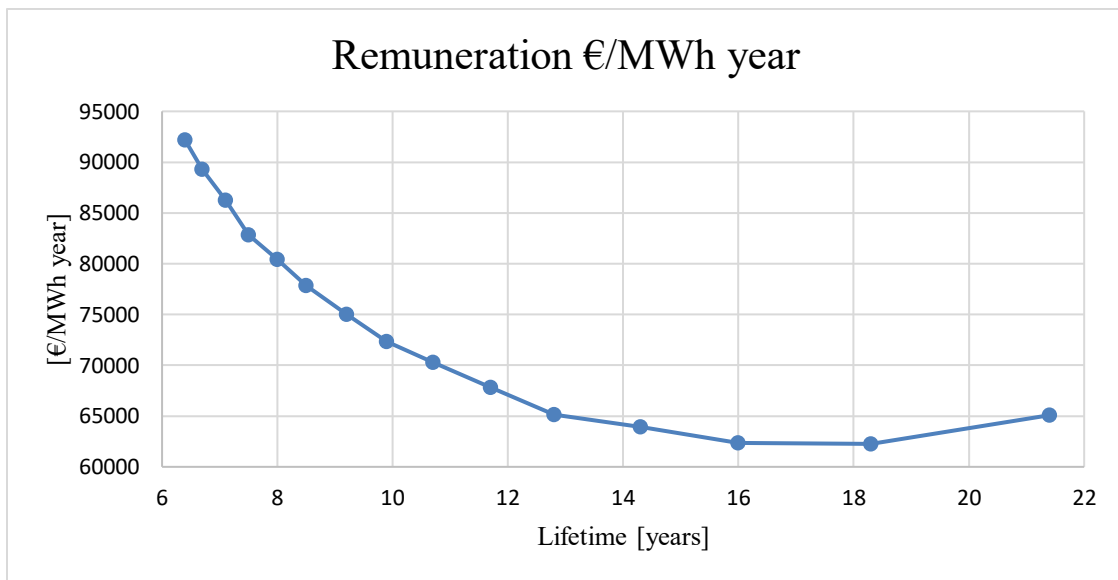
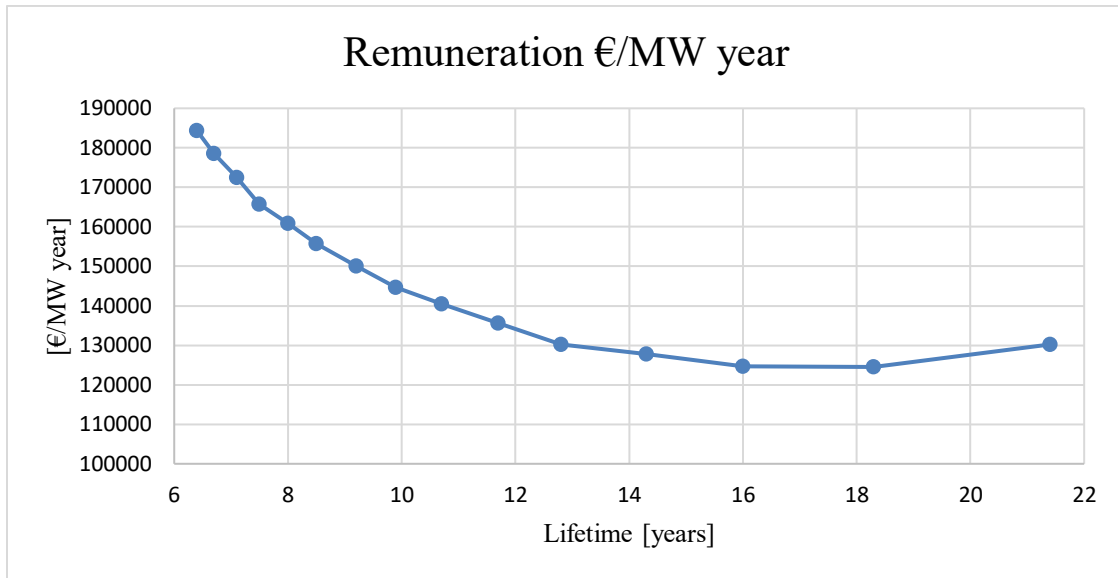
From the above plot it can be seen that too high cycling of the batteries would lead to a low lifetime of the system, and therefore require higher annual remuneration to cover the costs and the interests in a lower time. On the other hand, too low operation would lead to long lifetimes, and this would increase the amount of interests to be given over a longer period of financing. We can see that in this case the minimum remuneration required would be obtained considering between 450 and 600 cycles per year, corresponding to 15 to 19 years of lifetime under the previous assumption (and 14 to 18 years of financing). Under all the above cases of storage lifetime the DSCR would always be satisfactory, with values between 1.2 and 1.4, allowing for an adequate coverage of the financial costs. The same annual remuneration values are reported as €/MWh/year and €/MW/year, as described by the ARERA document in the following plots (Fig.147 and Fig.148), where the results were correlated to the system lifetime. Looking at the values per MW, we can see that the remuneration needed would be between 125 k€ and 145k€ /MW year.



Secondly, it was adopted the less optimistic hypothesis of 6000 cycles lifetime (100% to 70% of the initial storage capacity available). Once again, the resulting annual remuneration values are reported as function of the number of yearly cycles performed, which affect the system lifetime and the financing duration. For a lower lifetime it can be seen that the values of remuneration by Terna should be higher to cover the costs and to remunerate the investment enough. Like for the previous case, there was a range of minimum yearly remuneration between 320 and 420 cycles per year, corresponding to lifetimes between 14 and 18 years under the above hypothesis (and 13 to 17 years of financing). In this case, the DSCR would be satisfactory for lower acceptance ratios, as a longer financing period would allow to cover in an easier way the debt costs. Higher number of cycles, instead, would mean shorter lifetime and financing length, with consequent higher annual debt repayment. The plots of annual remuneration (Fig.149) and DSCR (Fig.150) are reported in the following.



Reporting the annual remuneration values in terms of €/MW/year (Fig.151), we could see that the values would be comprised between 125 k€/MW year and 185 k€/MW year. The point of minimum was similar to the previous case, while the upper values were much higher due to the lower lifetime. In order to get the right remuneration in accordance with the lifetime expected for the BESS, it might be interesting the proposal by Elettricità futura [6.03]. In their observations, it was suggested to define a maximum number of cycles per day for the system that should be respected by Terna in the allocation of the time shifting products and in the MSD operation. This way, a premature end of life of the system would be avoided, and it would be easier to comply with the obligations of the contracts, still being able to remunerate adequately the investment. For this reason, in the bid participation to be part of this storage supply mechanism, it would be suggested to offer one of the “minimum” remunerations required together with a specification of the maximum number of cycles/year corresponding.



Under the conservative hypothesis of 6000 cycles over lifetime, from the results of the above-described case, it might be suggested to offer a price of 125 k€/MW year (or 62.5 k€/MWh year) specifying a max number of 370 cycles/year (or 1/day). This price might be competitive in the bid, and the restriction to the number of cycles should allow a system lifetime of 16 years, which is comparable with the common lifetime of batteries of 15 years. Alternatively, if the battery lifetime was not well defined enough, it might be considered a lower restriction to the cycles and a lower system lifetime, so as not to exceed the expected lifetime, as an example with a price of 128 k€/MW year (or 64 k€/MWh year) and 14 years lifetime (420 cycles/year). Of course, these values are based on the hypothesis of investment costs for battery and installation of 350 k€/kWh, and they should be varied depending on the system real price. In addition, it should be remembered that as for the previous cases it was considered a financing with 75% bank loans at interest rate 5%, for a duration of 1 year lower than the system expected lifetime.



## 7 Conclusions

Over the last decades, the energy sector underwent significant changes to achieve decarbonization and reduce the global warming effect and the pollution related to the fossil power generations systems. In addition, the recent crisis due to the pandemic and the outbreak of the war in eastern Europe led to higher energy prices and difficulties in the energy supply. These phenomena caused in Europe a further commitment towards the achievement of energy independency thanks to renewable energy sources. However, with the increasing development of intermittent renewable energy technologies, like wind and solar, risks of overgeneration, congestions and grid imbalances are likely to grow. In this new scenario, energy storage technologies would play a key role in providing services to stabilize the grid and in time shifting the renewable energy generated, matching the energy demand with the generation.

This master thesis work has been developed in collaboration with Elettrostudio s.r.l., a company working in the renewable energy field. The company is currently working on the authorization process of three offshore wind farms that should be realized in the south of Italy. These offshore wind farms should reach a rated power of 495 MW each, possibly injecting large amounts of power in the national grid. Given the trend of increase of renewable generation, these additional wind farms might generate even more problems on the national grid due to overgeneration and imbalance effects. For this reason, the objective of this study was to determine if the realization of an energy storage system could have prevented the curtailment of the wind power while being able to self-sustain itself economically on the market.

In the first part of the thesis, the floating offshore wind technology has been described, as this represents something new and rapidly developing in the electricity generation sector. This is particularly interesting in Italy, given that by the end of 2022 only one small bottom-fixed offshore wind farm was in operation in Taranto, and Italy seems to have the greatest potential for offshore wind in the Mediterranean area. This study on the floating offshore wind allowed to highlight its high potential in terms of renewable energy generation, thanks to the undisturbed wind availability, and its potential lower visive impact. However, it also highlighted the critical points of this technology, which are mainly related to the ultra-deep-water applications, where moorings might be too costly, and where the power transmission technology is still not enough developed, both regarding the floating electrical substations and the submarine export cables. Moreover, the study on this technology and the available preliminary projects of the wind farms provided useful data to be used in the wind-storage coupling simulation. In fact, the project for the wind farm in Calabria was used as a reference to estimate a profile of wind power generation. A yearly wind profile of an onshore wind farm was scaled on the expected energy generation of the offshore wind farm, allowing to artificially create a realistic trend of the wind. This scaled profile was then used to estimate the wind power generation reaching the land, considering the wake losses, the transformation and transmission losses. The resulting profile of this calculation was used as an input of the wind-storage coupling simulation. In addition, the Italian TSO (Terna) provided some data about the power fluxes of a zone near the expected connection point of the offshore wind farm, which was also used in the first simulation.

Then, a brief overview of the Italian electricity markets was presented, so as to understand the main mechanisms through which the storage system could operate. In particular, the analysis was mainly



focused on the market of dispatching services, which could technically be the most remunerative thanks to the low prices for services down and high prices for services up. In this second part of the thesis, the historical results about the MSD ex-ante and MB market sessions were presented and elaborated to provide input data for the simulations. In particular, in this section, the volumes and the prices both for services up and down were presented, with two different possible cases: one referred to the region of Calabria only, and one to the whole Centre-South of Italy.

In the third part, a review of different storage technologies was presented, in order to decide which type of storage should have been considered for the simulations. Technologies like the liquid CO<sub>2</sub> energy storage were found to be very innovative, and they were considered to be interesting for experimentation. Power-to-X technologies based on hydrogen production via water electrolysis were considered as well, and they were found to be interesting concerning the momentum in the developing of the hydrogen supply chain and final uses. However, in the evaluation of a possible investment, the production and commercialization or use of hydrogen seemed to be too risky and inefficient if compared with the other energy storage solutions. In the end, the battery energy storage solution seemed to be the best one in terms of flexibility, reliability, and cost, despite its weaknesses. For this reason, in accordance with the company, this technology has been used to perform the simulations in two different scenarios.

At this point, a simple model of a battery energy storage system was developed to simulate its operation on the market. In the first scenario, it was investigated the possibility of reducing the curtailment of the wind power with a storage operating locally on the MSD in presence of a bottleneck in the connection between the local area and the remaining part of the national grid. The simulations were repeated five times, each time considering market data from a different year between 2018 and 2022. The simulations were performed cyclically, optimizing the ROI value, so as to determine the best combination of price offers to buy and sell energy on the market, supposing these values to be constant all over the year. In this case, it was found that the storage would have been able to partially reduce the curtailment, but still the severe bottleneck would have caused the unfeasibility of the wind farm project. Additionally, the storage would have not been able to sustain itself economically even operating on the MSD and solving the congestions generated by the wind farm. For these reasons it was concluded that a significant bottleneck would have mined the feasibility of both the wind farm and the storage system. Given that the results for the solution with C-rate 4 hours were very unsatisfactory, it was decided not to continue with the simulations for the C-rate 2 hours solution.

In a second scenario, then, it was supposed that the adequacy of the grid would have allowed the export of the wind power without any bottleneck, and the storage could have operated on the market of dispatching services to satisfy the requests of the whole Centre-South. As for the simulations in the first scenario, the market data about the whole Centre-South of Italy were considered for years between 2018 and 2019. Moreover, it was once again performed an optimization of the prices offered on the markets up and down over the year to achieve the best possible ROI. In this case, the local power data provided by Terna were not used, and the historical volumes on the MSD market were considered instead. A simple estimation of the effect of the wind farm was calculated subtracting it to the volumes up and increasing the volumes down. In this case, it was found that the preferred type of storage would have

been the one with C-rate 2 hours, compared to the C-rate 4 hours. This solution would have led to a larger number of cycles over the year thanks to the higher rated power. Thanks to the larger market volumes considered, the storage would have been able to achieve good economic results, under the hypothesis of acceptance of the offers by Terna. From the simulation results, it was seen that the best size of storage for the years considered would have been in the range between 4 and 300 MWh. In particular, without considering 2022 (for its extraordinariness) the best storage size would have been of around 40 MWh and 20 MW. It was also determined that the optimal offers on the market would have been on average of 39 €/MWh for services down and 155 €/MWh for services up.

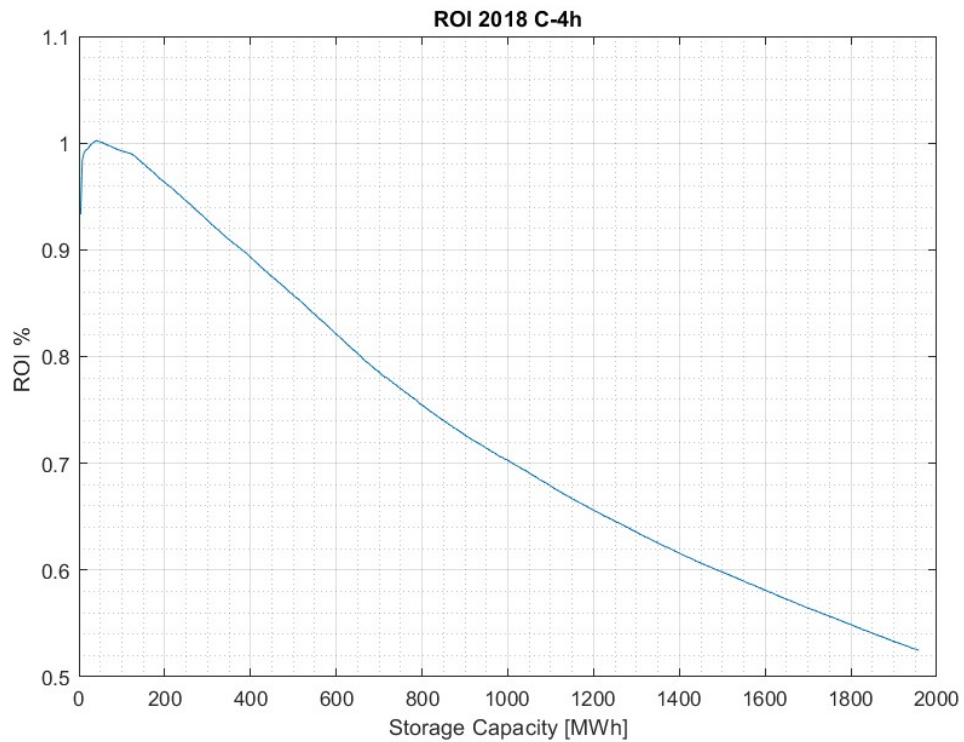
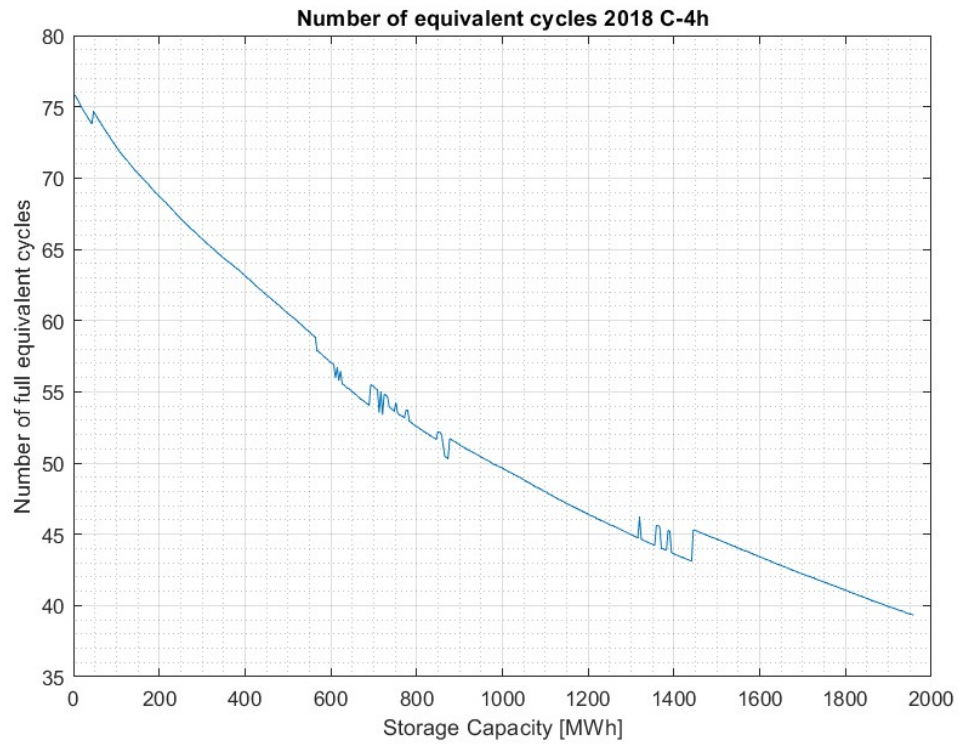
Given these results, the company decided to investigate the economic feasibility of a 200 MWh and 100 MW BESS solution operating on the MSD, as in the second scenario. For this size, it was found that on average the system would have been able to perform a maximum of 933 cycles/year in case all the appropriate offers were accepted. Starting from the average optimal prices above and the maximum number of cycles, a business plan was prepared, and the economic feasibility was studied as a function of the accepted offers on the market. From the results of the business plan, it was found that an investment on a storage system freely operating on the market would have been very risky, resulting to be feasible only with very high numbers of accepted offers and with low investment costs. In addition, it was found that the degradation phenomena would have been very dangerous for the economic results of the system, together with the low lifetime. For these reasons, in the end, it was decided to study a possible participation to the new bidding mechanism for the supply of the energy storage capacity that is being developed in Italy. This mechanism could possibly reduce the investment risks, shifting them to the TSO, which requires some capacity and remunerates it with fixed amounts to the owners.

Overall, this study was based on a simplified model of a BESS and a wind farm. For a more precise simulation, more data about the wind farm specifications would be needed, as well as better data about the wind availability, possibly taken from measurements on site. In addition, all the analysis was based on historical market data, supposing that the wind farm would not have influenced the market prices. A better model could be able to estimate the effects of the new wind power generation on the markets. Moreover, the competitiveness on the market might be considered, but still large uncertainties would persist on the offers accepted or refused by the TSO. For these reasons, in future developments, the analysis might be performed with more complex models considering also the future price trends, the contemporary participation to different markets and the behavior of the whole electric system, so as to reduce uncertainties on the system operation.

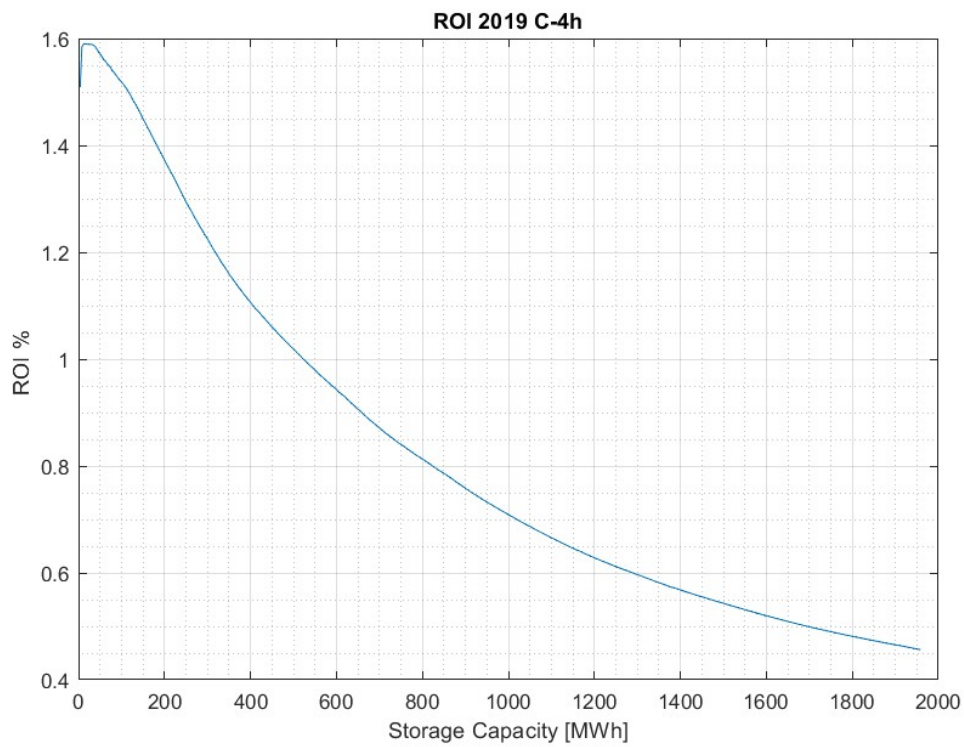
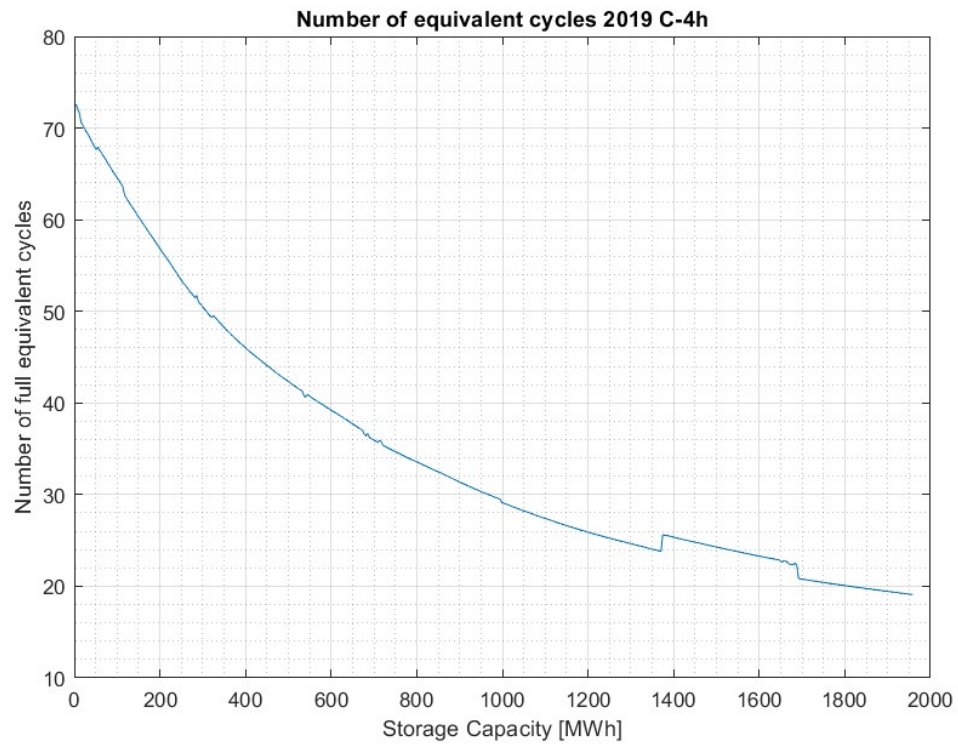


# Appendix A: Simulation 1 results

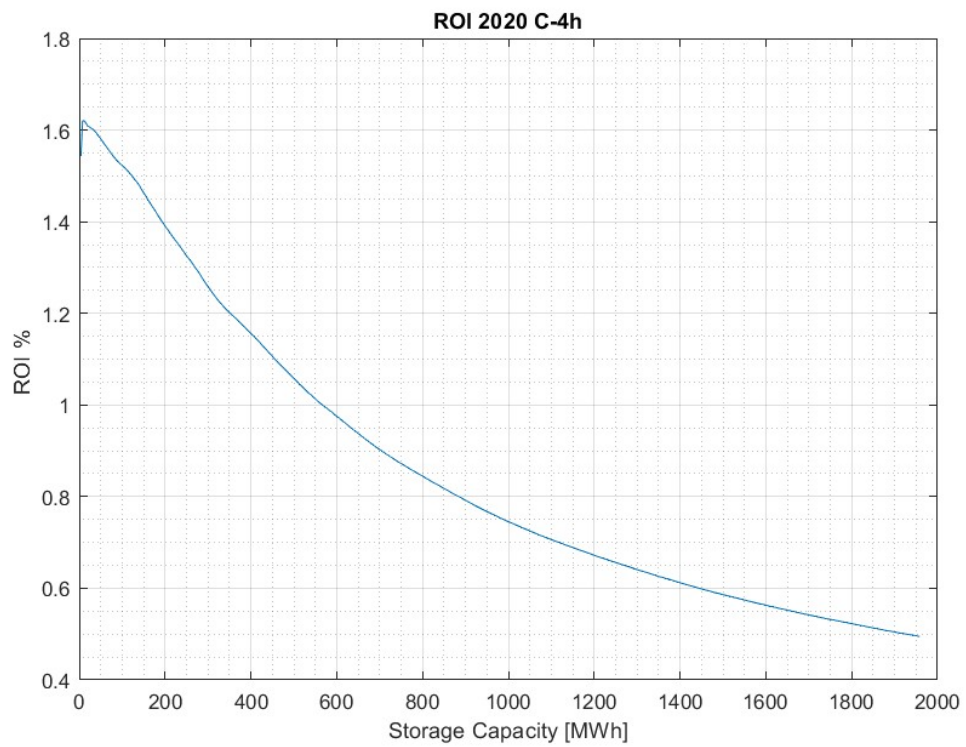
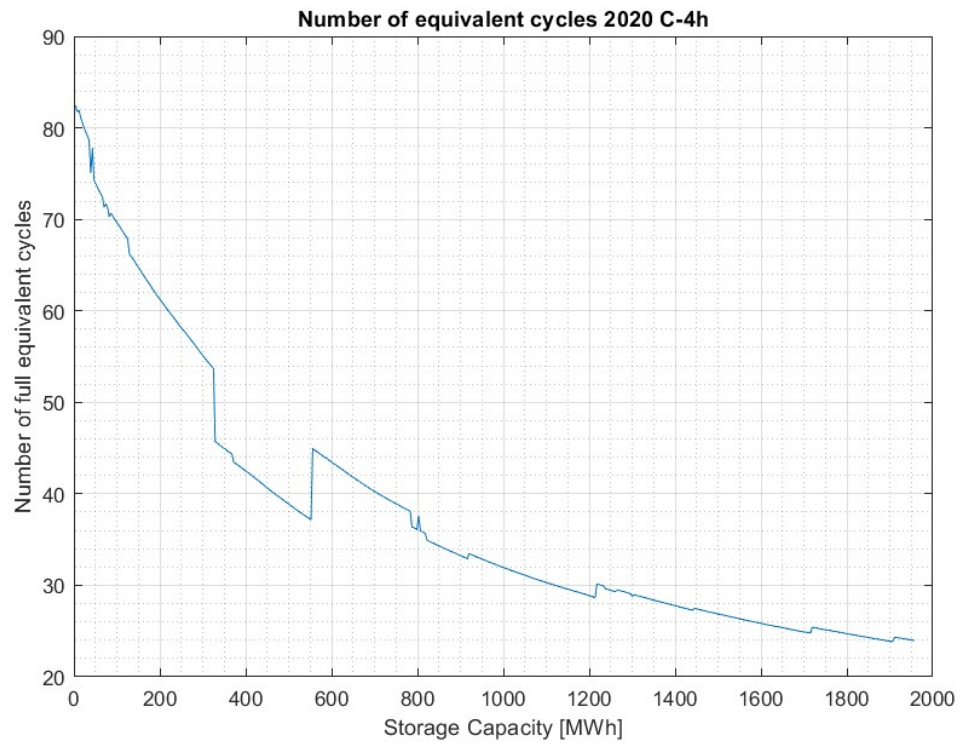
Simulation results for year 2018 for BESS with C-rate 4 hours in Calabria.



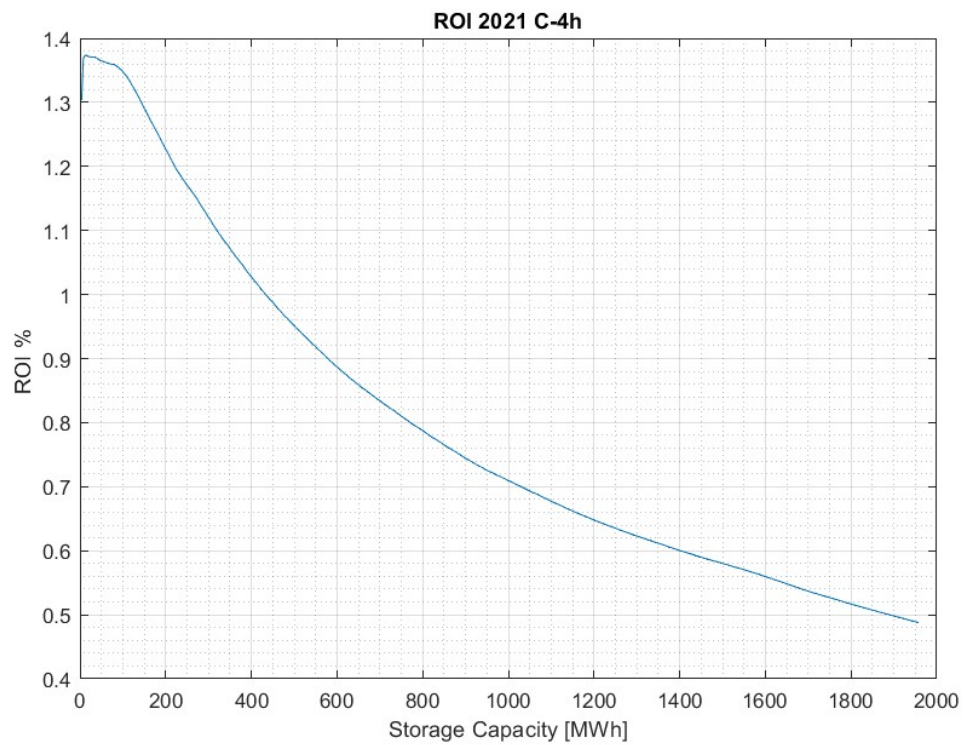
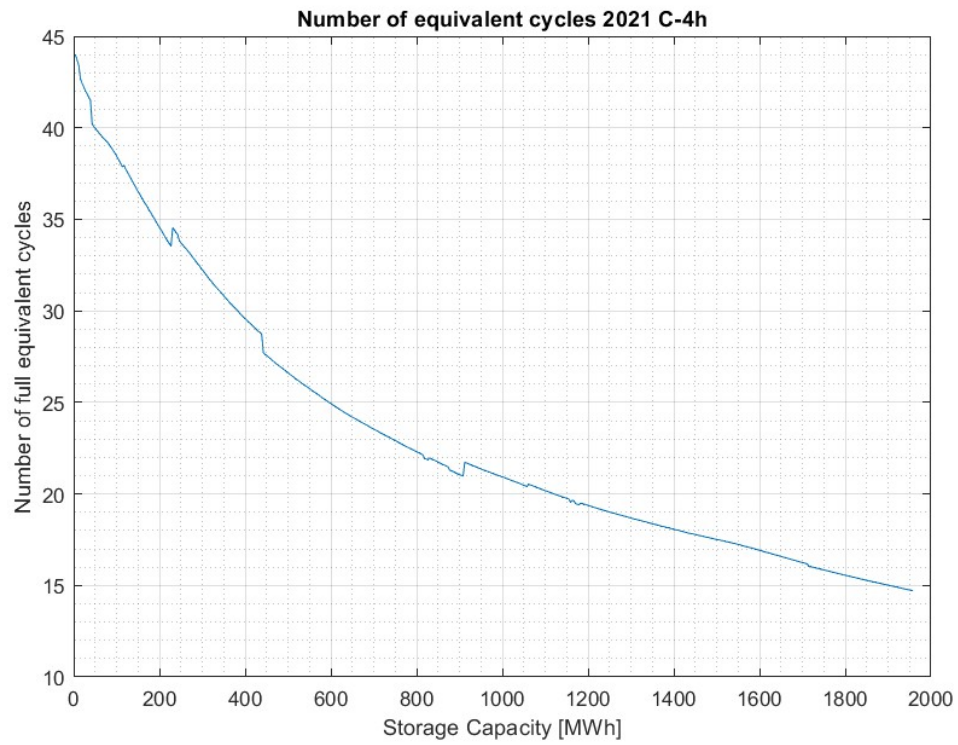
Simulation results for year 2019 for BESS with C-rate 4 hours in Calabria.



Simulation results for year 2020 for BESS with C-rate 4 hours in Calabria.

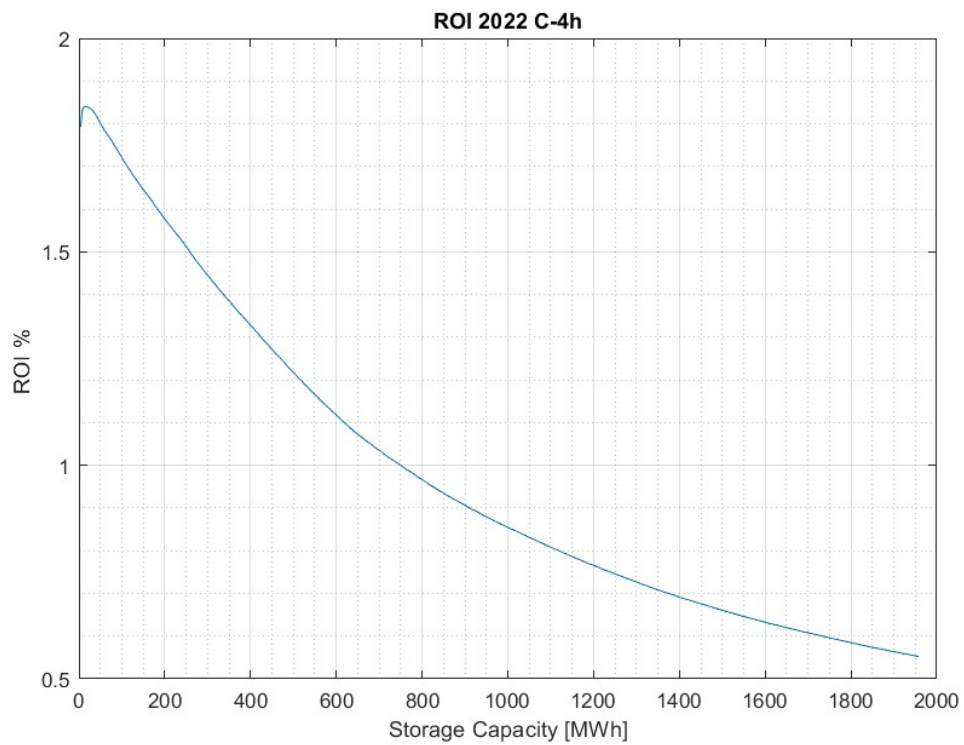
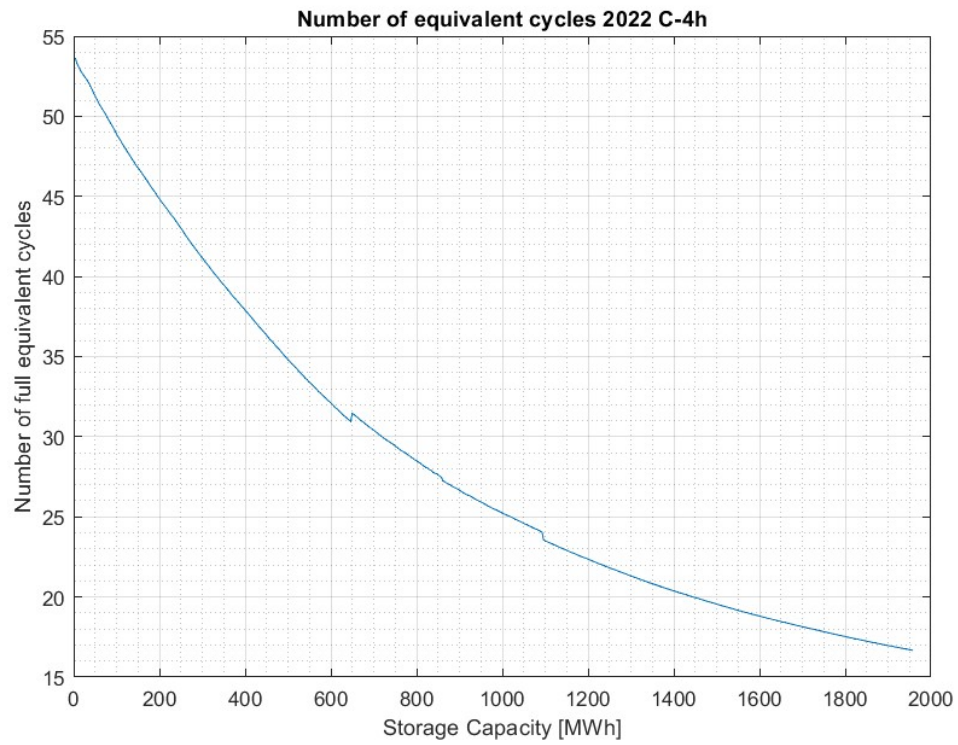


Simulation results for year 2021 for BESS with C-rate 4 hours in Calabria.





Simulation results for year 2022 for BESS with C-rate 4 hours in Calabria.

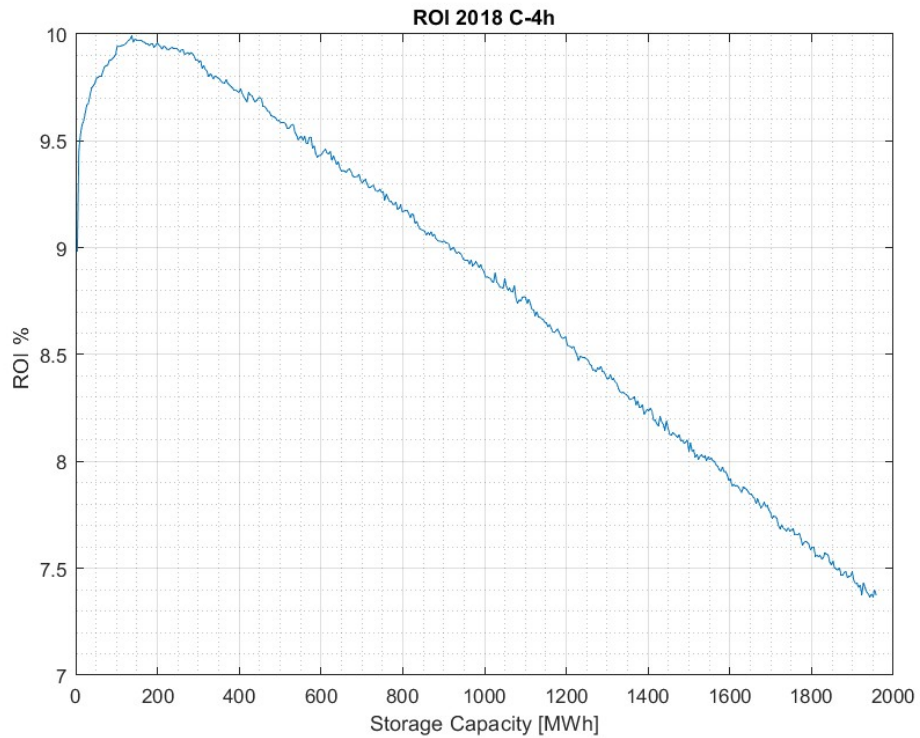
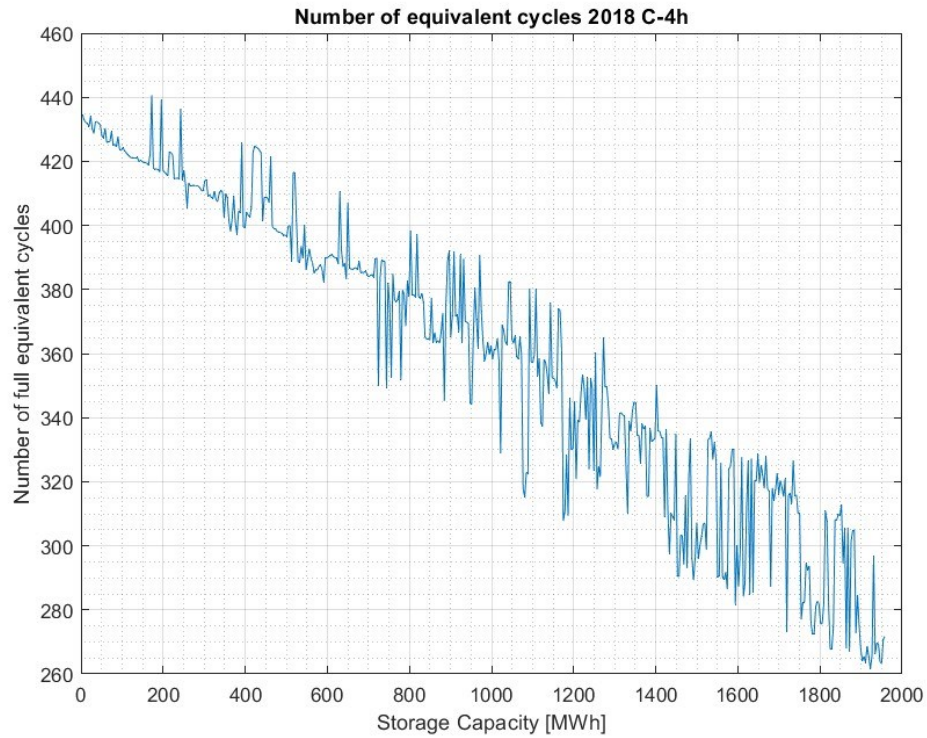




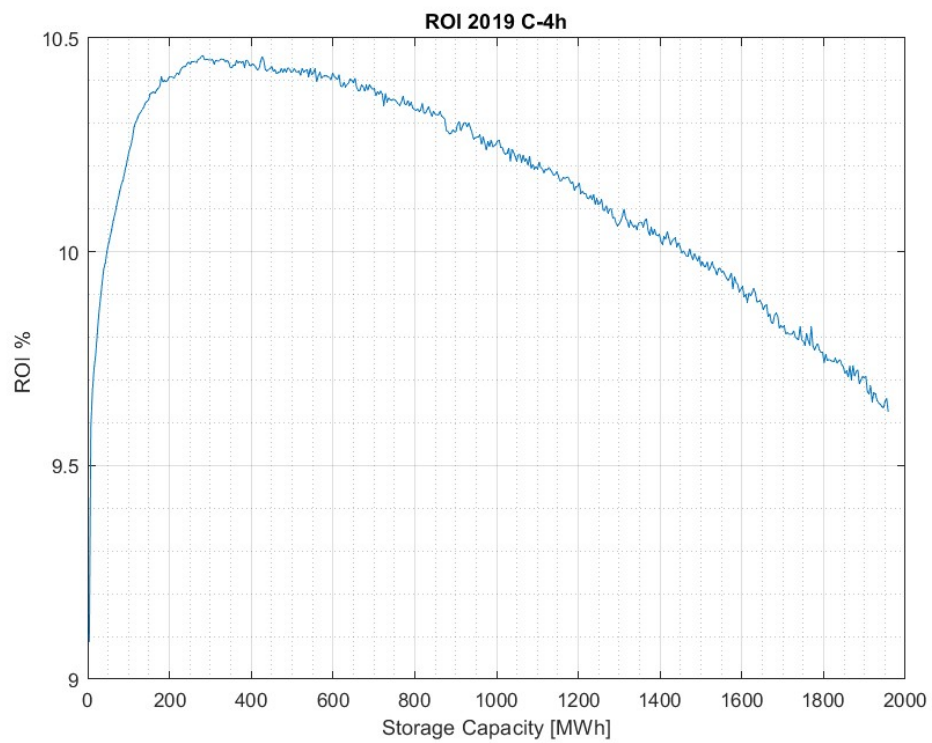
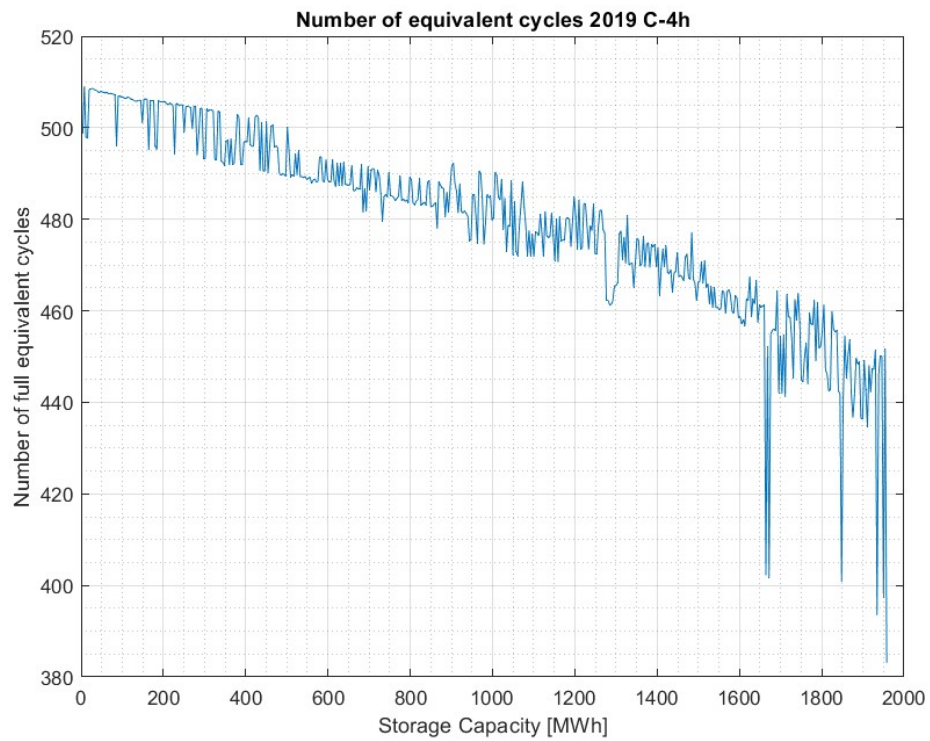


## Appendix B: Simulation 2 results

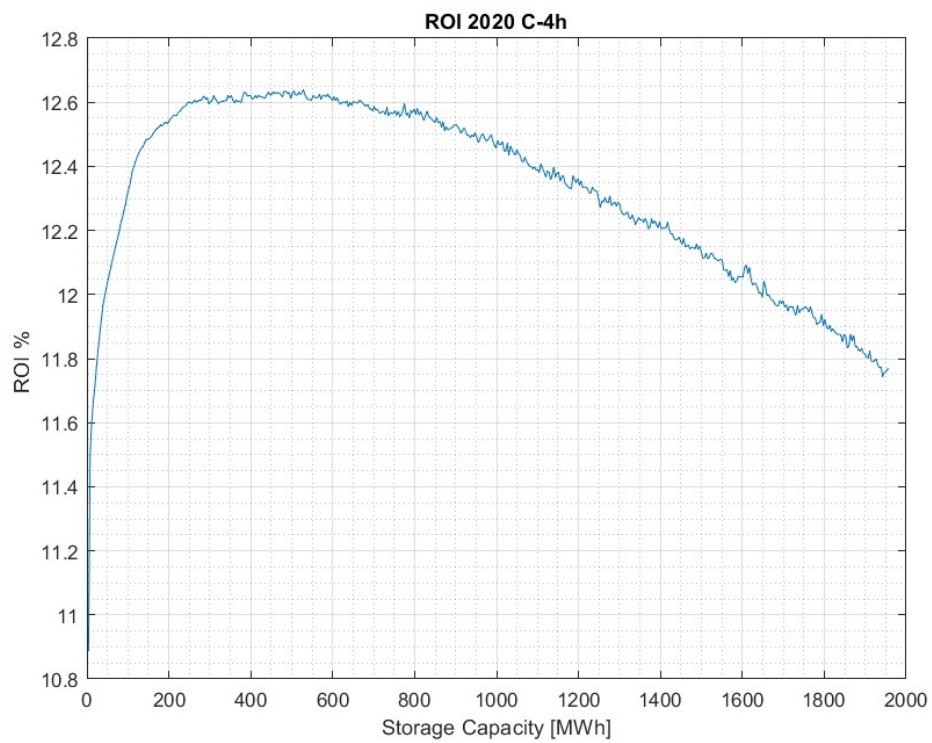
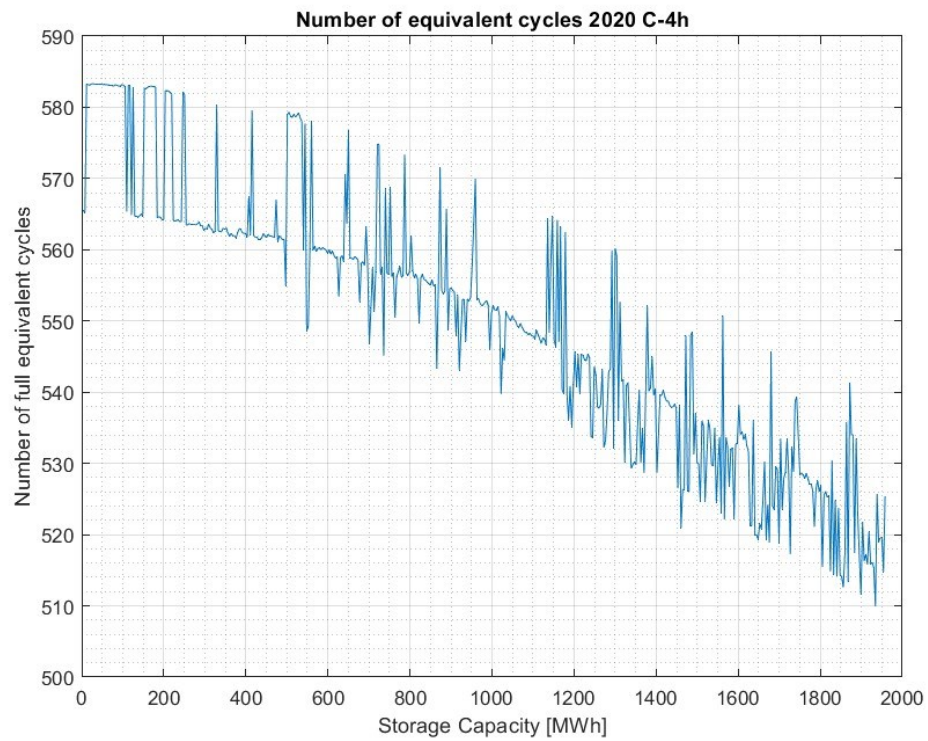
Simulation results for year 2018 for BESS with C-rate 4 hours



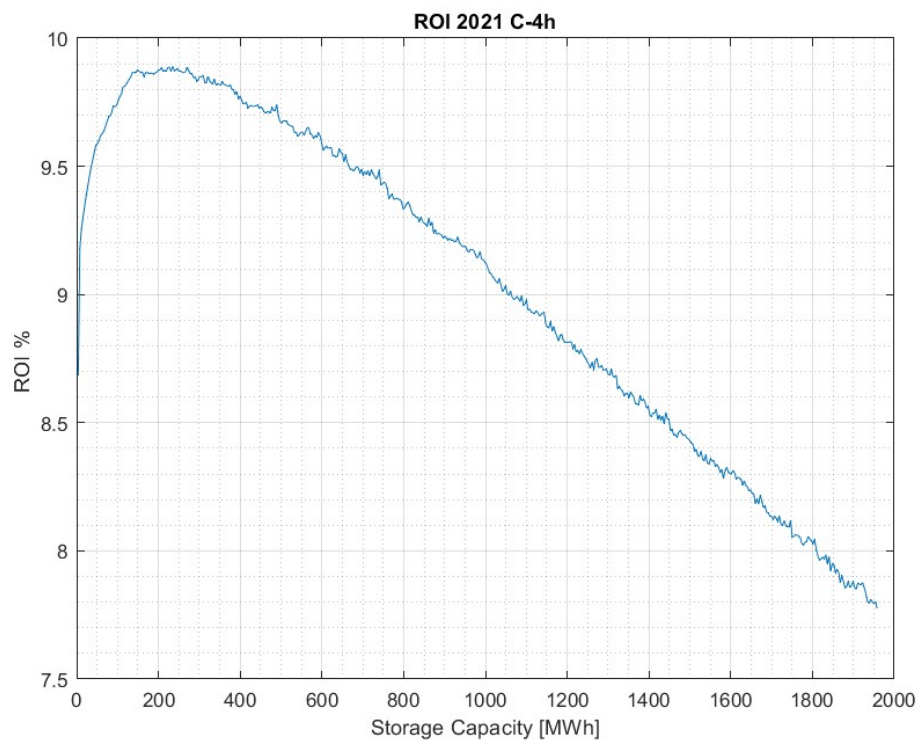
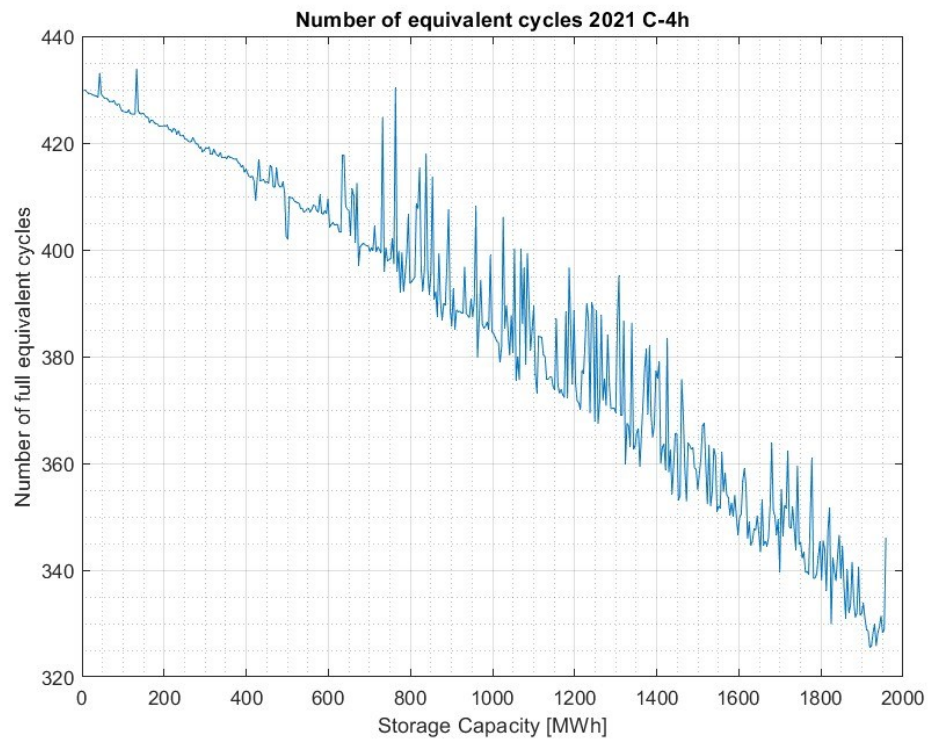
Simulation results for year 2019 for BESS with C-rate 4 hours



Simulation results for year 2020 for BESS with C-rate 4 hours

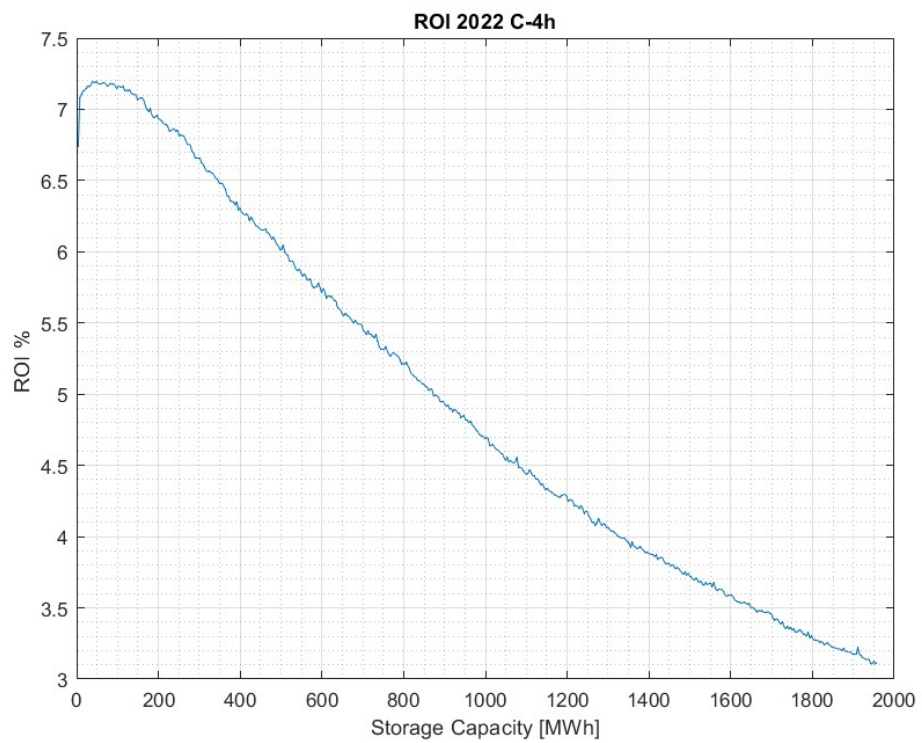
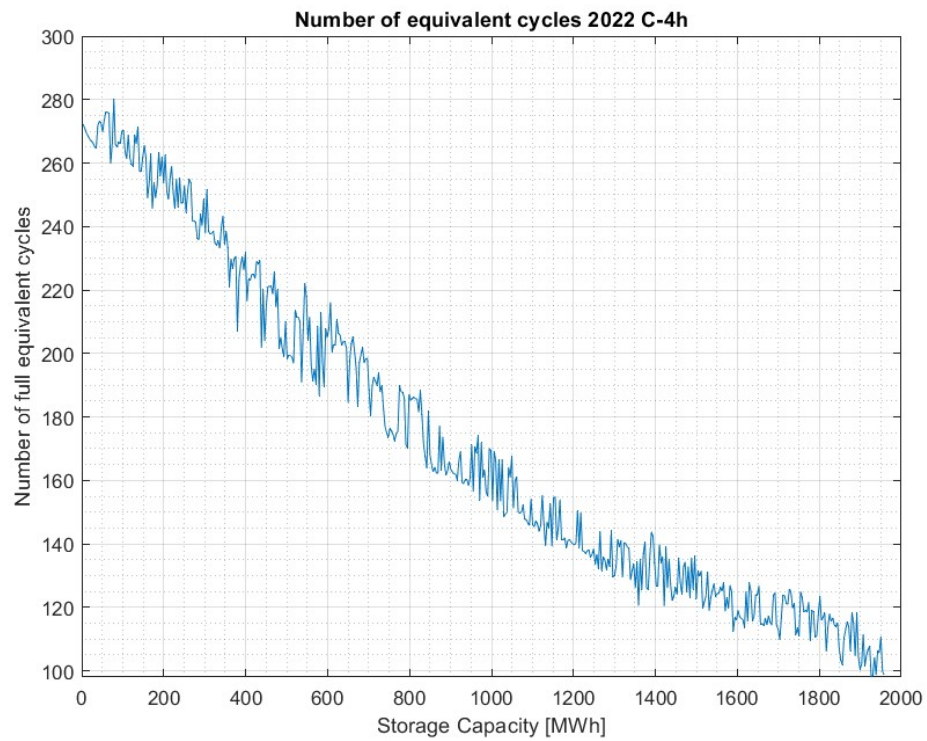


Simulation results for year 2021 for BESS with C-rate 4 hours

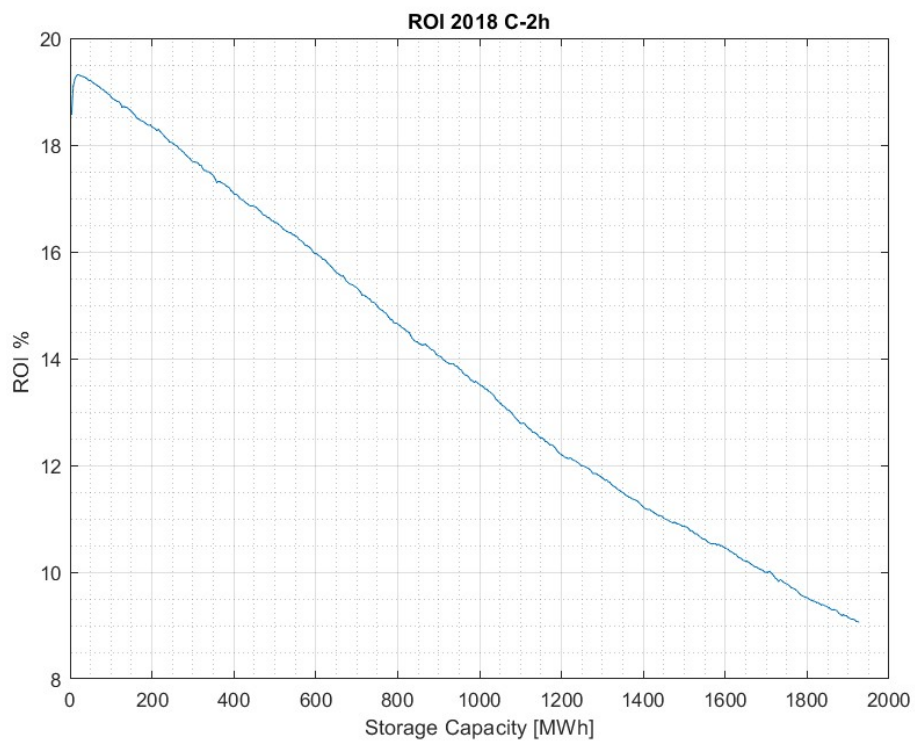
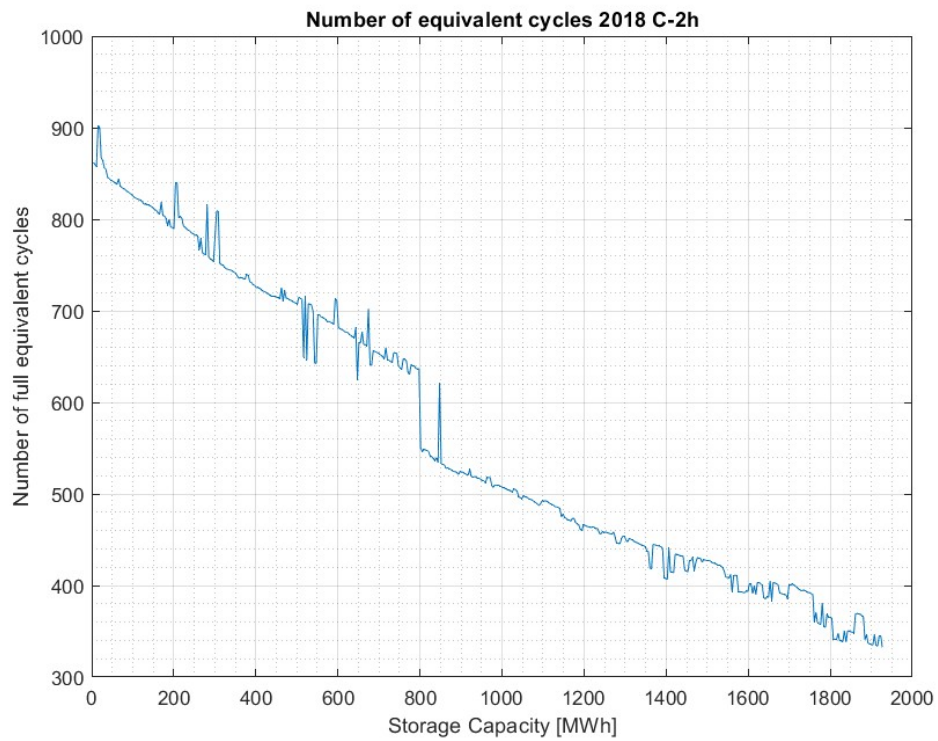




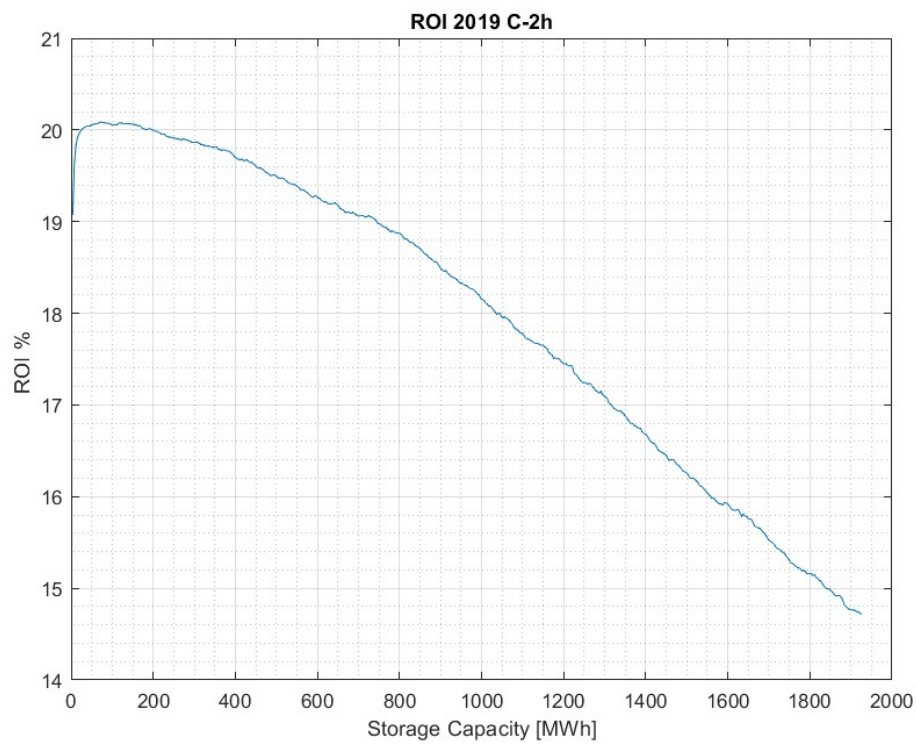
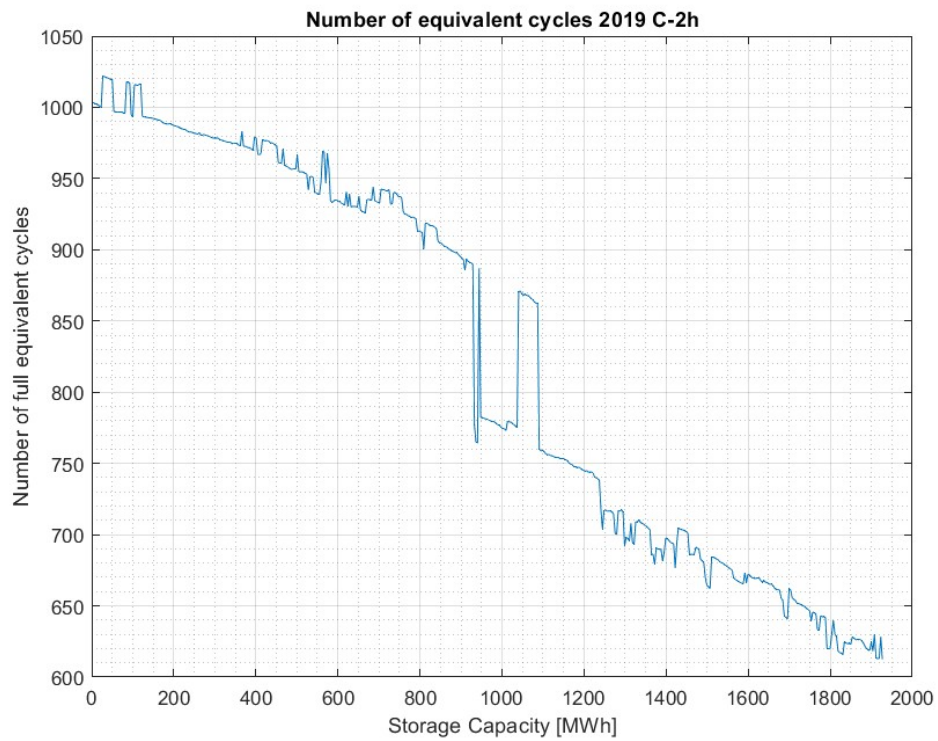
Simulation results for year 2022 for BESS with C-rate 4 hours



Simulation results for year 2018 for BESS with C-rate 2 hours

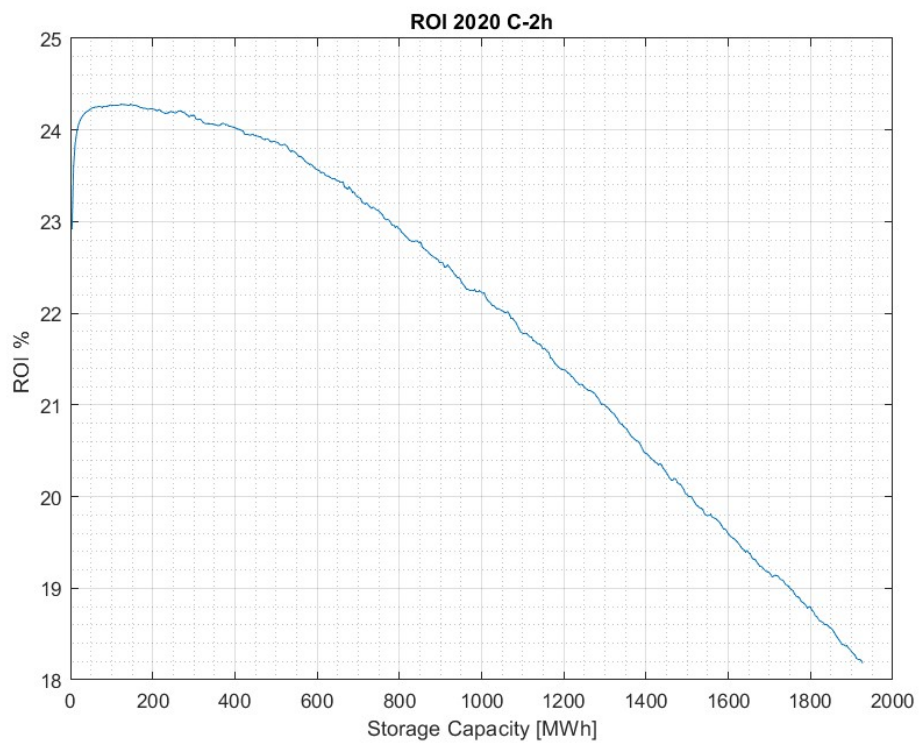
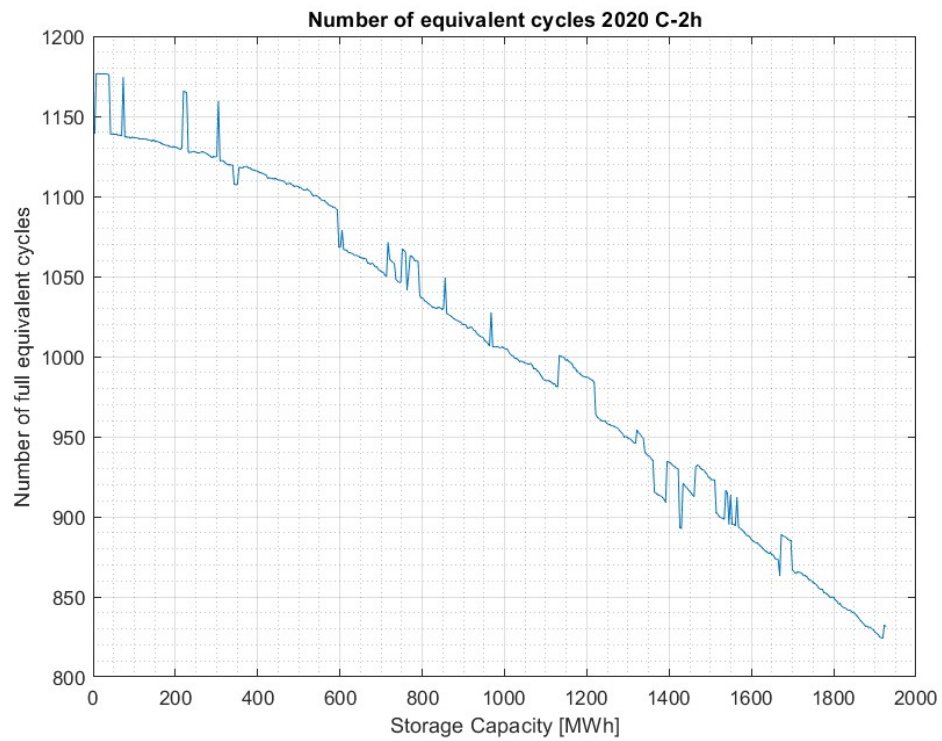


## Simulation results for year 2019 for BESS with C-rate 2 hours

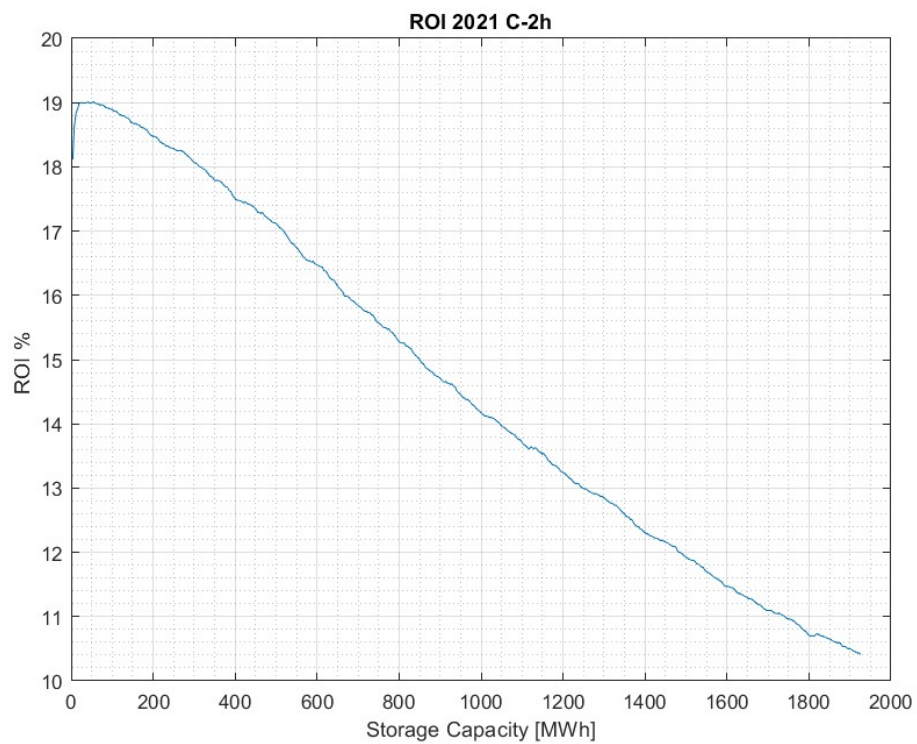
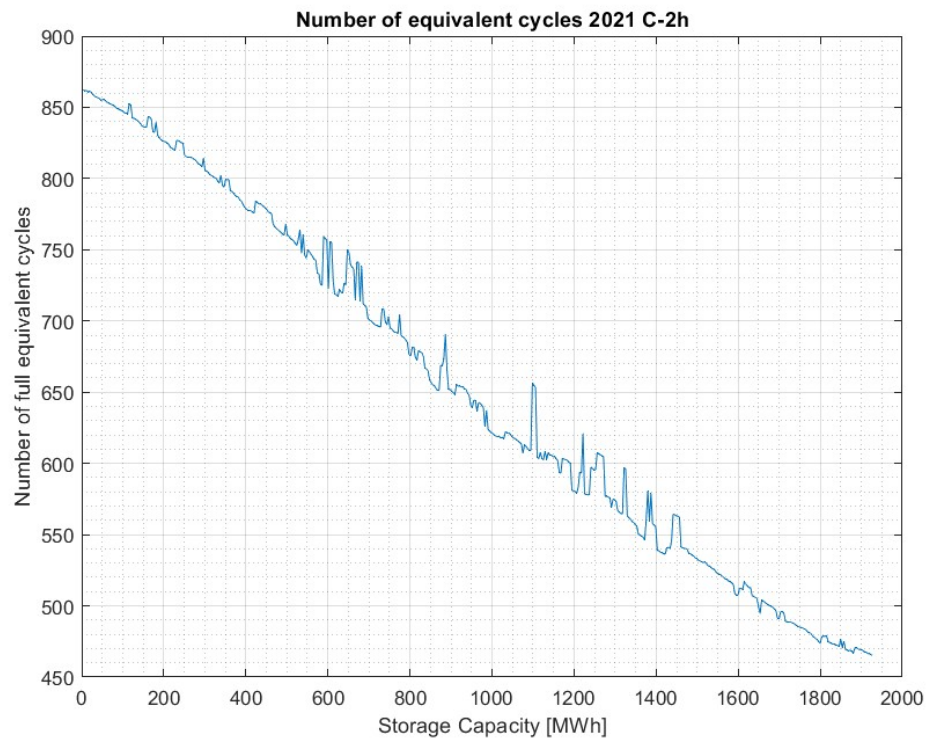




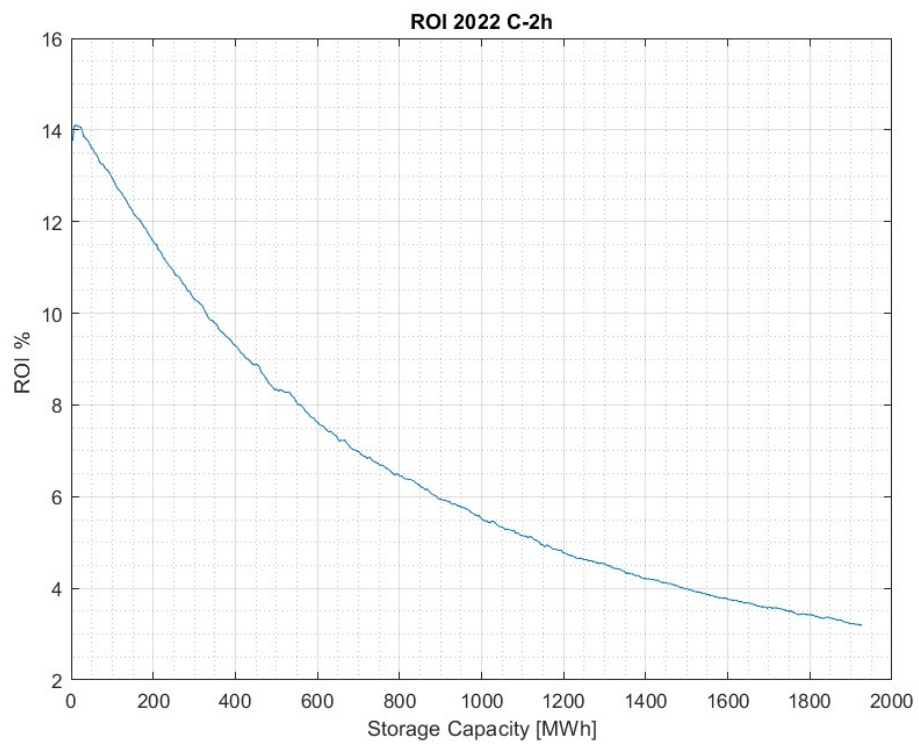
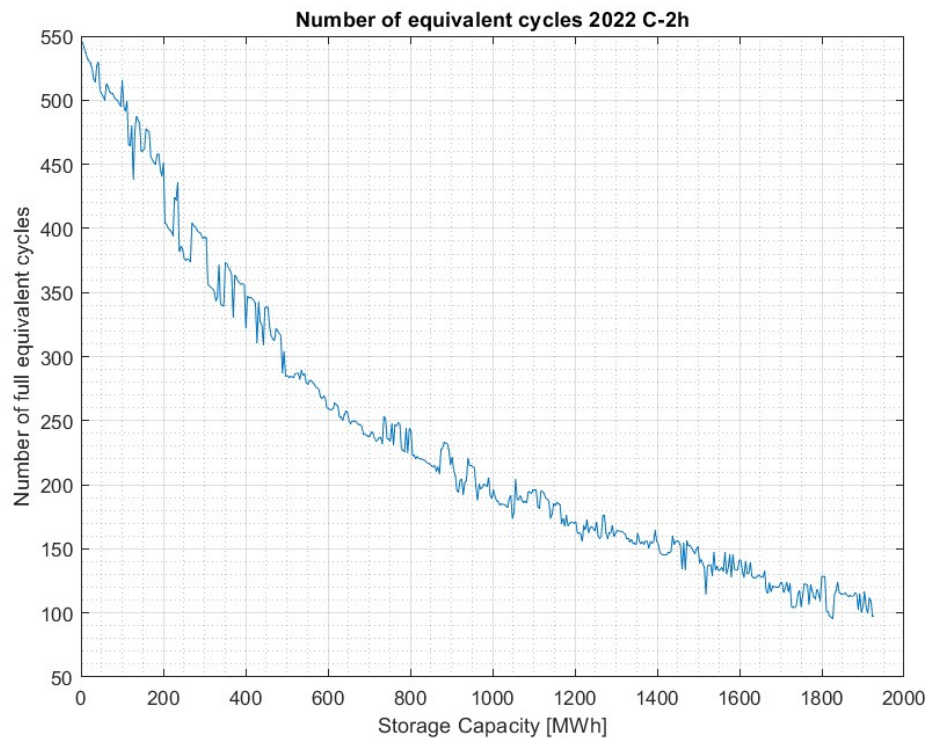
## Simulation results for year 2020 for BESS with C-rate 2 hours



Simulation results for year 2021 for BESS with C-rate 2 hours



Simulation results for year 2022 for BESS with C-rate 2 hours



## Bibliography

- [0.1] European Commission, Directorate-General for Budget, The EU's 2021-2027 long-term budget and NextGenerationEU : facts and figures, Publications Office of the European Union, 2021, <https://data.europa.eu/doi/10.2761/808559>
- [0.2] “Il Green Deal europeo illustra le strategie per fare dell'Europa il primo continente al mondo a impatto climatico zero entro il 2050, dando impulso all'economia, migliorando la salute e la qualità della vita delle persone e tutelando la natura e senza che nessuno sia escluso da questo processo”, [https://ec.europa.eu/commission/presscorner/detail/it/ip\\_19\\_6691](https://ec.europa.eu/commission/presscorner/detail/it/ip_19_6691)
- [0.3] UNFCCC <https://unfccc.int/>
- [0.4] “Global Climate Change” – NASA, <https://climate.nasa.gov/>
- [0.5] IPCC – Global warming of 1.5°C  
<https://ipccitalia.cmcc.it/ipcc-special-report-global-warming-of-1-5-c/>
- [0.6] “Global Greenhouse Gas Emissions Data”, EPA - United States Environmental Protection Agency, <https://www.epa.gov/ghgemissions/global-greenhouse-gas-emissions-data>
- [0.7] [https://unfccc.int/kyoto\\_protocol](https://unfccc.int/kyoto_protocol)
- [0.8] <https://unfccc.int/process-and-meetings/the-paris-agreement/the-paris-agreement>
- [0.9] [https://ec.europa.eu/commission/presscorner/detail/it/ip\\_20\\_2096](https://ec.europa.eu/commission/presscorner/detail/it/ip_20_2096)
- [0.10] [https://www.mise.gov.it/images/stories/documenti/PNIEC\\_finale\\_17012020.pdf](https://www.mise.gov.it/images/stories/documenti/PNIEC_finale_17012020.pdf)
- [0.11] “Piano Nazionale di Ripresa e Resilienza – Italia Domani”, PNRR - <https://www.governo.it/sites/governo.it/files/PNRR.pdf>
- [0.12] “Investimento 1.3 - Promozione impianti innovativi (incluso off-shore)”, <https://www.mite.gov.it/pagina/investimento-1-3-promozione-impianti-innovativi-incluso-shore>
- [0.13] “European Green Deal: Commission proposes transformation of EU economy and society to meet climate ambitions” [https://ec.europa.eu/commission/presscorner/detail/en/IP\\_21\\_3541](https://ec.europa.eu/commission/presscorner/detail/en/IP_21_3541)
- [0.14] “How Europe can cut natural gas imports from Russia significantly within a year” – IEA, <https://www.iea.org/news/how-europe-can-cut-natural-gas-imports-from-russia-significantly-within-a-year>
- [0.15] Ministry of Ecological Transition – Italian Gas imports  
[https://dgsaie.mise.gov.it/gas\\_naturale\\_importazioni.php?lang=en\\_US](https://dgsaie.mise.gov.it/gas_naturale_importazioni.php?lang=en_US)
- [0.16] “REPowerEU: energia sicura, sostenibile e a prezzi accessibili per l'Europa”, [https://ec.europa.eu/info/strategy/priorities-2019-2024/european-green-deal/repower-eu-affordable-secure-and-sustainable-energy-europe\\_it#le-azioni-di-repower-eu](https://ec.europa.eu/info/strategy/priorities-2019-2024/european-green-deal/repower-eu-affordable-secure-and-sustainable-energy-europe_it#le-azioni-di-repower-eu)
- [0.17] “IPCEI Idrogeno 1 (H2 Technology)”, Mise – <https://www.mise.gov.it/it/incentivi/ipcei-idrogeno-1-h2-technology>
- [0.18] “Documento di Descrizione degli Scenari Terna 2022”, August 2022, Terna - Snam. <https://www.terna.it/it/sistema-elettrico/rete/piano-sviluppo-rete/scenari>

- [0.19] “European Hydrogen Backbone”, <https://ehb.eu/>
- [1.1] New European Wind Atlas (NEWA), <https://map.neweuropeanwindatlas.eu/>
- [1.2] “Dedicated large-scale floating offshore wind to hydrogen: Assessing design variables in proposed typologies”, 2021, Omar S. Ibrahim, Alessandro Singlitico, Roberts Proskovics, Shane McDonagh, Cian Desmond, Jerry D. Murphy
- [1.3] ”Life cycle assessment of floating offshore wind farms: An evaluation of operation and maintenance”, 2021, Anna Garcia-Teruel, Giovanni Rinaldi, Philipp R. Thies, Lars Johanning, Henry Jeffrey.
- [1.4] Wind Europe – Wind Power Numbers daily,  
<https://windeurope.org/about-wind/daily-wind/capacity-factors>
- [1.5] Equinor – Hywind Tampen, <https://www.equinor.com/energy/hywind-tampen>
- [1.6] “Definition of the IEA 15-Megawatt Offshore Reference Wind Turbine”, March 2020, Gaertner, Evan, Jennifer Rinker, Latha Sethuraman, Frederik Zahle, Benjamin Anderson, Garrett Barter, Nikhar Abbas, Fanzhong Meng, Pietro Bortolotti, Witold Skrzypinski, George Scott, Roland Feil, Henrik Bredmose, Katherine Dykes, Matt Shields, Christopher Allen, and Anthony Viselli. Golden, CO: National Renewable Energy Laboratory. NREL/TP-5000-75698.
- [1.7] “Aquaterra Energy and Seawind Ocean Technology sign agreement for the development of world’s largest offshore floating wind and green hydrogen production project”,  
<https://aquaterraenergy.com/aquaterra-energy-and-seawind-ocean-technology-sign-agreement-for-the-development-of-worlds-largest-offshore-floating-wind-and-green-hydrogen-production-project/>
- [1.8] “Seawind’s innovative high-performing wind turbines”,  
<https://seawindtechnology.com/technologies/>
- [1.9] “A Surrogate-model-based Approach for Estimating the First and Second-order Moments of Offshore Wind Power”, December 2020, Behzad Golparvar, Petros Papadopoulos, Ahmed Aziz Ezzat, Ruo-Qian Wang.
- [1.10] “Mooring System Engineering for Offshore Structures”, 2019, Kai-Tung Ma, Yong Luo, Thomas Kwan, Yongyan Wu.
- [1.11] “Floating offshore wind - Economic and ecological challenges of a TLP solution”, 2018, Michael Kausche, Frank Adam, Frank Dahlhaus, Jochen Großmann.
- [1.12] “Motion control of a barge for offshore wind turbine (OWT) using gyro stabilizer”, 2019, Manmathakrishnan Palraj, Panneerselvam Rajamanickam
- [1.13] Principle Power – Windfloat, <https://www.principlepower.com/windfloat/advantage/installation>
- [1.14] SBM offshore – Float4Wind, [https://www.sbmoffshore.com/sites/sbm-offshore/files/documents/2022/Float4Wind%20Brochure\\_SBM%20Offshore\\_March%202022.pdf](https://www.sbmoffshore.com/sites/sbm-offshore/files/documents/2022/Float4Wind%20Brochure_SBM%20Offshore_March%202022.pdf)  
<https://www.sbmoffshore.com/creating-value/new-energies>
- [1.15] “Transformers for floating applications”, <https://www.hitachienergy.com/me/en/products-and-solutions/transformers/special-application-transformers/transformers-for-floating-applications>

- [1.16] “Cabling to connect offshore wind turbines to onshore facilities”, 2016, Narakorn Srinil, Offshore Wind Farms.
- [1.17] “Transmission Design and Analysis for Large-Scale Offshore Wind Energy Development”, 2018, Elpiniki Apostolaki-Iosifidou, Regina McCormack, Willett Kempton, Paul Mccoy, And Deniz Ozkan.
- [1.18] O. E. Oni, I. E. Davidson and K. N. I. Mbangula, "A review of LCC-HVDC and VSC-HVDC technologies and applications," 2016 IEEE 16th International Conference on Environment and Electrical Engineering (EEEIC), 2016, pp. 1-7, doi: 10.1109/EEEIC.2016.7555677.
- [1.19] T. W. May, Y. M. Yeap and A. Ukil, "Comparative evaluation of power loss in HVAC and HVDC transmission systems," 2016 IEEE Region 10 Conference (TENCON), 2016, pp. 637-641, doi: 10.1109/TENCON.2016.7848080.
- [1.20] Roberto Benato, Lorenzo Fellin, “Impianti Elettrici”, 2014.
- [1.21] “Progetto campo eolico nel tratto di mare a sud di Crotone”, Tecnoconsult, Repower.
- [2.1] GME - <https://www.mercatoelettrico.org/it/>
- [2.2] “Piano di Sviluppo 2021” Terna - [https://download.terna.it/terna/Piano\\_Sviluppo\\_2021\\_8d94126f94dc233.pdf](https://download.terna.it/terna/Piano_Sviluppo_2021_8d94126f94dc233.pdf)
- [2.3] TERNA - Transparency report – <https://www.terna.it/it/sistema-elettrico/transparency-report/download-center>
- [2.4] Bozza Decreto FER II - <https://cdn.rinnovabili.it/wp-content/uploads/2022/07/Bozza-DM-Fer2.pdf>
- [3.1] “Thermal, Mechanical, and Hybrid Chemical Energy Storage Systems”, 2020, Klaus Brun, Timothy Allison, Richard Dennis. <https://doi.org/10.1016/C2019-0-00430-X> – Chapter 7 – “Energy storage services”, Sebastian Freund, Scott Hume, Joseph Stekli.
- [3.2] “Compressed air energy storage in integrated energy systems: A review”, 2022, Elaheh Bazdar, Mohammad Sameti, Fuzhan Nasiri, Fariborz Haghighat.
- [3.3] “Diabatic Compressed Air Energy Storage (CAES) Systems: State of the Art”, 2022, M Soltani, Farshad Moradi Kashkooli, Heidar Jafarizadeh, Mohammad Hatefi, Hadi Fekri, Kobra Gharali, and Jatin Nathwanic.
- [3.4] “Mechanical Energy Storage Technologies” - “Chapter Three – Compressed Air Energy Storage”, 2020, Ahmad Arabkoohsar.
- [3.5] “Adiabatic Compressed Air Energy Storage” – EASE, <https://ease-storage.eu/energy-storage/technologies/>
- [3.6] “Diabatic Compressed Air Energy Storage” – EASE, <https://ease-storage.eu/energy-storage/technologies/>
- [3.7] “Adiabatic Compressed Air Energy Storage Systems”, 2022, Edward R.Barbour, Daniel L.F.Pottie.
- [3.8] Hydrostor - <https://www.hydrostor.ca/company/>

- [3.9] Zhang, Weiqi & Xue, Xiaodai & Feng, Liu & Mei, Shengwei. (2020). Modeling and experimental validation of Advanced Adiabatic Compressed Air Energy Storage with off-design Heat Exchanger. IET Renewable Power Generation. 14. 10.1049/iet-rpg.2019.0652.
- [3.10] Mei, S., Wang, J., Tian, F. et al. Design and engineering implementation of non-supplementary fired compressed air energy storage system: TICC-500. Sci. China Technol. Sci. 58, 600–611 (2015). <https://doi.org/10.1007/s11431-015-5789-0>
- [3.11] “LTA-CAES – A low-temperature approach to Adiabatic Compressed Air Energy Storage”, 2013, Daniel Wolf, Marcus Budt.
- [3.12] Venkataramani, Gayathri & Velraj, R.. (2021). Energy and Exergy Analysis of Isothermal Compressed Air Energy Storage System. 10.1016/B978-0-12-819723-3.00148-7.
- [3.13] Compressed Air Energy Storage – Siemens Energy, <https://www.siemens-energy.com/global/en/offerings/storage-solutions/thermo-mechanical-energy-storage/caes.html>
- [3.14] “Cryogenic Energy Storage”, Encyclopedia of Energy Storage, Volume 2, 2022, Pages 94-107, Xiaohui She, Tongtong Zhang, Yuanze Meng, Ting Liang, Xiaodong Peng, Lige Tong, Li Wang, Yongliang Li, Yulong Ding.
- [3.15] “Liquid air energy storage systems: A review”, Renewable and Sustainable Energy Reviews, Volume 146, August 2021, 111113, O. O’Callaghan, P. Donnellan.
- [3.16] Menezes, M.V.P.; Vilasboas, I.F.; da Silva, J.A.M. “Liquid Air Energy Storage System (LAES) Assisted by Cryogenic Air Rankine Cycle (ARC).” Energies 2022, 15, 2730. <https://doi.org/10.3390/en15082730>
- [3.17] “Optimal recovery of thermal energy in liquid air energy storage”, Energy, Volume 240, 1 February 2022, 122810, Zhongxuan Liu, Donghoi Kim, Truls Gundersen. <https://doi.org/10.1016/j.energy.2021.122810>
- [3.18] “Liquid Air Energy Storage” – EASE, <https://ease-storage.eu/energy-storage/technologies/>
- [3.19] Highview power – Projects - <https://highviewpower.com/plants/#uk-projects>
- [3.20] “Gravitational Energy Storage with Weights”, Encyclopedia of Energy Storage, Volume 3, 2022, Pages 64-73. Thomas Morstyn, Christoff D.Botha. <https://doi.org/10.1016/B978-0-12-819723-3.00065-2>
- [3.21] “Chapter 4 - Mechanical energy storage”, Thermal, Mechanical, and Hybrid Chemical Energy Storage Systems, 2021, Pages 139-247. Aaron Rimpel, KlauKrueger, Zhiyang Wang, Xiaojun Li, Alan Palazzolo, Jamshid Kavosi, Mohamad Naraghi, Terry Creasy, Bahar Anvari, Eric Severson, Eugene Broerman. <https://doi.org/10.1016/B978-0-12-819892-6.00004-6>
- [3.22] “Weights-Based Gravity Energy Storage Looks to Scale Up”, Engineering, Volume 14, July 2022, Pages 3-6. Sean O’Neill. <https://doi.org/10.1016/j.eng.2022.05.007>
- [3.23] ARES – GravityLine. <https://aresnorthamerica.com/gravityline/>
- [3.24] Energy Vault. <https://www.energyvault.com/>
- [3.25] Gravitricity. <https://gravitricity.com/>



- [3.26] Energy Dome - <https://energydome.com/>
- [3.27] “Energy Dome will prove a paradigm-shifting Utility Scale Energy Storage technology, the CO2 Battery, in its first Demonstrator.” - <https://energydome.com/energy-dome-will-prove-paradigm-shifting-long-duration-energy-storage-technology-the-co2-battery-in-its-first-technical-demonstration-project/>
- [3.28] “Innovation in batteries and electricity storage - A global analysis based on patent data”, September 2020, European Patent Office (EPO) & International Energy Agency (IEA). <https://www.iea.org/reports/innovation-in-batteries-and-electricity-storage>
- [3.29] Akhil, Abbas A., Huff, Georgianne, Currier, Aileen B., Hernandez, Jacquelynne, Bender, Donald Arthur, Kaun, Benjamin C., Rastler, Dan M., Chen, Stella Bingqing, Cotter, Andrew L., Bradshaw, Dale T., Gauntlett, William D., Eyer, James, Olinsky-Paul, Todd, Ellison, Michelle, and Schoenung, Susan. 2016. "DOE/EPRI Electricity Storage Handbook in Collaboration with NRECA". United States. <https://doi.org/10.2172/1431469>. <https://www.osti.gov/servlets/purl/1431469>.
- [3.30] OnLocation – “Electricity Storage Technology Review”, June 2020.
- [3.31] “Roadmap on stationary applications for batteries” – European commission - WG6 - Application and integration: Stationary <https://energy.ec.europa.eu/system/files/2022-01/vol-6-009.pdf>
- [3.32] Tesla Megapack - [https://www.tesla.com/it\\_it/megapack](https://www.tesla.com/it_it/megapack)
- [3.33] “UK’s Harmony Energy brings online Europe’s ‘largest battery storage system in MWh terms’” <https://www.energy-storage.news/uks-harmony-energy-brings-online-europes-largest-battery-storage-system-in-mwh-terms/>
- [3.34] “Moss Landing Battery Storage Project” <https://www.nsenergybusiness.com/projects/moss-landing/>
- [3.35] “Powin begins work on 1.9GWh Australian ‘Super Battery’ for BlackRock-owned developer” <https://www.energy-storage.news/powin-begins-work-on-1-9gwh-australian-super-battery-for-blackrock-owned-developer/>
- [3.36] Editor(s): Fu-Bao Wu, Bo Yang, Ji-Lei Ye, “Grid-scale Energy Storage Systems and Applications”, 2020, <https://doi.org/10.1016/B978-0-12-815292-8.12001-5>. (<https://www.sciencedirect.com/science/article/pii/B9780128152928120015> )
- [3.37] “Power to Fuel - How to Speed Up a Hydrogen Economy”, 2021, Giuseppe Spazzafumo. <https://doi.org/10.1016/C2019-0-05035-2>
- [3.38] “Ingegneria e sostenibilità: introduzione alle tecniche di produzione e ai metodi di impiego di idrogeno rinnovabile” Webinar by Fondazione Consiglio Nazionale degli Ingegneri.
- [3.39] IRENA (2020), “Green Hydrogen Cost Reduction: Scaling up Electrolysers to Meet the 1.5°C Climate Goal”, International Renewable Energy Agency, Abu Dhabi.
- [3.40] “Electrochemical Power Sources: Fundamentals, Systems, and Applications” - Chapter 13 - Hydrogen storage, Henrietta W.Langmi, Nicolaas Engelbrecht, Phillimon M. Modisha, Dmitri Bessarabov. <https://doi.org/10.1016/B978-0-12-819424-9.00006-9>

- [3.41] “Nanomaterials for Hydrogen Storage Applications”, 2021, Pages 249-264, - Chapter 14 - Solid-state hydrides for hydrogen storage. N.Rajesh Jesudoss Hynes, R.Sankaranarayanan, P.Senthamarai Kannan, Anish Khan, Aftab Aslam Parwaz Khan, Abdullah M.Asiri, Huriya Dzudzevic-Cancar. <https://doi.org/10.1016/B978-0-12-819476-8.00021-9>
- [3.42] “Alstom”, <https://www.alstom.com/solutions/rolling-stock/alstom-coradia-ilint-worlds-1st-hydrogen-powered-train>
- [3.43] “HESC – Suiso Frontier”, <https://www.hydrogenenergysupplychain.com/supply-chain/the-suiso-frontier/>
- [3.44] “Baxi Hydrogen Boiler”, <https://www.baxi.it/news-eventi/caldaia-idrogeno>
- [3.45] “Hybrid Renewable Energy Systems and Microgrids”, 2021, Pages 313-349. “9 - Fuel cell and hydrogen power plants”. Himadry ShekharDas, Md. Fahim F.Chowdhury, ShuhuiLi1Chee WeiTan. <https://doi.org/10.1016/B978-0-12-821724-5.00009-X>
- [3.46] SEMREV - Offshore renewable Hydrogen production- <https://www.lhyfe.com/our-production-units/offshore-ecological-hydrogen/>
- [3.47] “Green Hydrogen Unlocked: Brande Hydrogen” Whitepaper - <https://www.siemensgamesa.com/en-int/products-and-services/hybrid-and-storage/green-hydrogen/unlocked-brande-hydrogen-project>
- [4.01] Pubblicazioni statistiche Terna - <https://www.terna.it/it/sistema-elettrico/statistiche/pubblicazioni-statistiche>
- [5.01] Tesla Megapack Design - <https://www.tesla.com/megapack/design>
- [5.02] “New: Tesla Unveils Megapack Order Page & Pricing”, <https://www.thestreet.com/tesla/news/new-tesla-megapack-details-price>
- [5.03] “Degradation of Commercial Lithium-Ion Cells as a Function of Chemistry and Cycling Conditions”, Journal of The Electrochemical Society, Volume 167, Number 12. Yuliya Preger, Heather M. Barkholtz, Armando Fresquez, Daniel L. Campbell, Benjamin W. Juba, Jessica Romàn-Kustas, Summer R. Ferreira and Babu Chalamala. DOI 10.1149/1945-7111/abae37
- [6.01] “D.LGS. 210/21”- <https://www.normattiva.it/uri-res/N2Ls?urn:nir:stato:decreto.legislativo:2021-11-08;210>
- [6.02] “Documento per la consultazione 393/2022/R/EEL” - ARERA – <https://www.arera.it/it/docs/22/393-22.htm>
- [6.03] “Criteri e condizioni per il sistema di approvvigionamento a termine di capacità di stoccaggio elettrico, pompaggi” – Elettricità Futura - [https://www.elettricitafutura.it/Policy/Mercato-e-Reti/Criteri-e-condizioni-per-il-sistema-di-approvvigionamento-a-termine-di-capacit-di-stoccaggio-elettrico-pompaggi\\_4801.html](https://www.elettricitafutura.it/Policy/Mercato-e-Reti/Criteri-e-condizioni-per-il-sistema-di-approvvigionamento-a-termine-di-capacit-di-stoccaggio-elettrico-pompaggi_4801.html)
- [6.04] “L’accumulo elettrochimico di energia - Nuove regole, nuove opportunità”. Federazione ANIE, ANIE Energia, RSE, Confindustria. <https://anie.it/regole-e-opportunita-dellaccumulo-elettrochimico-di-energia-presentato-il-libro-bianco-3-0-di-anie-energia-e-rse-2/?contesto-articolo=/sala-stampa/notizie/#.Y-Je8XbMK38>